

If you have discovered material in Aston Publications Explorer which is unlawful e.g. breaches copyright, (either yours or that of a third party) or any other law, including but not limited to those relating to patent, trademark, confidentiality, data protection, obscenity, defamation, libel, then please read our [takedown policy](#) and [contact the service](#) immediately.



Kerr Nonlinearity in Optical Communication Systems

Abdallah Alsayed Ismail Ali

Doctor of Philosophy

Aston University

January 2020

©Abdallah Alsayed Ismail Ali, 2020

Abdallah Alsayed Ismail Ali asserts his moral right to be identified as the author of this thesis

This copy of the thesis has been supplied on condition that anyone who consults it is understood to recognise that its copyright belongs to its author and that no quotation from the thesis and no information derived from it may be published without appropriate permission or acknowledgement.

Aston University

Kerr Nonlinearity in Optical Communication Systems

Abdallah Alsayed Ismail Ali

Doctor of Philosophy

2020

SUMMARY

Single-mode fibers (SMFs) are approaching their nonlinear capacity limit soon, and the new technology for increasing the capacity per fiber like space-division multiplexing (SDM) is not ready yet. Therefore, mitigating the nonlinearity in SMFs becomes an important aspect of the current research. Optical phase conjugation (OPC) comes as a promising method for simultaneous compensation of dispersion and nonlinearity in optical fiber link for a broadband signal and in real-time. However, it is limited by the power and dispersion symmetry requirements around the mid-link OPC device. The power symmetry almost has been achieved by using Raman amplification. Another scheme for achieving the power symmetry was by achieving that for the nonlinear effective region instead of the total link through shifting those regions by adding a dispersive element collocated with the OPC. In this thesis, the two methods will be investigated in improving the symmetry around the mid-link OPC either through simulation or experimentally. A mathematical analysis for the latter method will be performed by estimating the four-wave mixing (FWM) power from the interactions of three tones propagating through the optical fiber. Then a closed-form formula for the nonlinear noise power from the transmission of Nyquist-shaped wave division multiplexed (WDM) signal will be driven. The closed-form will be used in predicting the performance of a system employing mid-link OPC with lumped amplification. In order to verify the mathematical results, simulations were run and give a good agreement with the theory. The closed-form formula is verified experimentally through the transmission of 4.08Tb/s WDM signal over 600km with mid-link OPC and 75km span is added after the OPC to improve the symmetry. The Raman amplification scheme in improving the power symmetry around the mid-link OPC has been tested with a real-time transceiver which proves the potential application of mid-link OPC in a real commercial system. The dispersion slope effect on the nonlinearity modeling is studied and a figure of merit is developed to predict when the dispersion slope needs to be considered in the models to give accurate results. The different OPC designs based on optical fiber are discussed and a wavelength shift-free OPC design is presented.

Keywords: Optical fiber, coherent optical communication system, Kerr nonlinearity, nonlinearity mitigation, optical phase conjugation

To my father.
In the memory of my mother and
for Eyad, Lena and Rabab.

ACKNOWLEDGMENT

First of all, countless thanks to ALLAH the almighty

I would like to express my sincere appreciation to my supervisor, Prof. Andrew Ellis for his continuous encouragement, support, patience, discussions, valuable comments, and excellent suggestions to improve the quality of this work.

Furthermore, I would like to acknowledge the prosperous teamwork with the professors, research fellows, and staff members at AIPT, the daily work and discussions with them helped me too much.

Thanks to my beloved family, my wife and my children Eyad and Lena, for their self-sacrifice, consistent love, support, understanding, and encouragement.

Finally, the work inside this thesis is partially supported by The Engineering and Physical Sciences Research Council (EPSRC) (PEACE (EP/L000091/1)) which is gratefully acknowledged.

Abdallah Ali

TABLE OF CONTENTS

SUMMARY	3
ACKNOWLEDGMENT	6
TABLE OF CONTENTS	7
LIST OF TABLES	11
LIST OF FIGURES	13
NOMENCLATURE	21
ABBREVIATIONS	25
1 Introduction	31
1.1 Capacity Demand	31
1.2 Fiber Optic Communication System	32
1.3 Capacity Crunch	33
1.4 Nonlinearity Effects Mitigation Methods	34
1.5 The Motivation for The Thesis Work	34
1.6 Thesis Organization	35
1.7 Collaboration Acknowledgements	36
2 Optical Communication System	39
2.1 Coherent Optical Communication system	40
2.1.1 Optical Transmitter	40
2.1.2 Coherent Receiver	42
2.1.3 Optical Channel	44

TABLE OF CONTENTS

2.2	Combating Kerr-Nonlinearities in Optical Fiber	56
2.3	Nonlinearity Compensation Methods	56
2.3.1	Digital Nonlinearity Compensation Methods	56
2.3.2	Optical Nonlinearity Compensation Methods	58
2.4	Optical Phase conjugation	58
2.5	OPC with Coherent Systems	59
2.6	Multiple Optical Phase Conjugation	62
2.7	The Efficiency of OPC Compensation	63
2.8	Optical Phase Conjugation with Pre-dispersion	64
2.9	Nonlinearity Mitigation Methods	67
2.9.1	Constellation Design	67
2.9.2	Transmitted Optical Pulse-Shaping	68
2.9.3	Symbol Rate Optimization	68
2.9.4	Nonlinear Noise Squeezing	68
2.9.5	Transmitted Data Encoding in the Nonlinear Frequency Domain	69
2.9.6	Conjugated Twin Waves	69
2.10	Performance Measure of Optical Communication System	70
2.10.1	Bit Error Rate	70
2.10.2	Signal to Noise Ratio	71
2.10.3	Optical Signal to Noise Ratio	71
2.10.4	Q-Factor	72
2.10.5	Error Vector Magnitude	73
2.10.6	Mutual Information	74
3	Mathematical Expressions for Fiber Nonlinearity in Lumped Amplified Systems	77
3.1	Four-Wave Mixing	78
3.2	Nonlinear Noise Power Spectral Density	81
3.2.1	Closed-form Expression for Nonlinear Noise Power Spectral Density	83
3.2.2	Optimum Pre-dispersion	92
3.2.3	Optimum Launch Power Density and SNR	93
3.3	Validation of the Mathematical Analysis	93
3.3.1	FWM Expression Validation	94
3.3.2	Nonlinear Noise Expressions Validation	97

TABLE OF CONTENTS

3.4	The Impact of Dispersion Slope on Modeling Fiber Nonlinearity in Ultra-Wideband Systems	101
3.4.1	FWM Power with Dispersion Slope	102
3.5	Conclusions	104
4	Optical Fiber Phase Conjugation Device	107
4.1	Optical Fiber Single-Pump Phase Conjugation Device	108
4.1.1	Pump Dithering	109
4.1.2	Phase Matching	111
4.1.3	Conjugation Bandwidth	111
4.1.4	Insertion Loss	112
4.1.5	Polarization Diversity	113
4.2	Optical Fiber Dual-Pump Phase Conjugation Device	114
4.2.1	Counter Dithering	118
4.2.2	Wavelength Shift-free OPC	120
4.3	Conclusions	126
5	Experimental Investigation of Nonlinearity in Optical Communication System	127
5.1	OPC Symmetry Improvement Through Pre-dispersion	128
5.1.1	Experimental Validation for FWM Expression	129
5.1.2	Nonlinear Noise Compensation Using Pre-dispersion	133
5.2	Real Time Nonlinearity Compensation Using OPC with Raman Amplification . .	147
5.2.1	Experiment Setup	148
5.2.2	Experiment Results and Discussions	151
5.3	Experimental Investigation for The Impact of Dispersion Slope on Modeling Fiber Nonlinearity	154
5.3.1	FWM Experiment	155
5.3.2	NLN Experiment	157
5.3.3	BER Measurement	159
5.4	Conclusions	161
6	CONCLUSIONS	163
6.1	Conclusions	163
6.2	Future Work Suggestions	164

TABLE OF CONTENTS

LIST OF PUBLICATIONS	166
REFERENCES	169
A FWM Power in Multi-Span System Employing OPC with Pre-Dispersion	199
A.1 Single Span FWM	200
A.2 Spans Before the OPC	201
A.3 Spans After the OPC	203
A.4 Total FWM Field and Power	204

LIST OF TABLES

2.1	Some experiments for nonlinearity mitigation in SSMF using OPC compensation. HNLf: Highly NonLinear Fiber - OOK: ON-Off Keying - OPC: Optical Phase Conjugation - SSMF : Standard Single Mode Fiber - SLA: Super Large Area - ULAF: Ultra Large Area Fiber.	62
2.2	BER formula for m-QAM modulation format for hard decision system with AWGN	71
3.1	Simulation parameters for FWM equation validation	94

LIST OF TABLES

LIST OF FIGURES

1.1	Total Internet Traffic Over Different Years including forecasts for the coming years. Source: Cisco VNI, 2019.	31
2.1	Block diagram for the optical coherent communication system.	40
2.2	Block diagram of the Mach-Zehnder modulator.	40
2.3	Block diagram of the IQ modulator.	41
2.4	(a) Single polarization coherent receiver setup. (b) 90° optical hybrid design. . .	43
2.5	FWM efficiency as a function of frequency separation for three different types of fiber.	54
2.6	The schematic for a multi-span lumped amplification system employing OPC. . .	64
2.7	Power and accumulated dispersion (D_{acc}) of multi-span system versus the distance.	65
2.8	Power versus the accumulated dispersion for a system with midlink OPC.	65
2.9	The schematic for a multi-span lumped amplification system employing OPC with pre-dispersion.	66
2.10	Power versus the distance and the accumulated dispersion is shown as a dotted line. The red line represents the pre-dispersion length.	66
2.11	Power versus the accumulated dispersion for a system with midlink OPC and pre-dispersion.	67
2.12	Error vector magnitude measurement for a constellation point. $E_{r,i}$ is the reference signal vector	73
3.1	Mid-link optical phase conjugation system with pre-dispersion. DE: Dispersion Element, $U_g^{(1,1)}$: The Four-wave mixing field in the first span and N: Number of spans	78

LIST OF FIGURES

3.2	Conceptual diagram for slicing the Nyquist WDM bandwidth into small frequency components	82
3.3	Integration boundaries shown as gray polygon , the square represent the approximation	83
3.4	Normalized coefficient ξ in lumped amplification system as a function of the span length.	91
3.5	FWM power of OPC system as a function of frequency separations between the two signals in three cases: without OPC or DE (red), with OPC only (blue) and with OPC and DE(green) for theory (lines) and simulation (markers).	95
3.6	The signal to noise ratio (SNR) of 224Gbps PM-16QAM transmitted over 10x100km SSMF link incorporating an OPC as a function of the launched power in two cases: without pre-dispersion (blue) and with pre-dispersion (green) for theory (lines) and simulation (markers).	96
3.7	The maximum signal to noise ratio (SNR) as a function of the number of spans with different span length 100 km (blue), 80 km (orange) and 60 km (green) in two cases: without pre-dispersion (solid - squares) and with pre-dispersion (dashed - circles) for theory (lines) and simulation (markers).	96
3.8	The signal to noise ratio (SNR) of the central channel of 17 WDM channels as a function of the total launched power density in three cases: Without OPC (red squares), with OPC only (purple diamonds) and with OPC and pre-dispersion (green circles) for theory (lines) and simulation (markers).	98
3.9	The maximum signal to noise ratio (SNR) of the central channel of 17 WDM channels as a function of the pre-dispersion for theory (dashed line) and simulation (markers). The optimum pre-dispersion (vertical line).	99
3.10	The Maximum signal to noise ratio (SNR) of the central channel of 17 WDM channels as a function of the span length in three cases: Without OPC (red), with OPC only (purple) and with OPC and pre-dispersion (green) for theory (lines) and simulation (markers).	100
3.11	FWM efficiency as a function of frequency separation between the three lasers normalized to the ratio of dispersion slope to the dispersion. The red hexagon represents the NLN boundaries affecting the signal with the same normalization. The top of the color bar is yellow then orange.	103

4.1	Basic single pump OPC design. PM: phase modulator. OBPF: optical bandpass filter. 3dB: 3dB coupler. HNLF: highly nonlinear fiber	108
4.2	Theoretical description of the spectrum of phase-modulated pump with two tones.	110
4.3	The output of PM modulator measured using an RF spectrum analyzer.	110
4.4	Single pump dual band OPC setup.	112
4.5	Polarization diversity loop setup.	113
4.6	Pump location with respect to the zero-dispersion wavelength to achieve wide-range phase matching.	114
4.7	Two orthogonal pump generation for polarization-insensitive OPC. PC: Polarization controller. PBC : polarization beam combiner	116
4.8	Polarization-independent dual-band OPC. PC: polarization controller.	117
4.9	The difference in Q factor between back-to-back (B2B) performance of 30 Gbaud 16QAM with the performance when the OPC inserted between Tx and Rx as a function of the phase difference between the two pumps	118
4.10	The Q factor of 30 Gbaud 16QAM as a function of OSNR at two cases back-to-back (B2B) performance and with the OPC inserted between Tx and Rx.	119
4.11	Experimental setup of dual-pump polarization insensitive OPC design.	120
4.12	Experimental setup of SBS threshold characterization.	121
4.13	The backscattered power from HNLF as a function of launched power into the fiber.	122
4.14	The RF spectrum of coherently received idler to show the effect of dithering suppression (a) Top HNLF1. (b) Lower HNLF2	122
4.15	The Spectrum of HNLF1 output with scrambled CW laser is fed the OPC.	123
4.16	The optical spectrum (0.1nm) after setting the OPC (a) Top HNLF1. (b) Lower HNLF2 (c) PBC output. C: Conjugate, S: Signal, P_1 : Pump1, P_2 : Pump2	124
4.17	The optical spectrum (0.1nm) in three cases (a) at HNLF1 output and $f_s - f_{Idler} = 0GHz$. (b) at OPC output and $f_s - f_{Idler} = 14GHz$. (c) at OPC output and $f_s - f_{Idler} = 28GHz$	125
4.18	The Q-factor as a function of the optical signal to noise ratio (OSNR) without OPC (dark blue circles) and with the OPC at three different frequency separations between the idler and the signal.	125

LIST OF FIGURES

5.1	Experimental setup of a discretely amplified system with dual pump OPC for measuring the FWM power.	129
5.2	FWM Power as a function of frequency separation between two CW lasers propagating through 2x100 km of SSMF without and with mid-link OPC, with OPC and DE. Exper.: Experiment.	130
5.3	FWM power as a function of frequency separation between two CW lasers propagating through 275km, with and without OPC and all the spans has the same input power (9dBm), without OPC and the 75km span has low input power (0 dBm).	131
5.4	FWM Power as a function of frequency separation between two CW lasers propagating through 6x100 km of SSMF without and with Mid-link OPC, with OPC and DE (75km span).	132
5.5	Experimental setup of back-to-back measurement of single-channel 30Gbaud PM-16QAM with and without the OPC.	133
5.6	OPC setup with dual pump. PM: polarization maintaining coupler. WSS: wavelength selective switch	134
5.7	Signal to noise (SNR) ratio as a function of the optical signal to noise ratio (OSNR) in back-to-back measurement of single-channel 30 Gbaud PM-16 QAM signal with or without the OPC.	135
5.8	Experimental setup of single-channel transmission over a different number of spans in different scenarios of a discretely amplified system with dual pump OPC.	136
5.9	The signal to noise ratio (SNR) of 30 Gbaud PM-16QAM channel transmitted over 2x100km as a function of the total launched power in three cases: Without OPC (blue triangles), with OPC only (red circles) and with OPC and added dispersion (yellow squares). b,c) The constellation digram for Polarization X and Y at 12dBm for the three cases.	137
5.10	The signal to noise ratio (SNR) of 30 Gbaud PM-16QAM channel transmitted over 2 x 200km spans and a 75 km span after the OPC as a function of the total launched power in the 75km span after the OPC with the optimum power launched in the other 2x100km spans.	138

5.11 The signal to noise ratio (SNR) of 30 Gbaud PM-16QAM channel transmitted over a different number of spans as a function of the total launched power in three cases: Without OPC (blue triangles), with OPC only (red circles) and with OPC and added dispersion (yellow squares). 139

5.12 WDM signal transmitter and receiver side setup. WDM: polarization maintaining wavelength division multiplexer 3dB: 3dB coupler. WSS: wavelength selective switch 140

5.13 (a) The signal to noise ratio (SNR) of 30 Gbaud PM-16QAM central channel of 17 WDM channels in back to back measurement as a function of the frequency separation between the center of the channels. (b) The spectrum of transmitted WDM channels. 141

5.14 The signal to noise ratio (SNR) of the single channel (circles) and the central channel of 17 WDM channels (triangles) as a function of the optical signal to noise ratio (OSNR) in back-to-back measurement with (red) or without the OPC inserted (blue). 142

5.15 The spectrum of OPC output after the HNLF and before filtering the pumps or the signal. 142

5.16 The signal to noise ratio (SNR) of the central channel of 17 WDM channels transmitted over different 2 x 300km spans as a function of the total launched power in three cases: Without OPC (blue triangles), with OPC only (red circles) and with OPC and added dispersion (yellow squares). 143

5.17 The constellation diagram of the symbols of the received central channel at total launch power of 16dBm : (a) without OPC , (b) with OPC only and (c) with OPC and added dispersion. 145

5.18 The optimum signal to noise ratio (SNR) of the different channels of 17 WDM channels transmitted over different 2 x 300km spans in two cases: with OPC only (red circles) and with OPC and added dispersion (yellow squares). 146

5.19 The signal to noise ratio (SNR) of the central channel of 17 WDM channels transmitted over different 2 x 300km spans as a function of the total launched power in two cases: (a) different added dispersion span lengths. (b) 75 km added dispersion span and an additional 100 km span. 147

5.20 Experimental setup of five channels transceivers over 2x50km SSMF spans pumped by a first-order pump laser at 1450nm using a dual-band OPC 148

LIST OF FIGURES

5.21	Transmitted 5 Channels Spectrum	149
5.22	Simulated and experimentally measured signal power profiles of the 50km SSMF span pumped by the first-order 1455nm laser	150
5.23	Experimentally measured (markers) and analytically fitted (lines) SNR versus OSNR (dB/0.1nm) for the central channel of five DPQPSK WDM channels (500Gb/s) back-to-back.	151
5.24	Experimentally measured (markers) and analytically fitted (lines) SNR versus signal launch power for single channel DP-QPSK transceiver.	152
5.25	Experimentally measured (markers) and analytically fitted (lines) SNR versus signal launch power per channel for five WDM channels DP-QPSK transceivers.	153
5.26	The constellation diagram of the signal at 10dBm without OPC and with OPC (red circled in Fig.(5.25)).	154
5.27	FWM measurement set-up to measure the effect of dispersion slope using DSF as a link. PM: polarization maintaining, OSA: optical spectrum analyzer	155
5.28	FWM Efficiency as a function the center frequency between two tunable lasers with fixed frequency separation	156
5.29	FWM efficiency as a function of frequency separation between two lasers showing experimental results (red and blue) and theory (green and light blue) with different laser frequencies. Blue and green curves shifted up by 5dB.	156
5.30	Experimental setup for the spectral notch method and the dashed line represents the addition to the setup for BER measurements.	157
5.31	NLN as a function of the signal bandwidth for Experiment (Markers) and Theory (Lines) using with (solid) and without (dashed) dispersion slope. Notch1: 193.275THz, Notch2: 193.75THz, Notch3: 194.25THz, Exp.: Experiment and Ap.: Approximation	158
5.32	NLN spectrum at 193.275THz and at 194.25THz at different ASE bandwidths	159
5.33	2THz ASE spectrum with 35Gbaud modulated signal inserted in 40GHz notch in the center of the ASE spectrum. (b) the modulated signal	159
5.34	BER as a function of the transmission bandwidth for experiment (markers) and theory (lines) with (solid) and without (dashed) dispersion slope for QPSK (triangle and diamond) and 16QAM (circle and square) signals at 193.3THz (blue and yellow lines) and at 194.25THz (green and purple lines) respectively.	160

LIST OF FIGURES

5.35 Constellation of 35 Gbaud-QPSK modulated signal at different notch locations and different ASE bandwidths	161
-----------------------------------------------------------------------------------------------------------------------------	-----

LIST OF FIGURES

NOMENCLATURE

$A(z, t)$	Slowly varying field envelope at time domain.
B_{ch}	a WDM channel bandwidth.
B	total WDM bandwidth.
B_n	Noise bandwidth.
c	Speed of light in free space.
D	Dispersion parameter.
E	Electric Field.
f	Frequency.
f_{fwm}	Four-wave mixing (Idler) frequency.
$F(x, y)$	The mode field distribution in the transverse plan.
G	Amplifier Gain.
h	Plank's constant.
I	Power spectral density.
I_{ase}	ASE noise Power spectral density.
I_{NLN}	Nonlinear noise Power spectral density.
$J_n(h)$	The n-Bessel function of the first kind.
L_d	DCE length.
L_{eff}	Effective length of fiber.
L	Total span length.
N	Number of spans.
k_0	Propagation constant at free space.
N_s	Number of WDM channels/subcarriers.

n	linear refractive index.
\bar{n}	Total refractive index (linear and nonlinear).
P	Total induced Polarization in fiber.
P	total Power launched in the fiber.
P_{ASE}	Amplified spontaneous emission noise power.
P_g	Four-wave mixing power.
$p(x)$	Probability of x.
R_s	Symbol rate.
t	Time.
ω	Angular Frequency.
v_g	Reference group velocity.
z	Distance along the fiber.
α	Attenuation.
β_1	Inverse group velocity .
β_2	Group velocity dispersion.
β_{2d}	DCE Group velocity dispersion.
β	Propagation constant.
β_x	The ratio of the accumulated dispersion in the DCE to the transmission span $\beta_x = \frac{ \beta_{2d} L_d}{ \beta_2 L}$.
ϵ_0	Vacuum permittivity.
$\chi^{(i)}$	The i^{th} material susceptibility.
\Re	Real part.
Δf	Frequency Separation.
$\Delta\beta$	phase mismatch.
γ	Nonlinear coefficient.
λ	Wavelength.
σ	variance.

η Conversion efficiency.
* Conjugate operator.

LIST OF FIGURES

ABBREVIATIONS

<i>ADC</i>	Analog to Digital Converter.
<i>ASE</i>	Amplified Spontaneous Emission.
<i>AWG</i>	Arbitrary Waveform Generator.
<i>AWGN</i>	Additive White Gaussian Noise.
<i>BER</i>	Bit Error Rate.
<i>BPF</i>	Band-Pass Filter.
<i>BPSK</i>	Binary Phase Shift Keying.
<i>B2B</i>	Back-to-Back.
<i>CD</i>	Chromatic Dispersion.
<i>CMOS</i>	Complementary metal-oxide semiconductor.
<i>CO – OFDM</i>	Coherent Optical OFDM.
<i>CW</i>	Continuous Wave.
<i>DAC</i>	Digital to Analog Converter.
<i>DBP</i>	Digital Back-Propagation.
<i>DE</i>	Dispersion Element.
<i>DCF</i>	Dispersion Compensating Fiber.
<i>DCM</i>	Dispersion Compensation Module.
<i>DD</i>	Direct Detection.
<i>DGD</i>	Differential Group Delay.
<i>DM</i>	Dispersion-Managed.
<i>DP</i>	Dual Polarization.

<i>DSF</i>	Dispersion Shifted Fiber.
<i>DSP</i>	Digital Signal Processing.
<i>EDFA</i>	Erbium-Doped Fiber Amplifier.
<i>EVM</i>	Error Vector Magnitude.
<i>FBG</i>	Fiber Bragg Grating.
<i>FEC</i>	Forward Error Correction.
<i>FFT</i>	Fast Fourier Transform.
<i>FIR</i>	Finite Impulse Response.
<i>FOPA</i>	Fiber Optical Parametric Amplifier .
<i>FWM</i>	Four-Wave Mixing.
<i>GVD</i>	Group Velocity Dispersion.
<i>GN</i>	Gaussian Noise.
<i>HNLFF</i>	Highly Non-Linear Fiber.
<i>IF</i>	Intermediate Frequency.
<i>IFFT</i>	Inverse FFT.
<i>IFWM</i>	Intra-channel FWM.
<i>IL</i>	Insertion Loss.
<i>IXPM</i>	Intra-channel XPM.
<i>IM</i>	Intensity Modulation.
<i>INFT</i>	Inverse NFT.
<i>IQ</i>	In-phase and Quadrature.
<i>ISI</i>	Inter-Symbol Interference.
<i>IVSTF</i>	Inverse VSTF.
<i>LO</i>	Local Oscillator.
<i>LPF</i>	Low Pass Filter.
<i>MIMO</i>	Multiple Input Multiple Output.
<i>MZM</i>	Mach-Zehnder Modulator.

<i>NLN</i>	Non-Linear Noise.
<i>NFT</i>	Non-Linear Fourier Transform.
<i>NLSE</i>	Non-Linear Schrödinger Equation.
<i>NRZ</i>	Non-Return to Zero.
<i>NZ – DSF</i>	Non-Zero Dispersion Shifted Fiber.
<i>OADM</i>	Optical Add Drop Multiplexer.
<i>OBPF</i>	Optical Band-Pass Filter.
<i>OFDM</i>	Orthogonal Frequency-Division Multiplexing.
<i>OPC</i>	Optical Phase Conjugation.
<i>OSA</i>	Optical Spectrum Analyzer.
<i>OSNR</i>	Optical Signal to Noise Ratio.
<i>OTDM</i>	Optical Time Domain Multiplexing.
<i>PC</i>	Polarization Controller.
<i>PBC</i>	Polarization Beam Combiner.
<i>PBS</i>	Polarization Beam Splitter.
<i>PCTW</i>	Phase-Conjugated Twin Waves.
<i>PDL</i>	Polarization Dependent Loss.
<i>PDM</i>	Polarization Division Multiplexing.
<i>PM</i>	Phase Modulation/Modulator.
<i>PMD</i>	Polarization Mode Dispersion.
<i>PPLN</i>	Periodically Poled Lithium Niobate.
<i>PRBS</i>	Pseudo-Random Binary Sequence.
<i>PSD</i>	Power Spectral Density.
<i>P1</i>	Pump1.
<i>P2</i>	Pump2.
<i>QAM</i>	Quadrature Amplitude Modulation.
<i>QPSK</i>	Quaternary Phase-Shift-Keying.

<i>RF</i>	Radio Frequency.
<i>RRC</i>	Root-Raised-Cosine.
<i>Rx</i>	Receiver.
<i>SBS</i>	Stimulated Brillouin Scattering.
<i>SDM</i>	Space Division Multiplexing.
<i>SE</i>	Spectral Efficiency.
<i>SMF</i>	Single Mode Fiber.
<i>SNR</i>	Signal to Noise Ratio.
<i>SOA</i>	Semiconductor Optical Amplifier.
<i>SOP</i>	State Of Polarization.
<i>SRS</i>	Stimulated Raman Scattering.
<i>SPM</i>	Self-Phase Modulation.
<i>SSMF</i>	Standard SMF.
<i>TIA</i>	TransImpedance amplifier.
<i>Tx</i>	Transmitter.
<i>VSTF</i>	Volterra Series Transfer Function.
<i>WDM</i>	Wave Division Multiplexing/Multiplexer.
<i>WSS</i>	Wavelength Selective Switch.
<i>XPM</i>	Cross-Phase Modulation.

LIST OF FIGURES

LIST OF FIGURES

Chapter 1

Introduction

1.1 Capacity Demand

Since the invention of the Internet, its traffic is growing higher every year. In 1992, the Internet networks carried traffic per day was around 100 gigabytes (GB). After ten years in 2002, Internet traffic became 100 gigabytes per second [1]. Figure.(1.1) shows the global internet traffic over different years collected from Cisco Visual Networking Index: Forecast and Trends, 2017 to 2022 [1]. By 2017, global Internet traffic became more than 45,000 GB per second.

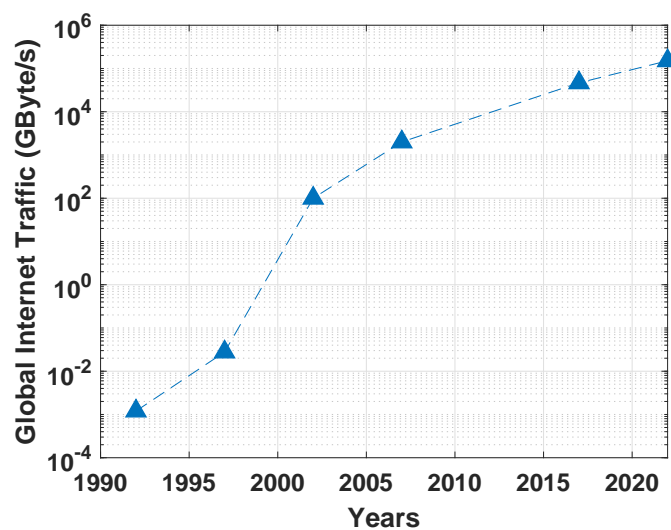


Figure 1.1. Total Internet Traffic Over Different Years including forecasts for the coming years. Source: Cisco VNI, 2019 [1].

1. INTRODUCTION

The forecasts show also steady exponential growth in the data traffic to reach by 2022, 396 Exabytes (EB) per month ($EB = 10^9$ Gigabyte) or 150,700 GB per second. This rapid increase in demand is forced by a variety of services such as video streaming, online gaming, machine to machine connections (such as smart meters, video surveillance, ...), etc.

Today most of the data traffic around the world go through optical networks and the optical fibers are forming the backbone of these networks. This is due to the very wide bandwidth spectrum of optical single mode fibers (SMFs) (40 THz) with carrier frequency 200 THz and low transmission loss (about 0.2 dB/km) [2]. This large bandwidth enables the fiber to carry a large amount of data. However, the nonlinear nature of the optical communication channel limits the amount of data transmitted over that channel [3].

1.2 Fiber Optic Communication System

Fiber-optic communication systems have been deployed since 1975 and made a revolution in the field of communication [4]. The system capacity of the optical communication network in the starting years was small. However, In 1990, the use of optical wavelength division multiplexing (WDM) with Erbium-Doped Fiber Amplifiers (EDFA) make an impressive increase in system capacity [5]. The new technology made a massive rise in system capacity to reach 1Tb/s by 2000 [6]. The WDM made a capacity radical increase by 1000 times in 10 years and this was achieved by adding more wavelengths to the system [7].

In the last decade, the research was focused on the enhancement of the use of the available optical bandwidth or in other words, increasing the spectral efficiency (SE) (which is expressed in bits per second per Hz) by employing advanced modulation format using both the polarization, amplitude and phase of the optical carrier. SE has been improved over the years. Up through the year 2000, the systems used on-off keying by simply changing the power between two levels, one of which becomes zero power. In 1996, bit rates per channel of WDM system increased from 2.5 Gb/s to 10 Gb/s then to 40 Gb/s in 2003 with the same channel spacing, which resulted in higher SE [7]. Additional improvement in SE is made by transmitting data over the two polarization of light through Polarization Division Multiplexing (PDM) with the four phases of

Quaternary Phase-Shift Keying (QPSK) which achieved 100Gb/s with channel spacing 50 GHz, which result in SE of 2 bits/s/Hz [8]. This enhancement in SE was continued in research to reach in the laboratory 11 b/s/Hz by using 128 Quadrature Amplitude Modulation with PDM (PDM-128QAM) [9]. Later, the ultra-high-order quadrature amplitude modulation has reached 4096-QAM with SE 15.8 bits/s/Hz [10] and 17.3 bit/s/Hz [11].

However, for the same transmission distance, increasing the spectral efficiency requires an improved signal to noise ratio (SNR) [2] to distinguish between the symbols in the receiver where the decision area for each symbol is decreased as the constellation level is increased. To increase the SNR, the signal power has to be increased and hence the optical fiber will be impacted by the intensity-dependent non-linear Kerr effects which will introduce distortions of the transmitted signal [12].

On the other hand, there are efforts to exploit the wide bandwidth of the optical fiber through using multiple bands (O+E+S+C+L+U) for example using C+L bands to transmit 54 Tb/s (16QAM) over 9150km using hybrid Raman-EDFA amplifications [13] instead of using C band only or using C+L+S bands to transmit real-time 240x200 GB/S (34 Gbaud DP-16QAM) with using frequency shifting to use only transponders in C-band. However, there is still work on optimizing the network component design to work properly with the other bands [14]. Again, using more bands with the same optical SNR (OSNR) for the same link length will inject more power in the optical fiber which will induce Kerr nonlinearities resulting in distortion to the transmitted signals and decreases the system performance.

As a result, the non-linearity will limit the amount of information that can be transmitted through the SMF which is called "non-linear Shannon limit" [15–17].

1.3 Capacity Crunch

As we closely approach the nonlinear capacity limit [15] and after using all physical dimensions of the signal propagating in the optical fiber, including time, frequency, quadrature phase, and polarization, in addition, the capacity demand is increasing continuously as shown in section (1.1), it is expected that there will be a capacity shortage within a decade. Although

1. INTRODUCTION

some new technologies such as optical space division multiplexing are under investigation by researchers [18], these technologies will not replace the current network. Therefore, some solutions to this problem were based on avoiding the need for high power, by decreasing the amplifier noise figure through using Raman amplifiers [19], or by making the signal propagation more tolerant to fiber nonlinearities such as pulse shaping [20]. On the other hand, the second approach was based on compensating the nonlinearity effects in the fiber through optical or digital methods.

1.4 Nonlinearity Effects Mitigation Methods

In order to avoid capacity crunch in SMF, nonlinearity mitigation has attracted great interest from the researchers in recent years. Several approaches have been introduced and they can be classified as optical signal processing and digital signal processing approaches. Optical signal processing includes, for example, optical backpropagation [21], optical pre-distortion [22], phase-sensitive amplifier [23], and mid-link optical phase conjugation (OPC) [24]. The use of coherent systems enabled the knowledge of the amplitude and the phase of the signal at the receiver and this knowledge enabled the compensation of the fiber transmission impairments using digital signal processing (DSP) [25]. Digital back-propagation (DBP) is a possible candidate for solving the fiber nonlinearity and dispersion in coherent systems [26]. However, the power requirements and complexity of DBP make real-time implementation is not possible in the current time. Furthermore, DBP is limited by the stochastic effects such as polarization mode dispersion (PMD) [27] and amplified spontaneous emission (ASE) noise [28]. Therefore, mid-link OPC attracted much interest again in recent years as a real-time all-optical signal processing method for parallel compensation of both intra-channel and inter-channel nonlinearity and dispersion fiber impairments.

1.5 The Motivation for The Thesis Work

The Kerr nonlinearity is considered as the main barrier for increasing the capacity of the current optical communication systems. Because it limits the increase of the OSNR or increasing the system bandwidth. With the increase of the system bandwidth, the wavelength dependence of the fiber parameters needs to be studied and in this thesis, the effect of the dispersion

slope on the modeling of the nonlinearity is studied. To overcome the Kerr nonlinearity, the midlink OPC method for nonlinearity compensation has attracted attention in recent years. However, the mathematical analysis for the compensation achieved by the OPC was limited and in this thesis, this gap is filled. Besides, the symmetry improvement for the current lumped amplification links was a challenge because of the fiber attenuation and in the thesis, an easy method for implementing the symmetry requirement for the OPC compensation is adopted to transmit 4.08 Tb/s WDM channels over 6 spans of 100 km. The OPC system for the real-time system was not tested before, which questions the validity of the OPC compensation in the currently deployed links and this is done in this work.

1.6 Thesis Organization

Chapter 2 introduces the background for this thesis. The optical communication system has been described including the transmitter, optical channel and coherent receiver. Then the different linear and nonlinear impairments of the optical channel have been discussed with focusing on the nonlinearity compensation using optical phase conjugation.

Chapter 3 reports the mathematical analysis, and verification using the simulation for the Kerr nonlinearities in multi-spans lumped amplification system employing mid-link OPC device and dispersion element after or before the OPC to enhance the power symmetry. The analysis for the nonlinear interactions of three tones has been conducted, then through the integration over the whole bandwidth, a closed-form expression for nonlinear noise has been introduced considering the amount of compensation from the mid-link OPC either with or without symmetry improvement. The mathematical results have been validated through simulations and showed a good agreement.

Chapter 4, presents the different designs and challenges of the optical phase conjugation device starting with single-band OPC design, then dual-band OPC. After that, the polarization diversity for the OPC is discussed. Finally a design of wavelength shift-free OPC with a 20nm conjugation bandwidth is introduced.

1. INTRODUCTION

Chapter 5 , reports the experimental validation of the mathematical models introduced in chapter (3). Starting with an experiment for the nonlinear interactions measurements between two tones in lumped amplification system which shows a perfect match with the theory. Then, an experiment for showing the benefit of improving the symmetry in the OPC link has been introduced for single-channel and WDM system transmission over different link lengths. The WDM transmission system used to verify the closed-form expression of nonlinear noise after considering the additional impairments from the OPC and the dispersion link. Next, Raman amplification is used instead of lumped amplification to achieve a high level of symmetry using a single pump backward Raman amplification. In this experiment, the first demonstrations of using the mid-link OPC with a real-time commercial transceiver is presented. Finally, the impact of dispersion slope on modeling the nonlinearity in wideband optical communication systems is studied and a figure of merit is developed for the required bandwidth to consider the effect of dispersion slope in the models used to evaluate the nonlinearity in optical communication systems.

Chapter 6, provides conclusions for the previous work and suggestions for future work.

1.7 Collaboration Acknowledgements

The work presented in this thesis will not be available without the collaborative work with my colleagues at AIPT. In all the work reported in this thesis, my supervisor Prof. Andrew Ellis has contributed to improving the quality of published research through suggestions, guidance and challenging my ideas. The simulations of coherent optical communication system done in chapter (3) used an offline digital signal processing (DSP) developed by Dr. Christian Sanchez, while I have operated the DSP and modified it to match with my simulation. Dr. Mohammad Al-Khateeb and Dr. Filipe Ferreira have trained me in the lab to operate the equipment properly and safely and to automate the control and the measurement of these devices. This lab training has given me the skills to plan, build and conduct my own experiments reported in this thesis in Chapter (4 and 5). In the reported experiment that used a Raman amplifier, Dr. Mingming Tan has helped in building the setup, measuring the Raman profile and setting power symmetry.

1.7 Collaboration Acknowledgements

While this thesis mainly contains my own research (published or to be published as a first or a second author), I have contributed to other research published during my PhD. For example, I helped the first author of [P10] to automate the experiment measurement. I have helped in mathematical analysis in [P3,P5]. Also, I helped in conducting the measurements in [P9,P11].

In this thesis, I will discuss in more details the work that I have published or intend to publish and listed in my List of Publications as:

Chapter 3 : [P7] and [P12]

Chapter 4 : [P1]

Chapter 5 : [P2], [P4],[P6] and [P8]

1. INTRODUCTION

Chapter 2

Optical Communication System

The research in optical fiber communication has started in the 1970s by developing low loss optical fiber and the development of semiconductor laser operating continuously at room temperature [4] which eased the development of a fiber-optics communication system. The first system was intensity modulation (IM) of semiconductor laser at the transmitter and direct detection (DD) using a square-law detector (photodiode) at the receiver (IM/DD system) [29]. The coherent system was under research in the 1980s by combining the received optical signal coherently with a continuous-wave optical field (narrow linewidth local oscillator (LO)) and showed many features such as high receiver sensitivity due to the gain from the LO signal and the ability of phase detection. However, in the 1990s, the commercial deployment of coherent systems was delayed by the invention of EDFA and the WDM which enabled the increase of the transmission capacity and distance of a single fiber [29].

With the exponential increase in the capacity demand and the need to meet this demand in parallel with the development in the speed of complementary metal-oxide semiconductor (CMOS) technology, the research in coherent optical communication system reanimated again [5, 30]. In 2004, there were several experiments for showing the benefit of the transmission using a coherent system employing polarization-multiplexed quadrature phase-shift keying (PM-QPSK) [31, 32]. Following that there were several experiments and commercial devices that support higher order modulation formats.

2. OPTICAL COMMUNICATION SYSTEM

2.1 Coherent Optical Communication system

The block diagram for an optical coherent communication system is shown in Fig. (2.1) consisting of an optical transmitter for modulating the digital data and prepare it for the optical channel, the optical channel which contains the optical fiber, optical amplifiers and any network devices, and finally, the optical receiver that recovers the transmitted digital data from the received impaired optical signal.

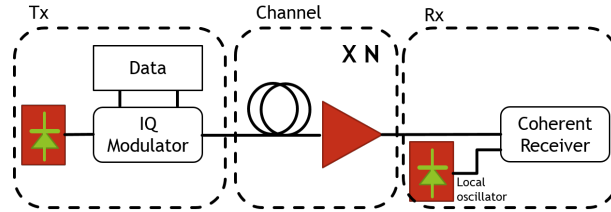


Figure 2.1. Block diagram for the optical coherent communication system.

2.1.1 Optical Transmitter

The optical IQ modulation is realized using Mach-Zehnder modulator (MZM) which is usually integrated on LiNbO₃ substrates where the phase depends on the applied voltage. The MZM is two parallel phase modulators in the interferometric structure as shown in Fig. (2.2).

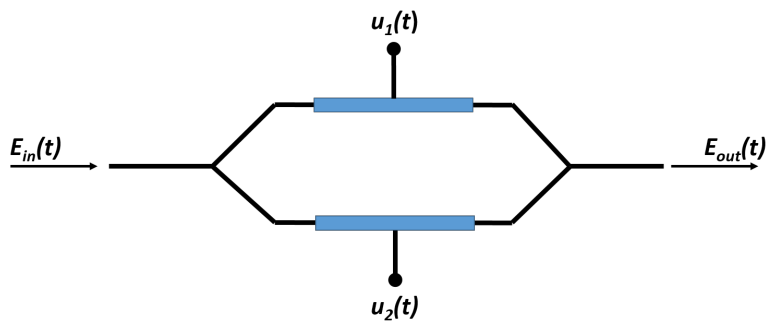


Figure 2.2. Block diagram of the Mach-Zehnder modulator.

Under the assumption of ideal coupling, the transfer function of the MZM can be written as [33],

$$\frac{E_{out}(t)}{E_{in}(t)} = \frac{1}{2} \left(e^{j\phi_1(t)} + e^{j\phi_2(t)} \right) \quad (2.1)$$

2.1 Coherent Optical Communication system

Where $\phi_i(t) = \pi \frac{u_i(t)}{V_{\pi_i}}$. $u_1(t)$ and $u_2(t)$ are the applied electric voltage signals represent the input data stream and V_{π} is the voltage required to produce a phase shift π from the phase modulator. For pure phase modulation, it is set $u_1(t) = u_2(t)$ and it is called push-push operation mode and the transfer function can be written as (assume that $V_{\pi_1} = V_{\pi_2} = V_{\pi}$)

$$\frac{E_{out}(t)}{E_{in}(t)} = e^{j\phi(t)} \quad (2.2)$$

and for pure amplitude modulation, the voltage set to $u_1(t) = -u_2(t)$ and this is called push-pull operation mode and similarly, the transfer function can be written as,

$$\frac{E_{out}(t)}{E_{in}(t)} = \cos(\phi(t)) \quad (2.3)$$

Based on the equation above, the MZM can be used as another approach for on-off keying and binary phase-shift keying (BPSK). However, for M-ary quadrature amplitude modulation (M-QAM) modulation format, In-Phase, Quadrature (IQ) modulator are needed.

IQ Modulator

The IQ modulator is dual nested two MZM modulators (work in push-pull operation mode) with an additional phase modulator on one arm to give the $\frac{\pi}{2}$ phase shift to give the quadrature signal, then the in-phase and quadrature signals are combined with a 3dB coupler. Fig.(2.3) shows the block diagram for the IQ modulator.

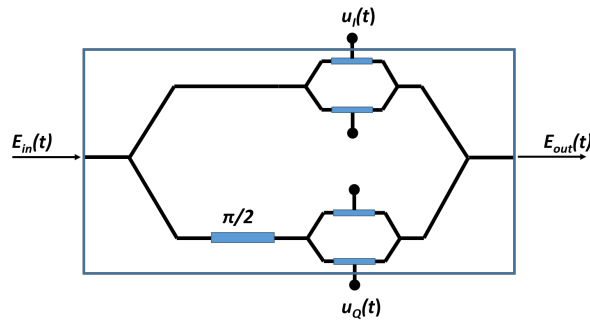


Figure 2.3. Block diagram of the IQ modulator.

2. OPTICAL COMMUNICATION SYSTEM

The transfer function for the IQ modulator can be written as,

$$\frac{E_{out}(t)}{E_{in}(t)} = \frac{1}{2}\cos(\phi_I(t)) + j\frac{1}{2}\cos(\phi_Q(t)) \quad (2.4)$$

The amplitude and phase modulation performed by the IQ modulator can be written as,

$$A_m = \left| \frac{E_{out}(t)}{E_{in}(t)} \right| \quad (2.5)$$

$$\phi_m = \arg\left(\frac{E_{out}(t)}{E_{in}(t)}\right) \quad (2.6)$$

For modulation formats such as 16QAM or higher, the driving electrical signal will not be binary and multilevel driving signals will be needed. However, there is some complex configuration that can use binary electrical driving signals such as tandem-QPSK transmitter [33]. For a polarization multiplexed signal, two IQ modulators will be needed for the two polarizations and the output will be combined using polarization beam combiner (PBC). The current commercial transmitter contains DAC plus digital signal processing chips for pulse shaping and pre-compensation.

2.1.2 Coherent Receiver

With using the coherent receiver, all the information of the received optical signal is transferred linearly to the electrical domain including amplitude, phase, frequency, and polarization. The coherent receiver configuration can be either homodyne where the signal is down-converted directly to a baseband signal or heterodyne where the signal is down-converted to an intermediate frequency (IF). This down-conversion will enable the demodulation and compensation of the transmission impairments in the electrical domain. The homodyne detection is difficult to implement in practice because of the high requirements of the frequency and phase locking of the received signal with the LO signal.

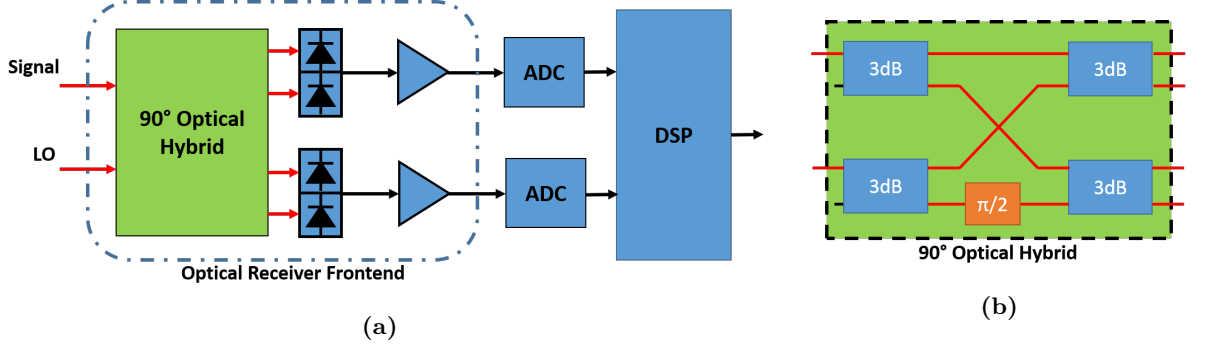


Figure 2.4. (a) Single polarization coherent receiver setup. (b) 90° optical hybrid design.

The coherent receiver has shown in Fig. (2.4a) consisting of two parts, an optical part called optical front-end and the electrical part. The received signal is mixed with LO signal using 2×4 90° optical hybrid. The detailed structure of the optical hybrid has been shown in Fig. (2.4b) and the output of the optical hybrid can be written as,

$$\begin{bmatrix} E_{O1} \\ E_{O2} \\ E_{O3} \\ E_{O4} \end{bmatrix} = \frac{1}{2} \begin{bmatrix} E_s + E_{LO} \\ E_s - E_{LO} \\ E_s + jE_{LO} \\ E_s - jE_{LO} \end{bmatrix} \quad (2.7)$$

Where E_s is the received signal. $E_s(t)$ can be written as [33],

$$E_s(t) = \sqrt{P_s} a(t) e^{j(\omega_c t + \phi_c + \phi(t))} \quad (2.8)$$

where P_s is the power of the received signal, $a(t)$ and $\phi(t)$ are the modulated signal amplitude and phase respectively. ω_c and ϕ_c are the angular frequency and the phase of the optical carrier. Similarly, E_{LO} is the electric field of the LO signal and can be written as,

$$E_{LO}(t) = \sqrt{P_{LO}} e^{j(\omega_{LO} t + \phi_{LO})} \quad (2.9)$$

where P_{LO} is the power of the LO signal, ω_{LO} and ϕ_{LO} are the angular frequency and the phase of local oscillator respectively. In Eq.(2.8) and Eq.(2.9), the Tx and Rx laser sources

2. OPTICAL COMMUNICATION SYSTEM

phase noise are neglected. The optical hybrid would then deliver the four optical signals to two pairs of balanced photodetectors producing the in-phase and quadrature components of the signal. Following the balanced photodiode, the current signal is amplified and converted to a voltage signal using a transimpedance amplifier (TIA). Then the electrical signal is converted into digital samples using an analog to digital converter (ADC) and processed by the digital signal processing unit for equalizing signal distortions such as chromatic dispersion and PMD and then error detection and correction are applied. The signal after the balanced photodiode (assuming that there are two identical photodiodes) can be written as [34],

$$\begin{aligned}
 I_I(t) &= R \left(E_{o1}(t)E_{o1}^*(t) - E_{o2}(t)E_{o2}^*(t) \right) \\
 &= \frac{1}{2}R \left((E_s(t) + E_{LO}(t))(E_s^*(t) + E_{LO}^*(t)) - (E_s(t) - E_{LO}(t))(E_s^*(t) - E_{LO}^*(t)) \right) \quad (2.10) \\
 &= 2\sqrt{P_s P_{LO}} a(t) \cos(\Delta\omega + \phi_c + \phi_{LO} + \phi(t))
 \end{aligned}$$

$$I_Q(t) = 2\sqrt{P_s P_{LO}} a(t) \sin(\Delta\omega + \phi_c + \phi_{LO} + \phi(t)) \quad (2.11)$$

Where R is the responsivity of the photodiode, $\Delta\omega = 2\pi\Delta f$ and Δf is the difference between LO and received signal frequencies and it is equal to zero for the homodyne receiver. For polarization multiplexed received signal, two coherent receivers such as the one shown in Fig. (2.4) are used to detect the two orthogonal polarization and the signal polarizations are initially separated using a polarization beam splitter (PBS).

2.1.3 Optical Channel

The two main parts of the optical channel are the optical fiber and the optical amplifiers. The first optical fiber design (with cladding) was in the 1960s with loss exceed 1000dB/km [4]. A great development happened in 1970 when the fiber loss was reduced to 20 dB/km [35] (in $1\mu m$ wavelength range). The loss has been decreased by operating the laser at wavelength $1.3\mu m$. Until the early 1980s, the transmitted data rate was limited to 100 Mb/s due to the modal dispersion in multimode fiber [4]. Then the data rate increased to 2Gb/s by the development

of SMF in 1981 [36]. Later, the dispersion-shifted fiber (DSF) was developed to operate at low attenuation window ($1.55\mu m$) and avoid the high dispersion of standard SMF (SSMF) in that region [37] and there no broadband practical technique for chromatic dispersion (CD) compensation was available in that time [5]. However, with the development of EDFA and WDM, DSF was not appreciated because of the non-linearities (Four-wave mixing (FWM)) generated and affected the signal and flourishes in low CD [38]. Another fiber has been developed called non-zero dispersion-shifted fiber (NZ-DSF) with low dispersion instead of zero dispersion at $1.55\mu m$ [39]. The NZ-DSF can be developed with positive or negative dispersion and this led to the development of dispersion management (DM) and the introduction of dispersion-compensating fiber (DCF) in the mid-1990s [40]. The development of the optical coherent systems with the ability to compensate for the dispersion inside the DSP chain has changed the need for DM system with SSMF in order to reduce the non-linearity [41]. The development of the optical fiber has continued to produce ultra-low loss optical fiber (≈ 0.14 dB/km) with a large effective area (to reduce the optical fiber nonlinear coefficient) for long haul transmission applications [42].

During the transmission over the optical fiber channel, the optical signal is distorted by different linear and nonlinear impairments. In the next sections, a brief description of these impairments will be introduced with more focus on the Kerr nonlinear impairments. The different impairments can be described using the wave equation or the simplified version, the nonlinear Schroedinger equation (NLSE). The electric field propagates inside the optical fiber can be described as,

$$E(z, t) = A(z, t)e^{j(\beta_0 z + \omega_c t)} \quad (2.12)$$

where $A(z, t)$ is the slowly varying complex envelope of the electric field, β_0 is the propagation constant and ω_c is the angular carrier frequency. The evolution of $A(z, t)$ along the optical fiber can be described using nonlinear Schroedinger equation (NLSE) as the following [38],

$$\frac{\partial A(z, t)}{\partial z} = -\frac{\alpha}{2}A(z, t) + j\frac{\beta_2}{2}\frac{\partial^2 A(z, t)}{\partial t^2} + \frac{\beta_3}{6}\frac{\partial^3 A(z, t)}{\partial t^3} - j\gamma|A(z, t)|^2 A(z, t) \quad (2.13)$$

where α , γ is the attenuation and nonlinear coefficients respectively. β_2 and β_3 are the first and

2. OPTICAL COMMUNICATION SYSTEM

second order dispersion respectively.

Attenuation

The fiber attenuation or loss is dependent on the wavelength of the transmitted signal. The main sources of the fiber loss [4] are the material absorption and Rayleigh scattering. Material absorption is due to the electronic (ultraviolet region) or vibrational (Infra-red region) resonance of the silica molecules or due to the absorption from the impurities. Rayleigh scattering is due to the random fluctuations of the refractive index during fabrications on a scale smaller than the optical wavelength. In the wavelength region $0.8\mu m$ to $1.6\mu m$, the loss is dominated by Rayleigh scattering which represents the fundamental limit of loss in optical fiber. It is described in Eq.(2.13) using the attenuation coefficient α . By considering only the fiber attenuation in 1/km, Eq.(2.13) can be written as,

$$\frac{\partial A(z, t)}{\partial z} = -\frac{\alpha}{2}A(z, t) \quad (2.14)$$

which can be solved as,

$$A(z, t) = A_{in}(t)e^{-\frac{\alpha}{2}z} \quad (2.15)$$

where $A_{in}(t)$ is the electric field complex envelope at the input of the fiber ($z = 0$) and z is the propagation distance along the fiber length L . Equation(2.15) can be written in terms of the power as,

$$P(z, t) = P_{in}(t)e^{-\alpha z} \quad (2.16)$$

where $P_{in}(t) = |A_{in}(t)|^2$ and represents the power of the electric field at the input of the fiber. Commonly, α is expressed in dB/km which can be related to 1/km through the equation,

$$\alpha(dB/km) = -\frac{10}{L} \log_{10} \left(\frac{P_{out}}{P_{in}} \right) = 10\alpha(1/km) \text{Log}_{10}(e) \quad (2.17)$$

The fiber loss is compensated using optical amplifiers, the optical amplification can be lumped (discrete) amplification or distributed amplification. Lumped amplification using EDFA is commonly used to compensate for the attenuation. Another lumped amplifier is a semiconductor

optical amplifier (SOA), however, it is not an attractive solution compared with the EDFA because of the polarization sensitivity and the nonlinear distortion to the WDM signal during the amplification process [4, 43]. EDFA is using an optical fiber doped with rare earth element (Erbium or Er) as the gain medium, however, distributed amplification or fiber Raman amplifier uses the transmission fiber as the gain medium using stimulated Raman scattering (SRS) occurring in the optical fiber where high power pump beam propagates through it. The energy of the pump is transferred to the signal through SRS as the two beams (pump and the signal) co-propagate along the fiber [38]. The Raman gain peak happens at 13 THz below the pump frequency with a large bandwidth around 6 THz. One of the main drawbacks of Raman amplifier, it does require high pump power to achieve high gain, for example, to achieve 30dB gain, 5W pump signal may be needed [4]. For long-haul transmission, the link is divided into several sections cascaded, each section with an amplifier and each optical amplifier adds noise to the signal and degrades the optical to signal ratio (OSNR) of the transmitted signal. This noise accumulation with the Kerr nonlinearities is the main limitation for extending the transmission distance. There are other types of optical amplifiers that use different phenomena for amplification such as Brillouin optical amplifier that uses stimulated Brillouin scattering (SBS) in a similar fashion for using SRS in Raman amplifiers [38]. However, the very narrow bandwidth of the Brillouin amplifier makes it unsuitable for WDM signal amplification. Fiber optic parametric amplifier (FOPA) is another candidate for wideband amplification [44] which uses a FWM of the signal with a high power pump signal for amplifying the signal. However, there are still efforts needed to test it with a higher-order modulation signal because of the effect of the nonlinear process on the amplified signal.

Chromatic Dispersion

The frequency dependence of the refractive index results in different spectral components of the propagated pulse travels at different speeds and this is called group velocity dispersion (GVD) [4] which causes pulse broadening. The contributions for GVD is coming either from material dispersion (wavelength dependence of the refractive index) or waveguide dispersion (core radius and index difference between core and cladding). It is described in Eq.(2.13) through β_2 and

2. OPTICAL COMMUNICATION SYSTEM

β_3 and the higher-order dispersion terms are neglected. The frequency-dependent propagation constant can be expanded around the carrier frequency ω_c as the following,

$$\beta(\omega) = \frac{wn}{c} = \beta_0 + \beta_1(\omega - \omega_c) + \frac{1}{2!}\beta_2(\omega - \omega_c)^2 + \frac{1}{3!}\beta_3(\omega - \omega_c)^3 + \dots + \frac{1}{m!}\beta_m(\omega - \omega_c)^m \quad (2.18)$$

where β_0 is the propagation constant, β_1 is the inverse group velocity ν_g ($\beta_1 = \frac{1}{\nu_g}$) and in general β_m can be written as,

$$\beta_i = \left. \frac{d\beta_{i-1}}{d\omega} \right|_{\omega=\omega_c} = \frac{d^i \beta(\omega)}{d\omega^i} \quad i = 1, 2, \dots, m \quad (2.19)$$

Frequently, the fiber dispersion is characterized using the dispersion parameter D and is expressed in (ps/nm/km) and dispersion slope parameter S (ps/nm²/km) and by changing the derivation from $d\omega$ to $d\lambda$ using the relation $c = \omega\lambda/(2\pi)$ where λ is the carrier wavelength and c is the speed of light, it can be related to the β_2 and β_3 as the following,

$$D = \frac{d}{d\lambda} \left(\frac{1}{\nu_g} \right) = -\frac{2\pi c}{\lambda^2} \beta_2 \quad (2.20)$$

$$S = \frac{dD}{d\lambda} = \left(\frac{2\pi c}{\lambda^2} \right)^2 \beta_3 + \left(\frac{4\pi c}{\lambda^3} \right) \beta_2 \quad (2.21)$$

By ignoring the Kerr-nonlinearity and attenuation, the transfer function for fiber dispersion can be obtained by solving Eq.(2.13) in the frequency domain and considering t is the retarded time which is delayed from the real-time by $\frac{z}{\nu_g}$ and it can be written as [4],

$$A(z, \omega) = A(0, \omega) e^{(-j\frac{1}{2}\beta_2\Delta\omega^2 - j\frac{1}{6}\beta_3\Delta\omega^3)L} \quad (2.22)$$

Equation (2.22) shows that the phase of the transmitted signal is changed by an amount that depends on the dispersion, frequency and propagation distance [38]. It worth mentioning that many references uses ω^2 instead of $\Delta\omega$ in Eq.(2.22) because it represents the baseband signal

[34,45] and it is written as,

$$H(z, \omega) = \frac{A(z, \omega)}{A(0, \omega)} = e^{-j\frac{1}{2}\beta_2\omega^2L} \quad (2.23)$$

The dispersion effect can be compensated by inserting a DCF at the end of each span which is suitable for a point-to-point link, however, it is difficult for a flexible routed optical network [33] which requires adaptive compensation. The optical coherent receiver has enabled the compensation of the accumulated dispersion in the electrical domain using large static digital filters. The compensation can be implemented in the time domain using a finite impulse response filter and the taps weights are calculated from the truncated impulse response from Eq.(2.23) or using least mean square to get the optimal tap weights. In order to avoid complex FIR filter in case of large accumulated dispersion, the dispersion can be compensated in the frequency domain either using an overlap-save method [46], or overlap-add method [47].

Polarization Mode Dispersion

The SMF can support the propagation of two orthogonal degenerate modes and for ideal symmetric cylindrical core, the two polarization modes will travel at the same speed and the two modes would not couple together [38]. However, due to the imperfect cylindrical core of SMF during fabrication or due to non-uniform mechanical stress over the fiber, the two modes will have different mode indices which are called birefringence [4]. This random varying birefringence produces random relative delays (also called differential group delay (DGD)) between the two polarization modes carrying the optical signal and it is called polarization mode dispersion (PMD). For the DD system, the uncompensated PMD leads to pulse broadening and causes inter-symbol interference (ISI) which limits the increase of the data rate [48]. Because of the random nature of the PMD, it is characterized using the root mean square of DGD between the two polarization modes ($L|\beta_{1x} - \beta_{1y}|$) after averaging over random perturbations and for large span length, the PDM is proportional to the square root of the span length which makes its impact less than the GVD [38].

$$\sigma_{DGD} \approx D_{PMD}\sqrt{L} \quad (2.24)$$

2. OPTICAL COMMUNICATION SYSTEM

where the PMD is described by D_{PMD} and it is in the range of $\sim 0.1ps/\sqrt{km}$. The PMD channel can be described with using Jones matrix [49, 50] which can be written as,

$$H(w) = \begin{bmatrix} h_{xx} & h_{xy} \\ h_{yx} & h_{yy} \end{bmatrix} = RP(\omega)R^{-1} \quad (2.25)$$

where R is a rotational matrix, and $P(\omega)$ is a diagonal matrix that corresponds to the DGD and it can be written as,

$$R = \begin{bmatrix} \cos(\frac{\theta}{2})e^{j\frac{\phi}{2}} & \sin(\frac{\theta}{2})e^{-j\frac{\phi}{2}} \\ -\sin(\frac{\theta}{2})e^{j\frac{\phi}{2}} & \cos(\frac{\theta}{2})e^{-j\frac{\phi}{2}} \end{bmatrix}, P(\omega) = \begin{bmatrix} e^{j\frac{1}{2}\omega\tau} & 0 \\ 0 & e^{-j\frac{1}{2}\omega\tau} \end{bmatrix} \quad (2.26)$$

where τ represents the DGD, θ and ϕ are the polar and azimuth angles respectively. The PMD can be avoided by using polarization-maintaining fiber, however, it is not a practical solution because the signal polarization needs to be aligned with the fast or slow axis of the fiber and in addition, all the components along the link should be designed using polarization maintaining components such as the amplifiers. In order to increase the data rate of DD systems, there were optical and electrical methods have been introduced to compensate for the PMD [51]. However, with the introduction of coherent systems, the PMD can be compensated in the DSP using an adaptive equalizer. The adaptive equalizer is 2x2 multiple-input multiple-output (MIMO) structure FIR filters to estimate the inverse Jones matrix of the channel [45]. There is another impairment related to the polarization modes is the polarization-dependent loss (PDL) where the two polarization components face different amplification or loss through the link. The PDL can also be compensated through the DSP [45] by considering the PDL effect in the Jones matrix.

Kerr Nonlinearity

The optical fiber as a dielectric material will respond nonlinearly to a high-intensity electric field. The total polarization P induced by the electric field can be written as the following,

$$\mathbf{P} = P_L + P_{NL} = \epsilon_0 \left(\chi^{(1)} \cdot \mathbf{E} + \chi^{(2)} : \mathbf{E}\mathbf{E} + \chi^{(3)} : \mathbf{E}\mathbf{E}\mathbf{E} + \dots \right) \quad (2.27)$$

where ϵ_0 is the vacuum permittivity and $\chi^{(j)}$ is the j th order susceptibility tensor of rank $(j + 1)$. The linear susceptibility $\chi^{(1)}$ is a function of the attenuation coefficient α and the refractive index n . The second-order susceptibility $\chi^{(2)}$ exists only in media that lacks inversion symmetry at the molecular level and therefore it vanishes in SiO₂ optical fiber because SiO₂ is symmetric molecule [38]. The third-order susceptibility $\chi^{(3)}$ is responsible for non-linear effects such as third-harmonic generation, FWM and nonlinear refraction (Kerr nonlinearity) in optical fiber. The nonlinear refraction is the intensity-dependence of the refractive index and leads to self-phase modulation (SPM) and cross-phase modulation (XPM). SPM is a self-induced intensity-dependent phase shift due to intense optical field propagation in optical fiber and leads to spectral broadening. On the other hand, XPM is the nonlinear phase shift of an optical field induced by a co-propagating field with a different wavelength or state of polarization. The non-linear coupling between two optical fields does not include any energy transfer between them. The effective refractive index of an optical field can be written as,

$$n(\omega, |E|^2) = n + n_2 |E|^2 \quad (2.28)$$

where n is the frequency-dependent refractive index and n_2 is the non-linear index coefficient and is related to $\chi^{(3)}$ through the relation,

$$n_2 = \frac{3}{8n} \Re(\chi^{(3)}) \quad (2.29)$$

2. OPTICAL COMMUNICATION SYSTEM

where \Re represents the real part. The relation between n_2 and the non-linear coefficient γ can be written as,

$$\gamma = \frac{n_2\omega}{cA_{eff}} \quad (2.30)$$

where A_{eff} is the effective mode area of the fiber. Assuming that two optical fields with angular frequencies ω_1 and ω_2 co-propagate in the optical fiber and linearly polarized along the x-axis and maintain their initial state of polarization. The total electric field can be written as,

$$E = \frac{1}{2}\vec{x}\left[\sum_{i=1}^2 E_i e^{j\omega_i t} + c.c.\right] \quad (2.31)$$

where *c.c.* short for complex conjugate. By substituting Eq.(2.31) into Eq.(2.28) and using the relation of total phase shift ($\phi = n(\omega, |E|^2)k_0L$) where $k_0 = \frac{2\pi}{\lambda}$ and L is the fiber length. The total nonlinear phase shift of the field at ω_1 can be written as,

$$\phi_{NL} = \phi_{SPM} + \phi_{XPM} = n_2k_0L(|E_1|^2 + 2|E_2|^2) \quad (2.32)$$

Equation (2.32) shows that in the absence of GVD, the effect of XPM to ϕ_{NL} is twice the SPM. The anomalous GVD has a reverse effect of SPM and the interplay between them can lead to soliton wave [52] which travels without any chirp through the optical fiber. In addition, GVD limits the XPM interaction by separating the pulses from each other. Another $\chi^{(3)}$ nonlinear effects that include the generation of new waves at other frequencies are FWM and third-harmonic generation (THG). The two phenomena require frequency and phase-matching conditions and for THG (3ω), it is difficult to achieve phase-matching conditions. FWM can be understood as the interactions of co-propagated three waves at frequencies f_1 , f_2 and f_3 interact nonlinearly to generate a fourth wave at frequency f_4 ,

$$f_4 = f_1 + f_2 - f_3 \quad (2.33)$$

2.1 Coherent Optical Communication system

It is also can be seen as, two photons at f_1 and f_2 are annihilated, and at the same time two photons at f_3 and f_4 are created with a condition,

$$f_1 + f_2 = f_3 + f_4 \quad (2.34)$$

The phase-matching condition for this process is $\Delta\beta = 0$ where $\Delta\beta$ is the phase mismatch term and can be written as,

$$\Delta\beta = \beta(\omega_1) + \beta(\omega_2) - \beta(\omega_3) - \beta(\omega_4) \quad (2.35)$$

The latter explanation of FWM is useful in understanding the parametric amplification of the signal co-propagated with two pumps and the generation of the idler wave. In a special case when $f_1 = f_2$, the idler signal will be located at $2f_1 - f_3$ and this is called a degenerate FWM. To show the effect of phase mismatch on the performance of FWM process, three signal frequencies f_1, f_2 and f_3 are assumed with powers P_1, P_2 and P_3 co-propagate in a single-span of optical fiber with length L attenuation, non-linear and dispersion coefficients α, γ and D respectively. The resulting FWM power efficiency η_{fwm} can be written as [53–58],

$$\eta_{fwm} = \frac{\alpha^2}{\alpha^2 + \Delta\beta^2} \left(1 + \frac{4e^{-\alpha L} \sin^2\left(\frac{\Delta\beta L}{2}\right)}{(1 - e^{-\alpha L})^2} \right) \quad (2.36)$$

In order to show the effect of phase mismatch due to the dispersion, three cases are assumed with different dispersion coefficients, SSMF with $D = 16$ ps/nm/km, NZDSF with $D = 4$ ps/nm/km and DSF with $D = 0.1$ ps/nm/km. All the fiber types are assumed to have the same attenuation coefficient ($\alpha = 0.2$ dB/km). The phase mismatch term are estimated using Eq.(2.35), Eq.(2.33) and Eq.(2.18) and considering only β_2 and it can be written as,

$$\Delta\beta = -4\pi^2\beta_2(f_1 - f_3)(f_2 - f_3) \quad (2.37)$$

2. OPTICAL COMMUNICATION SYSTEM

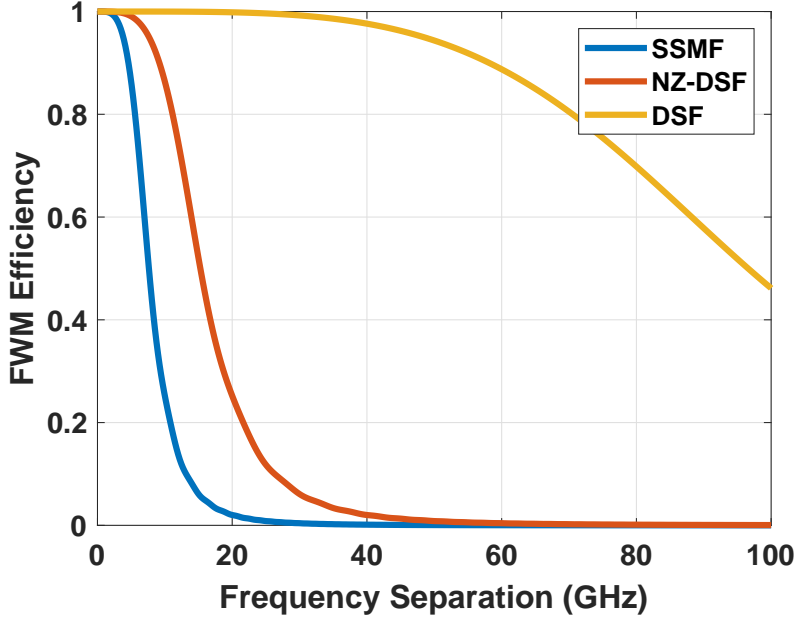


Figure 2.5. FWM efficiency as a function of frequency separation for three different types of fiber.

Figure (2.5) shows the FWM efficiency of the three types of optical fiber. It is clear that the maximum efficiency is when the phase mismatch is close to zero ($\Delta f \sim 0$). However, the dispersion has a different effect on the FWM efficiency in three fiber types and it is reduced with increasing the GVD. For SSMF, the efficiency is reduced to half at small frequency separation ($\Delta f \sim 8GHz$), while for NZ-DSF, it reaches the same value at almost the double frequency separation ($\Delta f \sim 16GHz$). However, for DSF, the FWM efficiency slowly declines with the frequency separation and reach half of the maximum at $\Delta f \sim 97GHz$. This may explain why the FWM is the main impediment in the transmission of WDM over DSF. The SPM and XPM can be considered as a special case of the FWM in Eq.(2.36) when $f_1 = f_2 = f_3$ (SPM) and when $f_1 = f_3$ and $f_1 \neq f_2$ (XPM) respectively [54]. For single-channel transmission, SPM is the dominant effect and sometimes divided into different intra-channel nonlinear effects. It is called (similar to inter-channel non-linear effects but in the time domain instead of frequency domain) intra-channel XPM (IXPM) and intra-channel FWM (IFWM) depending on whether the effects are caused by the own pulse or the neighboring pulses and leads to timing jitter and generation of echo pulses [59].

Nonlinear Scattering Effects

In the Kerr nonlinearities, no energy is transferred between the electromagnetic field and the dielectric medium which is called elastic non-linear effects [38]. Another stimulated inelastic effects that optical fiber medium plays an active role such as, stimulated Raman scattering (SRS) and stimulated Brillouin scattering (SBS) that has not been considered in NLSE in Eq.(2.13) needs to be discussed for their significant effect in optical fiber. The SBS and SRS are similar in that they include the generation of a signal whose frequency is downshifted from the incident signal. The incident signal is usually called the pump and the generated signal called the Stokes. However, there are a few differences between the SBS and SRS. The Stokes wave generated from SBS propagates in the backward direction while it occurs in both directions in the case of SRS. The threshold pump power for generating the Stokes is very small in the case of the SBS (~ 2 mW) compared with the SRS threshold (~ 500 mW). The SBS gain bandwidth is very narrow (< 100 MHz) while it is very broad for SRS (~ 40 THz). The peak value of SBS gain spectrum occurs for Stokes shift of ~ 11 GHz and ≈ 13.2 THz for the SRS.

The SRS can be a limiting factor in the transmission of ultra-wideband WDM systems by transferring the energy between the channels. However, it is also useful in making a low-noise wideband distributed amplifier. On the other hand, narrow bandwidth gain of the SBS limit its application in optical communication.

SBS has a negative impact in the application that uses high power CW laser (narrow linewidth) such as, FOPA, optical frequency shifters or OPC devices, where, as the launched power reach a critical level called SBS threshold, the amount of back-scattered power increase rapidly with the increase in the input power. Therefore, increasing the SBS threshold is quite important in such applications to use the high pump power efficiently. The backscattered Stokes waves grow exponentially along the fiber length and interrupting this growth can lead to a higher SBS threshold [38]. One way to do that to make inhomogeneous Brillouin shift ν_B along the fiber length by an amount more than the SBS gain bandwidth $\Delta\nu_B$ where the Stokes will stop to grow after the shift. The Brillouin shift of the SBS Stokes in the backward direction depends on the effective mode index n_p at the pump wavelength λ_p and the acoustic velocity ν_A according

2. OPTICAL COMMUNICATION SYSTEM

to the relation,

$$\nu_B = \frac{\Omega_B}{2\pi} = \frac{2n_p\nu_A}{\lambda_p} \quad (2.38)$$

where Ω_B is the frequency shift of the Stokes wave from the pump. The Brillouin shift can be changed along the fiber length by changing one of these parameters (ν_A or n_p). For example, changing the effective mode index n_p along the fiber length by changing the fiber parameters such as core diameter [60], stress [61], or temperature [62]. However, these methods are either cumbersome or require changing the fiber design. On the other hand, there is a simple and efficient method for increasing the SBS threshold by broadening the spectrum of the input signal (CW pump) using phase modulation to decrease its overlap with the narrow Brillouin gain spectrum [63], where the effective Brillouin gain will be reduced by $(1 + \frac{\Delta\nu_m}{\Delta\nu_B})$ where $\Delta\nu_m$ and $\Delta\nu_B$ are the modulated signal and Brillouin gain spectrum bandwidths respectively. This can be done using a single tone [63], multiple RF tones [64] or even using microwave noise source [65].

2.2 Combating Kerr-Nonlinearities in Optical Fiber

Reducing the impact of the optical fiber nonlinear effects on the system performance include methods that compensate for the effects of nonlinearity in the distorted signal and another methods that mitigate the impact of nonlinearity by making the signal more tolerant to the nonlinearity [66,67]. Based on that, the two terms will be used differently , nonlinearity compensation methods and nonlinearity mitigation methods.

2.3 Nonlinearity Compensation Methods

There are many methods have been developed over the years to compensate the nonlinearity in optical communication system and it can be mainly divided into two groups, digital nonlinearity compensation methods and optical nonlinearity compensation methods

2.3.1 Digital Nonlinearity Compensation Methods

Digital nonlinearity compensation methods are limited by the receiver bandwidth which limits the compensation to intra-channel nonlinear effects [66] and it is mainly based on reversing

the effect of the propagation in the optical fiber through digital signal processing and the complexity of implementing these algorithm remains as a barrier of implementing it for real-time transmission.

Digital Back Propagation

Digital backpropagation (DBP) is the most famous digital signal processing method for nonlinearity compensation [26]. In DBP, the deterministic signal-signal nonlinear effects are undone by solving the inverse nonlinear Schrödinger equation (NLSE) through virtual fiber to recover the transmitted signal from the received signal using the split-step Fourier method (SSFM) [38]. There are many drawbacks for the DBP, first, the required DSP complexity [68] due to excessive computational requirement, second, the limited compensation bandwidth due to the limited receiver bandwidth compared with the optical bandwidth [69], and the difficulty of nonlinearity compensation with the existence of polarization mode dispersion (PMD) [27], signal-noise nonlinear interactions [28] or transceiver noise [70].

Inverse Volterra Series transfer Function

The Volterra series can be used for approximating the response of a nonlinear system to a given input with considering the memory effects (in contrast with Taylor series) [71]. Therefore, the fiber nonlinear effects can be modeled using a Volterra series transfer function (VSTF) [72]. By truncating the VSTF to the third order and finding the inverse VSTF (IVSTF) [73], then it can be applied for the compensation of the impact of optical fiber nonlinearities [74–76]. IVSTF could perform better than DBP because of the avoidance of recursive frequency-time transitions (FFT and IFFT) [77]. In terms of complexity, IVSTF can be implemented in parallel achieving low computational load [74, 76]. However, it is still limited to the intra-channel nonlinear effects and the performance of IVSTF is decreased in the case of WDM transmission.

Perturbation based nonlinearity compensation

The perturbation method is based on an approximate solution of the NLSE in the time domain and it represents the effect of nonlinearity on the transmitted signal as a first-order perturbation

2. OPTICAL COMMUNICATION SYSTEM

term [78]. Perturbation based nonlinearity compensation needs prior information about the parameter of the optical fiber communication system [79] to estimate the perturbation coefficients. Therefore, the deployment of this method in a dynamically reconfigurable optical network is quite hard [80]. It can be applied either at the transmitter (Pre-compensation) [81] or at the receiver (Post-compensation) [82]. It is less complex than the digital backpropagation, however, it is still limited to the compensation of intra-channel nonlinear effects.

2.3.2 Optical Nonlinearity Compensation Methods

The Kerr nonlinearities can be compensated in the optical domain by either conjugating the signal in the middle of the link [83] and it is usually called mid-link optical phase conjugation, or transmitting another conjugated copy from the signal on another dimension along with the signal and it is called optical twin waves [84] or even implementing the fiber backpropagation at the receiver and it is called optical backpropagation. A separate section will be used for the optical phase conjugation because it is the subject of this thesis.

2.4 Optical Phase conjugation

The idea was first introduced theoretically by Yariv et. al. in 1979 [85] and Pepper et. al. in 1980 [83] that the signal can be restored by the use of a phase conjugation mirror in the middle of the propagation path and subsequent propagation through a second link with similar dispersive characteristics. In 1983, Fisher et al. showed through the simulation [86] that the combined effect of dispersion and self-phase modulation can be compensated by conjugating the signal in the middle of the optical fiber. The phase conjugation is equivalent to frequency inversion and it can be achieved using the second-order nonlinear effects in periodically poled Lithium-Niobate(PPLN) [87]. However, the PPLN device needs to operate at high temperatures to avoid the photorefractive effect in the Lithium-Niobate crystal which causes phase modification for phase-modulated signals [88]. Besides it can be realized using the third-order nonlinear effects in nonlinear medium like semiconductor optical amplifiers [89], SMF [90] or highly nonlinear fiber (HNLF) [88].

Experimental implementation of an OPC device, in an optical transmission system, was

demonstrated by Watanabe et al., for chromatic dispersion compensation in [89]. The use of OPC in nonlinearity compensation was, to the best of our knowledge, first experimentally shown in [24,91]. Since the first introduction of OPC, many experiments and numerical simulation have been done to show its effectiveness with different modulation techniques, different multiplexing system and different fiber lengths and types [22,90,92–106].

At first, it was used to compensate the fiber impairments in intensity modulation based transmission systems with different fiber lengths and different data rates using different implementation for phase conjugation, for example, for dispersion compensation [90,92–96], and for dispersion and nonlinearity compensation [97–99]. The use of the OPC with optical time division multiplexing (OTDM) was demonstrated for the first time in [100]. Afterwards, several experiments have been demonstrated for the using of OPC compensation with OTDM system with different fiber types and lengths and different data rates, for example [22,101–105]. In addition, the first field trial for the transmission of 40 Gb/s OTDM signal over 140 km of SSMF in deployed fiber network with dispersion compensation using mid-link OPC has been shown in [106]. The OPC has been used with the phase modulation system in [107] where 40-Gb/s differential phase-shift keying signal is transmitted over 3200 km of Lucent’s TrueWave reduced slope (TWRS) fiber using mid-link LiNbO₃ OPC with EDFA amplification and dispersion compensating modules (DCM) for dispersion compensation.

Furthermore, the OPC compensation is used with WDM systems. Watanabe and Chikama [91] demonstrated the compensation of FWM using mid-link OPC. Thereafter, many experiments for WDM direct detection systems using OPC compensation have been used with different modulation format, different channel spacing, different OPC devices and different fiber types and lengths, for example [87,108–114]. The use of OPC compensation in high data rates differential quadrature phase-shift keying has been shown in [112,115,116].

2.5 OPC with Coherent Systems

The coherent systems have many advantages over DD systems such as the improved signal to noise ratio, in addition, it gives the ability to compensate the dispersion using digital signal processing, moreover, it enabled the extraction of the amplitude, frequency, and phase informa-

2. OPTICAL COMMUNICATION SYSTEM

tion from an optical carrier, and consequently can achieve much higher capacity in the same bandwidth.

Numerical simulation [117] shows that the possibility of the transmission of 28 Gbaud PM-64QAM over 1920 km of SSMF with EDFA amplification using mid-link OPC with 2.5 improvements in Q-factor. Moreover, the simulation results show that the introduction of pre-dispersion before the OPC can make the transmission of nine WDM channels using OPC compensation close to using ideal DBP compensation. In [118], two channels are transmitted over 561 km of SSMF consisting of 6 spans with EDFA amplification using a mid-link electro-optic OPC device. One of the channels is 112-Gb/s PM-16QAM and the second is 10 Gb/s on-off-keying (OOK). Another experiment using phase conjugation in the digital domain in [119], where a single-channel 40-Gb/s 16-QAM polarization division multiplexed (PDM) coherent optical orthogonal frequency-division multiplexing (CO-OFDM) signal is successfully transmitted over 10,400-km ultra-large area fiber (ULAF) with mid-link digital phase conjugation. The experimental results show 4-dB improvement of power tolerance, and 53% increase in transmission reach. Another OFDM transmission experiment using mid-link OPC is done in [120], where a 604.7-Gb/s 16-QAM coherent optical OFDM super-channel is transmitted over 800-km of SSMF with 80 km span length and EDFA amplification. A pre-dispersion is applied to the signal before the OPC using 60 km DCM for better nonlinearity compensation. The results show a 4.8 dB improvement in the nonlinear threshold. This experiment has extended for the dual-polarization CO-OFDM system in [121], where 1.21-Tbit/s has been transmitted over 10x80-km of SSMF fibers with EDFA amplification. The improvement due to the nonlinearity compensation was 2.8 in the nonlinear threshold.

In [122], five WDM signals with 50-GHz spacing are transmitted over 800-km of Super-Large Area (SLA) fiber (has lower nonlinearity) using mid-link HNLF OPC device with 80 km span length and EDFA amplification. An Inverse dispersion fiber used for dispersion compensation and each WDM channel is modulated with 28-Gbaud DP-16QAM. The results show 0.9-dB improvement in the Q-factor and 1-dB improvement in the optimal transmission power. This experiment is repeated in [123] with 400-km of SSMF and backward distributed Raman amplification with 1.1-dB and 0.8-dB improvement in Q-factor for single-channel and 5-WDM channels

respectively. In addition to the experiment, the simulation has shown that the maximum reach can be increased to 2400 km with Q-factor equal to 8.5 dB.

Using the power symmetry introduced by Raman amplification, the maximum reach and the number of WDM channels have been increased in [124], where 7 channels of 114-Gb/s DP-QPSK have been transmitted over SSMF with Raman amplification and Midlink HNLF OPC. The use of OPC compensation has enabled the increase of maximum reach from 5200 km to 10400 km compared with a system with EDFA amplification. Using Silicon nano-wire as OPC device [125], 3 WDM channels of 32-Gbaud QPSK have been transmitted over 800-km of SSMF with 80-km span length and EDFA amplification. The results show a 3.6 dB improvement in the Q-factor. A large number of WDM channels have been successfully transmitted in [126], where 400-Gb/s optical 6-WDM super-channels have been transmitted over 2700-km with 75-km span length and bidirectional Raman amplification. Each sub-channel is modulated with 10-Gbaud PM-16QAM. The nonlinearity compensation using the HNLF mid-link OPC allows more than 50% increase in the maximum reach.

Table 2.1 summarizes some experiments of using mid-link OPC in the nonlinearity compensation of coherent optical communication system, it can be seen from the table the different experiments are trying to test the OPC with large bandwidth, high order constellation level, and increase the fiber maximum reach and try to achieve high compensation from the OPC.

In addition to the lab experiments, field experiments have been done to show the effectiveness of the Midlink OPC in fiber impairment compensation of deployed fiber. In [128], a 114-Gb/s single-channel PM-64QAM has been transmitted over 693.2km of deployed SSMF with different span lengths and EDFA amplification and the using the mid-link OPC enables the doubling of reach. Moreover, in [129], 6 WDM channels in two different bands are transmitted over 400-km of deployed SSMF with two different span lengths (90 and 110-km) with EDFA amplification and DCMs for dispersion compensation. Each WDM channel is modulated with 10-Gbaud 16-QAM. The results show a 0.4 improvement in the Q factor due to the use of mid-link OPC. The same field experiment is repeated [130] with 10-Gbaud 64QAM. The results show that 1.7-dB improvement in the Q factor due to the nonlinearity compensation using the mid-link OPC.

2. OPTICAL COMMUNICATION SYSTEM

Table 2.1. Some experiments for nonlinearity mitigation in SSMF using OPC compensation. HNLF: Highly NonLinear Fiber - OOK: ON-Off Keying - OPC: Optical Phase Conjugation - SSMF : Standard Single Mode Fiber - SLA: Super Large Area - ULAF: Ultra Large Area Fiber.

Nonlinearity Compensation in Coherent Optical Communication System Using Midlink OPC					
Authors	Transmitter	fiber Type	Fiber Maximum Reach (km)	OPC device	Improvement
Olsson et al. [118]	two channels (112 Gb/s PM-16QAM and 10 Gb/s OOK)	SSMF	561	Electro-Optic	3dB increase in span launch power
Chen et al. [119]	single-channel 40-Gb/s 16-QAM PDM CO-OFDM	ULAF	10400	Electro-Optic	4-dB improvement of power tolerance, and 53% increase in transmission reach
Du et al. [120]	604.7-Gb/s 16-QAM CO-OFDM super-channel	SSMF	800	HNLF	4.8 dB improvement in the nonlinear threshold
Morshed et al. [121]	1.21 Tbit/s PDM 16-QAM CO-OFDM super-channel	SSMF	800	HNLF	2.8 dB improvement in the nonlinear threshold
Ros et al. [122]	5-WDM channels (28-Gbaud DP-16QAM)	SLA	800	HNLF	0.9 dB improvement in the Q-factor
Sackey et al. [123]	5-WDM channels (28-Gbaud DP-16QAM)	SSMF	400	HNLF	0.8 dB improvement in Q-factor
Phillips et al. [124]	7 channels of 114 Gb/s DP-QPSK	SSMF	10400	HNLF	Doubling the maximum reach
Vukovic et al. [125]	3 WDM channels (32-Gbaud QPSK)	SSMF	800	Silicon nano-wire	3.6 dB improvement in the Q-factor
Ellis et al. [126]	400 Gb/s 6-WDM super-channels (10 Gbaud PM-16QAM)	SSMF	2700	HNLF	50% increase in the maximum reach
Al-Khateeb et al. [127]	3.6 Tb/s 30 WDM channels (30 Gbaud PM-QPSK)	SSMF	7600	HNLF	72% increase in the maximum reach

2.6 Multiple Optical Phase Conjugation

Instead of using single OPC near the middle of the link (Mid-link OPC), the use of multiple OPCs through the link for the compensation of fiber impairments can introduce extra improvement. The first experiment [131] for multiple OPCs (9-OPCs) used for the compensation of fiber impairments for eight channels WDM system and each channel was modulated with 32-Gbaud PM-16QAM with 50 GHz channel spacing over 6000 km of a Special type of fiber (TWRS) with 100 km span length and backward Raman amplification. The experiment tested the use of different fiber lengths with an OPC after each 600-km and found that for 3600 km, an improvement in the optimum launched power by 5 dB compared with 3 dB improvement from

the mid-link OPC, while for 6000 km there was a very small improvement.

In another experiment, twelve OPCs are used [132] for the compensation of nonlinearity and dispersion for 24 WDM Channels, each channel is modulated with 48-Gb/s DP-QPSK over 144-km of NZ-DSF with 12-km span length and bidirectional Raman pumping for amplification. The results reveal that 8-dB improvement in the optimum launch power. However, this high improvement probably is a result of the use of the special design of fiber (NZ-DSF) with dispersion symmetry and using a short span length which produces symmetric power profile.

The first experiment for multiple OPC has been repeated [133] with different fiber type and length, with only two OPCs, where 900 km of SSMF with 76 km span length and backward Raman amplification is used. The results show that the optimum power increased from -8 dBm (without OPC) to -3 dBm (with mid-link OPC) then to +2 dBm (with two OPCs) with 9.2 dB Q-factor. Although the improvement generated from the use of multiple OPC is substantial, it needs multiple OPC fiber designs which will introduce complexity to the link compared with mid-link OPC. Therefore, in this thesis, the use of the mid-link OPC is only considered.

2.7 The Efficiency of OPC Compensation

To achieve perfect dispersion and nonlinearity compensation using mid-link OPC, the power profile, nonlinearity and dispersion need to be symmetric with respect to the mid link OPC [88]. However, in optical communication systems which use lumped amplification, this condition is not achieved because the power profile is asymmetric around the OPC. The condition for perfect compensation was introduced by Watanabe [89,134] that the ratio of dispersion to nonlinearity is equal before and after OPC as the following,

$$\frac{\beta_2(-z)}{\gamma(-z)P(-z)} = \frac{\beta_2(z)}{\gamma(z)P(z)} \quad (2.39)$$

where z is a point on the z -axis and the sign refer to the location from the OPC (-ve means before the OPC), β_2 is the group velocity dispersion, γ is the nonlinear coefficient and P is the signal power and if the dispersion and nonlinear coefficient are uniforms over the fiber length, the power symmetry will need to be realized to make $P(z) = P(-z)$. One method to achieve the power

2. OPTICAL COMMUNICATION SYSTEM

symmetry is using short span lengths [24] which is not practical in the long haul transmission to use closely spaced amplifiers which will add noise to the signal. Another approach where the Raman amplification is used to achieve a nearly symmetrical power profile to increase the efficiency of OPC compensation [105, 107]. The use of nearly ideal OPC compensation was experimentally demonstrated [135] by using bidirectional Raman amplification with a small span length to achieve power symmetry and using a special type of fiber (NZ-DSF) which gives dispersion symmetry. The results show an 8 dB improvement in the nonlinear threshold (the performance peak at the optimum launch power). In addition to the asymmetry problem that affects the mid-link OPC compensation efficiency, the stochastic behavior of polarization mode dispersion (PMD) in polarization multiplexed systems has a great effect on the performance of systems use a mid-link OPC. A numerical simulation [136] shows that the optimum launch power decreased from +4.5 dBm to -1 dBm and the Q^2 factor also decreased by 5.2 dB when the PMD rose from 0 to $1 \text{ ps}/\sqrt{\text{km}}$.

2.8 Optical Phase Conjugation with Pre-dispersion

In the transmission systems with high bit-rate signals, the nonlinear effects can be modeled as a perturbation to the dispersion effects [137]. The nonlinear effects generated on two pulses (the signal and the conjugate copy) with the opposite value of accumulated dispersion will be with the opposite sign. To implement that, the power versus accumulated dispersion of the link needs to have a symmetric distribution of the nonlinear regions [138]. This can be viewed by plotting the power versus the accumulated dispersion and the nonlinearity can be compensated when the nonlinear regions are symmetric for the symmetric values of the pulse's accumulated dispersion.



Figure 2.6. The schematic for a multi-span lumped amplification system employing OPC.

Fig.(2.7) shows the power and the accumulated dispersion versus the distance through the link for the multi-span lumped amplification system employing midlink OPC shown in Fig.(2.6).

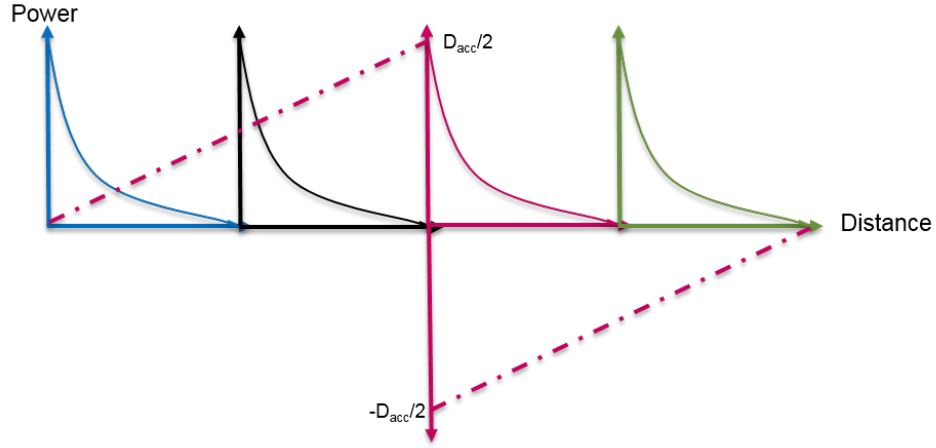


Figure 2.7. Power and accumulated dispersion (D_{acc}) of multi-span system versus the distance.

By plotting the power against the accumulated dispersion as shown in Fig. (2.8) which shows the asymmetric distribution for the nonlinear regions around the zero accumulated dispersion point.

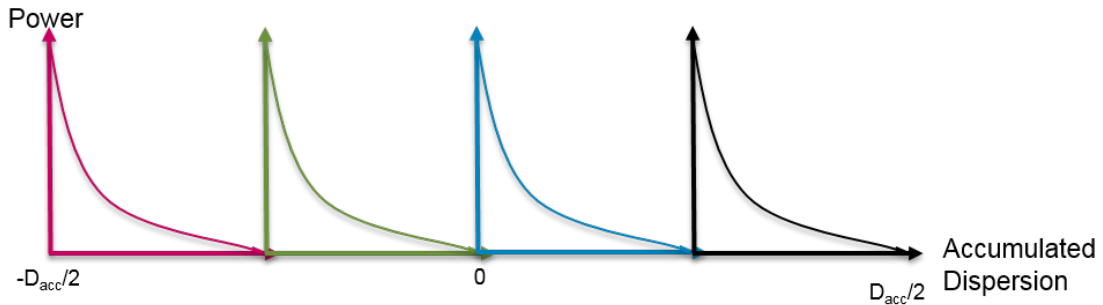


Figure 2.8. Power versus the accumulated dispersion for a system with midlink OPC.

Using this graphical method and as a solution for improving the nonlinearity compensation using mid-link OPC in the current deployed optical network with lumped amplification, Minzioni et. al. proposed in [138] instead of achieving the symmetry for the whole span length, it can be done for only the nonlinear effective region where the non-linearity highly affects the signal. The symmetry can be achieved through adding a suitable dispersive element before or after OPC to shift the nonlinear effective regions. From the graphical analysis, Minzioni concluded that the maximum compensation occurs when the accumulated dispersion of the dispersive element

2. OPTICAL COMMUNICATION SYSTEM

equal to $D(L - L_{eff})$, where D and L are the transmission fiber dispersion coefficient and span length respectively and L_{eff} is the effective length.

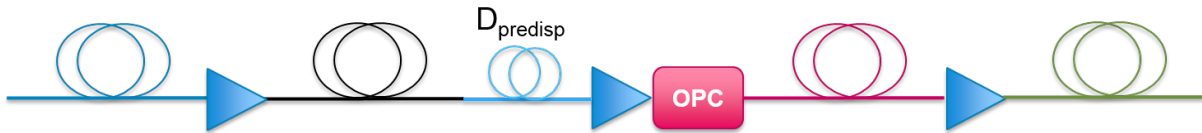


Figure 2.9. The schematic for a multi-span lumped amplification system employing OPC with pre-dispersion.

By adding a dispersion element before the OPC as shown in Fig.(2.9), the power and accumulated dispersion versus the distance can be plotted as shown in Fig.(2.10). Then by plotting the power versus the accumulated dispersion as shown in Fig.(2.11), the nonlinear effective region appears symmetric around the zero accumulated dispersion point. In other words, Fig.(2.11) shows that adding a dispersion element will improve the compensation of the nonlinear effects by the OPC where the nonlinear effective regions have been shifted and the symmetry is achieved between Areas 1 and 4 and Areas 2 and 3.

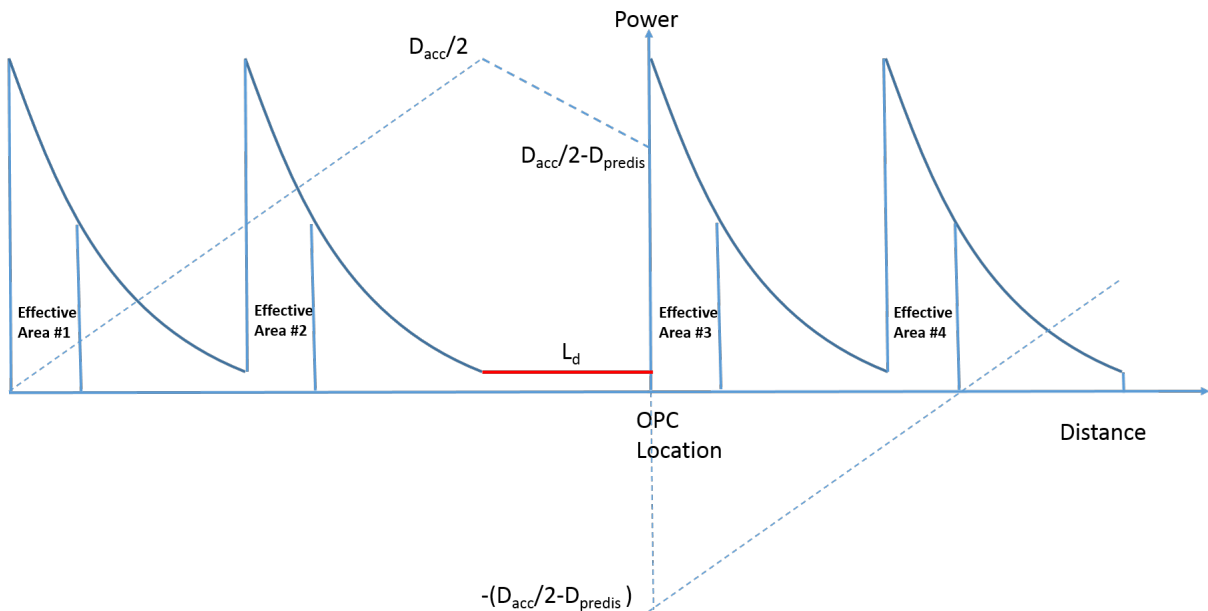


Figure 2.10. Power versus the distance and the accumulated dispersion is shown as a dotted line. The red line represents the pre-dispersion length.

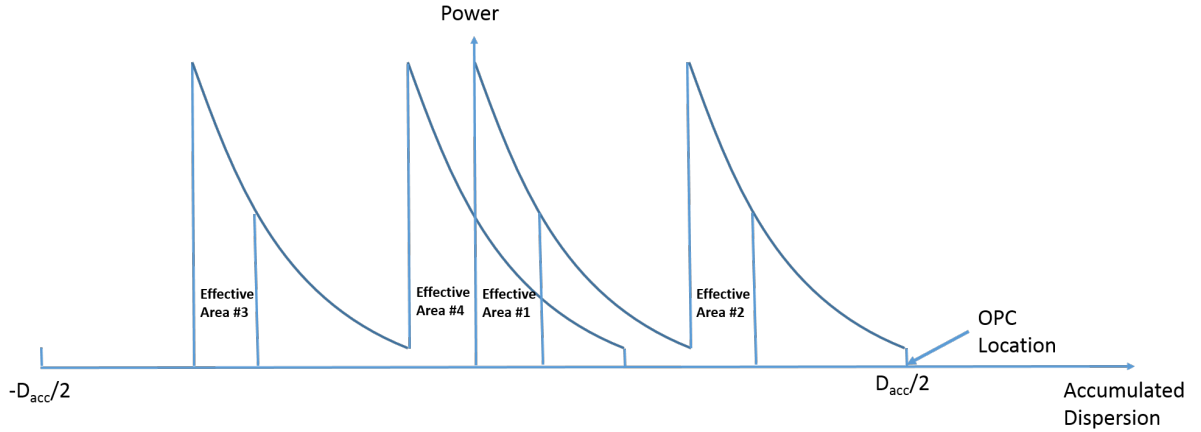


Figure 2.11. Power versus the accumulated dispersion for a system with midlink OPC and pre-dispersion.

In the next chapter, a mathematical analysis for this method will be derived and the condition for the accumulated dispersion of the dispersion element will be proved. In addition, the mathematical results will be validated through numerical simulations.

2.9 Nonlinearity Mitigation Methods

The terms mitigation and compensation are used generally interchangeably with nonlinearity compensation methods but the nonlinearity mitigation is used here for making the transmitted signal more tolerant to the effect of nonlinearity in optical fiber.

2.9.1 Constellation Design

Changing the design of the constellation through limiting the high-energy symbols reduces the peak to average power ratio. Therefore, the nonlinear effects on the signal are lowered and this is called geometric constellation shaping [139, 140]. In the geometric constellation, the symbols are more concentrated toward the center of the constellation diagram. However, the digital signal processing for the ring constellation is more complex than the uniform constellation and the optimum constellation shape depends on the channel condition which can be arbitrary. Instead of optimizing the location of the constellation points to approximate the Gaussian distribution, in probabilistic constellation shaping, the probability of the occurrence

2. OPTICAL COMMUNICATION SYSTEM

of the constellation points are Gaussian and again the low-energy symbols are more frequently transmitted than the high-energy ones [141–143].

Another approach for constellation design is the use of multi-dimension constellation design by using the polarization and different time slots with low cardinality on each dimension [144]. However, design complexity is increased by increasing the number of dimensions.

2.9.2 Transmitted Optical Pulse-Shaping

Instead of using non-return to zero (NRZ) pulses for the transmitted symbols, shaping the pulse shows tolerance for intra-channel nonlinear effects. Such as using a return to zero (RZ) pulses by carving the pulses at the transmitter [145] because the average power over the pulse width is reduced. However, RZ pulses need large bandwidth compared with the NRZ pulse transmission. Another approach for pulse shaping is using root-optimized Nyquist pulses [146] or using root polynomial pulses [20] with the same spectral efficiency as root raised cosine (RRC) pulses.

2.9.3 Symbol Rate Optimization

High baud-rate signal transmission can be replaced by low baud-rate subcarrier optimized to have the lowest nonlinear effects from the channel [147] then multiple subcarriers are multiplexed together in the digital domain at the transmitter [148] or in the optical domain using a comb laser source and multiple transmitters.

2.9.4 Nonlinear Noise Squeezing

Through optimizing the electronic dispersion pre-compensation to achieve symmetric dispersion map, the signal becomes more tolerant to the fiber nonlinearity where 0.9 dB improvement in the Q^2 has to be noticed from the transmission of PM-BPSK over 8000km due to dispersion pre-compensation at the transmitter [149]. However, for higher-order modulation like PM-16QAM, there is no improvement was noticed [150].

2.9.5 Transmitted Data Encoding in the Nonlinear Frequency Domain

By encoding the transmitted data in the nonlinear frequency domain through nonlinear Fourier transform (NFT), the transmitted data is not affected by the in-band nonlinear effects [151, 152]. In a similar fashion to orthogonal frequency division multiplexing (OFDM), the transmitted data are encoded using inverse NFT (INFT) and decoded at the receiver using NFT. Nonetheless, the computational complexity of the implementation of INFT and NFT [153], and the non-standard signal waveform and the constraint about the amplification scheme still need to be considered.

2.9.6 Conjugated Twin Waves

Another approach to mitigate the nonlinearity effects in the optical fiber by transmitting a conjugate copy of the signal along with the signal over another polarization which leads to correlated nonlinear distortions on the two waves, and coherently summing the signal and the conjugate copy at the receiver [154], the correlated distortions can then be removed. The idea was introduced by Han and Li [155] by transmitting two symbols and their conjugate on the two polarization through the special combination to be detected at the receiver by summing and subtracting the two polarization and to detect both the two symbols. Liu et. al. [84] succeeded to transmit 400-Gb/s super-channel over 12,800 km of TrueWave reduced slope (TWRS) fiber link with 80 km span length with EDFA amplification by transmitting the signal on one polarization and the conjugate copy on the second polarization. The super-channel is consisting of 8 channels each channel modulated with 32-Gbaud QPSK with the conjugate copy polarization multiplexed with the signal. The results show a significant improvement in nonlinearity reduction. This method has the benefits that it does not need any modification in the fiber link and also there are no restrictions on power and dispersion symmetry. However, the main drawback, it consumes half of the spectral efficiency for the conjugate copy. To overcome this redundancy, a modified PCTW scheme has been proposed, which, however, will suffer performance degradation (reduced SNR) [156–158] compared with PCTW.

The phase conjugated copy can be generated in the optical domain using high nonlinear fiber (HNLF) and transmitted on different wavelength [159], also it can be implemented in the time

2. OPTICAL COMMUNICATION SYSTEM

domain by transmitting the conjugated copy in a different time slot [160] or through different subcarrier in Orthogonal frequency-division multiplexed (OFDM) system [157].

2.10 Performance Measure of Optical Communication System

Measuring the performance of any system is a key in its operation and for the optical communication system there are different metrics used to evaluate the performance and most of them are related through analytical formulas in case of the additive white Gaussian noise (AWGN) channel. All the parameters listed below except bit error rate, optical signal to noise ratio (OSNR) and mutual information is developed for a hard decision system (making a decision based on the threshold).

2.10.1 Bit Error Rate

The bit error rate (BER) is the most accurate performance measure that can be used for evaluating the performance of the optical communication system where the BER is estimated as the following,

$$BER = \frac{\text{the number of bits received in error}}{\text{the total number of bits}} \quad (2.40)$$

Most of the published research reports the BER before the forward error correction (FEC) decoder and compares the results with the FEC threshold and uses it to predict the post-FEC BER. However, there was a debate [161] if the FEC should be implemented or the post-FEC performance can be predicted from the FEC threshold [162]. The nature of the burst error also may affect the FEC performance and two systems with the same BER can provide different post-FEC performance based on the nature of the error if it is burst or distributed [161]. The BER measurement can be time-consuming in case of high-quality signal because enough number of bits in error are needed which may require transmitting a long sequence, and the need for quick measurements such as signal to noise ratio (SNR) and error vector magnitude (EVM) may be required and analytical formula to link it to the BER values may be needed.

2.10.2 Signal to Noise Ratio

For m-QAM modulation format, the signal to noise ratio (SNR) can be estimated from the BER formula as the following,

$$BER = \frac{2}{\text{Log}_2(m)} \left(1 - \frac{1}{\sqrt{m}}\right) \text{erfc} \left(\sqrt{\frac{3 \cdot \text{SNR} \cdot \text{Log}_2(m)}{2(m-1)}} \right) \quad (2.41)$$

And it can be written for the different modulation format as the following,

Modulation Format	BER
PM-QPSK	$\frac{1}{2} \text{erfc} \left(\sqrt{\frac{\text{SNR}}{2}} \right)$
PM-16QAM	$\frac{3}{8} \text{erfc} \left(\sqrt{\frac{\text{SNR}}{10}} \right)$
PM-64QAM	$\frac{7}{24} \text{erfc} \left(\sqrt{\frac{\text{SNR}}{42}} \right)$

Table 2.2. BER formula for m-QAM modulation format for hard decision system with AWGN

2.10.3 Optical Signal to Noise Ratio

To describe the signal quality without taking the receiver penalties into account, the optical SNR (OSNR) can be used. The OSNR is the ratio of optical signal power P_{ch} to the noise (amplified spontaneous emission (ASE)) power P_{ase} in a given bandwidth B_{ref} .

$$OSNR = \frac{P_{ch}}{P_{ase}} \quad (2.42)$$

The OSNR is measured using an optical spectrum analyzer (OSA) that measures all the power in a given bandwidth. B_{ref} is commonly set to 0.1 nm (or 12.5GHz at 1550nm) which is the resolution of the early OSA devices [163]. The OSNR is widely used as a performance measure of optical fiber communication system, however, due to the Kerr nonlinearity in optical fiber, higher OSNR does not usually mean better performance. The relation between OSNR and SNR for polarization multiplexing system is given by [163]

$$OSNR = \frac{R_s}{B_{ref}} SNR \quad (2.43)$$

2. OPTICAL COMMUNICATION SYSTEM

where R_s is the symbol rate.

In practice, the OSNR is measured for a WDM system or a single channel according to IEC 61280-2-9:2009 standard [164] by measuring the total signal and noise power carried inside the channel bandwidth then the noise power is normalized to $B_{ref} = 0.1nm$. Because the noise power at the channel bandwidth is included in the signal power and is hard to extract. Therefore, the channel noise power can be estimated by interpolating the noise power value between channels. This is based on the assumption that the signal has a limited optical bandwidth whereas noise has a broadband distribution [165]. The measured channel power from the OSA is $P_{ch} + P_{ASE}$, so the noise inside the channel is subtracted (estimated from interpolation) from the signal and it is divided over the channel ASE noise after normalizing it to 0.1nm bandwidth. The measurement of the OSNR in Nyquist WDM transmission is challenging because there is no space between the channels to interpolate the noise and in that case, the two adjacent channels are switched off to be able to interpolate the noise. In addition, the OSNR has limited indication about the system performance because it does not consider the other channel impairments like dispersion, nonlinearity, polarization mode dispersion, etc., or the receiver and transmitter impairments such as the source relative intensity noise or receiver noise.

2.10.4 Q-Factor

For hard decision circuits with AWGN channel, the Q-factor is well established for on-off keying (OOK) direct detection optical systems and can be defined as [4],

$$Q = \frac{\mu_1 - \mu_0}{\sigma_1 + \sigma_0} \quad (2.44)$$

where μ_1 and μ_0 is the mean value amplitude of the received bit 1 or 0 respectively and σ_1 and σ_0 are the standard deviation of the received bit 1 or 0 amplitudes respectively. The relation between the BER and Q-factor can be written as,

$$BER = \frac{1}{2} \operatorname{erfc}\left(\frac{Q}{\sqrt{2}}\right) \quad (2.45)$$

Q-factors were often estimated from eye diagrams monitored on digital sampling oscilloscopes [3]. However, for higher order modulation, the results are still reported in terms of Q-factor and usually extracted from Eq.(2.45) after measuring the BER.

2.10.5 Error Vector Magnitude

Another faster signal quality metric that can be used for advanced modulation format is the error vector magnitude (EVM) which measures how the received constellation symbols are close to their reference constellation point [166] and can be linked to the BER [167] in case the signal is affected by additive Gaussian noise. The EVM is very useful in evaluating the performance of the system especially if the transmitted data is unknown which is a general case in the commercial transceiver.

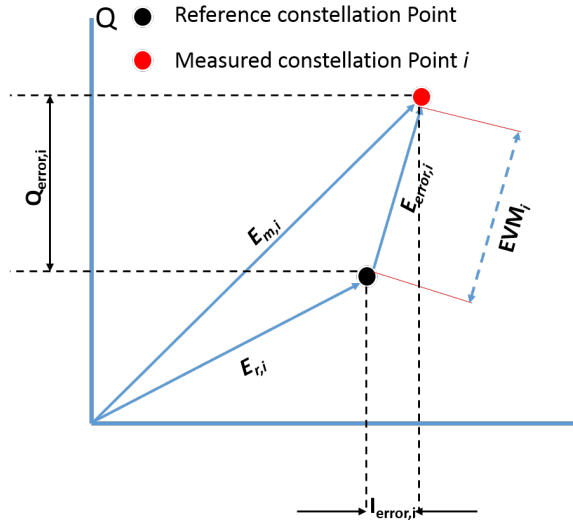


Figure 2.12. Error vector magnitude measurement for a constellation point. $E_{r,i}$ is the reference signal vector

Figure (2.12) shows the concept of EVM measurement where $E_{r,i}$ is the reference signal vector and usually is selected from the ideal transmitted signal vector, $E_{m,i}$ is the measured or the received signal vector and $E_{error,i}$ is the error vector i and can be estimated as,

$$|E_{error,i}|^2 = |E_{m,i} - E_{r,i}|^2 = I_{error,i}^2 + Q_{error,i}^2 \quad (2.46)$$

2. OPTICAL COMMUNICATION SYSTEM

EVM is defined as the root mean square of E_{error} , for a number of M randomly transmitted data [166] normalized to the longest reference (ideal or transmitted) vector $E_{r,p}$ (in some references the normalization is with respect to the average power of all reference symbols in the constellation $|Er, avg.|^2$) and can be written for a constellation point n as the following,

$$EVM_n = \frac{\sqrt{\frac{1}{M} \sum_{i=1}^M |E_{error,i}|^2}}{|E_{r,p}|} \quad (2.47)$$

The EVM gives an overall figure of merit for higher order modulation format such as m-QAM and large EVM leads to large BER and vice versa. In addition, EVM can be linked to the OSNR, BER and Q factor under the assumption that the signal is affected by an additive Gaussian noise and another certain assumption may be required as shown at [166–168]

2.10.6 Mutual Information

For non-uniform constellation such as probabilistic shaping or geometric constellation, and for a system employing a soft-decision decoder, the above metrics will not be accurate for measuring the performance because it is derived for the hard-decision systems with the assumption of uniform distribution of the symbols. the erfc formula for measuring the BER will not give accurate results because the number of bits in each constellation point is different. Therefore, the mutual information can be used as a general metric used in general to quantify the amount of information between two random variables [169] X and Y where in our case X will represent the transmitted signal and Y represents the received signal after passing through the optical fiber channel and affected by the channel different sources of noise where,

$$Y = X + N \quad (2.48)$$

where N represents the noise (additive Gaussian) from the channel with power spectral density N_0 and variance $\frac{N_0}{2}$. Assuming that the channel is memoryless and the transmitted symbols are independent and identically distributed according to $p(x)$ [17], the mutual information can be

2.10 Performance Measure of Optical Communication System

written as,

$$I(X Y) = \iint p(x, y) \cdot \log_2 \left(\frac{p(y|x)}{p(y)} \right) dx dy \quad (2.49)$$

where $p(x, y)$ is the joint probability between X (transmitted symbols) and Y (received symbols), $p(y)$ is the probability density function of the received symbols and $p(y|x)$ is the probability of observing y given the transmission of x. In practice, first, the transmitted and received symbols are normalized then a Gaussian channel [170] is assumed with circularly symmetric Gaussian distribution, so $p(y|x)$ can be written as,

$$p(y|x) = \frac{1}{\pi N_0} e^{-\frac{|y-x|^2}{N_0}} \quad (2.50)$$

After that, the variance of N_0 is calculated and the $p(x)$ from the transmitted symbols is estimated then finally, the integration in Eq.(2.49) is evaluated numerically, where $p(y|x)$ is evaluated using Eq.(2.50) and $P(y)$ is estimated as the following,

$$p(y) = p(y|x) \cdot p(x) \quad (2.51)$$

The mutual information can be estimated either using symbol-wise as above or bit-wise and in that case, it is called general mutual information (GMI) which is usually used with soft-decision decoding.

2. OPTICAL COMMUNICATION SYSTEM

Chapter 3

Mathematical Expressions for Fiber Nonlinearity in Lumped Amplified Systems

Accurate analytical models are a powerful tool in designing the transmission link of coherent optical communication system particularly when changing the design is high-cost like a submarine cable system case. While the numerical simulation can give an accurate prediction for the performance but large bandwidth, it becomes complex even with the use of high-speed computers. One of the early attempts to model the Kerr nonlinear noise in optical fiber was [171,172], where the non-linear effects such as SPM, XPM, and FWM are treated in the frequency domain as an FWM with the assumption that the effect of the non-linear noise can be considered as additive white Gaussian noise (AWGN) in highly dispersed link similar to the amplifier noise and this is the basis of what will be called later as the Gaussian Noise (GN) model [173]. This frequency-domain approach has attracted much interest and was validated through simulation and experimental works [173–182]. In spite of the criticism to the assumptions used in the frequency domain analysis such as assuming that the nonlinear noise is independent of the transmitted modulated signal [183, 184] and the frequency components of the propagating electric field are statistically independent of each other [185], these type of models are widely

3. MATHEMATICAL EXPRESSIONS FOR FIBER NONLINEARITY IN LUMPED AMPLIFIED SYSTEMS

used with a good matching with the experimental results [186–188]. In addition to the frequency domain models, another time-domain approach is used to model the non-linearity by treating the non-linear noise as a phase noise [185, 189–191].

For systems employing optical phase conjugation (OPC), there were some efforts to model the non-linearity, in [192], an expression for the FWM in OPC based systems is derived. In [193] the GN-model is applied to the system with OPC but without evaluating the double integration to get a closed-form. In [194], an analytical model is introduced to optimize the design of self-phase-modulation (SPM)-limited systems employing OPC. In [195] an analytical expression that anticipates the nonlinearity compensation of links with long span lengths and mid-link OPC is proposed. The power symmetry is a condition to get a compensation from the mid-link OPC, and in order to achieve the symmetry in lumped amplification mid-link OPC system, either to use short span lengths [91] or to collocate a dispersion element with the OPC [138] to enhance the regions where the fiber non-linearity has large impact to the same accumulated dispersion. In this chapter, a mathematical analysis is introduced for the signal-signal Kerr nonlinearity in the mid-link OPC system with pre-dispersion by driving the FWM power equation [53] then it is integrated over the signal bandwidth to get a closed-form for the non-linear noise [196]. The analytical results have been validated through simulations and used to predict the performance of a Nyquist super-channel wavelength division multiplexing (WDM) system.

3.1 Four-Wave Mixing

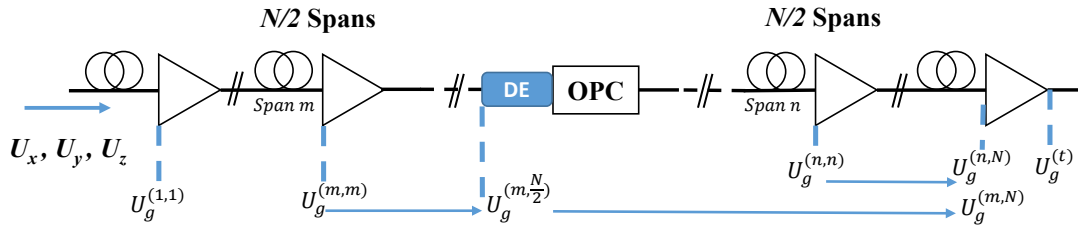


Figure 3.1. Mid-link optical phase conjugation system with pre-dispersion. DE: Dispersion Element, $U_g^{(1,1)}$: The Four-wave mixing field in the first span and N : Number of spans

In order to derive an expression of the FWM for a multi-span system with lumped amplification, the system shown in Fig. (3.1) is assumed with N identical standard SSMF spans of length L , dispersion β_2 , attenuation coefficient α and nonlinear coefficient γ . The attenuation is compensated using an EDFA at the end of each span. In the middle of the link, an ideal OPC device (no frequency conversion or insertion loss) is inserted. This is based on the reported shift-free [197] and low penalty OPC [127]. A dispersion element (DE) with total dispersion δ is inserted before or after the OPC based on the sign of dispersion, where the DE can be added before the OPC with δ has the opposite sign of β_2 or after the OPC with the same sign. For simplicity, it is assumed that the DE has length L_d and dispersion β_{2d} where $\delta = \beta_{2d}L_d$. The nonlinear impairment and insertion loss (IL) of the DE is ignored to simplify the equations and this can be justified by using a fiber Bragg grating (FBG) as DE where the IL is negligible and there are no nonlinear impairments.

The FWM field resulting from the interactions of three signal frequency components U_x , U_y and U_z at frequencies f_x , f_y and f_z with powers P_x , P_y and P_z can be found from the solution of the wave equation [198]. For the spans before the OPC, the input electric field amplitude at span m can be written as [55],

$$U_i^{(m)} = U_i e^{(m-1)(-\frac{\alpha}{2} + j\beta_i)L} G^{\frac{m-1}{2}} \quad (3.1)$$

where β_i is the propagation constant of U_i and $i = x, y$ or z . G is the power gain of the EDFA. Assuming that there no pump depletion and no parametric amplification from the FWM process and by solving the wave equation, the FWM field from span m can written as the following,

$$U_g^{(m,m)} = j2\gamma(U_x U_y U_z^* e^{(m-1)(-\frac{3}{2}\alpha + j(\Delta\beta + \beta_g))L} G^{\frac{3}{2}(m-1)}) e^{(-\frac{\alpha}{2} + j\beta_g)L} \frac{e^{(-\alpha + j\Delta\beta)L} - 1}{-\alpha + j\Delta\beta} \quad (3.2)$$

Where $U_g^{(j,k)}$ is the generated FWM field from span j measured at the end of span k and β_g is the propagation constant of the FWM field. $\Delta\beta$ is the phase mismatch between the three signals in the transmission fiber and for SSMF can be approximated by considering only the second-order dispersion in the Taylor series expansion of the propagation constant and it can

3. MATHEMATICAL EXPRESSIONS FOR FIBER NONLINEARITY IN LUMPED AMPLIFIED SYSTEMS

be written as [199, 200],

$$\Delta\beta = \beta_x + \beta_y - \beta_z - \beta_g = -4\pi^2\beta_2(f_x - f_z)(f_y - f_z) \quad (3.3)$$

$U_g^{(m,m)}$ linearly propagates to the middle of the link through $\frac{N}{2} - m$ spans and then through the DE. Then $U_g^{(m, \frac{N}{2})}$ is conjugated through the OPC and linearly propagates in the second half of the link. Assuming that the amplifiers are exactly compensating the span loss, the FWM field from span m measured at the end of the link can be written as,

$$U_g^{(m,N)} = -j2\gamma U_x^* U_y^* U_z e^{-j(m-1)\Delta\beta L} e^{-\frac{\alpha}{2}L} e^{-j\beta_{gd}L_d} \frac{e^{(-\alpha-j\Delta\beta)L} - 1}{-\alpha - j\Delta\beta} \quad (3.4)$$

Where β_{gd} is the propagation constant of the FWM field in the DE. For the spans after the OPC, U_i is linearly propagated to the middle of the link and through the DE and then is conjugated through the OPC and after that is propagated to the input of span n . The input electric field amplitude at span n can be written as,

$$U_i^{(n)} = U_i^* e^{(n-1)(-\frac{\alpha}{2})L} G^{\frac{n-1}{2}} e^{-j\frac{N}{2}\beta_i L} e^{j(n-\frac{N}{2}-1)\beta_i L} \quad (3.5)$$

Similarly, the FWM field generated from span n and measured at the end of the link can be written as,

$$U_g^{(n,N)} = j2\gamma U_x^* U_y^* U_z e^{j(n-N-1)\Delta\beta L} e^{-\frac{\alpha}{2}L} e^{-j(\Delta\beta_1 + \beta_{gd})L_d} \frac{e^{(-\alpha+j\Delta\beta)L} - 1}{-\alpha + j\Delta\beta} \quad (3.6)$$

Where $\Delta\beta_1$ is the equivalent phase mismatch for the DE.

By summing the FWM fields from all the spans at the end of the link [56] and considering the last amplifier, the total FWM field from all the spans $U_g^{(t)}$ can be written as,

$$U_g^{(t)} = \left(\sum_{m=1}^{\frac{N}{2}} U_g^{(m,N)} + \sum_{n=\frac{N}{2}+1}^N U_g^{(n,N)} \right) G \quad (3.7)$$

The total FWM field at the end of the link can be written as [196],

$$U_g^{(t)} = -4\gamma U_x^* U_y^* U_z e^{-jN\frac{\Delta\beta L}{4}} e^{-j\frac{\Delta\beta_1 L_d}{2}} e^{-j\beta_{gd}L_d} \frac{1}{(\alpha^2 + \Delta\beta^2)} \frac{\sin(\frac{N\Delta\beta L}{4})}{\sin(\frac{\Delta\beta L}{2})} \kappa \quad (3.8)$$

where,

$$\begin{aligned} \kappa = & \alpha \left(e^{-\alpha L} \sin\left(\frac{\Delta\beta L - \Delta\beta_1 L_d}{2}\right) + \sin\left(\frac{\Delta\beta L + \Delta\beta_1 L_d}{2}\right) \right) \\ & + \Delta\beta \left(e^{-\alpha L} \cos\left(\frac{\Delta\beta L - \Delta\beta_1 L_d}{2}\right) - \cos\left(\frac{\Delta\beta L + \Delta\beta_1 L_d}{2}\right) \right) \end{aligned} \quad (3.9)$$

Using Eq.(3.8), the total FWM power generated from all the spans at frequency f_g is calculated as the following [53],

$$P_g = |U_g^{(t)}|^2 = 16\gamma^2 P_x P_y P_z \frac{1}{(\alpha^2 + \Delta\beta^2)^2} \frac{\sin^2(\frac{N\Delta\beta L}{4})}{\sin^2(\frac{\Delta\beta L}{2})} \kappa^2 \quad (3.10)$$

If $\kappa = 1$, this represents the FWM equation from the half of the spans [56] without mid-link OPC. The ideal compensation for all inter-signal nonlinear effects can be achieved when κ is set to zero. This can be realized for a lossless fiber and with $L_d = 0$. A detailed derivation for Eq. (3.10) is available in appendix (A).

3.2 Nonlinear Noise Power Spectral Density

Equation (3.10) can be used to calculate the FWM power resulted from the non-linear interactions of two or three frequency tones. However, to estimate the effect of Kerr non-linearity on modulated signals with Nyquist WDM channels with bandwidth B , the bandwidth needs to be divided in N_s small frequency components [174] as shown in Fig. (3.2), with frequency separation Δf and sum all FWM products over the bandwidth where all the Kerr nonlinear effects such as SPM, XPM and FWM can be considered as a FWM between all the frequency components inside the full bandwidth B and under the assumptions that the non-linear noise is weak to medium (perturbation assumption) and the signal-noise non-linear interaction is negligible. f_x , f_y and f_z can be written using Δf as $f_i = i * \Delta f$ and $i = x, y$ or z . Equation

3. MATHEMATICAL EXPRESSIONS FOR FIBER NONLINEARITY IN LUMPED AMPLIFIED SYSTEMS

(3.3) can be written as,

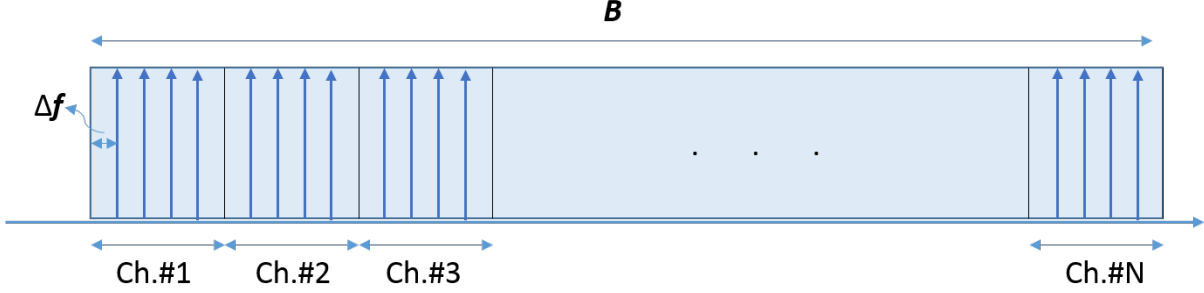


Figure 3.2. Conceptual diagram for slicing the Nyquist WDM bandwidth into small frequency components

$$\Delta\beta = -4\pi^2\beta_2(x-z)(y-z)\Delta f^2 \quad (3.11)$$

By making a constraint that f_g (the idler frequency) matches the frequency of interest reducing the triple summation to double summation and using the concept that the amount of energy scattered off the frequency component x should be equivalent to the energy scattered into the same frequency component [174], then setting $x = 0$, the phase mismatch can be written as the following,

$$\Delta\beta = 4\pi^2\beta_2z(y-z)\Delta f^2, \quad (3.12)$$

and assuming all the frequency components have the same power P , the non-linear noise power can be written as,

$$P_\xi = \frac{1}{2} \sum_{z=-\frac{N_s}{2}}^{\frac{N_s}{2}} \sum_{y=-\frac{N_s}{2}}^{\frac{N_s}{2}} P_g(y, z), \quad (3.13)$$

and the half is added due to the double-counting in the summation. By introducing new variable $w = y - z$ and changing the summation boundaries, the non-linear noise can be written as,

$$P_\xi = 8\gamma^2 P^3 \sum_{w=-\frac{N_s}{2}-y}^{\frac{N_s}{2}-y} \sum_{y=-\frac{N_s}{2}}^{\frac{N_s}{2}} \frac{1}{(\alpha^2 + 16\pi^4\beta_2^2z^2w^2\Delta f^2)^2} \frac{\sin^2(\frac{N4\pi^2\beta_2wz\Delta fL}{4})}{\sin^2(\frac{4\pi^2\beta_2wz\Delta fL}{2})} \kappa^2(w, z) \quad (3.14)$$

The summation in Eq.(3.14) can be solved numerically, however, it will be impractical for large bandwidth, for example, for the full C-band with Nyquist WDM system with bandwidth 4 THz, and in the case of $\Delta f = 100$ MHz, the number of summations will be 1.6×10^9 . In addition, Eq.(3.14) does not give insights into the maximum possible nonlinearity compensation. Therefore, a closed-form expression for Eq.(3.14) will be required and very useful.

3.2.1 Closed-form Expression for Nonlinear Noise Power Spectral Density

The approach in [174] will be adopted to derive a close-from expression for the non-linear noise power density starting from Eq.(3.14). By assuming that Δf is very small compared to the bandwidth, the summation in Eq.(3.14) can be converted to integration by taking the limits,

$$\lim_{\Delta f \rightarrow 0} P_{\xi} \tag{3.15}$$

$$P_{\xi} = \frac{8\gamma^2 P^3}{\Delta f^2} \int_{-\frac{B}{2}-f_1}^{\frac{B}{2}-f_1} \int_{-\frac{B}{2}}^{\frac{B}{2}} \frac{1}{(\alpha^2 + 16\pi^4 \beta_2^2 f_1^2 f_2^2)^2} \frac{\sin^2(\frac{N4\pi^2 \beta_2 f_1 f_2 L}{4})}{\sin^2(\frac{4\pi^2 \beta_2 f_1 f_2 L}{2})} \kappa^2(f_1, f_2) df_1 df_2 \tag{3.16}$$

Where $f_1 = y.\Delta f$ and $f_2 = w.\Delta f$. The boundaries for this integral is shown in figure (3.3) where the integration boundaries are represented by the gray polygon.

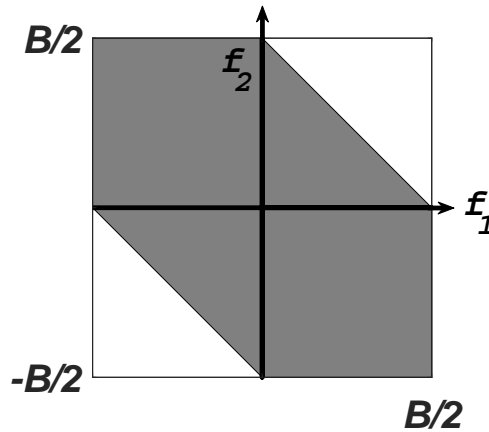


Figure 3.3. Integration boundaries shown as gray polygon , the square represent the approximation

By assuming large bandwidth, then the integration area can be approximated to the square

3. MATHEMATICAL EXPRESSIONS FOR FIBER NONLINEARITY IN LUMPED AMPLIFIED SYSTEMS

shape shown in Fig.(3.3) by changing f_2 boundaries from $(-\frac{B}{2} - f_1) \rightarrow (\frac{B}{2} - f_1)$ to $(-\frac{B}{2}) \rightarrow (\frac{B}{2})$ and considering that P_ξ is an even function, Eq.(3.16) can be written as,

$$I_\xi = 16\gamma^2 I^3 \int_0^{\frac{B}{2}} I_1 df_2 \quad (3.17)$$

Where $I_\xi = \frac{P_\xi}{\Delta f}$ and $I = \frac{P}{\Delta f}$ are the non-linear noise power spectral density (PSD) and signal PSD respectively and I_1 can be written as,

$$I_1 = \int_0^{\frac{B}{2}} \frac{1}{(\alpha^2 + (2\pi)^4 \beta_2^2 f_1^2 f_2^2)^2} \frac{\sin^2(\frac{N4\pi^2 \beta_2 f_1 f_2 L}{4})}{\sin^2(\frac{4\pi^2 \beta_2 f_1 f_2 L}{2})} \kappa^2(f_1, f_2) df_1 \quad (3.18)$$

The phase array term PA (\sin^2 fraction) can be expressed as a series of cosines as the following,

$$PA = \frac{\sin^2(\frac{N\Delta\beta L}{4})}{\sin^2(\frac{\Delta\beta L}{2})} = \frac{N}{2} + 2 \sum_{n=1}^{\frac{N}{2}-1} \left(\frac{N}{2} - n \right) \cos(n\Delta\beta L) \quad (3.19)$$

Again using the assumption of large bandwidth and because of $\Delta\beta^4$ in the denominator, $I_g = \frac{P_g}{\Delta f}$ can be neglected for large bandwidth values and the integration boundaries for df_1 can be changed to $0 \rightarrow \infty$. In addition, the variables can be exchanged $f = f_1 f_2$ and $df_1 = \frac{1}{f_2} df$, then I_1 can be written as,

$$I_1 = \frac{1}{f_2} \int_0^\infty \frac{1}{(\alpha^2 + (2\pi)^4 \beta_2^2 f^2)^2} \left(\frac{N}{2} + 2 \sum_{n=1}^{\frac{N}{2}-1} \left(\frac{N}{2} - n \right) \cos(n\Delta\beta L) \right) \kappa^2(f) df \quad (3.20)$$

The κ^2 term can be expanded as the following,

$$\begin{aligned} \kappa^2 = & \frac{1}{2}(1 + e^{-2\alpha L})(\alpha^2 + \Delta\beta^2) - e^{-\alpha L}(\alpha^2 + \Delta\beta^2) \cos(\Delta\beta L) + e^{-\alpha L}(\alpha^2 - \Delta\beta^2) \cos(\Delta\beta_1 L_d) \\ & - \frac{1}{2}e^{-2\alpha L}(\alpha^2 - \Delta\beta^2) \cos(\Delta\beta L - \Delta\beta_1 L_d) - \frac{1}{2}(\alpha^2 - \Delta\beta^2) \cos(\Delta\beta L + \Delta\beta_1 L_d) \\ & + 2e^{-\alpha L} \alpha \Delta\beta \sin(\Delta\beta_1 L_d) + e^{-2\alpha L} \alpha \Delta\beta \sin(\Delta\beta L - \Delta\beta_1 L_d) - \alpha \Delta\beta \sin(\Delta\beta L + \Delta\beta_1 L_d) \end{aligned} \quad (3.21)$$

3.2 Nonlinear Noise Power Spectral Density

By substituting Eq.(3.21) into Eq.(3.20), I_1 can be written as the following,

$$\begin{aligned}
I_1 = & \frac{1}{f_2} \int_0^\infty \frac{1}{(\alpha^2 + (2\pi)^4 \beta_2^2 f_2^2)} \left[\frac{1}{2} (1 + e^{-2\alpha L}) \left(\frac{N}{2} + 2 \sum_{n=1}^{\frac{N}{2}-1} \left(\frac{N}{2} - n \right) \cos(n\Delta\beta L) \right) \right. \\
& - e^{-\alpha L} \left(\frac{N}{2} \cos(\Delta\beta L) + 2 \sum_{n=1}^{\frac{N}{2}-1} \left(\frac{N}{2} - n \right) \cos(n\Delta\beta L) \cos(\Delta\beta L) \right) \\
& + e^{-\alpha L} \frac{(\alpha^2 - \Delta\beta^2)}{(\alpha^2 + \Delta\beta^2)} \left(\frac{N}{2} \cos(\Delta\beta_1 L_d) + 2 \sum_{n=1}^{\frac{N}{2}-1} \left(\frac{N}{2} - n \right) \cos(n\Delta\beta L) \cos(\Delta\beta_1 L_d) \right) \\
& - \frac{1}{2} e^{-2\alpha L} \frac{(\alpha^2 - \Delta\beta^2)}{(\alpha^2 + \Delta\beta^2)} \left(\frac{N}{2} \cos(\Delta\beta L - \Delta\beta_1 L_d) + 2 \sum_{n=1}^{\frac{N}{2}-1} \left(\frac{N}{2} - n \right) \cos(n\Delta\beta L) \cos(\Delta\beta L - \Delta\beta_1 L_d) \right) \\
& - \frac{1}{2} \frac{(\alpha^2 - \Delta\beta^2)}{(\alpha^2 + \Delta\beta^2)} \left(\frac{N}{2} \cos(\Delta\beta L + \Delta\beta_1 L_d) + 2 \sum_{n=1}^{\frac{N}{2}-1} \left(\frac{N}{2} - n \right) \cos(n\Delta\beta L) \cos(\Delta\beta L + \Delta\beta_1 L_d) \right) \\
& + 2e^{-\alpha L} \frac{\alpha\Delta\beta}{(\alpha^2 + \Delta\beta^2)} \left(\frac{N}{2} \sin(\Delta\beta_1 L_d) + 2 \sum_{n=1}^{\frac{N}{2}-1} \left(\frac{N}{2} - n \right) \cos(n\Delta\beta L) \sin(\Delta\beta_1 L_d) \right) \\
& + e^{-2\alpha L} \frac{\alpha\Delta\beta}{(\alpha^2 + \Delta\beta^2)} \left(\frac{N}{2} \sin(\Delta\beta L - \Delta\beta_1 L_d) + 2 \sum_{n=1}^{\frac{N}{2}-1} \left(\frac{N}{2} - n \right) \cos(n\Delta\beta L) \sin(\Delta\beta L - \Delta\beta_1 L_d) \right) \\
& \left. - \frac{\alpha\Delta\beta}{(\alpha^2 + \Delta\beta^2)} \left(\frac{N}{2} \sin(\Delta\beta L + \Delta\beta_1 L_d) + 2 \sum_{n=1}^{\frac{N}{2}-1} \left(\frac{N}{2} - n \right) \cos(n\Delta\beta L) \sin(\Delta\beta L + \Delta\beta_1 L_d) \right) \right] df
\end{aligned} \tag{3.22}$$

Using the trigonometric identities, the integration can be divided into a sum of integrations as,

$$I_1 = I_{11} - I_{12} + I_{13} - I_{14} - I_{15} + I_{16} + I_{17} - I_{18} \tag{3.23}$$

corresponding to each term in Eq.(3.21). I_{11} can be written as,

$$I_{11} = \frac{1}{2f_2} (1 + e^{-2\alpha L}) \int_0^\infty \frac{1}{(\alpha^2 + (2\pi)^4 \beta_2^2 f_1^2 f_2^2)} \left(\frac{N}{2} + 2 \sum_{n=1}^{\frac{N}{2}-1} \left(\frac{N}{2} - n \right) \cos \left((4\pi^2 \beta_2 L) n f \right) \right) df_1 \tag{3.24}$$

3. MATHEMATICAL EXPRESSIONS FOR FIBER NONLINEARITY IN LUMPED AMPLIFIED SYSTEMS

using the fact that the function inside the integration is even function, I_{11} can be rewritten as,

$$I_{11} = \frac{1}{4f_2} \frac{1}{(2\pi)^4 \beta_2^2} (1 + e^{-2\alpha L}) \lim_{R \rightarrow \infty} \int_{-R}^R \frac{1}{\frac{\alpha^2}{(2\pi)^4 \beta_2^2} + f^2} \left(\frac{N}{2} + 2 \sum_{n=1}^{\frac{N}{2}-1} \left(\frac{N}{2} - n \right) \cos \left((4\pi^2 \beta_2 L) n f \right) \right) df_1 \quad (3.25)$$

$$I_{11} = \frac{1}{4f_2} \frac{1}{(2\pi)^4 \beta_2^2} (1 + e^{-2\alpha L}) \Re \left[\lim_{R \rightarrow \infty} \int_{-R}^R \frac{1}{f - j \frac{\alpha}{(2\pi)^2 |\beta_2|}} \frac{1}{f + j \frac{\alpha}{(2\pi)^2 |\beta_2|}} \left(\frac{N}{2} + 2 \sum_{n=1}^{\frac{N}{2}-1} \left(\frac{N}{2} - n \right) \exp \left((4\pi^2 |\beta_2| L) n f \right) \right) df_1 \right] \quad (3.26)$$

Where \Re represents the real part operator. Now the integration in Eq.(3.26) can be evaluated using Cauchy's formula which can be written as,

$$\frac{1}{n!} \oint \frac{g(f)}{(f-a)^{n+1}} df = j2\pi g^{(n)}(a) \quad (3.27)$$

Where $g^{(n)}(a)$ is the n^{th} derivative of $g(f)$ evaluated at a and $g(f)$ is analytical function over the upper half of the complex plane, a is constant. For I_{11} , by setting $n = 0$ in Eq.(3.27) and then apply it for Eq.(3.26), therefore, I_{11} can be written as,

$$I_{11} = \frac{1}{16\pi |\beta_2| \alpha f_2} (1 + e^{-2\alpha L}) \left(\frac{N}{2} + 2 \sum_{n=1}^{\frac{N}{2}-1} \left(\frac{N}{2} - n \right) e^{-n\alpha L} \right) \quad (3.28)$$

In a similar fashion, integrations I_{12} to I_{18} can be evaluated. By defining a new variable β_x which represents the ratio of the pre-dispersion to single-span accumulated dispersion and can be written as,

$$\beta_x = \frac{|\beta_{2d}| L_d}{|\beta_2| L} \quad (3.29)$$

and using the facts that for our system $\beta_2 < 0$ and $\beta_{2d} > 0$ and $\beta_x < 1$, the evaluation of

3.2 Nonlinear Noise Power Spectral Density

the remaining integrations can be written as the following,

$$I_{12} = \frac{1}{8\pi|\beta_2|\alpha f_2} e^{-\alpha L} \left(\frac{N}{2} e^{-\alpha L} + \sum_{n=1}^{\frac{N}{2}-1} \left(\frac{N}{2} - n \right) (e^{-(n-1)\alpha L} + e^{-(n+1)\alpha L}) \right) \quad (3.30)$$

$$I_{13} = \frac{1}{8\pi|\beta_2|f_2} L e^{-\alpha L} \left(\frac{N}{2} \beta_x e^{-\beta_x \alpha L} + \sum_{n=1}^{\frac{N}{2}-1} \left(\frac{N}{2} - n \right) \left((n - \beta_x) e^{-(n-\beta_x)\alpha L} + (n + \beta_x) e^{-(n+\beta_x)\alpha L} \right) \right) \quad (3.31)$$

$$I_{14} = \frac{1}{16\pi|\beta_2|f_2} L e^{-2\alpha L} \left(\frac{N}{2} (1 + \beta_x) e^{-(1+\beta_x)\alpha L} + \sum_{n=1}^{\frac{N}{2}-1} \left(\frac{N}{2} - n \right) (n + 1 + \beta_x) e^{-(n+1+\beta_x)\alpha L} \right) \\ + \left(\frac{N}{2} - 1 \right) \beta_x e^{-\beta_x \alpha L} + \sum_{n=2}^{\frac{N}{2}-1} \left(\frac{N}{2} - n \right) (n - 1 - \beta_x) e^{-(n-1-\beta_x)\alpha L} \quad (3.32)$$

$$I_{15} = \frac{1}{16\pi|\beta_2|f_2} L \left(\frac{N}{2} (1 - \beta_x) e^{-(1-\beta_x)\alpha L} + \sum_{n=1}^{\frac{N}{2}-1} \left(\frac{N}{2} - n \right) \left((n + 1 - \beta_x) e^{-(n+1-\beta_x)\alpha L} \right. \right. \\ \left. \left. + (n - 1 + \beta_x) e^{-(n-1+\beta_x)\alpha L} \right) \right) \quad (3.33)$$

$$I_{16} = \frac{1}{8\pi|\beta_2|f_2} L e^{-\alpha L} \left(-\frac{N}{2} \beta_x e^{-\beta_x \alpha L} \sum_{n=1}^{\frac{N}{2}-1} \left(\frac{N}{2} - n \right) \left((n - \beta_x) e^{-(n-\beta_x)\alpha L} \right. \right. \\ \left. \left. - (n + \beta_x) e^{-(n+\beta_x)\alpha L} \right) \right) \quad (3.34)$$

3. MATHEMATICAL EXPRESSIONS FOR FIBER NONLINEARITY IN LUMPED AMPLIFIED SYSTEMS

$$I_{17} = \frac{1}{16\pi|\beta_2|f_2} L e^{-2\alpha L} \left(\frac{N}{2}(1 + \beta_x)e^{-(1+\beta_x)\alpha L} + \sum_{n=1}^{\frac{N}{2}-1} \left(\frac{N}{2} - n \right) \left((n + 1 + \beta_x)e^{-(n+1+\beta_x)\alpha L} + \left(\frac{N}{2} - 1 \right) \beta_x e^{-\beta_x \alpha L} - (n - 1 - \beta_x)e^{-(n-1-\beta_x)\alpha L} \right) \right) \quad (3.35)$$

$$I_{18} = \frac{1}{16\pi|\beta_2|f_2} L \left(\frac{N}{2}(1 - \beta_x)e^{-(1-\beta_x)\alpha L} + \sum_{n=1}^{\frac{N}{2}-1} \left(\frac{N}{2} - n \right) \left((n + 1 - \beta_x)e^{-(n+1-\beta_x)\alpha L} - (n - 1 + \beta_x)e^{-(n-1+\beta_x)\alpha L} \right) \right) \quad (3.36)$$

By evaluating the summations of geometric series for I_{11} to I_{18} , for instance,

$$I_{11} = \frac{1}{16\pi|\beta_2|\alpha f_2} (1 + e^{-2\alpha L}) \left(\frac{N}{2} + \frac{e^{-\alpha L}(N - 2 - Ne^{-\alpha L} + 2e^{-\frac{N}{2}\alpha L})}{(1 - e^{-\alpha L})^2} \right) \quad (3.37)$$

$$I_{12} = \frac{1}{8\pi|\beta_2|\alpha f_2} e^{-\alpha L} \left(\frac{N}{2} e^{-\alpha L} + \frac{(1 + e^{-2\alpha L})(N - 2 - Ne^{-\alpha L} + 2e^{-\frac{N}{2}\alpha L})}{2(1 - e^{-\alpha L})^2} \right) \quad (3.38)$$

It can be noticed easily that the second term in Eq.(3.37) and Eq.(3.38) are the same, therefore,

$$I_{11} - I_{12} = \frac{1}{16\pi|\beta_2|\alpha f_2} \frac{N}{2} (1 - e^{-2\alpha L}) \quad (3.39)$$

In like manner, $I_{13} - I_{14} - I_{15} + I_{16} + I_{17} - I_{18}$ can be evaluated to estimate I_1 as the following,

$$I_1 = \frac{N}{16\pi|\beta_2|f_2} \left(\frac{1 - e^{-2\alpha L}}{2\alpha} - L e^{-(1-\beta_x)\alpha L} \left(\beta_x e^{-\alpha L} \left(1 - \frac{2}{N} \right) - \beta_x + 1 \right) \right) \quad (3.40)$$

3.2 Nonlinear Noise Power Spectral Density

Equation (3.17) can be written as the following,

$$I_{\xi} = 16\gamma^2 I^3 I_x \int_0^{\frac{B}{2}} \frac{1}{f_2} df_2 \quad (3.41)$$

where $I_x = I_1 f_2$. Since the log function is not defined at 0, the integration boundaries are assumed to start from very small value B_{ϵ} compared with the signal bandwidth [174]. The following closed-form expressions for the nonlinear noise PSD is reached as,

$$I_{\xi} = \frac{N\gamma^2 \ln(\frac{B}{B_{\epsilon}})}{\pi|\beta_2|} I^3 \left(\frac{1 - e^{-2\alpha L}}{2\alpha} - L e^{-(1-\beta_x)\alpha L} \left(\beta_x e^{-\alpha L} \left(1 - \frac{2}{N} \right) - \beta_x + 1 \right) \right) \quad (3.42)$$

Equation (3.42) represents the non-linear noise PSD for a multi-span lumped amplification system with mid-link OPC with pre-dispersion to improve the symmetry around the OPC and consequently improve the compensation efficiency. However, it is still needed to separate the term for non-linearity compensation in Eq.(3.42). In order to do that the analysis in [174] will be repeated without the assumption of a large span length to find a closed-form for the non-linear PSD in multi-span lumped amplification system with flexible span length. The FWM power in multi-span system with lumped amplification can be written as [55, 56],

$$P_f = 16\gamma^2 P_x P_y P_z \frac{1}{(\alpha^2 + \Delta\beta^2)} \frac{\sin^2(\frac{N\Delta\beta L}{2})}{\sin^2(\frac{\Delta\beta L}{2})} \left(\frac{1}{4} (1 - e^{-\alpha L})^2 + e^{-\alpha L} \sin^2(\frac{\Delta\beta L}{2}) \right) \quad (3.43)$$

Following the same approach that has been used from Eq.(3.13) to Eq.(3.42) to find a closed-form expressions for nonlinear noise PSD. Similar to Eq.(3.17), $I_{\xi N}$ can be written as,

$$I_{\xi N} = 16\gamma^2 I^3 \int_0^{\frac{B}{2}} I_{1N} df_2 \quad (3.44)$$

The subscript N is used to refer to the results for multi-span system without OPC.

$$I_{1N} = \frac{1}{f_2} \int_0^{\infty} \frac{1}{(\alpha^2 + (2\pi)^4 \beta_2^2 f^2)} \left(N + 2 \sum_{n=1}^{N-1} \binom{N-n}{n} \cos(n(2\pi)^4 \beta_2^2 f^2 L) \right) \left(\frac{1}{4} (1 + e^{-2\alpha L}) - \frac{1}{2} e^{-\alpha L} \cos((2\pi)^4 \beta_2^2 f^2 L) \right) df \quad (3.45)$$

3. MATHEMATICAL EXPRESSIONS FOR FIBER NONLINEARITY IN LUMPED AMPLIFIED SYSTEMS

This is similar to the integration I_{11} and I_{12} in Eq.(3.28) and Eq.(3.30) for the double number of spans. Therefore the non-linear PSD can be written as

$$I_{\xi N} = \frac{N\gamma^2 \ln(\frac{B}{B_\epsilon})}{\pi|\beta_2|} I^3 \left(\frac{1 - e^{-2\alpha L}}{\alpha} \right) = \frac{N\gamma^2 \ln(\frac{B}{B_\epsilon}) L_{eff}}{\pi|\beta_2|} I^3 (1 + e^{-\alpha L}) \quad (3.46)$$

Equation (3.46) gives the dependence of non-linear noise PSD on the different parameters while it scales linearly with the number of spans and proportional to the cubic of transmitted signal PSD, it is also inversely proportional to the group velocity dispersion and the square of the effective area of the fiber A_{eff} where γ is defined in Eq. (2.30) as $\gamma = \frac{2\pi n_2}{\lambda A_{eff}}$. In addition, it has a logarithmic dependence on the bandwidth. γ should be multiplied by $\frac{8}{9}$ in case of polarization multiplexing with random birefringence. It can be seen from Eq.(3.46) that the more complex form, h_e in Eq. (22) in [174] will reduce to $(1 - e^{-2\alpha L})$ in case of solving the integration without making the assumption of large span length. Using Eq.(3.46), Eq.(3.42) can be written as the following,

$$I_\xi = \frac{N\gamma^2 \ln(\frac{B}{B_\epsilon})}{\pi|\beta_2|} I^3 \left(\xi_{\frac{N}{2}} - \xi_{OPC} \right) \quad (3.47)$$

Where $\xi_{\frac{N}{2}}$ scales the non-linear noise from the half of the spans and can be written as,

$$\xi_{\frac{N}{2}} = \frac{1 - e^{-2\alpha L}}{2\alpha} \quad (3.48)$$

ξ_{OPC} represents the OPC non-linearity compensation with the pre-dispersion and can be written as,

$$\xi_{OPC} = L e^{-(1-\beta_x)\alpha L} \left(\beta_x e^{-\alpha L} \left(1 - \frac{2}{N} \right) - \beta_x + 1 \right) \quad (3.49)$$

β_x is defined in Eq.(3.29) and it is usually less than one and excess dispersion ($\beta_x > 1$) would tend to decorrelate the conjugate signal from the signal before the OPC and rapidly degrade the performance. Setting $\beta_x = 0$, gives the compensation due to the OPC only and ξ_{OPC} will reduce to,

$$\xi_{OPC} = L e^{-\alpha L} \quad (3.50)$$

Equations (3.46) and (3.47) show that the insertion of the OPC affects only ξ while the logarithmic

3.2 Nonlinear Noise Power Spectral Density

mic dependence of the bandwidth still the same. By plotting ξ_{OPC} at Eq.(3.50) and Eq.(3.49) and plotting $\xi_{\frac{N}{2}}$ at Eq.(3.48) as the function of the transmission fiber span length as shown in Fig.(3.4), it can be seen that the maximum compensation coming from the OPC is when the transmission fiber span length equal to the effective length and this can be proved mathematically by solving Eq.(3.51).

$$\begin{aligned} \frac{\partial \xi_{OPC}}{\partial L} &= 0 \\ 1 - \alpha L &= 0 \quad i.e. \quad L = \frac{1}{\alpha} \approx L_{eff} \end{aligned} \quad (3.51)$$

It is worth mentioning that for span lengths smaller than the effective length, the non-linear

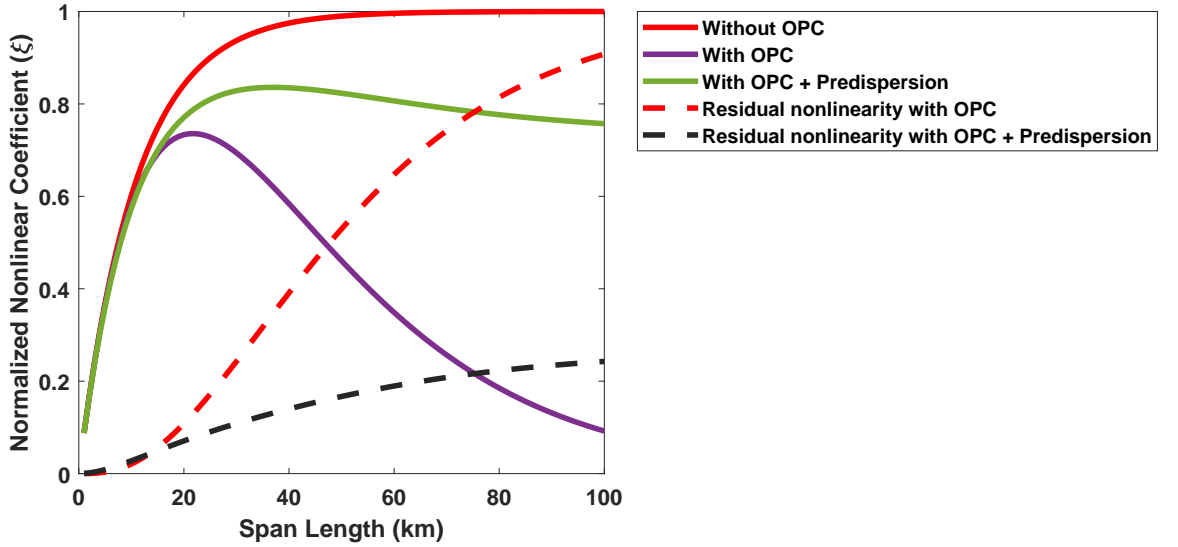


Figure 3.4. Normalized coefficient ξ in lumped amplification system as a function of the span length.

noise (red solid curve) is reduced significantly by reducing the span length. Therefore, the total non-linear noise will continue to decrease with decreasing the span length even when the OPC compensation started to decrease as shown in Fig. (3.4). For spans above 20 km, ξ_{OPC} for the system without pre-dispersion (purple solid line) started to decline sharply with increasing the span length due to the lack of symmetry in the power profile. However, adding the pre-dispersion with the OPC, ξ_{OPC} will decrease slowly with the span length increase (green solid line). The dashed curves represent $\xi_{\frac{N}{2}} - \xi_{OPC}$ for the OPC deployed systems with (dashed black line) and

3. MATHEMATICAL EXPRESSIONS FOR FIBER NONLINEARITY IN LUMPED AMPLIFIED SYSTEMS

without (dashed red line) pre-dispersion which represent the residual nonlinearity after OPC compensation. It shows that the residual nonlinearity is increasing fast with increasing the span length when the pre-dispersion is not employed with the OPC and starts to decrease slowly when the optimum pre-dispersion is added.

3.2.2 Optimum Pre-dispersion

The optimum pre-dispersion that gives the minimum non-linear noise I_ξ in Eq.(3.47) can be obtained by finding the value of β_x that minimize the value of ξ . Using Eq.(3.47) and solving the equation,

$$\frac{\partial \xi}{\partial \beta_x} = 0, \quad (3.52)$$

the condition for optimum pre-dispersion can be written as,

$$\beta_x = \frac{1}{1 - e^{-\alpha L}(1 - \frac{2}{N})} - \frac{1}{\alpha L} \quad (3.53)$$

For large span length ($e^{-\alpha L} \approx 0$), β_x can be reduced to,

$$\beta_x = (1 - \frac{1}{\alpha L}), \quad (3.54)$$

and using Eq.(3.29), it can be written,

$$|\beta_{2d}|L_d \approx (L - L_{eff})|\beta_2| \quad (3.55)$$

where L_{eff} is the effective length of SSMF and can be written as,

$$L_{eff} = \frac{1 - e^{-\alpha L}}{\alpha} \approx \frac{1}{\alpha} \quad (3.56)$$

Equation (3.55) proves the results concluded from graphical analysis in [138] about the optimum pre-dispersion to get the highest symmetry around the OPC.

3.2.3 Optimum Launch Power Density and SNR

Using the approach that the non-linear noise can be treated as an AWGN in case of large accumulated dispersion [3, 201, 202], the signal to noise ratio can be written as the following,

$$SNR = \frac{I}{I_{ase} + \eta I^3} \quad (3.57)$$

where I_{ase} represents the ASE noise PSD and can be written as,

$$I_{ase} = 0.5N(G - 1)Fh\nu \quad (3.58)$$

where F is the amplifier noise figure, h is Plank's constant and ν is the light frequency. η is the non-linear noise coefficient extracted from Eq.(3.47) as,

$$\eta = \frac{N\gamma^2 \ln(\frac{B}{B_c})}{\pi|\beta_2|} \xi \quad (3.59)$$

By solving $\frac{\partial SNR}{\partial I} = 0$,

$$I_\xi = \eta I^3 = \frac{I_{ase}}{2} \quad (3.60)$$

which means that the optimum SNR is when the non-linear noise PSD is half the ASE PSD and the optimum launch power density I_{opt} can be written as,

$$I_{opt} = \sqrt[3]{\frac{I_{ase}}{2\eta}} \quad (3.61)$$

By substituting Eq.(3.61) in Eq.(3.57), the optimum SNR is estimated at the optimum launch power as,

$$SNR_{opt} = \sqrt[3]{\frac{4\pi|\beta_2|}{27N\gamma^2 \ln(\frac{B}{B_c})\xi I_{ase}^2}} \quad (3.62)$$

3.3 Validation of the Mathematical Analysis

In order to derive the equations in sections (3.1) and (3.2), many assumptions are made and to verify that these assumptions do not accumulate to give inaccurate results, simulations were

3. MATHEMATICAL EXPRESSIONS FOR FIBER NONLINEARITY IN LUMPED AMPLIFIED SYSTEMS

run to verify these analytical expressions.

3.3.1 FWM Expression Validation

In order to validate Eq.(3.10), simulations were run using VPITransmissionMaker 9.5 for the system in Fig.(3.1) with the parameters shown Table (3.1) by transmitting two continuous-wave (CW) laser signals with 0 dBm powers in 10x100km SSMF with dispersion, attenuation and nonlinear coefficient equal to -20.4 ps²/km, 0.2 dB/km and 1.3 (W.km)⁻¹ respectively. The simulation was run with 8 samples per symbol. An ideal OPC (no insertion loss or frequency conversion) was implemented in Matlab. The DE was chosen according to Eq.(3.55) with accumulated dispersion $\delta = 1603$ ps². A filter is used to isolate the idler and power meter to measure its level for each simulation point. The FWM powers were measured at the end of the link at

Parameter	Value	Unit
Number of Spans	10	-
Span Length	100	km
Fiber Attenuation (α)	0.2	dB/km
Fiber Dispersion (β_2)	-20.4	ps ² /km
Fiber Nonlinear Coefficient (γ)	1.3	(W.km) ⁻¹
DE Accumulated Dispersion (δ)	1603	ps ² .

Table 3.1. Simulation parameters for FWM equation validation

different frequency separations (Δf) between the two CW lasers.

Figure (3.5) shows three different cases; multi-span system without OPC or pre-dispersion (red), with OPC only (blue) and with OPC and pre-dispersion (green).

The theory lines (solid) plotted using Eq.(3.10) and Eq.(3.43) and the markers represent the simulation results and it is clearly showing an excellent match between theory and simulation. Figure (3.5) shows that the FWM power is eliminated by the OPC in both cases (OPC with or without pre-dispersion) in the strong phase matching region compared with the case of not using the OPC. For the weakly phase-matched contributions, FWM power is rarely suppressed with the insertion of the OPC and then the FWM power has been suppressed by about 10 dB due to the in-line dispersion. In addition, the pre-dispersion affects the FWM efficiency and does not affect the phase array which causes the lobes.

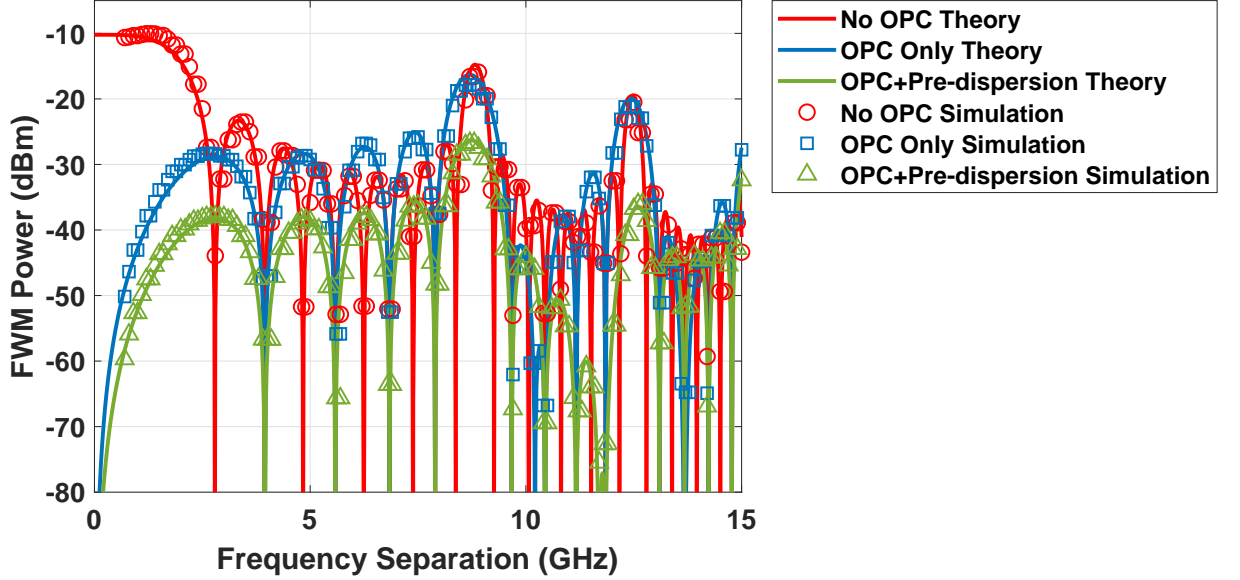


Figure 3.5. FWM power of OPC system as a function of frequency separations between the two signals in three cases: without OPC or DE (red), with OPC only (blue) and with OPC and DE (green) for theory (lines) and simulation (markers).

Using the same transmission link in Fig.(3.1), the performance of 224 Gbps PM-16QAM signal operating at 193.1 THz is simulated. VPITransmissionMaker 9.5 is used for fibre transmission and Matlab for signal recovery and performance measurement. The transmitted bits was 2^{20} bits per polarization, and the modulated optical signals was simulated with 8 samples per symbol. The PMD and dispersion slope were ignored because it is out of the scope of these simulations. An EDFA were used with 6dB noise figure at the end of each span to compensate the loss. The SNR was measured from error vector magnitude (EVM). Figure (3.6) shows the SNR as a function of the fiber input power, in the two scenarios and compared theory (solid lines) with simulations (symbols).

The theory curves (solid lines) plotted by substituting Eq.(3.14) and Eq.(3.58) in Eq.(3.57). The simulation results closely match the theoretical curves with an error less than 0.3 dB measured at the optimum SNR value and show that the pre-dispersion will produce an improvement in SNR measured at the optimum power about 3 dB compared with OPC system without DE. Figure (3.7) shows the maximum SNR for different link lengths and with different span lengths (100 km(blue), 80 km(orange) and 60 km(green)) and with consistent 3 dB improvement due

3. MATHEMATICAL EXPRESSIONS FOR FIBER NONLINEARITY IN LUMPED AMPLIFIED SYSTEMS

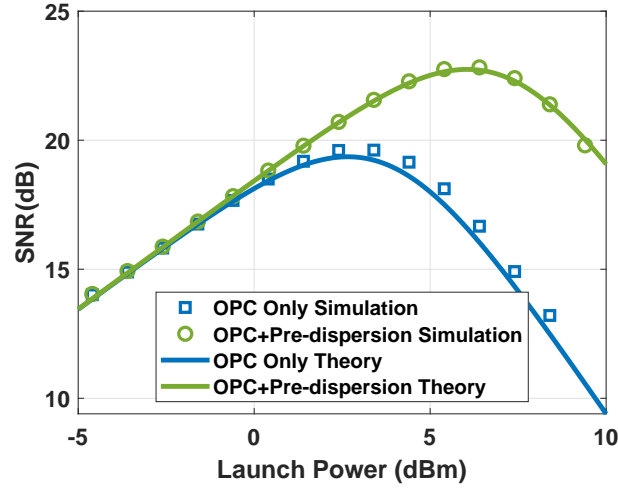


Figure 3.6. The signal to noise ratio (SNR) of 224Gbps PM-16QAM transmitted over 10x100km SSMF link incorporating an OPC as a function of the launched power in two cases: without pre-dispersion (blue) and with pre-dispersion (green) for theory (lines) and simulation (markers).

to the pre-dispersion and changing the span length (from 60 to 80 km) does not affect the compensation efficiency due to the pre-dispersion with the OPC which match the theoretical results (black dashed line) in Fig.(3.4).

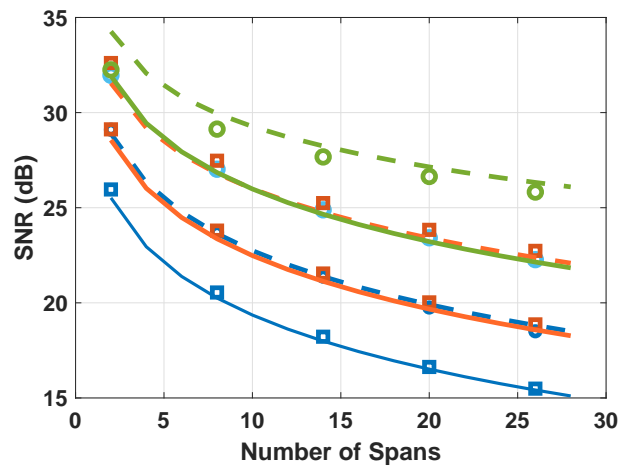


Figure 3.7. The maximum signal to noise ratio (SNR) as a function of the number of spans with different span length 100 km (blue), 80 km (orange) and 60 km (green) in two cases: without pre-dispersion (solid - squares) and with pre-dispersion (dashed - circles) for theory (lines) and simulation (markers).

3.3.2 Nonlinear Noise Expressions Validation

In order to validate the analytical results for the non-linear noise PSD, a Nyquist WDM system is simulated using Matlab for the signal generation, recovery and performance measurement and VPITransmissionMaker 9.8 for fiber transmission and optical components. The simulated system employed 17 channels of 28-Gbaud PM-16QAM (on 30GHz grid) which were transmitted using the same transmission link shown in Fig. (3.1) with 10x100 km SSMF and using the same simulation parameters shown in Table (3.1). An ideal OPC (no insertion loss or frequency conversion) was implemented in Matlab and inserted in the middle of the link.

The transmitted bits were 2^{19} bits per polarization, and the simulations were conducted with 64 samples per symbol. The PMD and dispersion slope were omitted because they are outside the scope of these simulations. An EDFA (with 5dB noise figure) was used at the end of each span to compensate for the fiber loss.

Root-raised-cosine filters with a roll-off factor of 0.05 were used for pulse shaping. A preamble (1024 bits) containing constant amplitude zero autocorrelation sequences for time synchronization and channel estimation purposes was transmitted together with the information data. At the receiver, time synchronization was performed using the Schmidl & Cox autocorrelation metric [203], while fine-time synchronization and channel impulse response estimation were performed using cross-correlation with the training sequence. The signal was pre-dispersed before the OPC and the insertion loss for the pre-dispersion element was ignored. The residual dispersion from the DE was compensated by the digital signal processing at the receiver.

The performance was compared using the signal to noise ratio (SNR), either calculated for the theoretical results from Eq.(3.57) or extracted from direct error counting according to (for PM-16QAM signal),

$$BER = \frac{3}{8} \operatorname{erfc} \left(\sqrt{\frac{SNR}{10}} \right) \quad (3.63)$$

Three systems were investigated: without OPC (red squares), with OPC in the middle of the link (purple diamonds), and with OPC and pre-dispersion (green circles) before the OPC with the optimum accumulated dispersion (1256 ps/nm) calculated from Eq.(3.53). Theoretical

3. MATHEMATICAL EXPRESSIONS FOR FIBER NONLINEARITY IN LUMPED AMPLIFIED SYSTEMS

results are plotted by substituting Eq.(3.47) and Eq.(3.58) in Eq.(3.57) as lines for the three different cases. When no OPC is used, Eq.(3.47) is replaced by Eq.(3.46).

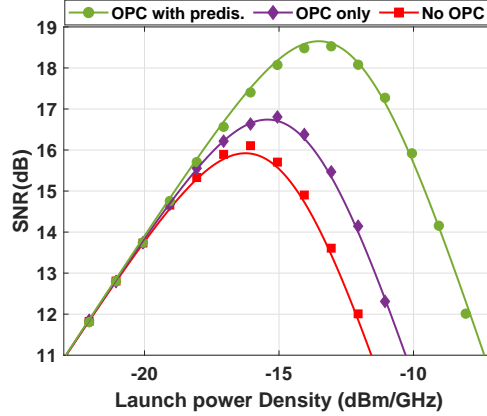


Figure 3.8. The signal to noise ratio (SNR) of the central channel of 17 WDM channels as a function of the total launched power density in three cases: Without OPC (red squares), with OPC only (purple diamonds) and with OPC and pre-dispersion (green circles) for theory (lines) and simulation (markers).

Figure (3.8) shows the obtained SNR as a function of the total launch power density (measured at the input of the fiber). It can be observed that the simulation results match with the theory for the three cases. The difference between the simulated results and the analytical results is smaller than 0.12 dB at the optimal launch power density. For this system, the improvement due to OPC alone is less than 0.8 dB, but increases to 2.7 dB due to the improved symmetry when pre-dispersion is employed.

Next, the simulations were run at different pre-dispersion values to verify the optimum pre-dispersion concluded by Eq.(3.53) and for each pre-dispersion value, the launch power was swept to get the maximum SNR. Figure (3.9) shows the maximum SNR for the central channel as a function of the pre-dispersion (the accumulated dispersion of the DE) which closely matches the predictions of Eq.(3.53). The theory line was plotted using Eq.(3.62). There is good matching between the theory and the simulation and also the results show that even adding a pre-dispersion less than the optimum value still improves the system performance. Furthermore, the curve is asymmetric around the optimum pre-dispersion value and this can be explained through the

power versus the accumulated dispersion curve in Fig.(2.11) and it can be seen that shifting the power to the right or the left will give completely different compensation because the power profile of the lumped amplification is not symmetric.

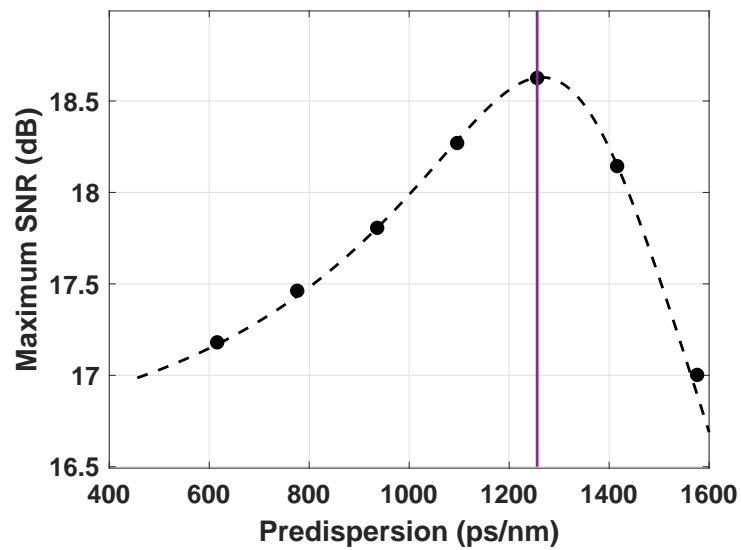


Figure 3.9. The maximum signal to noise ratio (SNR) of the central channel of 17 WDM channels as a function of the pre-dispersion for theory (dashed line) and simulation (markers). The optimum pre-dispersion (vertical line).

Finally, as shown in Fig. (3.10), the system is simulated over different span lengths for a 10 span system (variable transmission reach) for the three cases (without OPC (red), with OPC only (purple) and with OPC accompanied with pre-dispersion (green)). The SNR was estimated from the error vector magnitude (EVM) because the received signal was error-free in the high SNR region. For each simulation point, a power sweep was performed with a step size of 0.5 dB, enabling the optimum to be estimated. For the theoretical results, the optimum launch power, and maximum SNR was plotted using Eq.(3.61) and Eq.(3.62).

3. MATHEMATICAL EXPRESSIONS FOR FIBER NONLINEARITY IN LUMPED AMPLIFIED SYSTEMS

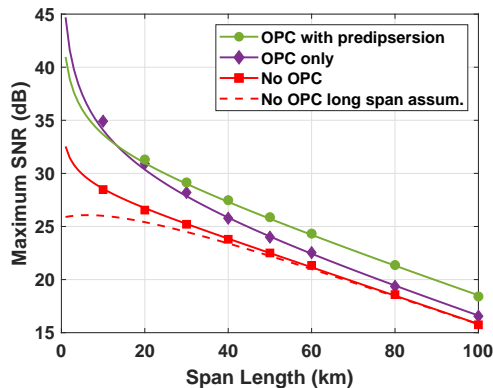


Figure 3.10. The Maximum signal to noise ratio (SNR) of the central channel of 17 WDM channels as a function of the span length in three cases: Without OPC (red), with OPC only (purple) and with OPC and pre-dispersion (green) for theory (lines) and simulation (markers).

The simulation results match the analytical predictions with a difference of less than 0.2 dB. In addition, whilst the benefit of OPC becomes increasingly significant for short span lengths because the symmetry condition has been improved, the beneficial effect of pre-dispersion starts to decrease for spans shorter than 50km and the pre-dispersion is not effective for spans less than the effective length of the SSMF and this is the reason for the cross-over in Fig. (3.10). For system without OPC (red), the dashed line is plotted using Eq.(21) in [174] which gives the analytical predictions for systems without OPC under the approximation of long span lengths, while the solid line was plotted using Eq.(3.46) which gives the analytical predictions for systems without OPC without this approximation. The results show that the simulation points (markers) match with the solid line for long and small span lengths while the dashed line clearly breaks down, as expected, below 40km.

Although the OPC have been assumed with zero penalties in deriving Eq.(3.47), an additional penalty from the OPC can be added to the denominator of Eq.(3.57) under the assumption that these penalties can be considered as AWGN. In addition, by comparing the numerical results of Eq.(3.14) with the analytical model from Eq.(3.47), the model works for bandwidth greater than 250GHz with less than 0.3 dB difference from the numerical integration, and the difference starts to increase with decreasing the bandwidth as the large bandwidth assumption has been violated. For channels with large guard bands, these guard bands might need to be considered into the integration boundaries in a similar manner to [204].

3.4 The Impact of Dispersion Slope on Modeling Fiber Nonlinearity in Ultra-Wideband Systems

In order to meet the high capacity demand in the core network and instead of using new immature technology like space division multiplexing (SDM), optical fiber transmission extending beyond the C-band is now used by employing the large bandwidth of the currently installed SSMF through using multiple telecom optical wavelengths bands [13]. As it has been introduced above, the nonlinear noise has been well modeled by assuming constant fiber parameter with respect to the wavelength and by ignoring some other nonlinear phenomenon like stimulated Raman scattering (SRS) which needs ultra-wide bandwidth to evolve [38] and introduces frequency-dependent loss or gain. However, it is obvious that as signal bandwidths continue to expand, such wavelength-independent parameter assumptions may become inaccurate and a more detailed understanding of bandwidth dependent effects will become increasingly important. Efforts to include the SRS effect in the models in case of ultra-wide bandwidth have been done [205–207].

In addition, the wavelength dependence of the dispersion has been considered in the GN-model [181] by including the third-order dispersion (dispersion slope) β_3 in the phase matching term $\Delta\beta$. The effect of the dispersion slope on the nonlinear noise PSD from the transmission of 1THz WDM signal over 80km SSMF single span was negligible even with increasing the value of β_3 by a factor of ten [181]. However, 1THz may not be wide enough bandwidth to notice the effect of dispersion slope (in SSMF with dispersion around $-20 \text{ ps}^2/\text{km}$) and it is required to know when the dispersion slope should be considered in the Kerr nonlinearity evaluation models to get accurate results.

In this part, the effect of dispersion slope is analyzed on the nonlinear performance of wide-band signals, proposing a normalized parameter beyond which dispersion slope must be taken into account.

3. MATHEMATICAL EXPRESSIONS FOR FIBER NONLINEARITY IN LUMPED AMPLIFIED SYSTEMS

3.4.1 FWM Power with Dispersion Slope

Equation (3.43) shows the FWM power resulted from the interaction of three frequencies in a multi-span lumped amplification system and in the previous analysis, the phase mismatching term has been approximated by considering only the second-order dispersion β_2 as shown in Eq.(3.3). Now the same term will be derived including the terms till the second-order dispersion and dropping the higher-order dispersion terms. By expanding the propagation constant using Taylor series [38] around frequency f_0 ,

$$\beta(\omega_i) = \beta_0 + \beta_1 (\omega_i - \omega_0) + \frac{1}{2}\beta_2 (\omega_i - \omega_0)^2 + \frac{1}{6}\beta_3 (\omega_i - \omega_0)^3 + \dots \quad (3.64)$$

Where β_0 is a constant phase shift and β_1 is the inverse of the group velocity v_g ($\beta_1 = \frac{1}{v_g}$). The phase mismatching term can be written as,

$$\Delta\beta = \beta(\omega_x - \omega_0) + \beta(\omega_y - \omega_0) - \beta(\omega_z - \omega_0) - \beta(\omega_x + \omega_y - \omega_z - \omega_0) \quad (3.65)$$

By substituting Eq.(3.64) into Eq.(3.65), the phase mismatch can be written as,

$$\Delta\beta = -(2\pi)^2\beta_2(f_x - f_z)(f_y - f_z)\left(1 + \pi\frac{\beta_3}{\beta_2}((f_x - f_0) + (f_y - f_0))\right) \quad (3.66)$$

it is assumed that f_z is located at the center of the bandwidth and the phase mismatch term can be written as,

$$\Delta\beta = -(2\pi)^2\beta_2(f_x - f_z)(f_y - f_z)\left(1 + \pi\frac{\beta_3}{\beta_2}((f_x - f_z) + (f_y - f_z))\right) \quad (3.67)$$

Conventionally Eq.(3.67) is further approximated by considering β_3 to be zero as shown in Eq.(3.3). From Eq.(3.67), there are *three* regimes of strong phase matching ($\Delta\beta \approx 0$), where two of the frequencies are close to each other ($f_x \approx f_z$ and $f_y \approx f_z$) and a third when,

$$\pi\frac{\beta_3}{\beta_2}((f_x - f_z) + (f_y - f_z)) = -1, \quad (3.68)$$

3.4 The Impact of Dispersion Slope on Modeling Fiber Nonlinearity in Ultra-Wideband Systems

and for the case of degenerate FWM, the condition to notice the effect of the dispersion slope (third matching region) can be written as,

$$|df| = \frac{1}{2\pi} \frac{\beta_2}{\beta_3} \quad (3.69)$$

In order to analyze the FWM in the case of dispersion slope, 80 km single DSF span is assumed with dispersion (β_2) $-0.54 \text{ ps}^2/\text{km}$ and second-order dispersion (β_3) $0.131 \text{ ps}^3/\text{km}$ and attenuation 0.26 dB/km at 193.6 THz . By substituting Eq.(3.67) into Eq.(3.43), the FWM can be plotted as a function of the normalized frequency separation as shown in Fig.(3.11).

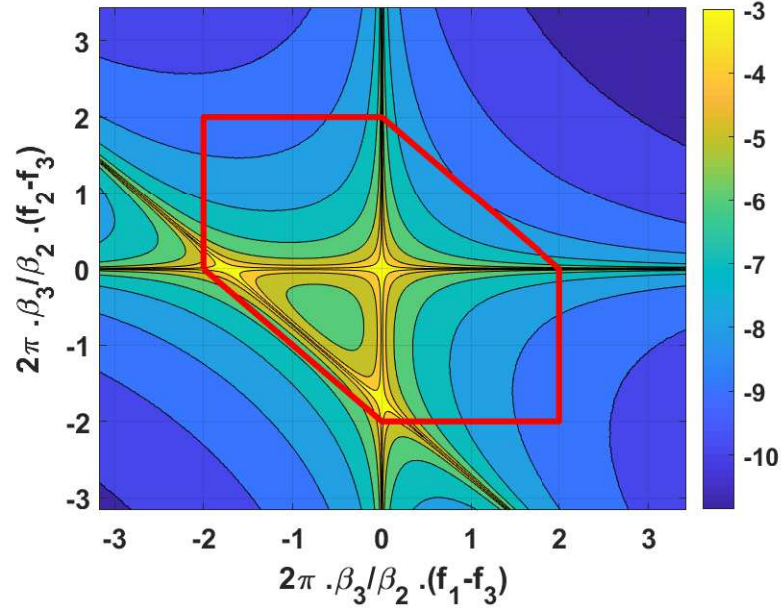


Figure 3.11. FWM efficiency as a function of frequency separation between the three lasers normalized to the ratio of dispersion slope to the dispersion. The red hexagon represents the NLN boundaries affecting the signal with the same normalization. The top of the color bar is yellow then orange.

The blue regions represent low FWM efficiency due to weak phase matching. The yellow areas represent the three areas of strong phase matching. The dispersion slope has three key effects. Firstly, the appearance of an additional strongly phase-matched region (diagonal yellow peak), secondly, the modification of phase matching in the region bounded by the three strongly phase-matched regions, and a slight change in the rate of decay in the weakly phase-matched area.

3. MATHEMATICAL EXPRESSIONS FOR FIBER NONLINEARITY IN LUMPED AMPLIFIED SYSTEMS

These general features remain irrespective of the fiber type, although the width of the strongly phase-matched regions (yellow) decreases with β_2 . The red polygon bounds the region where signals may interact to produce mixing products at the center of the signal band, and scales with fiber dispersion and bandwidth. Additional strongly phase-matched mixing products are clearly to be expected if the polygon includes all three phase matching peaks. Based on Eq.(3.67) and the results in Fig.(3.11), for SSMF with $\beta_2 \approx -20$ ps²/km and $\beta_3 \approx 0.13$ ps³/km, this occurs with bandwidths around 20THz, assuming a center frequency of 193.6 THz and require 40THz to make an effect inside the signal bandwidth and for non-zero dispersion-shifted fiber (NZ-DSF) ($\beta_2 \approx -5$ ps²/km) ~ 5.9 THz and require 11.8THz bandwidth to make an effect on the signal. However, an increase in nonlinear noise (NLN) may occur before these bandwidths and should be calculated by integrating Eq.(3.43) for single-span taking into account dispersion slope as the following,

$$I_\xi = 16\gamma^2 I^3 \iint_B \frac{1}{\left(\alpha^2 + (2\pi)^4 \beta_2^2 f_a^2 f_b^2 \left(1 + \pi \frac{\beta_3}{\beta_2} (f_a + f_b) \right)^2 \right)} \left(\frac{1}{4} (1 - e^{-\alpha L})^2 + e^{-\alpha L} \sin^2 \left(\frac{(2\pi)^2 \beta_2 f_a f_b \left(1 + \pi \frac{\beta_3}{\beta_2} (f_a + f_b) \right) L}{2} \right) \right) df_a df_b \quad (3.70)$$

Where $f_a = f_x - f_z$ and $f_b = f_y - f_z$. These analysis will be verified experimentally in Chapter (5)

3.5 Conclusions

An analytical result have been introduced for the FWM produced from the interaction of three frequencies in a multi-span lumped amplified system with mid-link OPC and pre-dispersion. Then the results are developed to get a closed-form expression for the non-linear noise PSD. The model can be used to predict the amount of improvement due to the insertion of OPC and also the impact of adding a dispersion element with the OPC to improve the symmetry. The same model can be used to predict the optimum launch power and estimate the optimum SNR. In addition, the closed-form expression have been developed for nonlinear noise

PSD in a multi-span system without OPC to consider the short span lengths. The results have been validated through simulation in different scenarios and show good agreement.

3. MATHEMATICAL EXPRESSIONS FOR FIBER NONLINEARITY IN LUMPED AMPLIFIED SYSTEMS

Chapter 4

Optical Fiber Phase Conjugation Device

The ultrafast nonlinear response of silica gives the OPC an advantage over the other nonlinearity compensation methods where the dispersion and Kerr nonlinearity can be compensated simultaneously (under symmetry conditions) and in real-time without any additional delay in the system. The OPC showed a great improvement either in increasing the transmitted data rate [208] or in extending the maximum reach [127] through nonlinearity compensation. The OPC device has some requirements to be practically deployed. First, to be polarization-insensitive. Second, to have low insertion penalties and these penalties can be linear due to ASE noise from the amplifier used to compensate for the OPC insertion loss or phase distortions from the pump phase converted to the idler or nonlinear penalties from XPM from the pumps or the FWM process. Third, to conjugate large bandwidth with flat response, to cover the whole C-band without the need to split the broadband signal. Finally to have a compact size which is not our interest in this chapter. Therefore, a careful design of the OPC device is important to avoid these different penalties. In this chapter, the different designs of the OPC using optical fiber are discussed and the main sources of the different impairments in each design are studied. Starting with polarization-dependent single pump OPC then moving to the dual-pump OPC with different configurations. Finally, the experimental implementation of a wavelength shift-free OPC device

4. OPTICAL FIBER PHASE CONJUGATION DEVICE

are discussed.

4.1 Optical Fiber Single-Pump Phase Conjugation Device

The basic optical parametric OPC design is shown schematically in Fig. (4.1) and the phase conjugation medium is the highly nonlinear fiber (HNLF) where the FWM process happens. A SSMF or DSF can be used but at the expense of lower conversion efficiency or high insertion loss because of the low nonlinear coefficient.

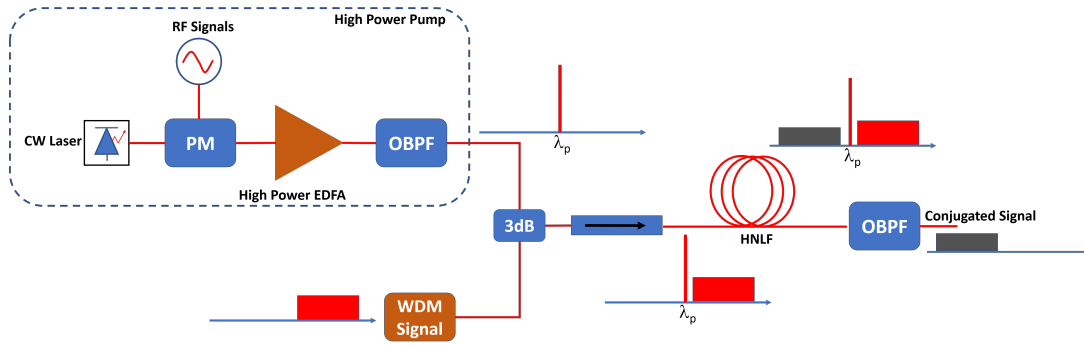


Figure 4.1. Basic single pump OPC design. PM: phase modulator. OBPF: optical bandpass filter. 3dB: 3dB coupler. HNLF: highly nonlinear fiber

The signal is multiplexed with a pump and launched into the HNLF then the pump and signal are filtered out using an optical bandpass filter (OBPF). Usually, the high power pump is generated using a CW laser followed by a high power EDFA. To avoid degrading the performance of the OPC with spontaneous emission (ASE) from the high power EDFA, a narrow bandwidth OBPF is used at the output. If the signal field can be described as,

$$E_s(t) = |E_s|e^{j(\omega_s t + \phi_s)} \quad (4.1)$$

and the pump field as,

$$E_p(t) = |E_p|e^{j(\omega_p t + \phi_p)} \quad (4.2)$$

then the idler signal from a degenerate FWM can be written as [38],

$$E_{Idler} = \varkappa |E_{Idler}| e^{j[(2\omega_p - \omega_s)t + (2\phi_p - \phi_s)]} \quad (4.3)$$

4.1 Optical Fiber Single-Pump Phase Conjugation Device

where $|E_{Idler}| = |E_p|^2|E_s|$, \varkappa is a proportional constant representing the FWM efficiency and is depending on the HNLF nonlinear coefficient γ and length L . $|E_s|$, $|E_p|$, ω_s , and ω_p are the signal and the pump field amplitudes and angular frequencies respectively. The conversion efficiency η from the signal to the idler can be written (in case of phase matching) as [209],

$$\eta = \varkappa^2 P_p^2 \quad (4.4)$$

where $P_p = |E_p|^2$ is the pump power. Equation (4.4) shows that the conversion efficiency is a function of fiber parameters and pump power. Increasing the pump power will be limited by the SBS and an optical isolator is used after the 3dB coupler to block the backward SBS reflections from the HNLF. However, these reflections will reduce the useful pump power passed through the HNLF after exceeding the SBS threshold as discussed in Ch.(2).

4.1.1 Pump Dithering

To increase the SBS threshold, the CW laser is modulated with one or more sinusoidal radio frequency (RF) signals before amplification to broaden the narrow linewidth of the CW laser beyond the SBS gain bandwidth. Each added tone will increase the SBS threshold by a factor of 3 (assuming that every PM modulator will produce two spectral lines in addition to the CW laser spectral line and neglecting the high order side-bands). The phase-modulation of the pump with two tones can be represented through ϕ_p as the following,

$$\phi_p = h_1 \sin(2\pi f_1 t) + h_2 \cos(2\pi f_2 t) \quad (4.5)$$

where h_1 and h_2 are the modulation indexes of the two tones and f_1 , f_2 are the frequencies of the RF tones. By substituting Eq.(4.5) into Eq.(4.2) and using Jacobi-Anger expansion [210], the dithered pump field can be written as,

$$\begin{aligned} E_p(t) &= |E_p| e^{j(2\pi f_p t)} e^{j(h_1 \sin(2\pi f_1 t) + h_2 \cos(2\pi f_2 t))} \\ &= |E_p| e^{j(2\pi f_p t)} \sum_{n_1=-\infty}^{\infty} J_{n_1}(h_1) e^{j2\pi n_1 f_1 t} \sum_{n_2=-\infty}^{\infty} J_{n_2}(h_2) e^{j2\pi n_2 f_2 t} \end{aligned} \quad (4.6)$$

4. OPTICAL FIBER PHASE CONJUGATION DEVICE

where f_p is the pump frequency, $J_n(h)$ is the n-th Bessel function of the first kind. If h_1 and h_2 have been chosen to make $J_1(h_1) = J_2(h_2)$ and the higher order components are zero, the output of the phase modulator can be plotted as shown in Fig.(4.2).

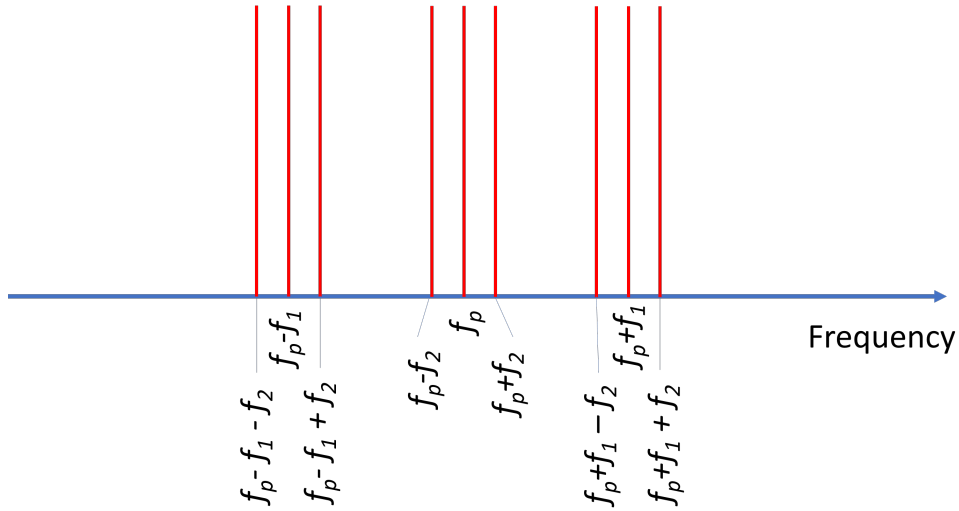


Figure 4.2. Theoretical description of the spectrum of phase-modulated pump with two tones.

However, Fig.(4.2) represents the ideal case of a phase modulated pump signal where there are no side-bands from the phase modulator. The actual output of the phase modulator is shown in Fig.(4.3) where there are many side-bands for the two tones and the main lines have slightly different amplitudes.

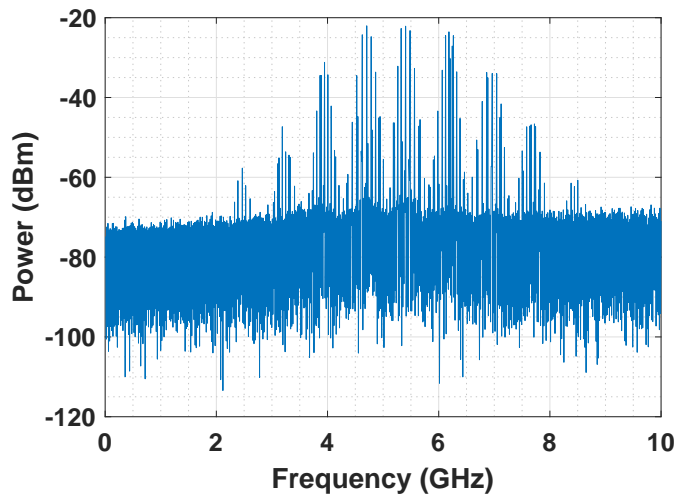


Figure 4.3. The output of PM modulator measured using an RF spectrum analyzer.

Figure (4.3) is plotted by mixing the output of the phase modulator with a CW laser signal and the output is fed to a photodiode which is connected to an RF spectrum analyzer. The phase of the pump will be transferred doubled to the idler as shown in Eq.(4.3), therefore, using many RF tones to increase the SBS threshold will distort the conjugated signal (or the idler). This phase distortion can be removed through the DSP in the coherent receiver before recovering the carrier phase [211] or using counter dithering between the pump and the signal [209]. In addition to the phase conversion between the pump and the conjugate, any fluctuations in the pump amplitude will be transferred to the signal and this can reduce the SNR of the conjugated signal [38].

4.1.2 Phase Matching

The conversion efficiency is highly dependent on the phase matching between the pump and the signal as a result of the FWM process. The linear phase mismatch term has been defined in Eq.(2.35) and it can be written for a degenerate FWM (by considering only the first-order dispersion) as the following,

$$\Delta\beta = -\beta_2(\omega_p - \omega_s)^2 \quad (4.7)$$

In order to minimize the phase mismatch in the single pump OPC shown in Fig.(4.1), the pump wavelength λ_p should be chosen close to the zero-dispersion wavelength of the HNLF λ_0 . The dithering is expected to reduce the phase matching as it is affecting the phase of the pump. In addition, the phase matching will be high when the signal is close to the pump and decrease with moving far from the pump and this may produce an uneven conjugated signal in case of using wideband WDM signal where the channels close to the pump will have different phase mismatching from the channels away from the pump.

4.1.3 Conjugation Bandwidth

The single-band OPC setup in Fig.(4.1) produces a mirrored conjugate on the other side of the pump according to Eq.(4.3) where the idler will be located at $f_{Idler} = 2f_p - f_s$. This frequency shift will make a restriction on the signal bandwidth. For example, to cover the full C-band using a single OPC, the pump (and the zero-dispersion wavelength) should be located

4. OPTICAL FIBER PHASE CONJUGATION DEVICE

on the edge of the C-band, and in that case, the conjugate will be located either in the L-band or the S-band which may require different optical components. In addition, if part of the conjugate is located in C-band and another part in L-band due to the pump location, the amplification of the conjugate signal may not be available using a single amplifier and it may need two parallel amplifiers, one for each band. This can be solved partially by using two OPCs in parallel and the signal band is divided and a conjugate is generated for each half using one OPC.

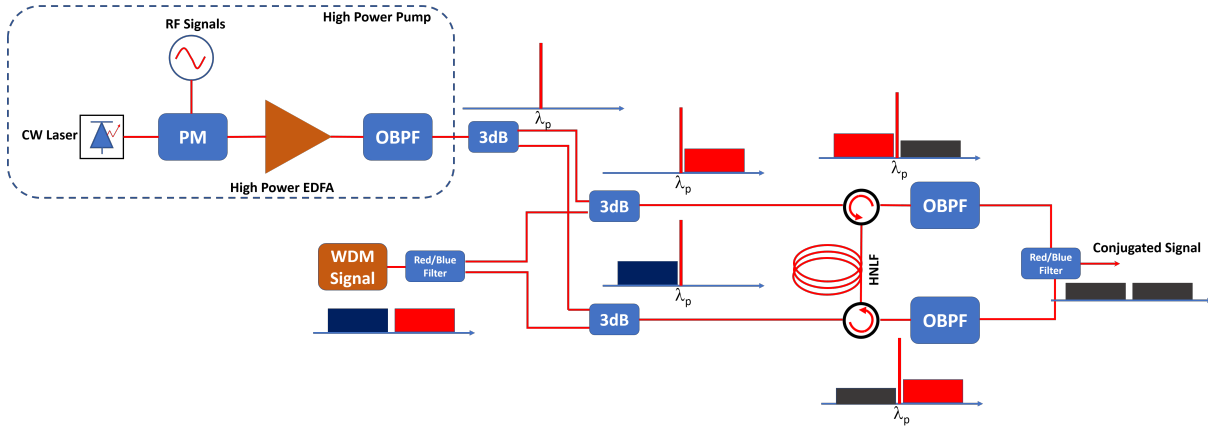


Figure 4.4. Single pump dual band OPC setup.

In Fig.(4.4), the signal band is split using a red/blue filter or wavelength selective switch (WSS) and each band is combined with the pump and counter-propagated through the HNLF. Then the pump and the signal are filtered out and the conjugated two bands are combined again using another red/blue filter or WSS. However, there is a bandwidth gap (around 50GHz) that needs to be left between the two bands because of the roll-off factor of the filter.

4.1.4 Insertion Loss

The OPC setup is adding insertion loss to the link which can be compensated with an EDFA which adds an ASE noise to the link. This insertion loss either is due to the losses from the different components or due to the conversion efficiency in the conjugation process. The components' loss can be reduced to some limit by optimizing its performance during the manufacturing process. In addition, the conversion efficiency can be improved by using the OPC as a FOPA [212,213]. However, this will require a high power pump that needs dithering with

multiple tones to increase the SBS threshold and unfortunately, this additional phase will distort the idler [212].

4.1.5 Polarization Diversity

The FWM process is greatly dependent on the polarization and the conversion efficiency is dependent on the relation of the states of polarization (SOP) between the pump and the signal. The maximum efficiency happens when the SOP of both the input pump and the signal is linearly polarized and maintain their SOP during the propagation (this is the assumption of Eq.(4.3)). If the polarization of the pump and the signal are completely orthogonal, no idler field will be generated. While the SOP of the pump can be selected, it is often random for the signal. Therefore, a polarization-independent OPC design is required. The design of the OPC in Fig. (4.1) or Fig. (4.4) is considered as a polarization-sensitive setup because the two polarization components of the signal will be conjugated unequally. In order to use the OPC to get the conjugate of polarization multiplexed (PM) signal, a polarization diversity loop is required where the two polarization components of the pump and the signal are split into two orthogonally polarized components and each aligned polarization component of pump and signal is combined in HNLF. There are slightly different configurations but the main polarization diversity loop is shown in Fig.(4.5) [214].

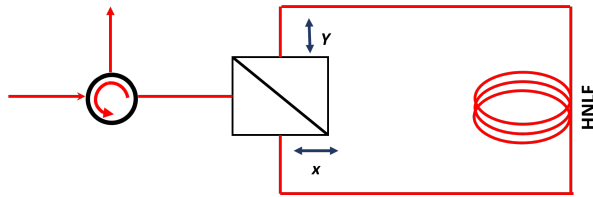


Figure 4.5. Polarization diversity loop setup.

In [208], the polarization diversity loop has been used with a single pump OPC shown schematically in Fig.(4.1). The need for the polarization diversity loop can be avoided by using dual pump OPC.

4. OPTICAL FIBER PHASE CONJUGATION DEVICE

4.2 Optical Fiber Dual-Pump Phase Conjugation Device

Instead of using a single pump for phase conjugation, two pumps can be used and in order to achieve phase matching, their wavelengths are chosen to be located symmetrically around the zero-dispersion wavelength of the HNLF as indicated in Fig.(4.6).

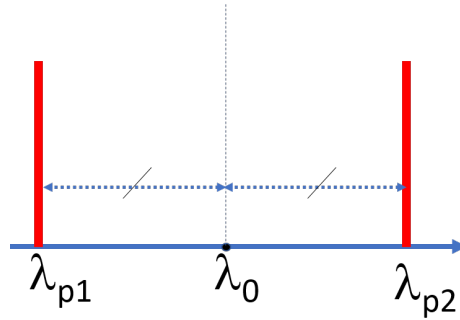


Figure 4.6. Pump location with respect to the zero-dispersion wavelength to achieve wide-range phase matching.

$$f_0 = \frac{c}{\lambda_0} = \frac{f_{P_1} + f_{P_2}}{2} \quad (4.8)$$

and in that case, the idler resulted from the non-degenerate FWM will be located at,

$$f_{Idler} = f_{P_1} + f_{P_2} - f_s = 2f_0 - f_s \quad (4.9)$$

Eq.(4.9) shows that the two pumps symmetrically around the zero-dispersion wavelength/frequency of HNLF are equivalent to a single pump at the zero-dispersion wavelength/frequency.

Using two pumps in the OPC setup has many positive features over a single pump. The polarization diversity loop is not required for the polarization-insensitive conjugation process by using two linear orthogonally polarized pumps [215, 216] and the conversion efficiency will be independent of the signal polarization. In addition, although the phase modulation of the pump resulting from the dithering will be transferred to the idler, modulating the two pumps out of phase [217] where $\phi_{P_1} + \phi_{P_2} = 0$ will theoretically cancel this phase at the idler and it is usually called counter-dithering.

4.2 Optical Fiber Dual-Pump Phase Conjugation Device

The scalar representation of the field in Eq.(4.3) is not suitable to describe the FWM in polarization-insensitive OPC. Therefore, the vector representation of the field is used and the degenerate FWM between the two orthogonal polarization fields is set to zero. Also, x, y are assumed to be the polarization components and pump 1 is launched with polarization x and pump 2 is launched with polarization y . The idler field resulting from degenerate and non-degenerate FWM can be written as [216],

$$E_{Idler}^x = \varkappa \left[|E_{p_1}^x|^2 |E_s^x| e^{j2\pi(2f_{p_1}-f_s)+j(2\phi_{p_1}-\phi_s)} + |E_{P_1}^x| |E_{P_2}^y| |E_s^y| e^{j2\pi(f_{p_1}+f_{p_2}-f_s)+j(\phi_{p_1}+\phi_{p_2}-\phi_s)} \right] \quad (4.10)$$

$$E_{Idler}^y = \varkappa \left[|E_{p_2}^y|^2 |E_s^y| e^{j2\pi(2f_{p_2}-f_s)+j(2\phi_{p_2}-\phi_s)} + |E_{P_1}^x| |E_{P_2}^y| |E_s^x| e^{j2\pi(f_{p_1}+f_{p_2}-f_s)+j(\phi_{p_1}+\phi_{p_2}-\phi_s)} \right] \quad (4.11)$$

The first term in Eq.(4.10) and Eq.(4.11) represent the unwanted degenerate FWM, and when the two pumps are symmetrically far from the zero-dispersion wavelength of HNLF, the phase-matching conditions are achieved for these terms when the signal is close to the pump [38]. So, if a guard band is considered between the pump and the signal, these two terms can be dropped as the following,

$$E_{Idler}^x = \varkappa |E_{P_1}^x| |E_{P_2}^y| |E_s^y| e^{j2\pi(f_{p_1}+f_{p_2}-f_s)+j(\phi_{p_1}+\phi_{p_2}-\phi_s)} \quad (4.12)$$

$$E_{Idler}^y = \varkappa |E_{P_1}^x| |E_{P_2}^y| |E_s^x| e^{j2\pi(f_{p_1}+f_{p_2}-f_s)+j(\phi_{p_1}+\phi_{p_2}-\phi_s)} \quad (4.13)$$

Equation (4.12) and (4.13) show that the conversion efficiency for the polarization components are identical and equal to,

$$\eta = \varkappa^2 P_1 P_2 \quad (4.14)$$

In addition, the effect of the pump dithering on the idler can be removed by modulating the

4. OPTICAL FIBER PHASE CONJUGATION DEVICE

two pumps out of phase to make $\phi_{p1} + \phi_{p2} = 0$. Furthermore, the conjugation of E_s^x will be generated at y polarization and vice versa and this can be used as an advantage for developing frequency shift-free OPC as it will be shown later. This can be understood physically through the concept that the polarization dependence of the FWM arises from the condition of angular momentum conservation among the four interacting photons (two pumps, signal, and idler) in the optical fiber (isotropic medium) [38]. When the two pumps are orthogonally polarized, their angular momentum is zero. To keep this value (based on the conservation of angular momentum), the signal and idler photons must be orthogonally polarized [38]. The schematic OPC design in Fig.(4.1) and Fig.(4.4) is polarization-dependent and it can be upgraded to be polarization-insensitive by changing the pump part.

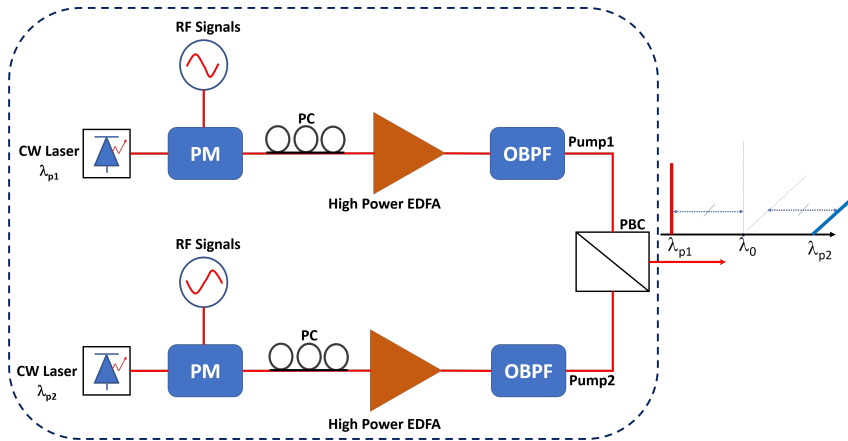


Figure 4.7. Two orthogonal pump generation for polarization-insensitive OPC. PC: Polarization controller. PBC : polarization beam combiner

Figure (4.7) shows a schematic design for two orthogonal pump generation where the polarization controller with PBS is used to ensure the orthogonality between the two pumps by maximizing the power of each pump at the output of the PBS. In [127], the dual-band OPC is used with orthogonal polarization pumps.

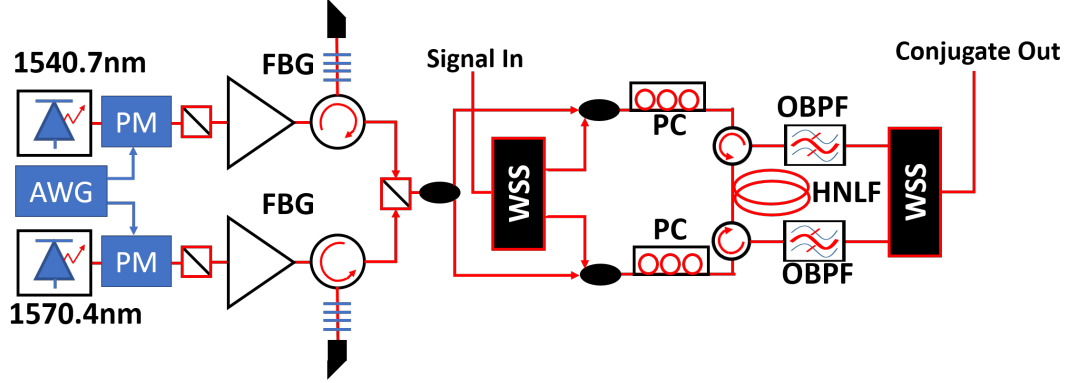


Figure 4.8. Polarization-independent dual-band OPC. PC: polarization controller.

Figure (4.8) shows the experimental setup of dual-band polarization-independent OPC. The two pump lasers with linewidth $< 10\text{kHz}$ (at $\lambda_{p1} = 1540.7\text{nm}$ and $\lambda_{p2} = 1570.4\text{nm}$) were amplified using high power EDFAs then the amplified pumps were filtered using a circulator and fiber Bragg grating (FBG) (1 nm) (the OBPF as described in Fig.(4.7) to filter out the ASE noise from EDFAs). To achieve a high level of orthogonality between the two pumps, the pump generation is done using polarization maintaining components such as high power EDFA, circulator, and fiber Bragg grating (FBG), and a PBS is used at the input of each high power EDFA to ensure that only one polarization component is amplified. Finally, two copies of the orthogonally polarized pumps were created (using a 3dB splitter). A wavelength selective switch (WSS) (instead of the red/blue filter in Fig.(4.7)) was used to split the signal into two bands [127] to create two independent OPCs for the two bands. A 3dB coupler was used to combine each signal band with the two orthogonally polarized pumps. A polarization controller was used before the HNLF on each path to minimize polarization walk-off and to optimize the polarization independence of the conjugation process. The two bands combined with the pumps were counter propagated in the HNLF ($L = 100\text{m}$, $\lambda_0 = 1557\text{nm}$, $\gamma = 28\text{W/km}$, dispersion slope = $0.024\text{ps/nm}^2/\text{km}$) via two circulators, as shown in Fig.(4.8). Each propagation direction along the HNLF formed an independent OPC, one for each band. The circulators enabled the extraction of signals, conjugates, and pumps after passing through the HNLF. Tunable OBPFs were used to remove the high-power pumps from the output of each OPC. Finally, a WSS was used at the output of the OPC to filter and combine the conjugated signals on each

4. OPTICAL FIBER PHASE CONJUGATION DEVICE

band. Although every effort can be done to launch orthogonal pumps initially, because the two pumps have different wavelengths, they emerge differently as they passed through the different optical components with different birefringence for each pump. Therefore, this may lead to a polarization-dependent loss (PDL) in the OPC.

4.2.1 Counter Dithering

The two fiber laser based pumps in Fig.(4.8) were phase modulated with two RF tones (with frequencies at 60MHz and 600MHz) with the opposite phase for each pump (counter-dithering) to avoid transferring this additional phase to the conjugate. To show the effect of dithering on the system performance, a 30 Gbaud 16QAM signal was transmitted back-to-back with the Rx without and with the OPC inserted between the Tx and Rx. To isolate the effect of dithering, a single polarization signal is used to avoid any effect from PDL. The signal was received using a 100Gsample/s coherent receiver and processed using built-in DSP (Tektronix OM4245). The performance is evaluated using the Q-factor measured from the EVM. Figure (4.9) shows the

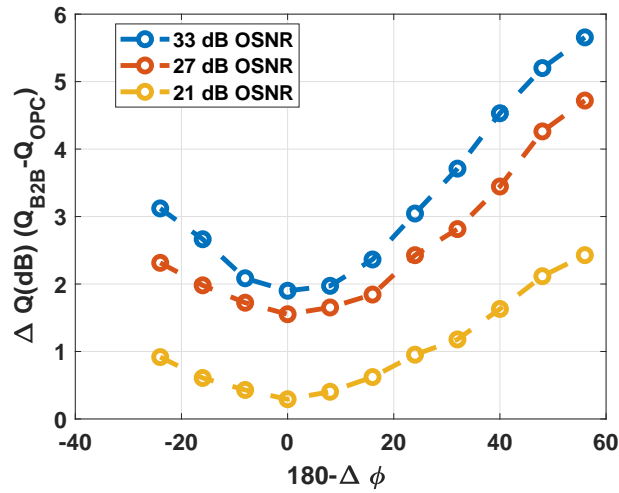


Figure 4.9. The difference in Q factor between back-to-back (B2B) performance of 30 Gbaud 16QAM with the performance when the OPC inserted between Tx and Rx as a function of the phase difference between the two pumps

effect of the transferred phase from the pump to the idler at a different value of phase difference between the modulated signals of each pump. The performance is measured using the difference in Q-factor between the signal and idler ΔQ . The lowest penalty occurs when the two pump

4.2 Optical Fiber Dual-Pump Phase Conjugation Device

signals are out of phase or when $\Delta\phi = 180$ and the penalty increases with the phase difference ϕ decreases. The dithering effect is high for high OSNR and it is reduced at low OSNR because the ASE penalty is overcoming the penalties arising from the dithering which appears as a reduced slope in the orange curve in Fig.(4.9). Even at the out of phase point, there is still residual dithering causing some penalty. The residual dithering is due to the mismatch in the electrical characteristic of the RF components [218] and this appears as a difference in the phase response of the two PMs. The response of the PM is shown in Fig.(4.3).

To improve the dithering suppression, an electrical low pass filter (LPF) (with a 3dB cut-off frequency of 750MHz) is used after the RF amplifier to suppress the high order frequency components produced by the nonlinearity of the RF amplifiers. The performance of the back-to-back measurements of 30 Gbaud 16QAM is repeated with and without the OPC. Noise from the EDFA is used as an ASE source then shaped using a WSS and amplified using another EDFA. The output of the EDFA is connected to an optical attenuator (to sweep OSNR) then added with the signal at the input of the Rx using a 3dB coupler.

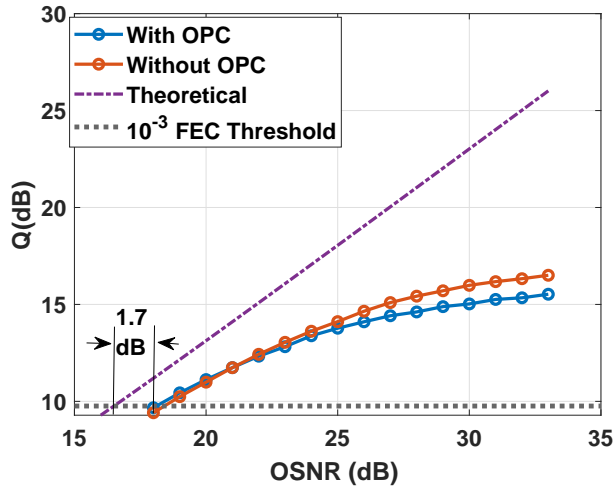


Figure 4.10. The Q factor of 30 Gbaud 16QAM as a function of OSNR at two cases back-to-back (B2B) performance and with the OPC inserted between Tx and Rx.

Figure (4.10) shows the performance of the B2B system compared with the system where the OPC is inserted between the Tx and Rx as a function of the OSNR. The penalty due to residual dithering has been decreased to 1dB at high OSNR (>26dB) and for low OSNR, it is

4. OPTICAL FIBER PHASE CONJUGATION DEVICE

reduced to a very small value close to zero. The implementation penalty is 1.7dB compared with the theory.

4.2.2 Wavelength Shift-free OPC

For the OPC design in Fig.(4.8), a guard band is required in the center between the two pumps to avoid any penalty due to the roll-off factor of the band splitting filter. One solution to save this guard band is using two OPCs with a polarization diversity loop [197] and conjugate each signal component of the polarization using one OPC. Eq.(4.12) and Eq.(4.13) show that the generation of the conjugate of E_s^x will be located at y polarization and vice versa. Although the previous work [197,219] was followed in calling this design as a wavelength shift-free, this almost applies if it is used to conjugate single-channel centered at f_0 , where f_0 is defined in Eq.(4.8). While the other channels will face some shift based on their locations from f_0 . An OPC with 10nm conjugation bandwidth has been designed and used for the transmission of single-channel 31.75 PM-16QAM over dispersion-managed 10 spans with 80km fiber length per span [197]. In this experiment, a wavelength shift-free polarization-insensitive OPC is introduced with 20 nm conjugation bandwidth.

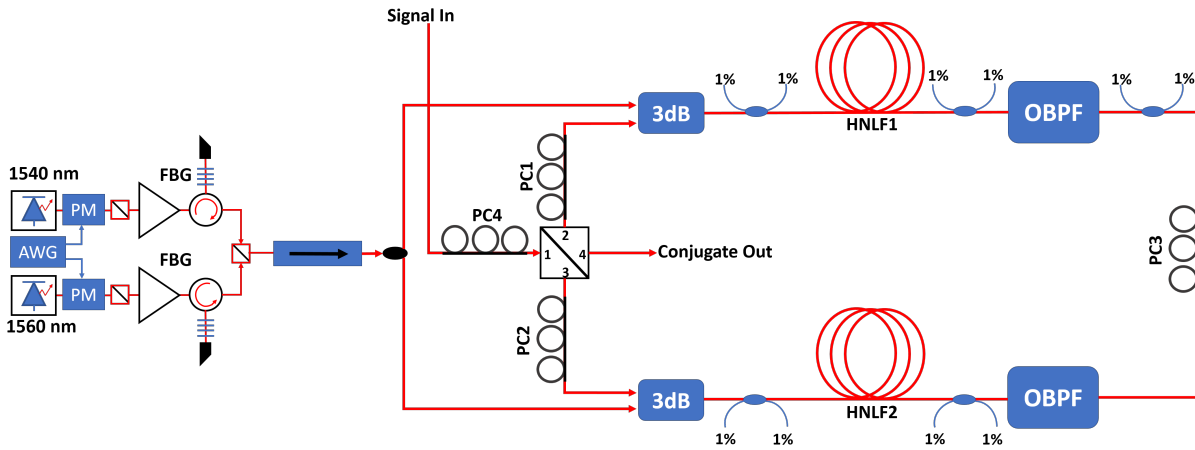


Figure 4.11. Experimental setup of dual-pump polarization insensitive OPC design.

Figure (4.11) shows the experimental setup of polarization-insensitive dual-pump wavelength shift-free OPC. The pump generation setup is similar to the one used in the setup of Fig.(4.8) with two pumps tuned at 1560nm (semiconductor laser, linewidth<100kHz) and 1540nm (fiber

4.2 Optical Fiber Dual-Pump Phase Conjugation Device

laser, linewidth < 10 kHz). The WDM signal with arbitrary polarization is split into two orthogonal polarization components (port 1 and 2 of PBS) using 4 ports PBS. The two polarization components counter propagate in the opposite direction. Each polarization component is combined with a copy of two orthogonal pumps with a 3 dB coupler then propagated through the HNLFs (two identical HNLFs ($L = 100$ m, $\lambda_0 = 1550$ nm, $\alpha \approx 1.2$ dB/km, $\gamma = 21.4$ W/km, dispersion slope at 1550 nm ≈ 0.041 ps/nm²/km)) to generate the idler on the other polarization axis. The pump is filtered using OBPF to prevent the pump from entering the second HNLF. After that, the orthogonal signal and idler travel through the other OPC. Next, PC3 is used to get the idler polarization components combined at port 4 of PBS. PC1, PC2 are used to increase the conjugation efficiency by aligning the signal polarization component with one pump. PC4 is used to test the polarization-insensitive property of the OPC. An isolator is used after the pump generation part to prevent the backward signal power and any SBS power.

Pump Power Setting

To decide the amount of pump power to be launched into the HNLF, the HNLFs SBS threshold were characterized.

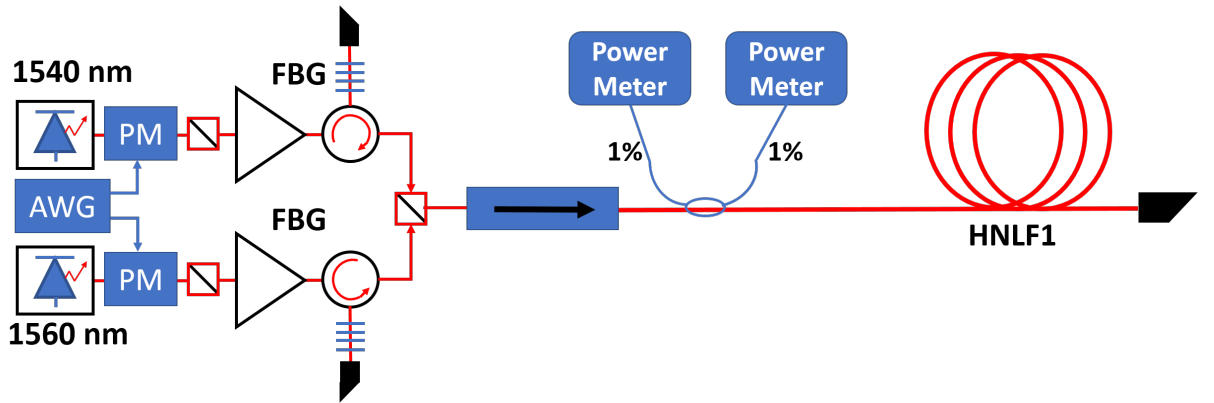


Figure 4.12. Experimental setup of SBS threshold characterization.

Figure (4.12) shows a simple setup that was used to characterize the SBS threshold. The power was swept by changing the EDFA output power and measured the input and reflected power using 1% coupler. For low power values, 30% coupler was added after the isolator.

4. OPTICAL FIBER PHASE CONJUGATION DEVICE

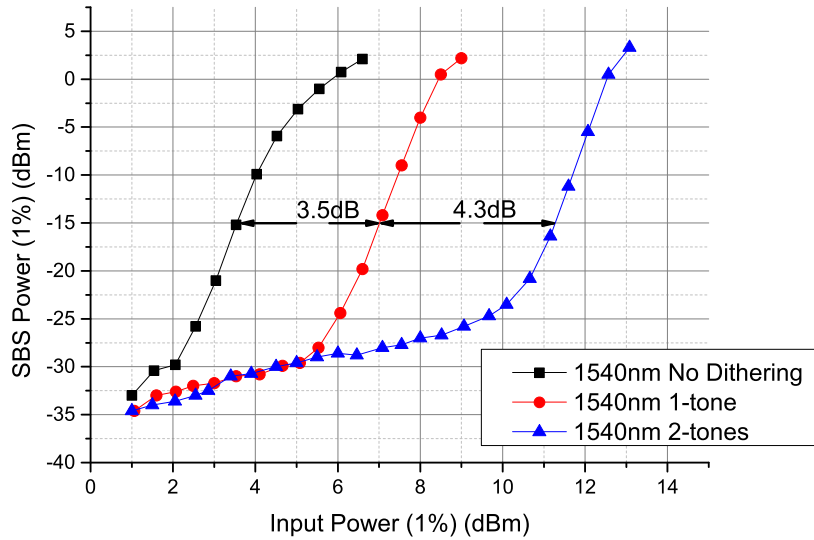


Figure 4.13. The backscattered power from HNLF as a function of launched power into the fiber.

Figure (4.13) shows the backscattered power as a function of the launched power. The dithering has improved the SBS threshold by around 7.8 dB and increased the SBS threshold to around 30dBm, which is used as the launched power in the HNLF.

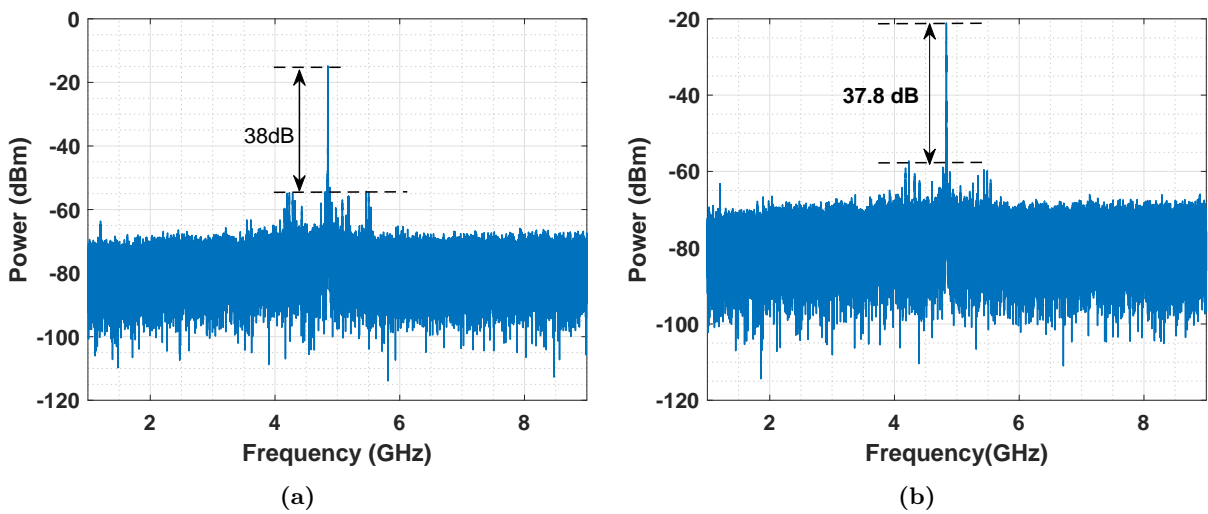


Figure 4.14. The RF spectrum of coherently received idler to show the effect of dithering suppression (a) Top HNLF1. (b) Lower HNLF2

4.2 Optical Fiber Dual-Pump Phase Conjugation Device

In order to check the effect of the pump dithering on the idler, the OPC was used to conjugate a CW laser signal with random polarization using a polarization scrambler. The scrambled CW laser is connected to the OPC and the conjugate is received coherently by mixing the idler with another CW laser with a small frequency difference (5GHz) from the idler frequency and the mixing is fed to a photodiode. The output of the photodiode is connected to the RF spectrum analyzer. Figure (4.14) shows the spectrum of the coherently received idler and shows that the suppression of the dithering is around 38dBc (relative to the idler).

Polarization Setting

To show the importance of the polarization controllers PC1 and PC2 in Fig.(4.11), again the scrambled CW laser signal was used as the input to the OPC and the output of the HNLF is monitored using the 1% coupler (at the end of HNLF) which is connected to the optical spectrum analyzer (OSA). Figure (4.15) shows the spectrum of the top HNLF output before setting.

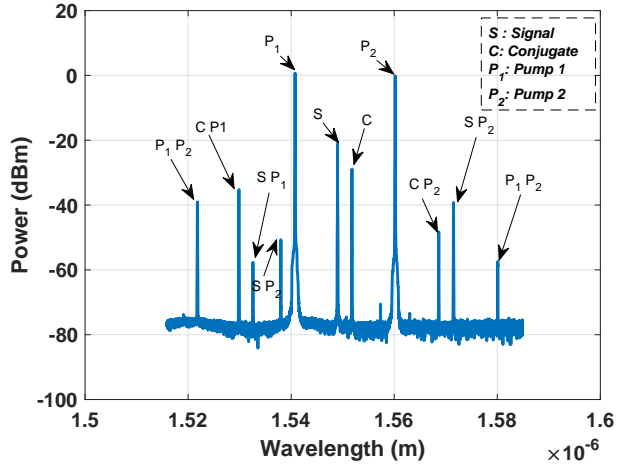


Figure 4.15. The Spectrum of HNLF1 output with scrambled CW laser is fed the OPC.

First of all, it is ensured that the polarization of the two pumps is orthogonal by minimizing the degenerate FWM between the two pumps (P_1P_2 in Fig.(4.15)). Through PC1 (or PC2 for the second polarization component of the signal), the signal polarization component was set aligned with pump2 (pump1) through minimizing the degenerate FWM between the signal and pump1 (pump2) (the spectrum line $S P_1(S P_2)$ in Fig.(4.15)). Then the setting is repeated to the

4. OPTICAL FIBER PHASE CONJUGATION DEVICE

other polarization component of the signal through PC2. Next, the OSA should be connected to the output of the PBC and the PC2 is set to maximize the conjugate (the idler) and minimize the signal.

Figure (4.16) shows the optical spectrum of the OPC after setting. The degenerate FWM between the two pumps is minimized to around 38 dB below the pump to ensure orthogonal pumps. Figure (4.16a) shows the spectrum at output of the HNLF1 where the signal polarization is set aligned with pump 1 and orthogonal to pump2 using PC1 in Figure(4.11), the degenerate FWM (SP_2) between the signal S and pump1 P_2 is minimized or between the conjugate C and pump 1 (CP_1). On the other side in Fig.(4.16b), SP_1 or CP_1 is minimized to make the signal polarization in that fiber aligned with pump2 and orthogonal to pump1. Figure (4.16c) shows the spectrum of the PBC output (port 4) where the signal component is suppressed by around 28dB using PC3. However, due to the conversion efficiency (6dB), the signal is 22dB below the conjugate.

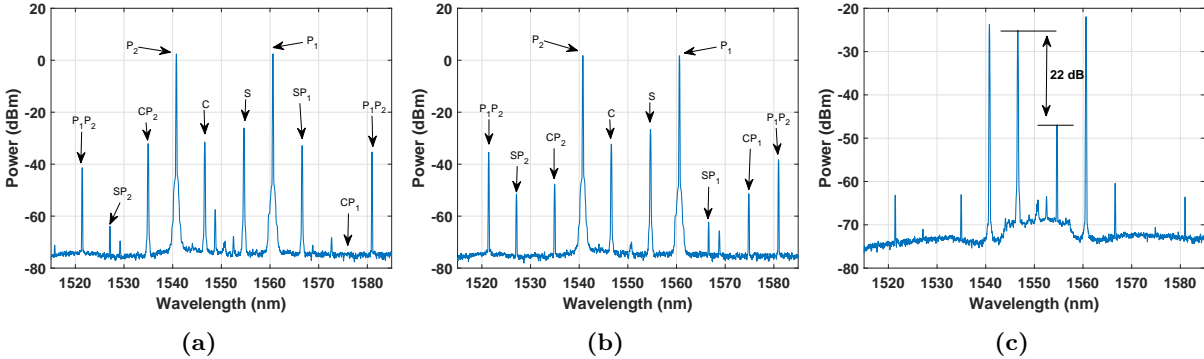


Figure 4.16. The optical spectrum (0.1nm) after setting the OPC (a) Top HNLF1. (b) Lower HNLF2 (c) PBC output. C: Conjugate, S: Signal, P_1 : Pump1, P_2 : Pump2

In order to test the wavelength shift-free property of the OPC, the setup shown in Fig.(5.5) is used to characterize the OPC using a 28-Gbaud PM-QPSK signal in back-to-back configuration and measured the Q-factor (calculated from the EVM) as a function of the OSNR in four cases, first, the signal (and the conjugate) is located at the center between the two pumps, second, the channel is moved by 14GHz from the center between the two pumps, third, the channel center frequency is 28GHz away from the center frequency between the two pumps and finally, without the OPC. Figure(4.17c) shows the spectrum at the first three cases.

4.2 Optical Fiber Dual-Pump Phase Conjugation Device

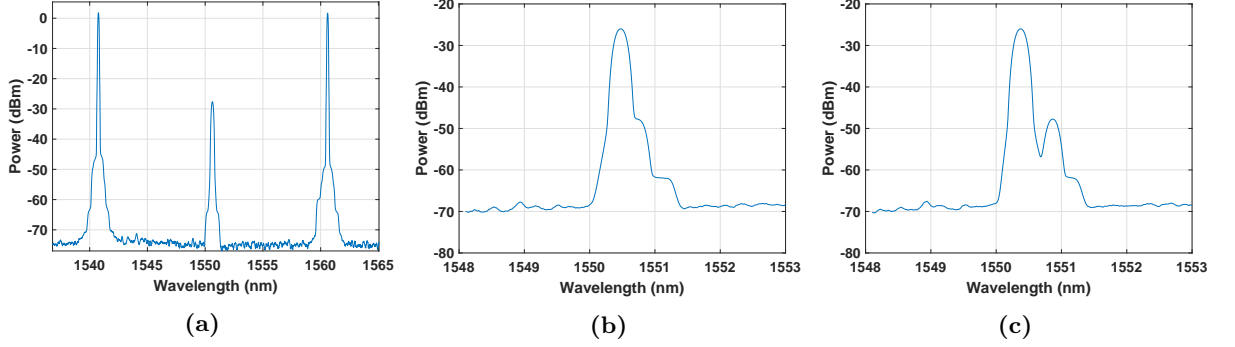


Figure 4.17. The optical spectrum (0.1nm) in three cases (a) at HNLFF1 output and $f_s - f_{idler} = 0GHz$. (b) at OPC output and $f_s - f_{idler} = 14GHz$. (c) at OPC output and $f_s - f_{idler} = 28GHz$.

Figure (4.17a) shows the spectrum of the HNLFF1 output where the channel at the center between the two pumps where the conjugate is generated without any shift ($f_{idler} = \frac{f_{P1}+f_{P2}}{2}$). Figures(4.17b and 4.17c) show the spectrum at the output of the OPC when the signal is separated from the idler by 14GHz ($f_{idler} = \frac{f_{P1}+f_{P2}}{2} - 14GHz$) and 28GHz ($f_{idler} = \frac{f_{P1}+f_{P2}}{2} - 28GHz$) respectively. Figure (4.18) shows the Q-factor as a function of the OSNR without OPC (dark blue circles) and with the OPC at three different frequency separations between the idler and the signal: 1) 0 GHz (oranges squares) 2) 14 GHz (green upward-pointing triangles) 3) 28 GHz (white blue right-pointing triangles).

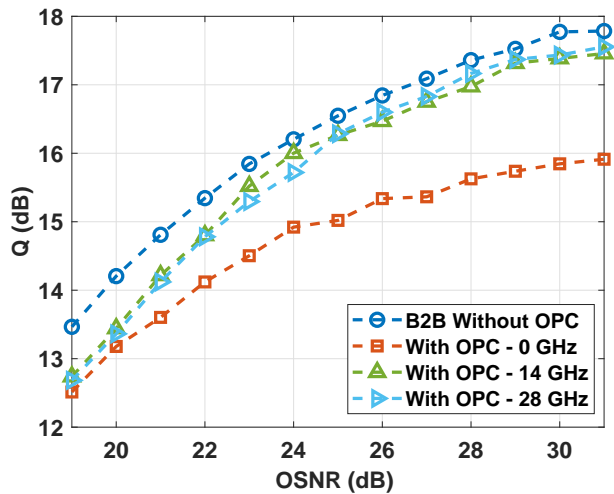


Figure 4.18. The Q-factor as a function of the optical signal to noise ratio (OSNR) without OPC (dark blue circles) and with the OPC at three different frequency separations between the idler and the signal.

4. OPTICAL FIBER PHASE CONJUGATION DEVICE

The difference between the Q-factor for the B2B system without OPC and with OPC at frequency separations (between the signal and the idler) of 14 GHz or 28 GHz is due to the residual dithering transferred from the pumps to the idler which is low (~ 0.5 dB) for a QPSK signal compared with 16QAM. For the case of zero frequency separation between the signal and the idler, the crosstalk from the unwanted original signal on the idler is reducing the performance [220] by around 1.8dB (combined with the dithering) at high OSNR (31dB). This is reduced to less than 1 dB at low OSNR (19dB). The source of this crosstalk is coming from the small extinction ratio PBS (around 28dB) and nonideal orthogonality between the pumps. This extinction ratio is translated in the suppression of the signal by 22dB below the phase conjugated idler as shown in Fig.(4.16c). Improving the PBS extinction ratio can reduce these penalties to very small values [197].

4.3 Conclusions

The design challenges of the OPC device have been discussed. The effect of counter dithering in dual pump OPC on the conjugated signal has been studied and the effect of residual dithering introduces around 2 dB penalties in the Q factor of 30 Gbaud 16QAM signal in high OSNR values. By improving the dithering setup, these penalties are reduced to around 0.5 dB. The design challenges of shift-free dual pump OPC have been investigated with 20nm conjugation bandwidth and the main challenge with this design is the extinction ratio of the PBS which needs to be above 30 dB.

Chapter 5

Experimental Investigation of Nonlinearity in Optical Communication System

In this chapter, the improvement in nonlinearity compensation as a result of improving the power symmetry around the mid-link OPC is investigated experimentally. The power symmetry is achieved in two different ways.

First, in a system with lumped amplification, through using a dispersion element collocated with the OPC which is sometimes called a pre-dispersion. A SSMF span is used after the OPC to do the function of the DE in Fig.(3.1). The theoretical results that is derived in chapter (3) is validated starting with validating Eq.(3.10) that represents the FWM between two or three frequency tones, then an experiment was conducted to show the effect of symmetry improvement through additional dispersion on modulated channels whether single channel or WDM system. Using wideband signal ($\sim 0.56\text{THz}$) transmission, the analytical results are validated for nonlinear noise developed in chapter (3) (Eq.(3.42), Eq.(3.46)) using Eq.(3.57). Eq.(3.42) is derived under the assumption of ideal frequency shift-free OPC (zero insertion penalty) and lossless dispersion element without nonlinear impairments. Eq.(3.57) is modified to consider the nonidealities in the experiment compared with the theory.

5. EXPERIMENTAL INVESTIGATION OF NONLINEARITY IN OPTICAL COMMUNICATION SYSTEM

Second, a single pump backward Raman amplification is used instead of lumped amplification [221] to improve the symmetry around the OPC and get better nonlinearity compensation. Both of the two methods give good nonlinearity compensation, however, the first method will be more efficient for the currently installed lumped amplified links. In the experiment of symmetry improvement through Raman amplification, the first use of mid-link OPC for dispersion and nonlinearity compensation with real-time transceiver through is demonstrated using two OPCs to avoid any frequency shifting and data scrambling due to the conjugation process.

Finally, the impact of dispersion slope on the nonlinear noise for wide-bandwidth signals is investigated and the analysis is verified experimentally [222]. A figure of merit for estimating the required bandwidth is introduced to consider the effect of the dispersion slope in the nonlinearity modeling.

5.1 OPC Symmetry Improvement Through Pre-dispersion

Few experimental demonstrations have been done for the use of DE with OPC to improve the symmetry. 13 km of SSMF has been used to work as a dispersion compensating module (DCM) inserted before the OPC and before the receiver to compensate the nonlinearity and dispersion from the transmission of 10Gbps on-off keying [223] and differential phase-shift keying (DPSK) [224] over 600km of non-zero dispersion-shifted fiber (NZ-DSF). In chapter (3), it has been shown, through mathematical analysis and simulations, the benefit of adding a pre-dispersion element collocated with the OPC to improve the symmetry and developed analytical models to describe the FWM power [53] generated from system with OPC and pre-dispersion then the analysis were developed to get a closed-form expression for the nonlinear noise [196] from this system. This closed-form can be used to estimate the amount of improvement in the nonlinearity compensation from OPC due to the symmetry enhancement. In this experiment, these benefits were proved and the mathematical analysis in chapter (3) was validated experimentally [225] by adding a 75km span with reduced input power, it is shown that such a span enhances the nonlinearity compensation efficiency of the OPC.

5.1.1 Experimental Validation for FWM Expression

Equation (3.10) describes the FWM power from the interactions of three frequencies in a multi-span system employing mid-link OPC with and without DE inserted before or after the OPC with the right dispersion coefficient. The equation has been validated through simulation in section (3.3.1) with the perfect matching between the theory and the simulation results. In this part, the FWM equation (3.10) has been validated experimentally [225] and the benefit of adding a DE with the OPC on the nonlinearity compensation efficiency for a different number of spans is shown.

Experiment Setup

To experimentally validate Eq.(3.10), a 2x100km SSMF lumped amplification system with OPC was built and a 75km span of SSMF was added after the OPC to work as a DE. According to Eq.(3.53), the optimum length for the SSMF after the OPC should be $\approx 78.3\text{km}$. However, Fig.(3.9) shows that a DE with accumulated dispersion close to the optimum pre-dispersion continues to give an improvement in nonlinearity compensation from the OPC [196] with less efficiency. The SSMF has attenuation and nonlinear coefficients 0.2 dB/km and 1.3 (W.km)^{-1} respectively. The experiment setup is shown in Fig.(5.1) where the FWM power generated from two CW lasers was measured with 9dBm power launched into the fiber. The FWM power was measured as a function of the frequency separation between the two lasers using a high resolution (150MHz) OSA. The signal has been conjugated through a polarization-insensitive dual-band OPC [127] as described in detail in chapter (3).

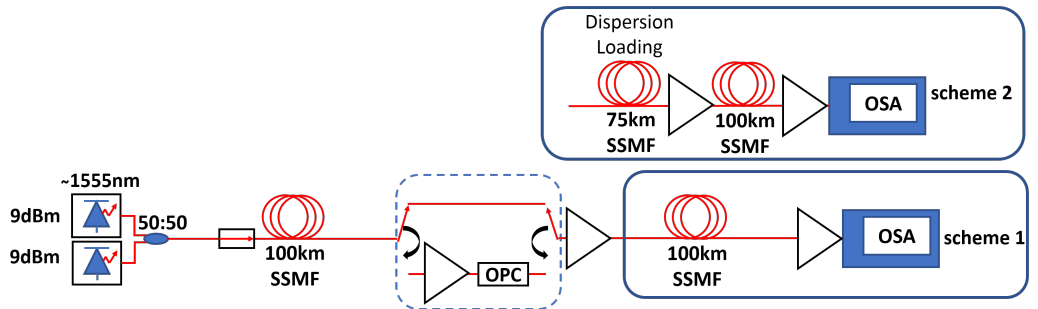


Figure 5.1. Experimental setup of a discretely amplified system with dual pump OPC for measuring the FWM power.

5. EXPERIMENTAL INVESTIGATION OF NONLINEARITY IN OPTICAL COMMUNICATION SYSTEM

Results and Discussion

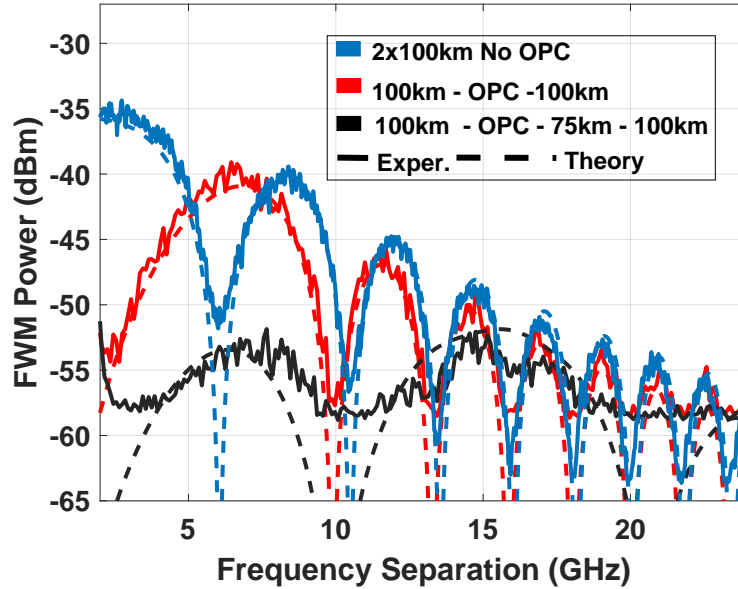


Figure 5.2. FWM Power as a function of frequency separation between two CW lasers propagating through 2x100 km of SSMF without and with mid-link OPC, with OPC and DE. Exper.: Experiment.

Figure (5.2) shows the FWM power, as a function of frequency separation, generated from the interaction between the two CW lasers as they propagate through the different systems. Figure (5.2) represents the FWM power for 2x100km spans without OPC (blue curve), 2x100km spans with mid-link OPC (red curve), and the black curve represents the response of 2x100km with OPC and DE (75km span) deployed after the OPC (see scheme 2 in Fig.(5.1)). To ensure that the nonlinearity generated in the DE (75km span) is not affecting the nonlinearity compensation efficiency, the input power has been decreased to the 75km span to 0dBm (9dB lower than the launched power to the 100km spans). The results show that adding the OPC (without the DE, 200km link) has suppressed the FWM power by ~ 5 dB for the strong phase-matched region (first lobe) and that improvement starts to diminish with increasing the phase mismatch (higher frequency separation). By deploying the DE (75km span), it can be seen that the OPC has improved the nonlinearity compensation efficiency by around 18 dB compared to the 2x100km without OPC (i.e. 13dB over the system with OPC and no DE element). Theoretical results are plotted on the same figure as dashed lines using Eq.(3.10) (red and black curves) and using the

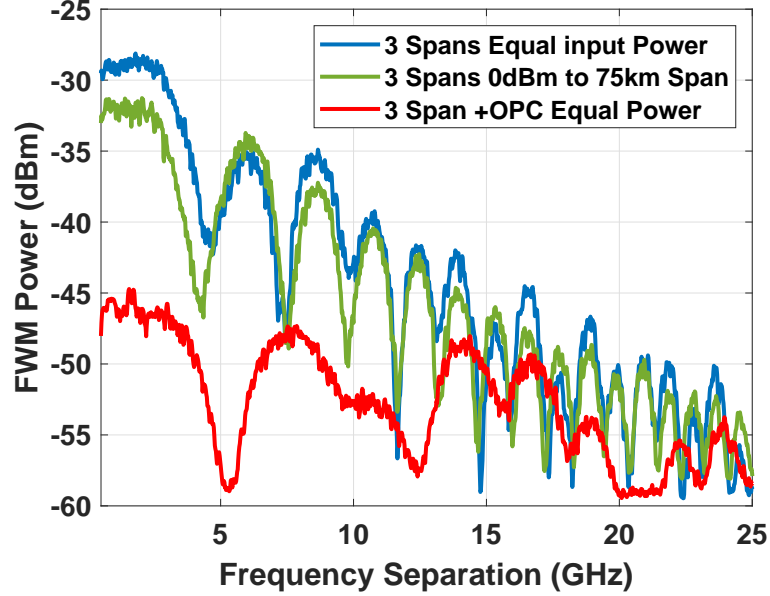


Figure 5.3. FWM power as a function of frequency separation between two CW lasers propagating through 275km, with and without OPC and all the spans has the same input power (9dBm), without OPC and the 75km span has low input power (0 dBm).

conventional FWM equation (3.43) [56] of multi-span for the blue curve. The results show that there is a good match with the experimental results. A small difference between experiment and theory is observed for the system with both OPC and DE which is believed is due to additional FWM from the 75km span and from the effect of the ASE noise generated from the added amplifier. This small nonlinearity from 75km is observable even with the decrease in the launch power of 9dB due to the reduction in FWM from the 100km spans induced by the dispersion loaded OPC.

This is explored more fully in Fig.(5.3) which shows the FWM power as a function of the frequency separation for three different configurations of 275 km (2x100km+75km)(see scheme 2 in Fig.(5.1)). Firstly, without OPC (green) with the power launched into the 75km span equal to 0 dBm. Secondly, without OPC also (blue) but with 9dBm launched power in 75km. It can be seen that the FWM power has increased by ~ 3 dB (compared with the green curve) due to the increased power in the 75km span. Finally, three spans system with OPC and increased input power (9 dBm) to the 75km span (red). Comparing this red curve to the black curve in Fig.(5.2) reveals the additional nonlinearity from the 75km span. It is clear that

5. EXPERIMENTAL INVESTIGATION OF NONLINEARITY IN OPTICAL COMMUNICATION SYSTEM

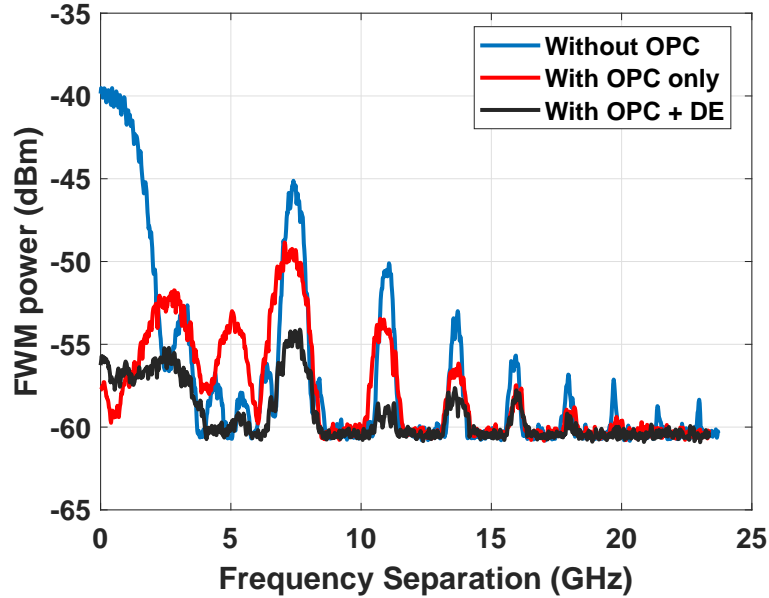


Figure 5.4. FWM Power as a function of frequency separation between two CW lasers propagating through 6x100 km of SSMF without and with Mid-link OPC, with OPC and DE (75km span).

the compensation efficiency provided by the OPC was decreased to 10 dB due to the excess nonlinearities generated within the DE element (75km of SSMF). However, operation in the dispersion loading scheme still gives a good reduction in net mixing efficiency of at least 8 dB when compared to either the 2 spans (200km) system or the three spans (275km) system without OPC. In Fig.(5.4), the number of spans were upgraded to 6 spans and the measurements are taken in the three cases, without OPC (blue curve), with OPC only (red curve) and with OPC followed by the DE (75km span)(black curve) and with the same input power for all the spans, it can be seen that the improvement from DE with OPC is around 5 dB over the system with OPC only. This confirms that this method can be used either by decreasing the input power to the 75km span and get only the dispersion effect from the DE and sacrificing some OSNR performance due to power reduction or using the same power in all the spans with less improvement in nonlinearity compensation due to the additional nonlinearity from the DE as shown in Fig.(5.4).

5.1.2 Nonlinear Noise Compensation Using Pre-dispersion

Improving the symmetry using pre-dispersion can lead to better improvement in the nonlinearity compensation using the OPC as shown through mathematical analysis and simulation in Chapter (3) and experimentally using CW laser signals in the experiment presented in section (5.1). In this experiment, the work in section (5.1) is extended to the transmission of modulated signals over different number of spans using a single channel and WDM multiplexed signal.

Experiment Setup

Figure (5.5) shows the schematic of the experimental setup of a back-to-back (B2B) measurement of 30 Gbaud PM-16QAM signal with and without the OPC to show the insertion penalty of the OPC.

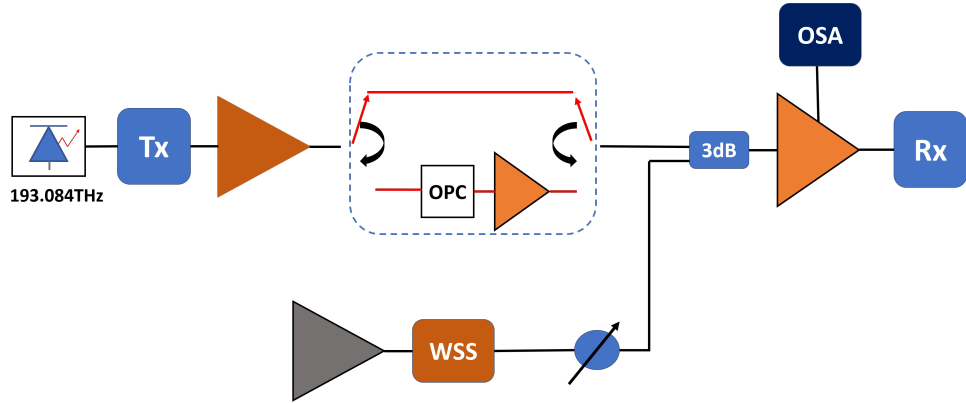


Figure 5.5. Experimental setup of back-to-back measurement of single-channel 30Gbaud PM-16QAM with and without the OPC.

A CW-laser tuned at 193.084 THz was modulated using a dual-polarization optical IQ modulator (Tektronix OM5110) derived by four electrical signals that were generated from four digital to analog converters (DACs) of 56 GSa/s arbitrary waveform generator (AWG - Keysight M8195A). The DACs input signal is coming from a pseudo-random bit sequence (PRBS) of $2^{15}-1$ were encoded and mapped to PM-16QAM symbols. In addition, a root-raised cosine filter with a roll-off factor of 0.1 was used inside the AWG for pulse shaping. The raw data rate for the single-channel is 240Gbits/s. The AWG decorrelates the generated symbols of the two polarizations by adding a delay of 4096 symbols.

5. EXPERIMENTAL INVESTIGATION OF NONLINEARITY IN OPTICAL COMMUNICATION SYSTEM

The OPC used in this experiment was described in detail in section(4.2). A single band from

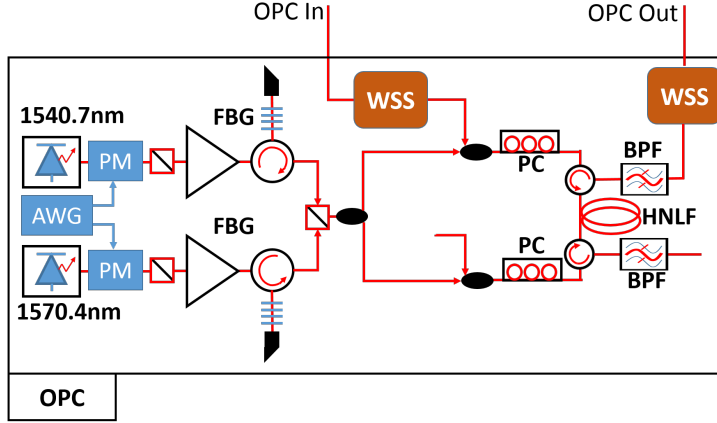


Figure 5.6. OPC setup with dual pump. PM: polarization maintaining coupler. WSS: wavelength selective switch

the polarization-insensitive dual-band OPC described is used in Fig.(4.8) as shown in Fig.(5.6). A WSS is used at the input of the OPC to remove the out of band noise and hence improve the conversion efficiency of the conjugation. In addition, an EDFA was used after the OPC to compensate for its insertion loss ($IL \approx 20\text{dB}$). An EDFA was used as an ASE source then the ASE spectrum was shaped and flattened using a WSS. A variable optical attenuator was used to control the ASE noise level then combined with the signal and amplified at the input of the coherent receiver. The OSA is connected to the monitor port of the EDFA.

The coherent receiver consisted of a polarization diversity 90-degree hybrid (Tektronix OM4245), a local oscillator (LO), four balanced photodiodes, 70GHz, 100GSa/s real-time oscilloscope (Tektronix DPO77004SX) (work as analog to digital converter (ADC)) and offline digital signal processing processed in Matlab (Tektronix OMA). First, FIR filter was applied to eliminate out of band noise, then the dispersion (or residual dispersion when using the OPC) is compensated by applying the mathematical model $H(\omega) = e^{j\beta_2\omega^2/2}$ for the received samples in the frequency domain. Then clock recovery is used to interpolate the clock frequency of the ADC. After that, an adaptive (least mean square) filter that uses radius directed algorithms (with 15 taps) is used to de-multiplex the two polarizations. Finally, the frequency and phase DSP stage is used to estimate and compensate for the frequency offset and the phase noise. The value of dispersion

5.1 OPC Symmetry Improvement Through Pre-dispersion

compensated in the DSP was dependent on the system setup (number of spans) and whether a mid-link OPC was used in the link or not. With the OPC system, the DSP compensates for the residual dispersion resulted from the dispersion slope or the dispersion from the 75km span. The receiver then calculates all the parameters that quantify the received signal quality, such as BER (from the decoded bit sequence) and EVM (from the constellation). The SNR is used over all the thesis to match the theoretical results whenever possible. The results are shown for the average performance over the two polarizations and the difference in the SNR of the two polarizations is less than 0.6 dB for all the results. The SNR is calculated from the BER using Eq.(3.63) and the OSNR is measured at 0.1-nm resolution bandwidth using the OSA.

Figure (5.7) shows the B2B measurement of the SNR as a function of the OSNR. OPC insertion degrades the SNR with different values as the signal pass through the OPC. In low OSNR, this penalty is small (around 0.4 dB) because the ASE is dominant. However, at high OSNR, it increases to reach around 1 dB. This degradation in performance is due to different impairments in the OPC such as residual transferred phase from the phase-modulated pumps to the idler, and the nonlinear impairments from Kerr nonlinearities in HNLF (XPM or FWM).

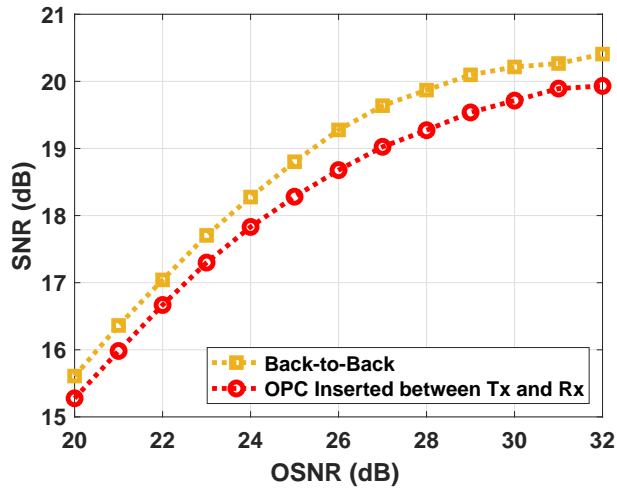


Figure 5.7. Signal to noise (SNR) ratio as a function of the optical signal to noise ratio (OSNR) in back-to-back measurement of single-channel 30 Gbaud PM-16 QAM signal with or without the OPC.

Next, the transmission setup shown in Fig.(5.8) was built for nonlinearity compensation with

5. EXPERIMENTAL INVESTIGATION OF NONLINEARITY IN OPTICAL COMMUNICATION SYSTEM

or without symmetry improvement. The transmission link contains N spans with span length 100km of SSMF ($\alpha = 0.2$ dB/km, $D = 17$ ps/nm/km). An EDFA is used at the end of each span to compensate for the span loss. The number of spans was changed from 2 spans to 4, 6 or 8 spans. In order to improve the power symmetry in the link, a 75km was added after the OPC to work as a dispersion element. All the measurements are done in three cases, 1) without OPC and with attenuator to represent the IL of the OPC (blue triangles in the results). 2) with OPC only connected in the middle of the link (red circles). 3) with OPC followed by an additional 75km span work as a dispersion element (yellow squares) as discussed in chapter (3). The SNR is measured from the error bits counting through using Eq.(2.41).

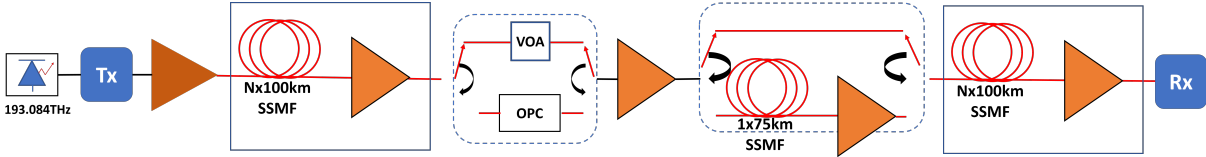


Figure 5.8. Experimental setup of single-channel transmission over a different number of spans in different scenarios of a discretely amplified system with dual pump OPC.

The measurements were started with 2 spans of 100km for the three cases described above. Figure. (5.9) shows the SNR as a function of the total launch power in the spans. In the linear regime, it can be seen that the system without OPC has a better performance than the system with OPC and this is due to the impairment added by the OPC device in the link. For the nonlinear region, the OPC alone adds a small improvement in the SNR by around 0.9 dB (measured at launch power of 12 dBm).

This improvement in the performance (due to the nonlinearity compensation using the OPC) has increased significantly by enhancing the symmetry by adding the 75km span to shift the nonlinear effective region. About 3 dB improvement in the SNR can be noticed at the highly nonlinear region (measured at 12 dBm launched power) compared with the system with OPC only and 4 dB compared with the system without OPC. The performance of the system without OPC at the optimum launch power is better than the system with OPC due to the penalties generated from the OPC device. However, for long haul link, it is expected that the noise from the link will exceed the penalties from the OPC. To minimize the nonlinearity added by the 75km

5.1 OPC Symmetry Improvement Through Pre-dispersion

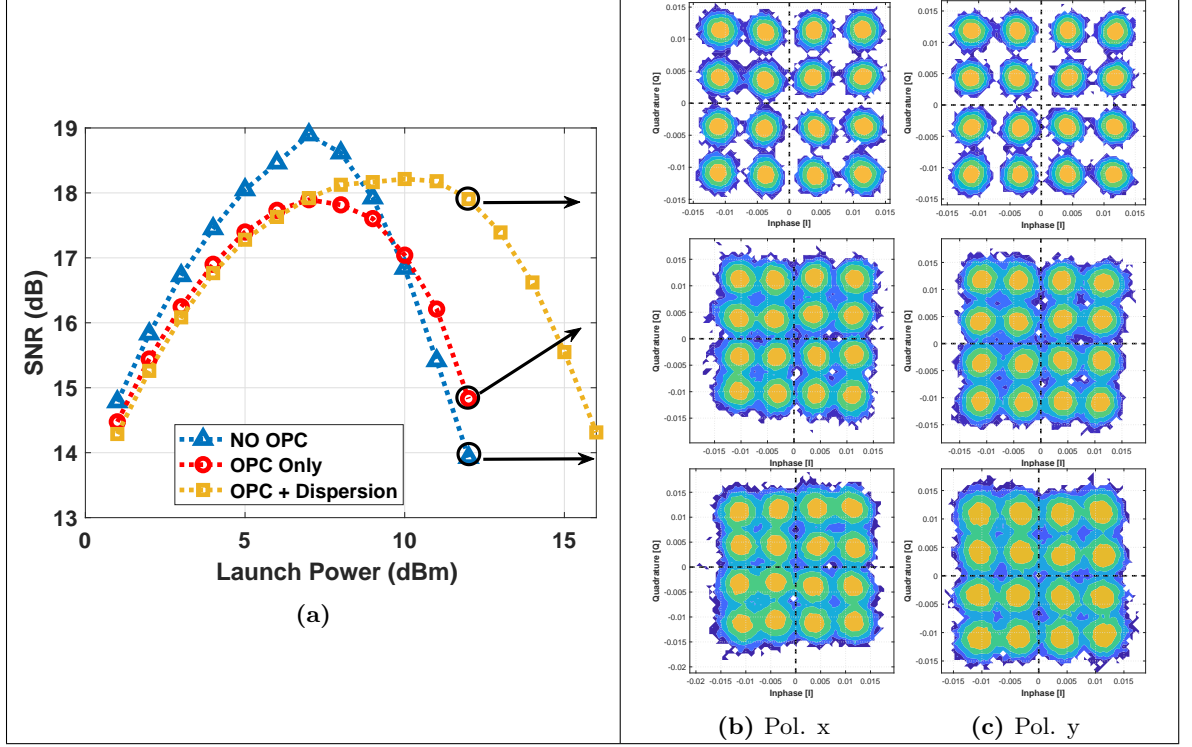


Figure 5.9. The signal to noise ratio (SNR) of 30 Gbaud PM-16QAM channel transmitted over 2x100km as a function of the total launched power in three cases: Without OPC (blue triangles), with OPC only (red circles) and with OPC and added dispersion (yellow squares). b,c) The constellation diagram for Polarization X and Y at 12dBm for the three cases.

span, the launch power was set in the transmission spans to 11dBm, then the launched power was swept in the 75km span and the SNR of the signal is measured at the Rx. Figure (5.10) shows the SNR as a function of the launched power in the 75km span. The additional 75km span degrades the SNR by small value (less than 0.15 dB) in the linear regime compared with the system with OPC only. It is clear that if the 11 dBm launched power in the transmission spans is used, the SNR will be degraded by around 0.6 dB. Therefore, the launched power was fixed in the 75km span to 7 dBm to avoid any additional nonlinearity from the span and this value is used in measuring the results in Fig.(5.9), Fig.(5.11), and Fig.(5.16).

5. EXPERIMENTAL INVESTIGATION OF NONLINEARITY IN OPTICAL COMMUNICATION SYSTEM

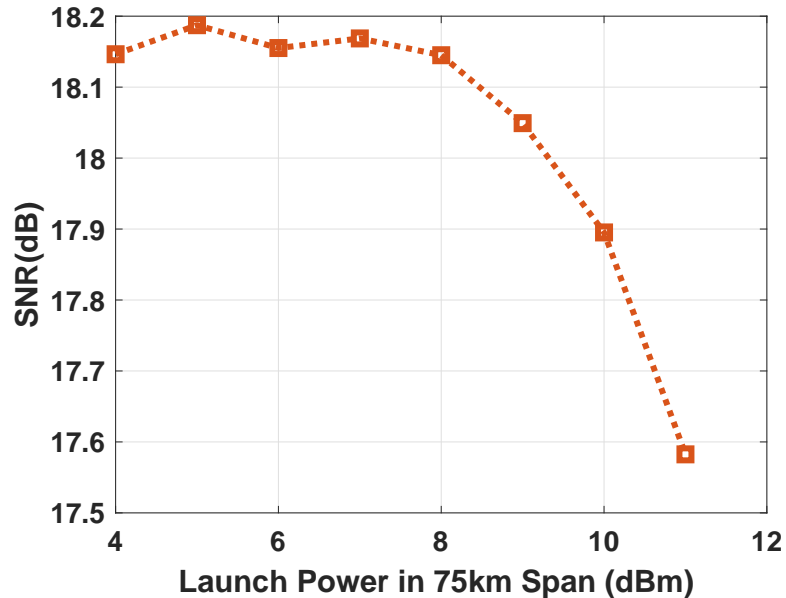


Figure 5.10. The signal to noise ratio (SNR) of 30 Gbaud PM-16QAM channel transmitted over 2 x 200km spans and a 75 km span after the OPC as a function of the total launched power in the 75km span after the OPC with the optimum power launched in the other 2x100km spans.

The same conclusion can be drawn from the constellation diagrams shown in Fig.(5.9) plotted from the received symbols at total launched power 12dBm. While the constellation points overlapping in the system without OPC or with OPC only, there some clear gaps between the constellation points in the case of the added dispersion with the OPC that improved the nonlinearity compensation.

The previous measurements were repeated for three different number of spans (4, 6, and 8 spans), the results are shown in Fig.(5.11).

5.1 OPC Symmetry Improvement Through Pre-dispersion

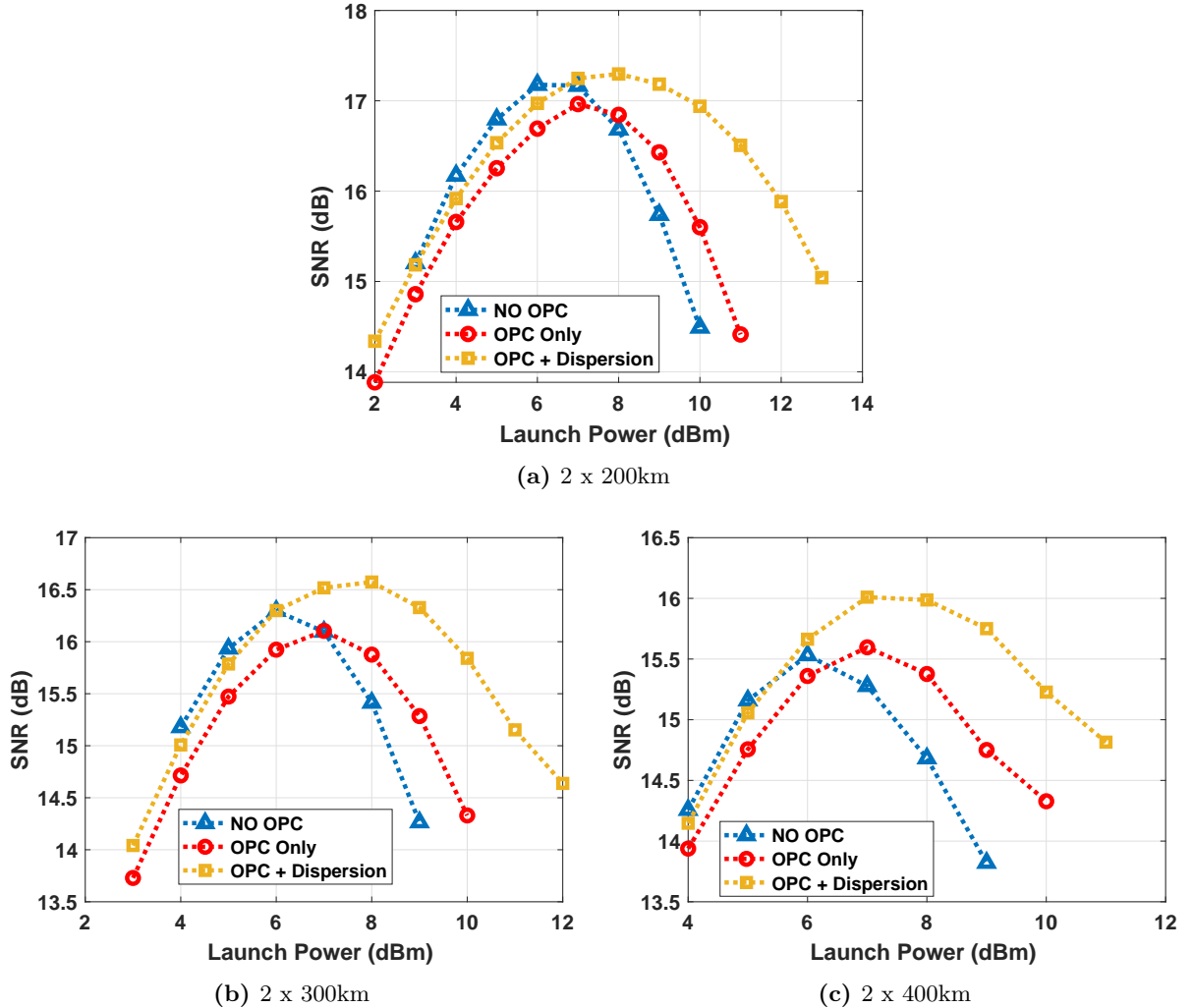


Figure 5.11. The signal to noise ratio (SNR) of 30 Gbaud PM-16QAM channel transmitted over a different number of spans as a function of the total launched power in three cases: Without OPC (blue triangles), with OPC only (red circles) and with OPC and added dispersion (yellow squares).

Figure (5.11) shows that the nonlinearity compensation with OPC only has increased slightly and this because the nonlinearity has increased with increasing the number of spans where more nonlinearity will allow more compensation. The OPC is compensating some SPM nonlinearities (as a single channel only is transmitted) even with the low symmetry in the link. The compensation should be increased slightly with increasing the nonlinearity in the link. This is in a match with the theoretical and simulation results shown in Fig.(3.5) where the OPC only show a high level of compensation at low-frequency separation where the phase matching is high. There is

5. EXPERIMENTAL INVESTIGATION OF NONLINEARITY IN OPTICAL COMMUNICATION SYSTEM

a still improvement due to the additional dispersion (75km span) by around 1dB (measured at 10dBm launched power).

In order to investigate the performance of the system with the nonlinear impairments associated with multiple channels (such as XPM and FWM) and also, to validate the theoretical results (Eq.(3.42)) for nonlinear noise which was derived under the assumption of large bandwidth, the transmitter side were upgraded to WDM multiplexing system. Fig.(5.12) shows the transmitter side and receiver side for the WDM system.

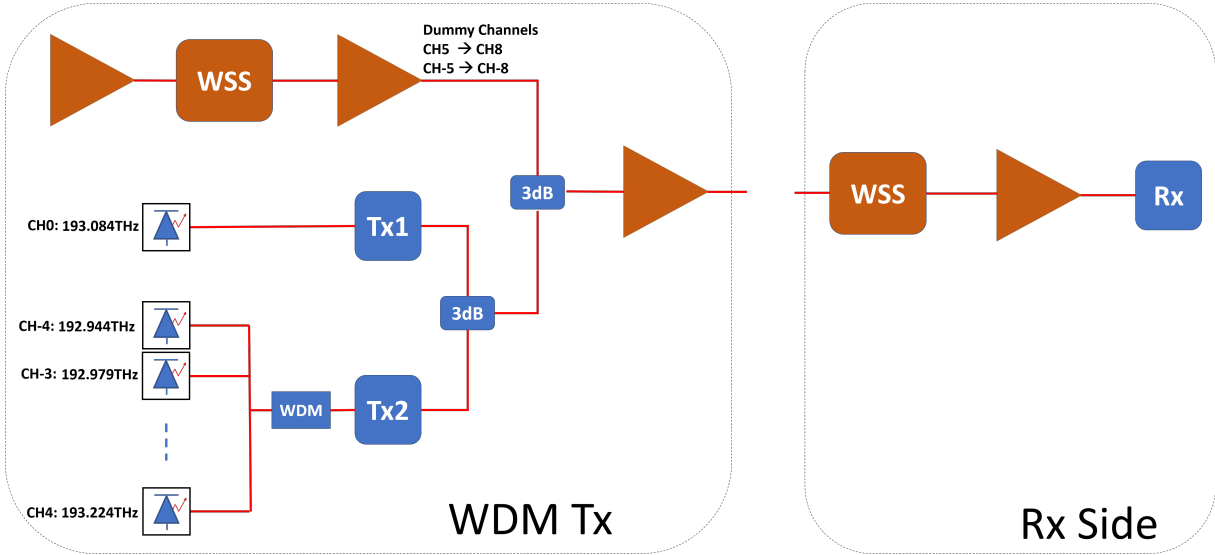


Figure 5.12. WDM signal transmitter and receiver side setup. WDM: polarization maintaining wavelength division multiplexer 3dB: 3dB coupler. WSS: wavelength selective switch

Eight C-band lasers were operating on a 35GHz grid extending from 192.944 THz to 193.049THz (CH-4 to CH-1) and from 193.119 to 193.224THz (CH1 - CH4) and combined using PM-WDM coupler. The 8 Lasers were modulated using another dual-polarization optical IQ modulator (Tektronix OM5110). The IQ modulator was derived by the other 4 ports of the AWG described above and included in Fig.(5.8). The 8 WDM modulated channels with 30 Gbaud PM-16QAM were multiplexed with the output of transmitter 1 (Tx1) which was used in single-channel transmission. A WSS was used to shape and flatten the ASE spectrum produced by an EDFA to generate 8 dummy channels to emulate real channels [226], then the 8 dummy channels were amplified by another EDFA. The dummy channels are multiplexed with the real channel

5.1 OPC Symmetry Improvement Through Pre-dispersion

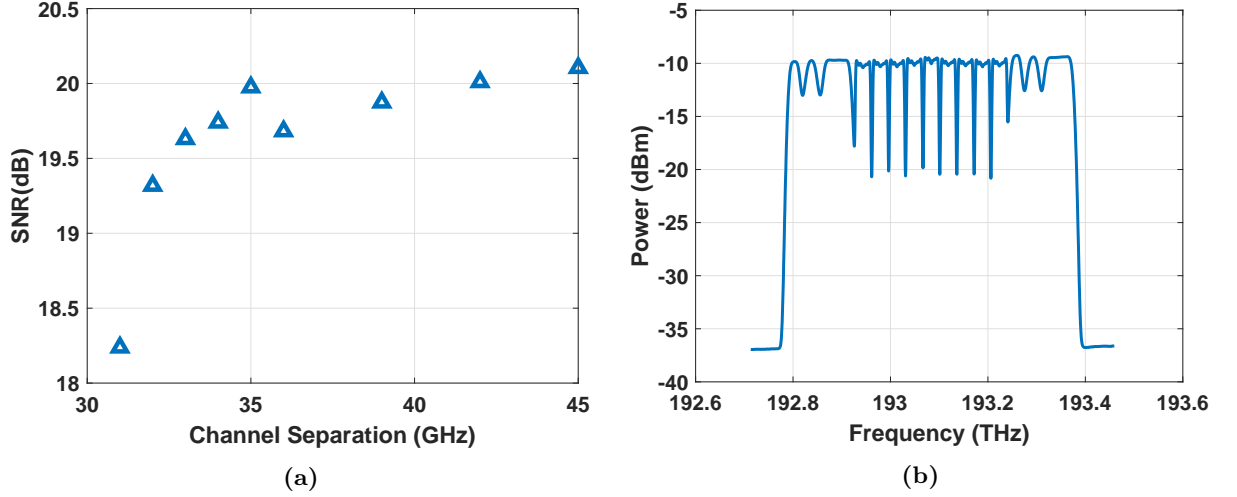


Figure 5.13. (a) The signal to noise ratio (SNR) of 30 Gbaud PM-16QAM central channel of 17 WDM channels in back to back measurement as a function of the frequency separation between the center of the channels. (b) The spectrum of transmitted WDM channels.

using 3 dB coupler and amplified using another EDFA before transmission. The dummy channel EDFA was used to make all the channels level are the same as the modulated channels level. In the beginning, the channel separation were swept in B2B (Tx connected directly to the Rx) to choose the optimum channel separation without sacrificing the performance. Fig.(5.13a) shows the back-to-back SNR of the central channel as a function of the frequency separation between the channels at 27dB OSNR. There is a significant penalty when the channels are very close then it decreases with increasing the channel separation. 35GHz channel separation was chosen as the optimum point. Fig.(5.13b) shows the transmitted 17-WDM channels spectrum (0.1nm OSA resolution) with total bandwidth 590GHz. On the receiver side, a WSS was used as OBPF to select the channel under test (the central channel) which amplified using an EDFA before the Rx.

Again, the B2B measurements shown in Fig.(5.7) were repeated but with the WDM channels to check if there are additional penalties for the insertion of the OPC with the WDM system. Figure(5.14) shows the SNR as a function of the OSNR for the central channel of the 17 WDM channel. The results are similar to the single-channel B2B measurements shown in Fig.(5.7).

5. EXPERIMENTAL INVESTIGATION OF NONLINEARITY IN OPTICAL COMMUNICATION SYSTEM

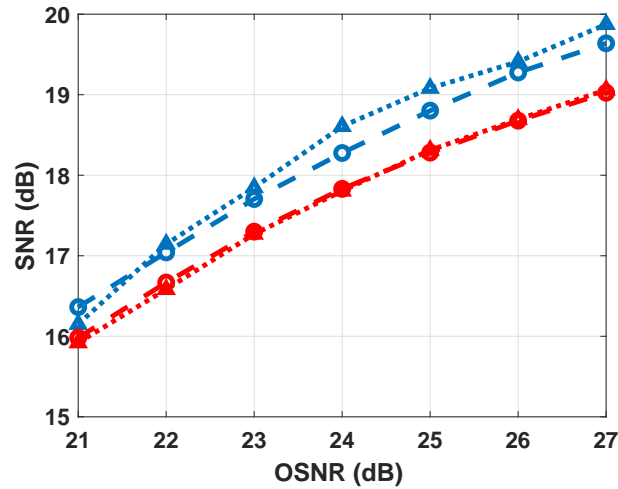


Figure 5.14. The signal to noise ratio (SNR) of the single channel (circles) and the central channel of 17 WDM channels (triangles) as a function of the optical signal to noise ratio (OSNR) in back-to-back measurement with (red) or without the OPC inserted (blue).

Next, the 17 WDM modulated signals were transmitted over 6 spans of 100km SSMF and the measurement is done for the central channel in the three cases, with attenuator to represent the OPC insertion loss, with OPC only, and with OPC and the 75km span.

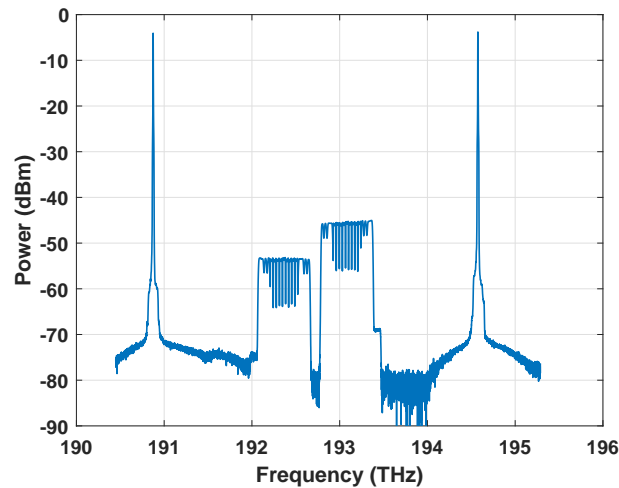


Figure 5.15. The spectrum of OPC output after the HNLF and before filtering the pumps or the signal.

Figure.(5.15) shows the spectrum (0.1nm OSA resolution) of the WDM signal at the output of the OPC monitoring (1% coupler). The conversion efficiency is around -7 dB and it is

5.1 OPC Symmetry Improvement Through Pre-dispersion

measured as the ratio of the conjugate power when the pumps are on to the signal power when the pumps are off.

Figure (5.16) shows the experimentally measured (markers) and analytically fitted (dashed lines) SNR as a function of the total launched power in three cases, with fixed attenuation (represents the insertion loss of the OPC) and amplifier (Blue Triangles), with mid-link OPC only (red circles), and with OPC and additional 75km span to improve the nonlinearity compensation through enhancing the power symmetry (yellow squares).

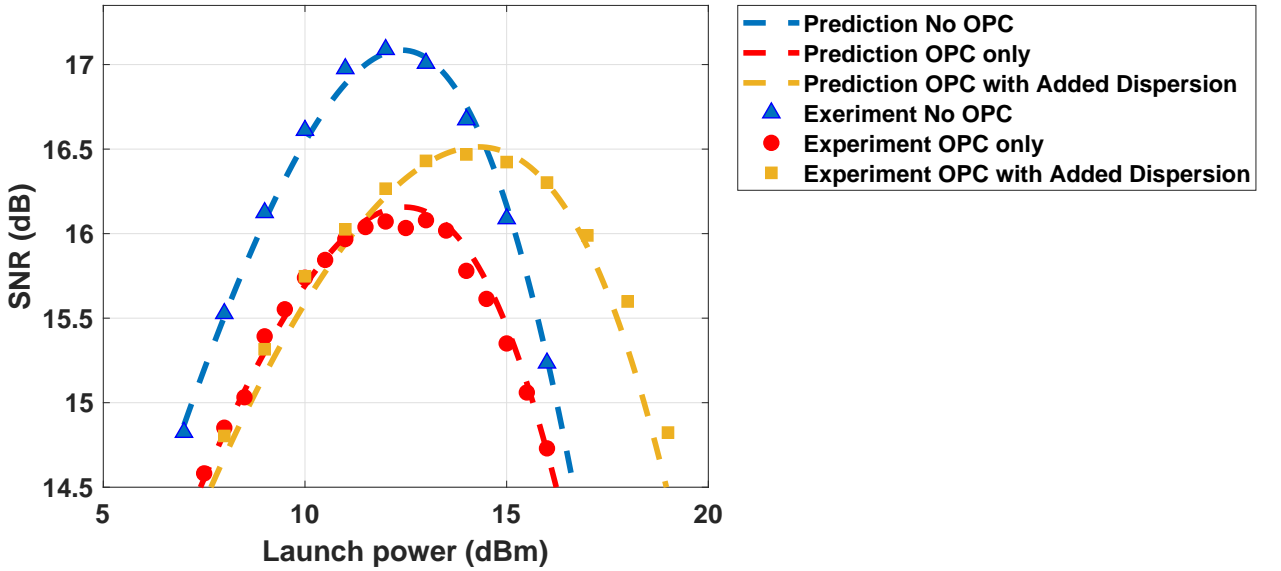


Figure 5.16. The signal to noise ratio (SNR) of the central channel of 17 WDM channels transmitted over different 2 x 300km spans as a function of the total launched power in three cases: Without OPC (blue triangles), with OPC only (red circles) and with OPC and added dispersion (yellow squares).

The dotted curve was plotted using a modified version from Eq.(3.57) by considering the transceiver SNR limit (Fig.(5.7)), the total ASE noise from the link, the ASE noise from the OPC, and the nonlinear noise from the link. The SNR can be written as,

$$SNR = \frac{I}{\frac{I}{SNR_{Tx}} + I_{ase} + I_{OPC} + I_{NLN} + I_{N75}} \quad (5.1)$$

where I is the total launched power spectral density $I = \frac{P}{B}$, where P is the total launch power and B is the total WDM signal bandwidth (595 GHz). SNR_{Tx} is the maximum achievable SNR

5. EXPERIMENTAL INVESTIGATION OF NONLINEARITY IN OPTICAL COMMUNICATION SYSTEM

by the transceiver in a back-to-back configuration. It is extracted from Fig.(5.7) and it is about 20.4 dB without the OPC insertion penalty and 19.9 dB with the OPC insertion penalty. I_{ase} is the ASE PSD noise defined in Eq.(3.58) with EDFA noise figure 5 dB, I_{OPC} is assumed roughly to improve the theoretical matching with the experimental results, and I_{NLN} is the nonlinear noise from the link defined in the theoretical model in Eq.(3.46) for the system without OPC, and Eq.(3.47) for the system employing OPC with the fiber parameters mentioned below. I_{N75} is the nonlinearity from the 75km span which can not be ignored in the WDM system and it is calculated using Eq.(3.46) with $N = 1$ and the same fiber parameters of the other spans and launch power 10 dBm. The parameters used in the theoretical predictions were $\gamma = 1.3$ /dB/km, $\alpha = 0.2$ dB/km, and $D = 17$ ps/nm/km. For the system without OPC (blue line), I_{N75} and I_{OPC} are set to zero.

Using the mid-link OPC only in that lumped amplification system without any power symmetry improvement does not give any improvement as the inter-channel nonlinear effects are dominant in the WDM system. The symmetry improvement allowed around a 2 dB increase in the allowable launched power (at SNR of 15dB). In the linear regime, the penalty from the OPC is around 1 dB in the high OSNR and decreases to less than 0.5 dB in the low OSNR in agreement with the B2B measurements in Fig.(5.14). There is a good agreement between the theoretical predictions and the experimental results.

The constellations digram in Fig.(5.17) shows the nonlinearity compensation due to the improved symmetry as clear space between the constellation points compared with the overlapped constellation points due to the excess nonlinearity either in system without OPC or with OPC only.

The lower enhancement in nonlinearity compensation of WDM signals in the OPC system with additional dispersion compared with the single-channel system maybe belongs to the additional nonlinearity from the 75km span with WDM system. Using a broadband FBG for adding dispersion can lead to a better performance close to the theoretical results shown in Chapter (3) where the FBG adds the required dispersion without significant attenuation or inducing nonlinear effects compared with the SSMF or DCF [227].

5.1 OPC Symmetry Improvement Through Pre-dispersion

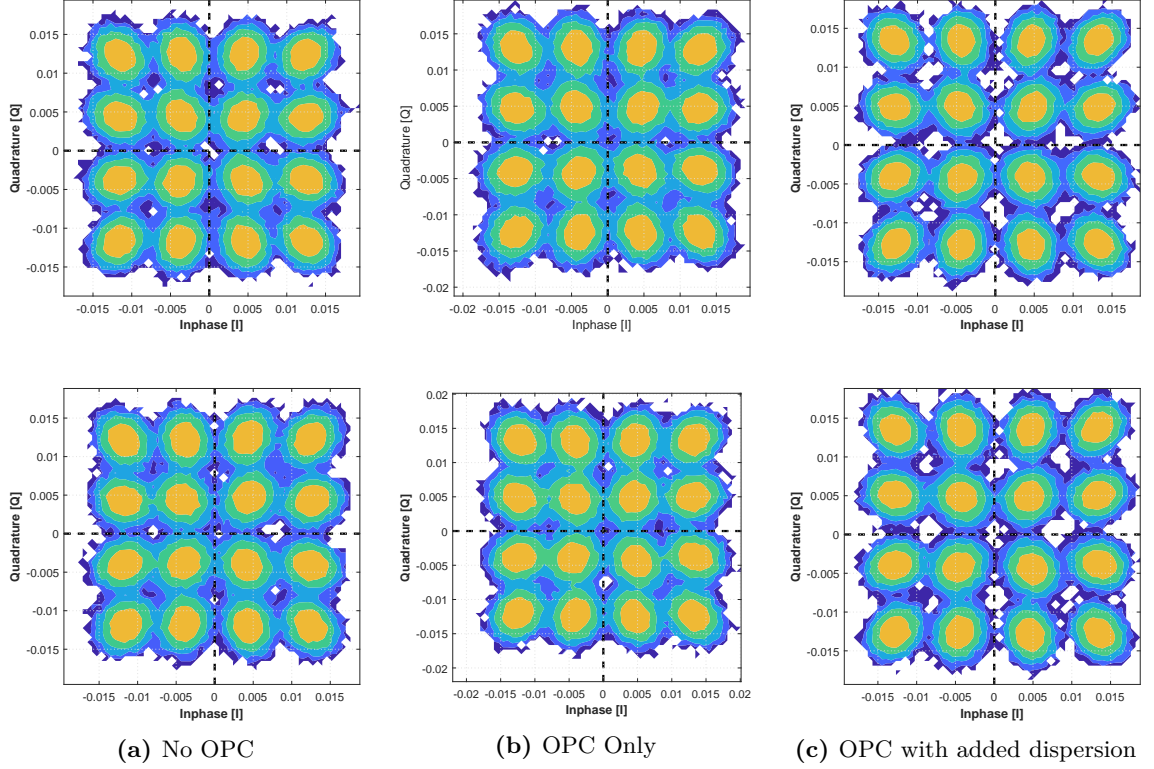


Figure 5.17. The constellation diagram of the symbols of the received central channel at total launch power of 16dBm : (a) without OPC , (b) with OPC only and (c) with OPC and added dispersion.

Figure (5.18) shows the optimum SNR for the different channels in the system with OPC only and with OPC plus additional dispersion, the fluctuations in the SNR between the channels is around 0.3 dB and the results in Fig. (5.18) confirm the compensation improvement presented in Fig.(5.16). The overlapping between channel 4 and the neighbour dummy channel degraded its performance.

5. EXPERIMENTAL INVESTIGATION OF NONLINEARITY IN OPTICAL COMMUNICATION SYSTEM

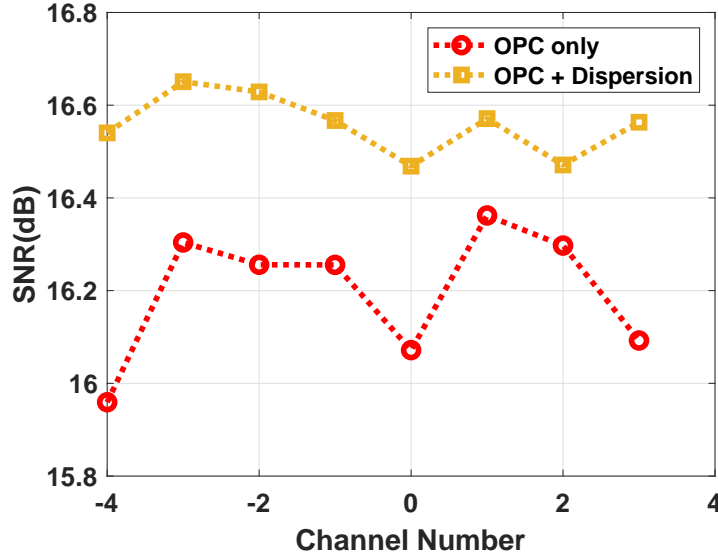


Figure 5.18. The optimum signal to noise ratio (SNR) of the different channels of 17 WDM channels transmitted over different 2 x 300km spans in two cases: with OPC only (red circles) and with OPC and added dispersion (yellow squares).

After that, the dispersion span length after the OPC was swept with using a different number of spans (25km, 50 km, 75km, and 100km). Figure (5.19a) shows the SNR as a function of the total launch power for different lengths of dispersion element. The results show that adding a dispersion after the OPC less than the optimum value can lead to some improvement (0.3 dB at the optimum launch power), however, the highest performance occurs when using a dispersion close to the optimum value. However, using a span length (100km) longer than the 75km span length (green curve) degrades the performance to less than the performance of the system with OPC only (blue curve).

To ensure that the improvement in the nonlinearity compensation by the mid-link OPC is due to the additional dispersion element collocated with the OPC to enhance the symmetry and is not due to the location of the OPC in the link, 3 spans before the OPC were used and 4 spans after the OPC then the same total launched power was set in all the spans. Fig.(5.19b) shows the SNR of the central channel of 17 WDM channels as a function of the total launch power in 7 (3+4) spans (blue curve) and the SNR in Fig.(5.16) is for a system of 6 span (3+3) and additional 75km span after the OPC (yellow curve). The results show that adding extra span after the OPC does not give an improvement in symmetry and then in nonlinearity compensation.

5.2 Real Time Nonlinearity Compensation Using OPC with Raman Amplification

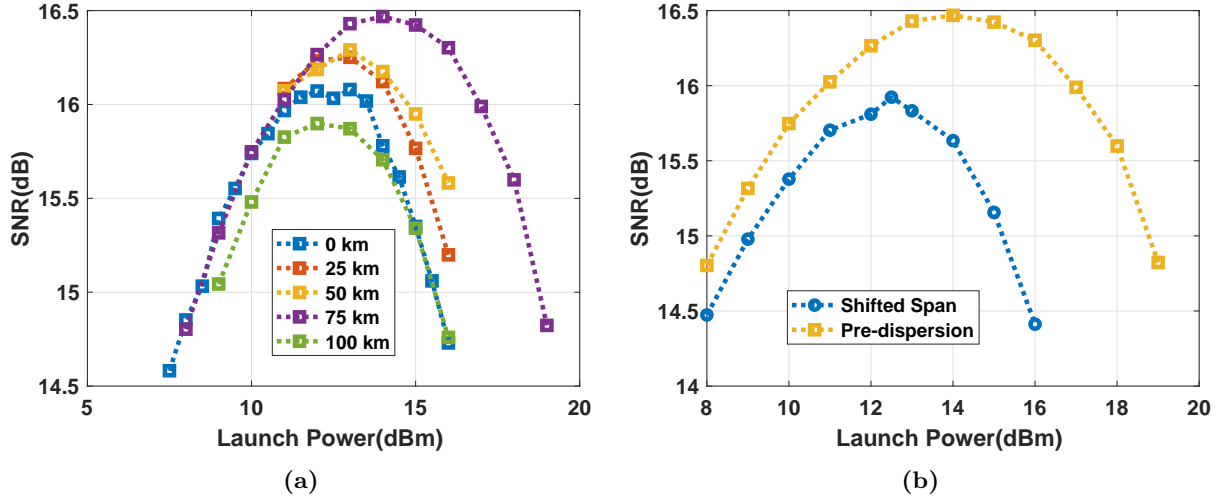


Figure 5.19. The signal to noise ratio (SNR) of the central channel of 17 WDM channels transmitted over different 2 x 300km spans as a function of the total launched power in two cases: (a) different added dispersion span lengths. (b) 75 km added dispersion span and an additional 100 km span.

5.2 Real Time Nonlinearity Compensation Using OPC with Raman Amplification

The OPC has two main features, It compensates the nonlinear impairments for all transmitted channels using the same device and next, it compensates it in real-time without additional complexity at the receiver compared with the digital approaches [68]. OPC has been tested successfully with a WDM system [127, 132, 208, 228] where reasonable power and dispersion symmetry around the OPC has been implemented. However, whilst a limited level of digital nonlinearity compensation has been implemented for certain commercial transponders [229], real-time processing feature of the OPC has not been tested yet, because firstly the frequency shifting accompanying phase conjugation process results in different transmitter and the receiver operating frequencies, and secondly because of the data scrambling inherent in the conjugation process. In this experiment, It is demonstrated that the use of two optical phase conjugations enables real time (commercial) transponders to be deployed without any modification. The cascaded phase conjugations are implemented using the two different waveband inputs of a previously reported dual-band OPC [127], which simultaneously eliminates the residual phase conjugation and achieves the consistency of the wavelengths in the transmitter and the receiver.

5. EXPERIMENTAL INVESTIGATION OF NONLINEARITY IN OPTICAL COMMUNICATION SYSTEM

Effectively, the signal input in one band is used as a conventional mid-link OPC, and the other signal input for the other band is used to convert the conjugated signal to the original signal as an end-link OPC before the receiver.

5.2.1 Experiment Setup

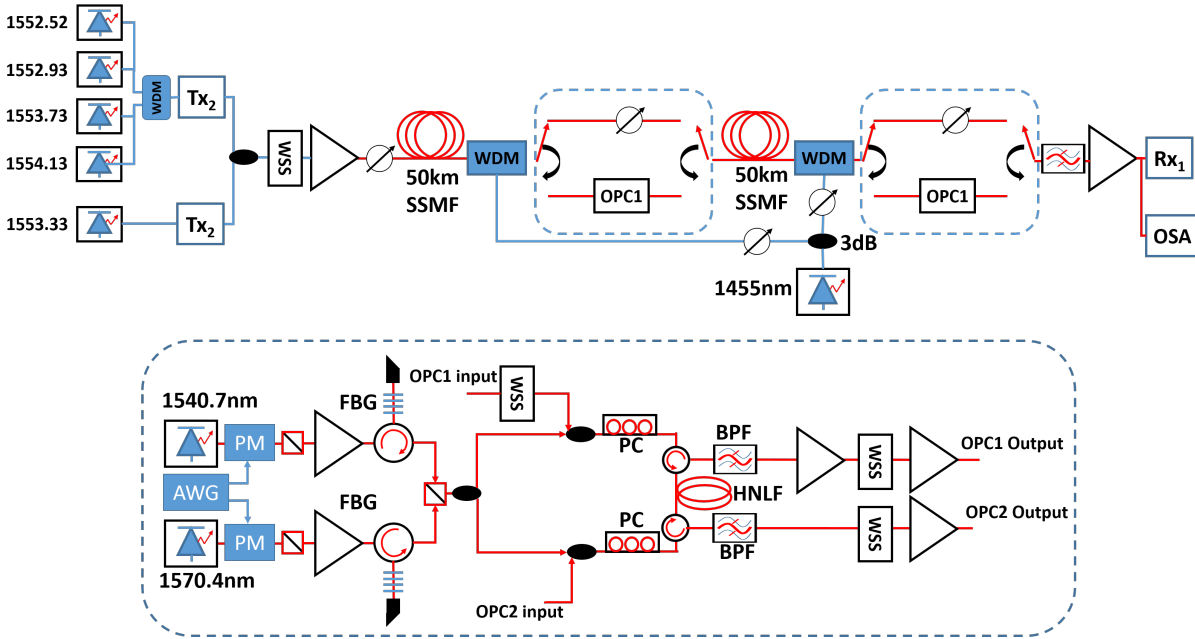


Figure 5.20. Experimental setup of five channels transceivers over 2x50km SSMF spans pumped by a first-order pump laser at 1450nm using a dual-band OPC

Figure (5.20) shows the system setup which includes the DP-QPSK commercial real-time transponders (Ciena WaveLogic 3), a dual-band OPC, and 2x50km SSMF first-order backward-pumped link. Four narrow-linewidth ($<100\text{kHz}$) lasers ranging from 1552.52nm to 1554.13nm spaced at 50GHz were combined before being injected into the modulator input of the first Ciena WaveLogic 3 transponder, where they were bulk modulated with DP-QPSK data at 35Gbaud. The channel under test at 1553.33nm was generated using a second Ciena WaveLogic 3 transponder, also configured to generate DP-QPSK modulated signal at 35Gbaud. The data format was based on internally generated $2^{10}-1$ pseudo-random bit sequences (PRBS), fully processed in real-time into Nyquist pulse shaped channels by the transponder DSP. The channel under test and the other four IQ modulated signals were to give an aggregate 5x100Gb/s DP-

5.2 Real Time Nonlinearity Compensation Using OPC with Raman Amplification

QPSK signal. The optical spectrum of the transmitted signal is shown in Fig.(5.21).

The Raman-amplified link was a first-order backward (BW) pumped distributed Raman amplifier (DRA) which exactly compensated the ~ 9.8 dB loss from the 50.4km transmission fiber of each span. For simplicity, only one pump laser at 1450nm was used and the pump power on each path was controlled by a variable optical attenuator (VOA). The signal output from the first span could be transmitted either with or without the OPCs. The detailed experimental setup of the OPC is shown in Fig.(5.20) (bottom). The OPC was a polarisation insensitive,

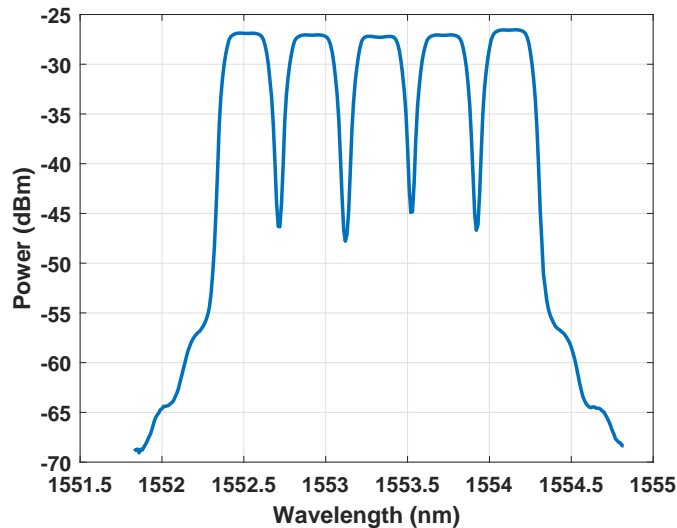


Figure 5.21. Transmitted 5 Channels Spectrum

dual-signal-band, dual-orthogonally polarised pump configuration [127]. In this experiment, the dual-band OPC was used as two separate OPCs, with a band for each OPC around the zero-dispersion wavelength ~ 1557 nm. The OPC1 signal input allowed the signals to be conjugated to the second wavelength band (1556.97 to 1558.58nm), and the OPC2 input allowed the conjugated signal to be converted back to the original wavelengths. The OPC has been described in detail in chapter (3). The insertion loss of this dual-band OPC was 20dB compensated by EDFAs.

5. EXPERIMENTAL INVESTIGATION OF NONLINEARITY IN OPTICAL COMMUNICATION SYSTEM

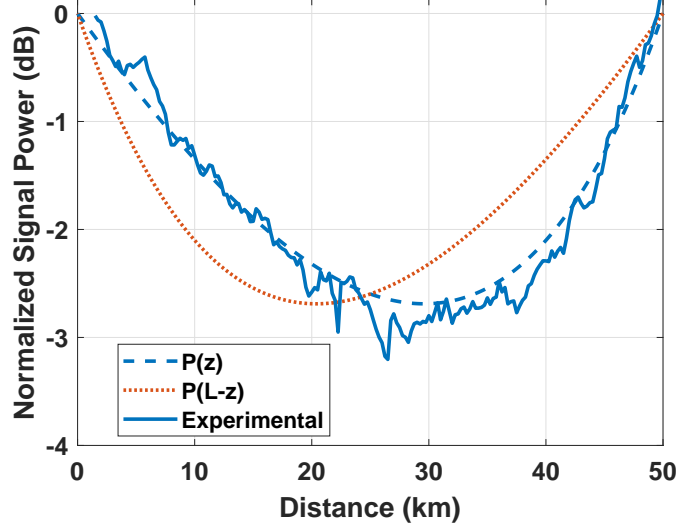


Figure 5.22. Simulated and experimentally measured signal power profiles of the 50km SSMF span pumped by the first-order 1455nm laser

Figure (5.22) shows the simulated and experimentally measured signal power profiles along the fiber using the first-order distributed Raman amplification (DRA) scheme. The signal power profile was measured by an optical time-domain reflectometer. The power symmetry over the link can be estimated using the equation [230],

$$Symmetry = \left(1 - \frac{\int_0^{\frac{L}{2}} |P(z) - P(L-z)| dz}{\int_0^{\frac{L}{2}} P(z) dz} \right) * 100\% \quad (5.2)$$

where $P(z)$ is the power of the simulated transmitted signal as a function of the fiber length. $P(z)$ and $P(L-z)$ are shown as dashed and dotted line respectively in Fig.(5.22). By solving this integration numerically using the simulation results, it is found that the first-order BW-pumping scheme provides 89.4% signal power symmetry over 50.4km SMF. The first-order pump power for each span was 360mW. Higher symmetry allows more effective fiber nonlinearity compensation, however, requiring a more complicated Raman configuration such as forward pumping, high-order pumping [231, 232]. First-order BW-pumping was used here, as it has been widely deployed commercially and is cost-effective. After transmission the channel-under-test was detected by the second WaveLogic 3 transponder and the engineering wire used to interrogate the transponder for pre-FEC BER values, and interpolated samples at the center of

5.2 Real Time Nonlinearity Compensation Using OPC with Raman Amplification

each bit slot to enable constellation diagrams to be plotted. BER results were converted to an equivalent signal-to-noise (SNR) assuming the white noise [208].

5.2.2 Experiment Results and Discussions

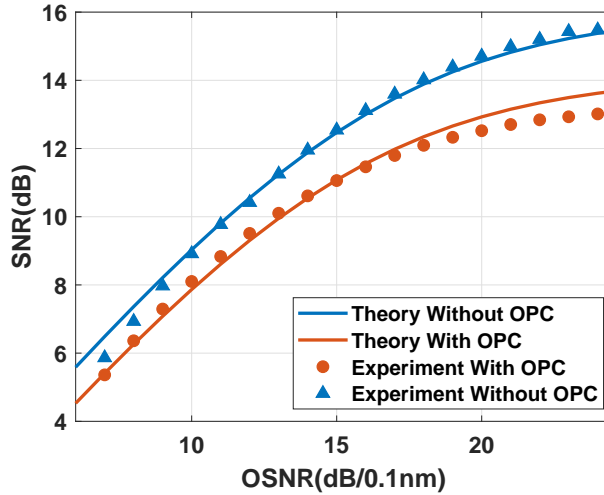


Figure 5.23. Experimentally measured (markers) and analytically fitted (lines) SNR versus OSNR (dB/0.1nm) for the central channel of five DPQPSK WDM channels (500Gb/s) back-to-back.

The back-to-back SNR for the central channel versus signal OSNR is presented in Fig.(5.23). In Fig.(5.23) to (5.25), "with OPC" means with both OPC 1 (mid-link OPC) and OPC 2 (end-link OPC). The SNRs without OPC show better SNR (0.5dB to 2dB) compared with that with OPC. This was because the residual dithering tones caused the imperfect mismatching between two phase-modulators of counter-dithering parts causing interference with the modulated signal, and therefore limited the maximum SNR achieved by the transceiver and OPC system. These residual tones can be removed by making the two PM modulators on the same substrate to have identical properties and in that case, the modulated lines will have the same level around the carrier and will be fully canceled with the right counter phase.

Fig.(5.24) shows the experimentally measured and analytically fitted SNR versus signal launch power over 2x50km SSMF Raman amplified link for single-channel and for five WDM channels transmission in Fig.(5.25). Analytical modeling [196] enables the received SNR to be calculated, considering ASE noise (P_{ASE}), the transceiver SNR limit without and with OPC (using the results in Fig.(5.23)). In addition, the first ($f[P^2P_{ASE}]$) and second-order

5. EXPERIMENTAL INVESTIGATION OF NONLINEARITY IN OPTICAL COMMUNICATION SYSTEM

($f[P^2(P^2P_{ASE})]$) parametric noise amplification [233, 234] (signal-noise nonlinear interactions), and it can be simplified to:

$$SNR = \frac{P}{N_{TR} + 2P_{ASE} + N_{OPC} + 2\eta\Gamma p^3 + 2\Gamma p^2(3 + 6\Gamma p^2)} \quad (5.3)$$

where P is the transmitted signal power, $N_{TR} = \frac{P}{SNR_{max}}$ and SNR_{max} is the maximum achievable back-to-back SNR without or with OPC from Fig.(5.23). N_{OPC} represents the ASE noise power introduced by the OPC, Γ is the effective nonlinearity coefficient which scales logarithmically with signal bandwidth (equation (27) in ref [3]), and η is the proportion of nonlinear noise remaining after compensation.

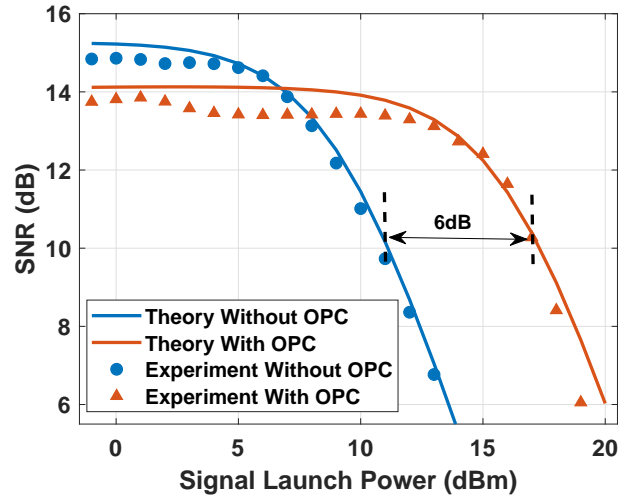


Figure 5.24. Experimentally measured (markers) and analytically fitted (lines) SNR versus signal launch power for single channel DP-QPSK transceiver.

A 6dB increase in the allowable launch power was observed in the nonlinear regime (measured at an SNR of 10dB which is used as a benchmarker instead of using 8.5dB pre-FEC threshold (7% overhead) because the data was not available at that point for the 5 channels setup) for the single-channel case, with the improvement dominated by residual inter-signal nonlinear noise (4th term in the denominator of equation (5.3)) corresponding to about 94% compensation of the nonlinear noise (relative to the back-to-back performance in Fig.(5.23)). This is slightly better than anticipated from dispersion-power symmetry due to the improved effectiveness of the OPC for strongly phase-matched signals which dominated the performance

5.2 Real Time Nonlinearity Compensation Using OPC with Raman Amplification

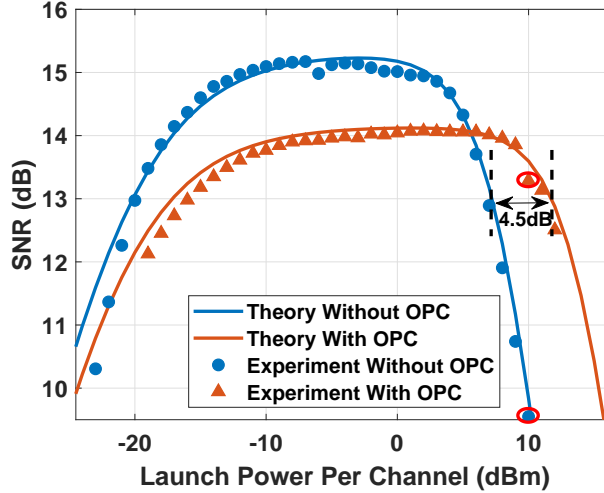


Figure 5.25. Experimentally measured (markers) and analytically fitted (lines) SNR versus signal launch power per channel for five WDM channels DP-QPSK transceivers.

in the single-channel case. In the case of 5 channels transmission, due to the additional nonlinear noise associated with the increase in signal bandwidth, the allowable launch power in the nonlinear regime without compensation was reduced by approximately 2dB in accordance with the increase in bandwidth ($10 \cdot \log_{10}(\ln(5))$), however, the beneficial impact of the OPC remains ~ 6 dB (at a SNR of 10dB). Here however, the nonlinearity compensation was reduced to the 90% anticipated from the dispersion power symmetry. The nonlinear threshold increase can be further improved by enhancing the efficiency of fiber nonlinearity compensation, such as increasing the link symmetry with an optimized Raman technique [235]. In both cases, the SNR without OPC at the optimum launch power was 1dB better than that with OPC due to degradations in maximum achievable SNR associated with the OPC, for example from residual phase modulation arising from imperfect counter dithering [232]. However, for the signal power in the nonlinear regime, i.e., at 10dBm without and with OPC, the SNR with OPC was about 4 dB better than that without OPC. Figure (5.26) shows the effect of the insertion of the OPC on nonlinearity compensation where the constellation diagram for the system with OPC was also much clearer than the system without OPC which showed the nonlinearity compensation in such short link.

5. EXPERIMENTAL INVESTIGATION OF NONLINEARITY IN OPTICAL COMMUNICATION SYSTEM

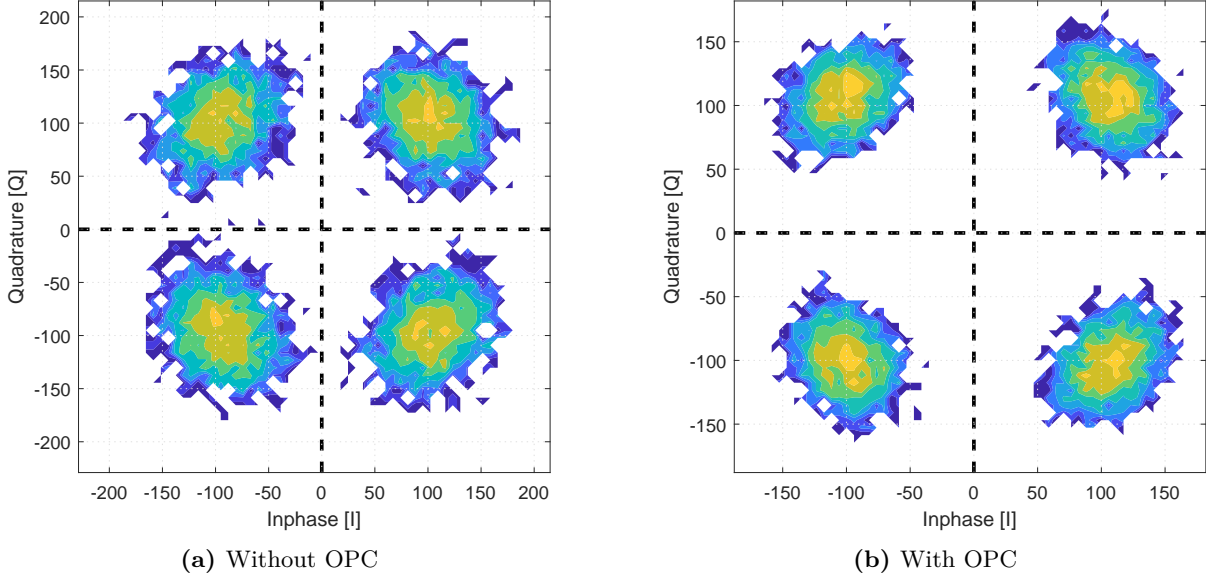


Figure 5.26. The constellation diagram of the signal at 10dBm without OPC and with OPC (red circled in Fig.(5.25)).

5.3 Experimental Investigation for The Impact of Dispersion Slope on Modeling Fiber Nonlinearity

In this part, the analysis in section (3.4) is validated experimentally. Doing an experiment with wide-bandwidth is challenging because of the limited availability of devices those work on different optical bands. Therefore the analysis will be verified by experimentally measuring the nonlinear noise (NLN) and system performance over a dispersion-shifted fiber (DSF) link, which scales the effects to narrower bandwidths. In particular, the effect of dispersion slope is significant if the product of 2π times signal bandwidth and third-order dispersion coefficient exceeds the second-order dispersion coefficient ($\beta_3\Delta\omega > \beta_2$), and may influence system performance before the dispersion zero is hit.

5.3 Experimental Investigation for The Impact of Dispersion Slope on Modeling Fiber Nonlinearity

5.3.1 FWM Experiment

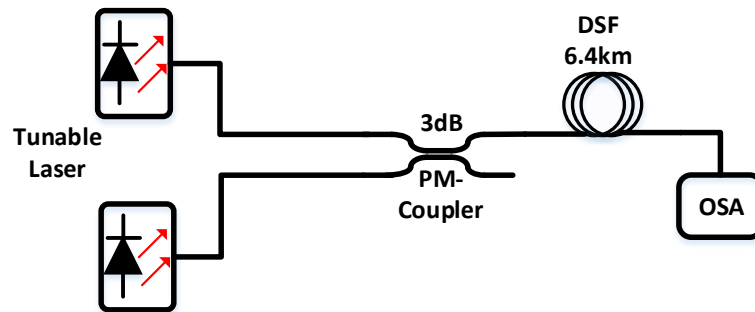


Figure 5.27. FWM measurement set-up to measure the effect of dispersion slope using DSF as a link. PM: polarization maintaining, OSA: optical spectrum analyzer

First of all, the zero-dispersion frequency of the DSF has been characterized using the setup in Fig.(5.27) by using tunable lasers with fixed frequency separation (400GHz) and swept the center frequency between the two lasers over the whole C-band. The idler power was measured using a high-resolution OSA. Figure (5.28) shows the idler power as a function of the center frequency between the two lasers and the results show that the zero-dispersion frequency is around 194.1THz. Then a fine sweeping from 193.7THz to 194.5 was run with reducing the frequency separation between the two lasers to 100GHz and again the zero-dispersion frequency was found at 194.1THz.

5. EXPERIMENTAL INVESTIGATION OF NONLINEARITY IN OPTICAL COMMUNICATION SYSTEM

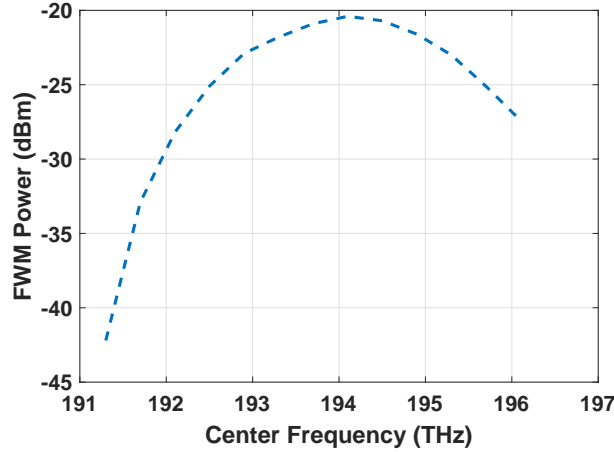


Figure 5.28. FWM Efficiency as a function the center frequency between two tunable lasers with fixed frequency separation

The other parameters of the DSF come from the manufacturer are $\beta_2 = -0.54 \text{ ps}^2/\text{km}$, $\beta_3 = 0.131 \text{ ps}^3/\text{km}$ and attenuation $0.26 \text{ dB}/\text{km}$ at 193.6 THz . The DSF has been employed to experimentally verify the accuracy of the normalized analytical model as shown in Fig.(5.27). First, the FWM efficiency (Fig.(3.11)) was verified by combining two tunable continuous-wave lasers using polarization-maintaining coupler and launching at 15 dBm into a 6.4 km length of DSF with the same parameters as used for Fig.(3.11), recording the idler power as a function of frequency separation with a high resolution (150 MHz) optical spectrum analyzer (Fig. (5.29)).

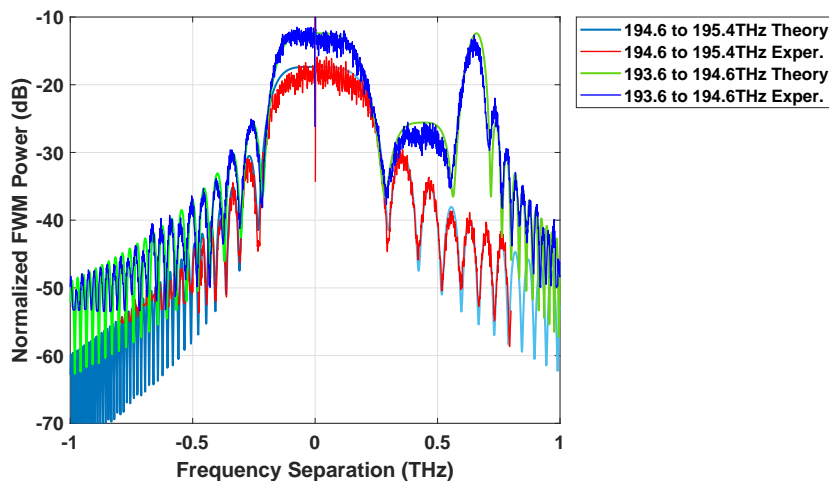


Figure 5.29. FWM efficiency as a function of frequency separation between two lasers showing experimental results (red and blue) and theory (green and light blue) with different laser frequencies. Blue and green curves shifted up by 5 dB .

5.3 Experimental Investigation for The Impact of Dispersion Slope on Modeling Fiber Nonlinearity

Two different frequency ranges were selected to illustrate the changes in efficiency due to the emergence of dispersion slope effects. For the lower curves (red and light blue), one laser was fixed at 194.6THz, whilst the other was swept up to 195.4THz. The effect of dispersion slope is quite small and only appears as a slight asymmetry between the weakly phase-matched idler powers for positive and negative detuning. With the fixed laser tuned to 193.6THz, closer to the dispersion zero (green and dark blue), the impact of dispersion slope becomes significant and appears as an enhancement in the FWM efficiency between 0.2 and 0.5 THz with an extra peak around 0.65 THz separation. Excellent matching with the theoretical predictions may be observed by substituting the DSF fiber parameters in Eq.(3.69) (frequency separation = 0.656 THz).

5.3.2 NLN Experiment

The NLN PSD was measured using the spectral notch method [236] as shown in Fig.(5.30) where a notch is generated in the center of the spectrum and using high-resolution OSA, the FWM power generated in the central notch can be measured. The spectrum was used to determine the output power spectral density (and by implication the relative input power spectral density). An EDFA was used as a source of the ASE. The ASE was further amplified by a second EDFA and shaped using two wavelength selective switches (WSS) to give a flat rectangular spectrum representing highly dispersed Nyquist WDM channels with a launched PSD of $0.75 \mu W/GHz$ and a 10GHz notch in the middle of the spectrum representing the location of the channel under test.

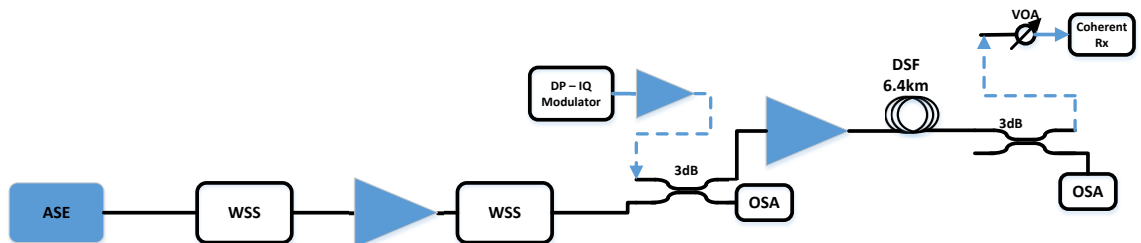


Figure 5.30. Experimental setup for the spectral notch method and the dashed line represents the addition to the setup for BER measurements.

5. EXPERIMENTAL INVESTIGATION OF NONLINEARITY IN OPTICAL COMMUNICATION SYSTEM

Three different central notch locations were measured (193.275, 193.75 and 194.25 THz), representing high, intermediate, and low dispersion spectral regions of the fiber respectively. Figure (5.31) shows the measured and analytically predicted (taking into account residual background ASE from the WSS cascade) NLN PSD using Eq.(3.70). At small bandwidth, all notches have similar NLN PSDs and for the notch centered at 193.275THz (high dispersion case), the NLN follows the expected logarithmic increase with bandwidth. However, for lower dispersions (notches at 193.75THz and 194.25THz), this logarithmic dependence only holds up to a certain bandwidth, beyond which the dispersion slope takes effect.

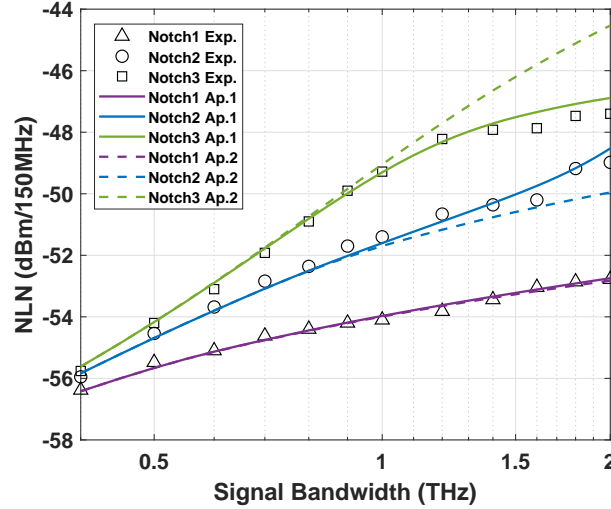


Figure 5.31. NLN as a function of the signal bandwidth for Experiment (Markers) and Theory (Lines) using with (solid) and without (dashed) dispersion slope. Notch1: 193.275THz, Notch2: 193.75THz, Notch3: 194.25THz, Exp.: Experiment and Ap.: Approximation

At moderate dispersion (193.75THz), the additional phase-matching condition results in an increase in NLN, reminiscent of the step changes observed in few-mode fiber when additional modes become phase-matched [237]. However, for the lowest dispersion (194.25THz), the effect is to reduce the rate of growth, as widely separated signals are less well phase-matched thanks to the dispersion slope. Analytical predictions according to the two approximations considered here, $\beta_3 = 0$ (dashed) (approximation 1) and $\beta_3 \neq 0$ (solid), are also shown where β_2 is adjusted to the correct value at the center of each band. Despite adjustment of β_2 to the center of the band (approximation 2), inclusion of dispersion slope is necessary for wider bandwidths

5.3 Experimental Investigation for The Impact of Dispersion Slope on Modeling Fiber Nonlinearity

($\Delta f > \frac{\beta_2}{\pi\beta_3}$). Figure (5.32) shows the spectrum of the notches at 193.275 and 194.25 THz at different bandwidths of the ASE spectrum shown as different line colors.

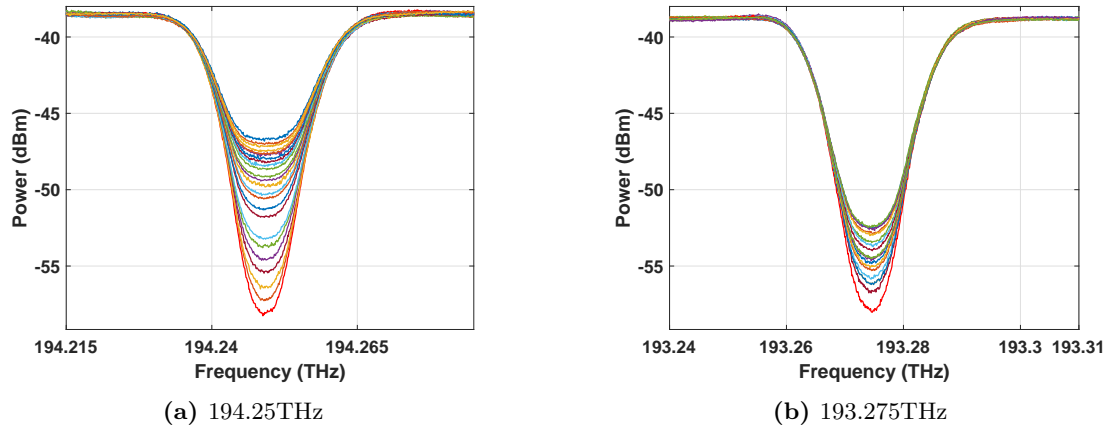


Figure 5.32. NLN spectrum at 193.275THz and at 194.25THz at different ASE bandwidths

5.3.3 BER Measurement

Finally, the impact of the NLN was verified by measuring the bit error rate (BER) for 35Gbaud PM-QPSK and PM-16QAM signals (Fig. (5.30)). The central notch was increased from 10GHz to 40GHz using the WSS and a modulated signal, generated and received using a commercial Ciena WaveLogic 3 transceiver, was inserted in the notch using a 3 dB coupler. The channel was tested at 193.3 THz and at 194.25THz.

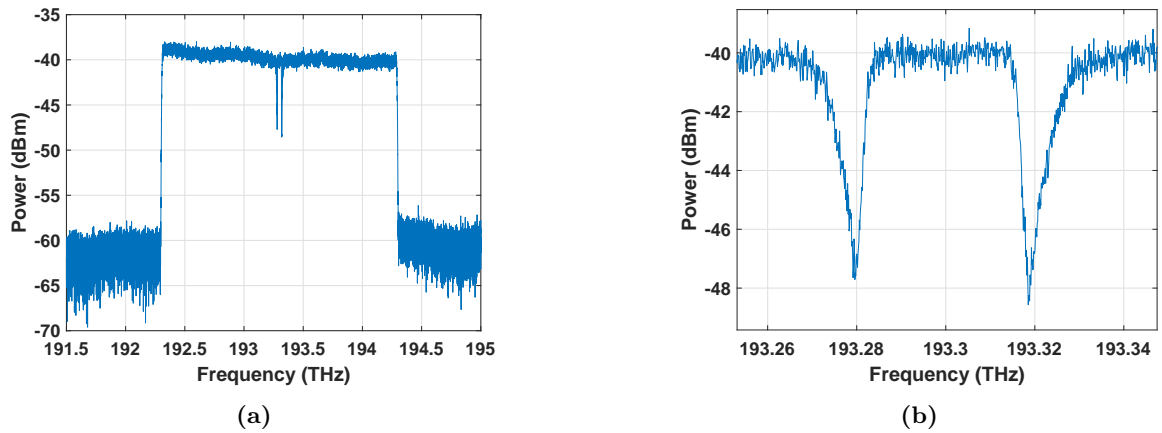


Figure 5.33. 2THz ASE spectrum with 35Gbaud modulated signal inserted in 40GHz notch in the center of the ASE spectrum. (b) the modulated signal

5. EXPERIMENTAL INVESTIGATION OF NONLINEARITY IN OPTICAL COMMUNICATION SYSTEM

The data format was based on internally generated $2^{10}-1$ pseudo-random bit sequences (PRBS), fully processed in real-time into Nyquist pulse shaped channels by the transponder DSP. An EDFA was used after the transmitter to equalize the power spectral densities. Figure(5.33) shows a 2THz ASE spectrum with the 40GHz notch in the middle of the band and the modulated signal inserted inside the notch and it shows clearly in Fig.(5.33b). Figure (5.34) shows the measured BERs as a function of the transmission bandwidth and curve fits based on calculating NLN using approximation 1 (dashed lines) and approximation 2 (solid lines) with using Eq. (3.57) to estimate the SNR and the conventional dependence of BER on SNR as in Eq.(3.63). The results confirm that in addition to predicting FWM efficiencies [56, 238], Eq. (3.70) can be effectively used to estimate NLN and system performance in the presence of significant effects of dispersion slope.

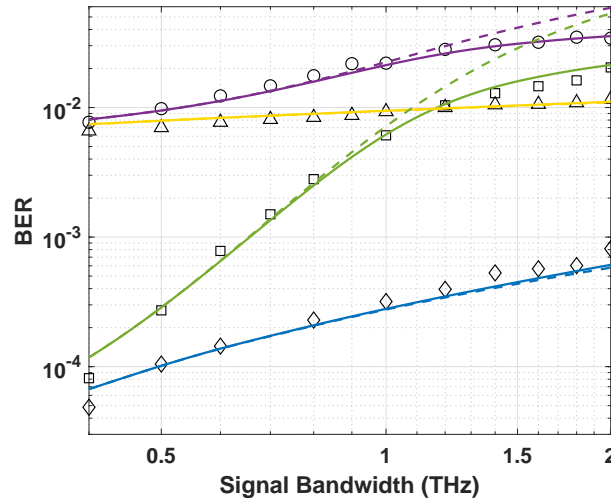


Figure 5.34. BER as a function of the transmission bandwidth for experiment (markers) and theory (lines) with (solid) and without (dashed) dispersion slope for QPSK (triangle and diamond) and 16QAM (circle and square) signals at 193.3THz (blue and yellow lines) and at 194.25THz (green and purple lines) respectively.

The same effect can be shown using the constellation of the received signal. Figures (5.35a) and (5.35b) show the constellation of the received QPSK modulated signal at the top point of blue curve (at 2THz of transmitted signal bandwidth) and green curve in Fig.(5.34) respectively and Fig.(5.35c) shows the constellation at the lowest point in the green curve (194.25THz). The constellation in Fig.(5.35a) has high distortion compared with the constellation in Fig.(5.35b)

at the same bandwidth but at a different center frequency. The constellation in Fig.(5.35c) is for low bandwidth of 0.25THz and has more space between the constellation points which is translated in low BER in Fig.(5.34)).

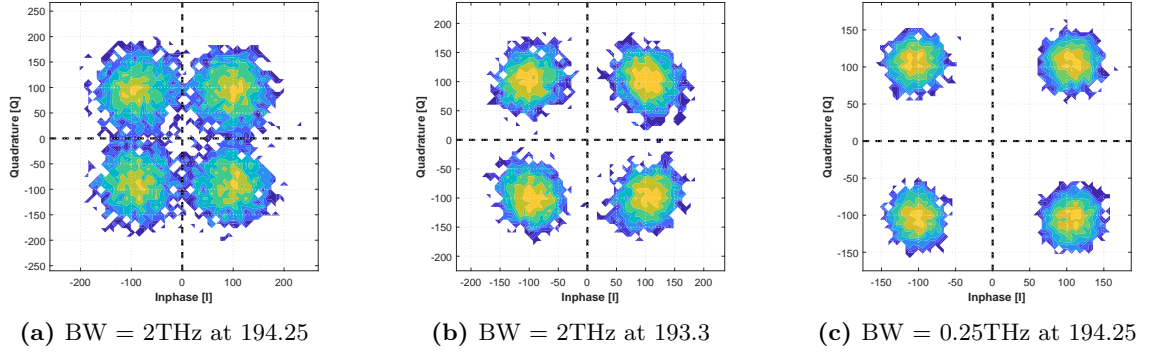


Figure 5.35. Constellation of 35 Gbaud-QPSK modulated signal at different notch locations and different ASE bandwidths

5.4 Conclusions

The mathematical analysis of the FWM and NLN has been verified experimentally and 4.08Tb/s 17 WDM channels have been transmitted over 600 km. For the first time, the OPC with real-time transceiver is experimentally presented using a dual-band OPC device simultaneously acting as both mid-link and end-link OPC, which remains the consistency of the wavelength in the transmitter and receiver and therefore allows the use of the commercially deployed optical transceivers in the OPC system. It is demonstrated that, in a 2x50km SSMF link pumped by a first-order Raman laser, a 6dB nonlinear threshold improvement with both single-channel 100Gb/s DP-QPSK transmission, and with five DP-QPSK WDM channels. The impact of dispersion slope on NLN generation has been experimentally verified the predictions using DSF. The analytical predictions suggest that dispersion slope may be safely neglected until $BW > \frac{\beta_2}{\pi\beta_3}$, approximately 40 THz for fiber with dispersion $\sim -20ps^2/km$.

5. EXPERIMENTAL INVESTIGATION OF NONLINEARITY IN OPTICAL COMMUNICATION SYSTEM

Chapter 6

CONCLUSIONS

6.1 Conclusions

For the first time, an analytical expression has been introduced for measuring the impact of the FWM in a multi-span lumped amplification system employing OPC with a dispersion element (to improve the symmetry). Besides, a novel closed-form expression for measuring the impact of nonlinearity on the transmission of WDM signals in a system with mid-link OPC has been presented. These expressions are used successfully to predict the performance of 17 WDM channels transmitted over 10 spans of 100km SSMF and it is also used to estimate the optimum dispersion required around the OPC to get the best performance. The results have been validated through the simulations and showed a good agreement within a margin of error of less than 0.2dB.

Through experimental works, the benefit of adding a DE with the OPC to enhance the non-linearity effects compensation has been proved where the FWM power (from the transmission of two 9dBm tones over 200km of SSMF) has been suppressed by around 18 dB compared with the system without OPC. In addition to the performance improvement, the link length also can be increased by 75km. Using the OPC without dealing with improving the symmetry through dispersion management gives a 5dB improvement over the system without OPC. The results are in a perfect matching with the theoretical analysis introduced in chapter (3). The transmission of a 30 Gbaud PM-16QAM signal over different link lengths has shown also the benefit of this method

6. CONCLUSIONS

in improving the symmetry and enhancing the performance of the OPC nonlinearity compensation, wherein the highly nonlinear regime, a 4 dB improvement in SNR is noticed over the system without OPC and 3 dB over the system with OPC but without symmetry improvement. 4.08Tb/s 17 WDM PM-16QAM channels have been transmitted over 6 spans of SSMF (span length 100km) with OPC and additional dispersion, the improvement in SNR has decreased (to ~ 1.8 dB) compared with the 4 dB improvement in the performance of the single-channel system. This is probably due to the additional nonlinear impairment from the additional dispersion span.

The mid-link OPC has shown good performance in compensating the nonlinearity in a transmission system with a real-time transceiver. The nonlinearity compensation enabled a 6dB improvement in the nonlinear threshold for a single channel (100Gb/s PM-QPSK) transmitted over 2 spans (2x50km) with mid-link OPC and backward Raman amplification. Moreover, 4.5dB improvement in the nonlinear threshold for 5 WDM channels transmission over the same link has been noticed. These experiments indicated the need to decrease the penalty added by the insertion of the OPC device in the link. These different penalties have been discussed in detail then a wavelength shift-free OPC is introduced with 20nm conjugation bandwidth. The results have shown that the main barrier in designing the OPC device is overcoming the SBS power without affecting the performance of the conjugated signal. The effect of dispersion slope on modeling the fiber nonlinearity impacts has been analyzed. This analysis has been investigated experimentally by scaling the problem to small bandwidths by using DSF instead of SSMF. The results show that when the whole SMF bandwidth (~ 40 THz) is occupied, the models for nonlinearity impacts will need to consider the effect of the dispersion slope to produce accurate results.

6.2 Future Work Suggestions

The OPC design needs to be improved to increase the conversion efficiency and reduce the penalties due to counter dithering. Another conjugation medium may need to be investigated where the required pump power for conjugation can be small. Using the OPC with a higher-order modulation format such as 256QAM is required without adding an extra penalty that

overcomes the gain from the nonlinearity compensation.

The current OPC design is suitable for point to point communication and a novel design may be needed to work inside the optical network. The inherent frequency shift property of the conjugation process can be used as a feature for routing.

The nonlinearity in a lumped amplified system with a highly dispersive link is found to be Gaussian and therefore the nonlinear noise is treated as additive white Gaussian noise (AWGN). The OPC introduces a gradual dispersion compensation. The insertion of midlink OPC on the Gaussian distribution of the received symbols needs to be studied through extensive simulations and experimental work.

In ultra-wideband communication over an optical fiber link that employs midlink OPC, the stimulated Raman scattering will affect the power distribution over the span length, and also the dispersion slope will not be compensated using the OPC. These effects need to be studied and modeled particularly in the case when a high level of power symmetry is achieved around the OPC.

Noise-signal nonlinear interactions have been studied analytically and through simulations. However, these interactions need to be investigated experimentally by compensating the signal-signal nonlinearity through the use of short span lengths ($\sim 20\text{km}$) with a higher-order Raman pumping (to achieve the maximum possible symmetry) for amplification with a midlink OPC.

LIST OF PUBLICATIONS

- [P1] **Abdallah A. I. Ali** and Andrew D. Ellis, “Design challenges of optical parametric device for Kerr Nonlinearity compensation,”in Photonics. Multidisciplinary Digital Publishing Institute. To be submitted in a Special Issue entitled “Optical Parametric Amplifiers”, 2020.
- [P2] Andrew D. Ellis, **Abdallah A. I. Ali** et al., “Nonlinear compensation based on optical phase conjugation,”To be submitted in IEEE Journal of Selected Topics in Quantum Electronics focusing on Optical Signal Processing, 2020.
- [P3] Mohammad A. Z. Al-Khateeb, **Abdallah Ali**, and Andrew Ellis. ”Basic Optical Fiber Nonlinear Limits.” Optical Communication Systems: Limits and Possibilities: 63. Jenny Stanford Publishing, 2019.
- [P4] **Abdallah A. I. Ali**, Mingming Tan, Mohammad A. Z. Al-Khateeb, Charles Laperle, Andrew D. Ellis¹ ”First Demonstration of Optical Phase Conjugation with Real Time Commercial Transceiver” 2019 European Conference on Optical Communication (ECOC), Dublin, Ireland, 2019, pp. 1-3.
- [P5] Abdulaziz E. Elfiqi, **Abdallah A.I. Ali**, Ziad A. El-Sahn, Kazutoshi Kato, Hossam M.H. Shalaby,”Theoretical analysis of long-haul systems adopting mode-division multiplexing”, Optics Communications, Volume 445, 2019, Pages 10-18.
- [P6] **A. A. I. Ali**, M. Al-Khateeb, T. Zhang, F. Ferreira and A. Ellis, ”Enhanced Nonlinearity Compensation Efficiency of Optical Phase Conjugation System,” 2019 Optical Fiber Communications Conference and Exhibition (OFC), San Diego, CA, USA, 2019, pp. 1-3.
- [P7] **A. A. I. Ali**, C. S. Costa, M. A. Z. Al-Khateeb, F. M. Ferreira and A. D. Ellis, ”An Expression for Nonlinear Noise in Optical Phase Conjugation Systems With

- Lumped Amplifiers,” in *IEEE Photonics Technology Letters*, vol. 30, no. 23, pp. 2056-2059, 1 Dec.1, 2018.
- [P8] **A. A. I. Ali**, F. Ferreira, M. Al-Khateeb, D. Charlton, C. Laperle and A. D. Ellis, ”The Impact of Dispersion Slope on Fiber Nonlinearity in Ultra-Wideband Optical Communication System,” 2018 European Conference on Optical Communication (ECOC), Rome, 2018, pp. 1-3.
- [P9] Mohammad A. Z. Al-Khateeb, Mingming Tan, Md. Asif Iqbal, **Abdallah Ali**, Mary E. McCarthy, Paul Harper, and Andrew D. Ellis, ”Experimental demonstration of 72 % reach enhancement of 3.6Tbps optical transmission system using mid-link optical phase conjugation,” *Opt. Express* 26, 23960-23968 (2018)
- [P10] Zhang, Tingting, C. Sanchez, M. Al-Khateeb, **Abdallah Ali**, M. Tan, Pavel Skvortcov, Ian Phillips, Stylianos Sygletos, and Andrew Ellis. ”224-Gb/s Carrier-Recovery-Free Doubly Differential 2ASK-8PSK for Short-Reach Optical Networks.” *IEEE Photonics Technology Letters* 30, no. 16 (2018): 1463-1466.
- [P11] Mohammad A. Z. Al-Khateeb, Md. Asif Iqbal, Mingming Tan, **Abdallah Ali**, Mary McCarthy, Paul Harper, and Andrew D. Ellis, ”Analysis of the nonlinear Kerr effects in optical transmission systems that deploy optical phase conjugation,” *Opt. Express* 26, 3145-3160 (2018).
- [P12] **A. A. I. Ali**, C. S. Costa, M. A. Z. Al-Khateeb, F. M. Ferreira and A. D. E. Aston, ”Four-wave mixing in optical phase conjugation system with pre-dispersion,” 2017 Opto-Electronics and Communications Conference (OECC) and Photonics Global Conference (PGC), Singapore, 2017, pp. 1-3.
- [P13] T. Zhang, C. Sanchez, **A. A. I. Ali** and A. Ellis, ”Nonamplified 100Gbps doubly differential QPSK optical signal transmission over 80 km SSMF without carrier recovery,” 2017 Opto-Electronics and Communications Conference (OECC) and Photonics Global Conference (PGC), Singapore, 2017, pp. 1-2.

6. CONCLUSIONS

REFERENCES

- [1] C. V. Forecast, “Cisco visual networking index: Forecast and trends, 2017–2022,” *White paper, Cisco Public Information*, 2019.
- [2] R.-J. Essiambre, R. W. Tkach, and R. Ryf, “Fiber nonlinearity and capacity: Single-mode and multimode fibers,” *Optical Fiber Telecommunications VI B, I. Kaminow*, pp. 1–37, 2013.
- [3] A. Ellis, M. McCarthy, M. Al Khateeb, M. Sorokina, and N. Doran, “Performance limits in optical communications due to fiber nonlinearity,” *Advances in Optics and Photonics*, vol. 9, no. 3, pp. 429–503, 2017.
- [4] G. P. Agrawal, “Fiber-optic communication systems,” *John Wiley & Sons*, vol. 222, 2012.
- [5] P. J. Winzer, D. T. Neilson, and A. R. Chraplyvy, “Fiber-optic transmission and networking: the previous 20 and the next 20 years,” *Optics Express*, vol. 26, no. 18, pp. 24 190–24 239, 2018.
- [6] A. H. Gnauck, R. Tkach, A. Chraplyvy, and T. Li, “High-capacity optical transmission systems,” *Journal of Lightwave Technology*, vol. 26, no. 9, pp. 1032–1045, 2008.
- [7] R.-J. Essiambre and R. W. Tkach, “Capacity trends and limits of optical communication networks,” *Proceedings of the IEEE*, vol. 100, no. 5, pp. 1035–1055, 2012.
- [8] T. Xia, G. Wellbrock, D. Peterson, W. Lee, M. Pollock, B. Basch, D. Chen, M. Freiburger, M. Alfiad, H. de Waardt *et al.*, “Multi-rate (111-Gb/s, 2x43-Gb/s, and 8x10. 7-Gb/s)

REFERENCES

- transmission at 50-GHz channel spacing over 1040-km field-deployed fiber,” in *2008 34th European Conference on Optical Communication*. IEEE, 2008, pp. 1–4.
- [9] D. Qian, M.-F. Huang, E. Ip, Y.-K. Huang, Y. Shao, J. Hu, and T. Wang, “High capacity/spectral efficiency 101.7-Tb/s WDM transmission using PDM-128QAM-OFDM over 165-km SSMF within C-and L-bands,” *Journal of Lightwave Technology*, vol. 30, no. 10, pp. 1540–1548, 2012.
- [10] M. Terayama, S. Okamoto, K. Kasai, M. Yoshida, and M. Nakazawa, “4096 QAM (72 Gbit/s) single-carrier coherent optical transmission with a potential SE of 15.8 bit/s/Hz in all-Raman amplified 160 km fiber link,” in *Optical Fiber Communication Conference*. Optical Society of America, 2018, pp. Th1F–2.
- [11] S. L. Olsson, J. Cho, S. Chandrasekhar, X. Chen, E. C. Burrows, and P. J. Winzer, “Record-high 17.3-bit/s/Hz spectral efficiency transmission over 50 km using probabilistically shaped PDM 4096-QAM,” in *2018 Optical Fiber Communications Conference and Exposition (OFC)*. IEEE, 2018, pp. 1–3.
- [12] A. Ellis, F. Ferreira, T. Zhang, and M. Al Khateeb, “Limits of optical fibre communication systems,” in *2018 20th International Conference on Transparent Optical Networks (ICTON)*. IEEE, 2018, pp. 1–4.
- [13] J.-X. Cai, Y. Sun, H. Zhang, H. G. Batshon, M. V. Mazurczyk, O. V. Sinkin, D. G. Foursa, and A. Pilipetskii, “49.3 Tb/s transmission over 9100 km using C+ L EDFA and 54 Tb/s transmission over 9150 km using hybrid-Raman EDFA,” *Journal of Lightwave Technology*, vol. 33, no. 13, pp. 2724–2734, 2015.
- [14] Y. Mori, “Ultra-wide band ROADM,” in *WS07 - Ultra-wideband communications Workshop in The 45th European Conference on Optical Communication (ECOC), Dublin*, 2019.
- [15] A. D. Ellis, J. Zhao, and D. Cotter, “Approaching the non-linear Shannon limit,” *Journal of Lightwave Technology*, vol. 28, no. 4, pp. 423–433, 2009.

-
- [16] A. Ellis and M. Sorokina, *Optical Communication Systems: Limits and Possibilities*. CRC Press, 2019.
- [17] P. Bayvel, R. Maher, T. Xu, G. Liga, N. A. Shevchenko, D. Lavery, A. Alvarado, and R. I. Killey, “Maximizing the optical network capacity,” *Philosophical Transactions of the Royal Society A: Mathematical, Physical and Engineering Sciences*, vol. 374, no. 2062, p. 20140440, 2016.
- [18] D. Richardson, J. Fini, and L. Nelson, “Space-division multiplexing in optical fibres,” *Nature Photonics*, vol. 7, no. 5, pp. 354–362, 2013.
- [19] M. Nissov, C. Davidson, K. Rottwitt, R. Menges, P. Corbett, D. Innis, and N. S. Bergano, “100 Gb/s (10/spl times/10 Gb/s) WDM transmission over 7200 km using distributed Raman amplification,” in *Integrated Optics and Optical Fibre Communications, 11th International Conference on, and 23rd European Conference on Optical Communications (Conf. Publ. No.: 448)*, vol. 5. IET, 1997, pp. 9–12.
- [20] A. Karar, Y. Gao, J. Cartledge, S. Gazor, M. O’Sullivan, C. Laperle, A. Borowiec, and K. Roberts, “Mitigating intra-channel nonlinearity in coherent optical communications using ISI-free polynomial pulses,” in *OFC 2014*. IEEE, 2014, pp. 1–3.
- [21] S. Kumar and D. Yang, “Optical backpropagation for fiber-optic communications using highly nonlinear fibers,” *Optics letters*, vol. 36, no. 7, pp. 1038–1040, 2011.
- [22] S. Watanabe, S. Kaneko, and T. Chikama, “Long-haul fiber transmission using optical phase conjugation,” *Optical Fiber Technology*, vol. 2, no. 2, pp. 169–178, 1996.
- [23] S. L. Olsson, B. Corcoran, C. Lundström, M. Sjödin, M. Karlsson, and P. A. Andrekson, “Phase-sensitive amplified optical link operating in the nonlinear transmission regime,” in *European Conference and Exhibition on Optical Communication*. Optical Society of America, 2012, pp. Th–2.

REFERENCES

- [24] W. Pieper, C. Kurtzke, R. Schnabel, D. Breuer, R. Ludwig, K. Petermann, and H. Weber, “Nonlinearity-insensitive standard-fibre transmission based on optical-phase conjugation in a semiconductor-laser amplifier,” *Electronics Letters*, vol. 30, pp. 724–726, 1994.
- [25] J. C. Geyer, C. R. Fludger, T. Duthel, C. Schulien, and B. Schmauss, “Simple automatic nonlinear compensation with low complexity for implementation in coherent receivers,” in *36th European Conference and Exhibition on Optical Communication*. IEEE, 2010, pp. 1–3.
- [26] E. Ip and J. M. Kahn, “Compensation of dispersion and nonlinear impairments using digital backpropagation,” *Journal of Lightwave Technology*, vol. 26, no. 20, pp. 3416–3425, 2008.
- [27] G. Gao, X. Chen, and W. Shieh, “Influence of PMD on fiber nonlinearity compensation using digital back propagation,” *Optics Express*, vol. 20, no. 13, pp. 14 406–14 418, 2012.
- [28] D. Rafique and A. D. Ellis, “Impact of signal-ASE four-wave mixing on the effectiveness of digital back-propagation in 112 Gb/s PM-QPSK systems,” *Optics Express*, vol. 19, no. 4, pp. 3449–3454, 2011.
- [29] K. Kikuchi, “Coherent optical communication systems,” in *Optical Fiber Telecommunications VB*. Elsevier, 2008, pp. 95–129.
- [30] A. Ellis, N. M. Suibhne, D. Saad, and D. Payne, “Communication networks beyond the capacity crunch,” 2016.
- [31] M. G. Taylor, “Coherent detection method using DSP for demodulation of signal and subsequent equalization of propagation impairments,” *IEEE Photonics Technology Letters*, vol. 16, no. 2, pp. 674–676, 2004.
- [32] R. Noe, “PLL-free synchronous QPSK polarization multiplex/diversity receiver concept with digital I&Q baseband processing,” *IEEE Photonics Technology Letters*, vol. 17, no. 4, pp. 887–889, 2005.

-
- [33] M. Seimetz, *"High-order modulation for optical fiber transmission"*. Springer, 2009, vol. 143.
- [34] K. Kikuchi, "Fundamentals of coherent optical fiber communications," *Journal of Light-wave Technology*, vol. 34, no. 1, pp. 157–179, 2015.
- [35] F. Kapron, D. B. Keck, and R. D. Maurer, "Radiation losses in glass optical waveguides," *Applied Physics Letters*, vol. 17, no. 10, pp. 423–425, 1970.
- [36] J. Yamada, S. Machida, and T. Kimura, "2 Gbit/s optical transmission experiments at 1.3 μm with 44 km single-mode fibre," *Electronics Letters*, vol. 17, no. 13, pp. 479–480, 1981.
- [37] K. Monham, R. Plastow, A. Carter, and R. Goodfellow, "1.3 Gbit/s transmission over 107 km of dispersion-shifted monomode fibre using a 1.55 μm multimode laser," *Electronics Letters*, vol. 21, no. 14, pp. 619–620, 1985.
- [38] G. Agrawal, *Nonlinear Fiber Optics*, 5th ed. Amsterdam ; Boston: Academic Press, 2013.
- [39] A. R. Chraplyvy, R. W. Tkach, and K. L. Walker, "Optical fiber for wavelength division multiplexing," Jul. 5 1994, uS Patent 5,327,516.
- [40] A. M. Vengsarkar, A. E. Miler, and W. Reed, "Highly efficient single-mode fiber for broadband dispersion compensation," in *Optical Fiber Communication Conference*. Optical Society of America, 1993, p. PD13.
- [41] D. McGhan, C. Laperle, A. Savchenko, C. Li, G. Mak, and M. O'Sullivan, "5120 km RZ-DPSK transmission over G652 fiber at 10 Gb/s with no optical dispersion compensation," in *Optical Fiber Communication Conference*. Optical Society of America, 2005, p. PDP27.
- [42] T. Hasegawa, Y. Yamamoto, and M. Hirano, "Optimal fiber design for large capacity long haul coherent transmission," *Optics Express*, vol. 25, no. 2, pp. 706–712, 2017.
- [43] M. J. Connelly, *"Semiconductor optical amplifiers"*. Springer Science & Business Media, 2007.

REFERENCES

- [44] M. Marhic, N. Kagi, T.-K. Chiang, and L. Kazovsky, "Broadband fiber optical parametric amplifiers," *Optics letters*, vol. 21, no. 8, pp. 573–575, 1996.
- [45] M. S. Faruk and S. J. Savory, "Digital signal processing for coherent transceivers employing multilevel formats," *Journal of Lightwave Technology*, vol. 35, no. 5, pp. 1125–1141, 2017.
- [46] J. C. Geyer, C. R. Fludger, T. Duthel, C. Schulien, and B. Schmauss, "Efficient frequency domain chromatic dispersion compensation in a coherent polmux QPSK-receiver," in *Optical Fiber Communication Conference*. Optical Society of America, 2010, p. OWV5.
- [47] R. Kudo, T. Kobayashi, K. Ishihara, Y. Takatori, A. Sano, and Y. Miyamoto, "Coherent optical single carrier transmission using overlap frequency domain equalization for long-haul optical systems," *Journal of Lightwave Technology*, vol. 27, no. 16, pp. 3721–3728, 2009.
- [48] C. Poole, R. Tkach, A. Chraplyvy, and D. Fishman, "Fading in lightwave systems due to polarization-mode dispersion," *IEEE Photonics Technology Letters*, vol. 3, no. 1, pp. 68–70, 1991.
- [49] D. Penninckx and V. Morénas, "Jones matrix of polarization mode dispersion," *Optics Letters*, vol. 24, no. 13, pp. 875–877, 1999.
- [50] W. Shieh and I. Djordjevic, *OFDM for optical communications*. Academic Press, 2009.
- [51] F. Buchali and H. Bülow, "Adaptive PMD compensation by electrical and optical techniques," *Journal of Lightwave Technology*, vol. 22, no. 4, p. 1116, 2004.
- [52] P. Knight and A. Miller, *Optical solitons: theory and experiment*. Cambridge University Press, 1992, vol. 10.
- [53] A. A. Ali, C. S. Costa, M. A. Al-Khateeb, F. M. Ferreira, and A. D. Ellis, "Four-wave mixing in optical phase conjugation system with pre-dispersion," in *2017 Opto-Electronics and Communications Conference (OECC) and Photonics Global Conference (PGC)*. IEEE, 2017, pp. 1–3.

-
- [54] M. A. Z. Al-Khateeb, A. Ali, and A. Ellis, “Basic optical fiber nonlinear limits,” *Optical Communication Systems: Limits and Possibilities*, p. 63, 2019.
- [55] K. Inoue, “Phase-mismatching characteristic of four-wave mixing in fiber lines with multistage optical amplifiers,” *Optics letters*, vol. 17, no. 11, pp. 801–803, 1992.
- [56] D. Cleland *et al.*, “Precise modelling of four wave mixing products over 400 km of step-index fibre,” *Electron. Lett.*, vol. 28, pp. 1171–1173, 1992.
- [57] D. Cleland, X. Gu, J. Cox, and A. Ellis, “Limitations of WDM transmission over 560 km due to degenerate four wave mixing,” *Electronics Letters*, vol. 28, no. 3, pp. 307–309, 1992.
- [58] A. Ellis and W. Stallard, “Four wave mixing in ultra long transmission systems incorporating linear amplifiers,” in *IEE Colloquium on Non-Linear Effects in Fibre Communications*. IET, 1990, pp. 6–1.
- [59] P. V. Mamyshev and N. A. Mamysheva, “Pulse-overlapped dispersion-managed data transmission and intrachannel four-wave mixing,” *Optics Letters*, vol. 24, no. 21, pp. 1454–1456, 1999.
- [60] K. Shiraki, M. Ohashi, and M. Tateda, “Suppression of stimulated Brillouin scattering in a fibre by changing the core radius,” *Electronics letters*, vol. 31, no. 8, pp. 668–669, 1995.
- [61] N. Yoshizawa and T. Imai, “Stimulated Brillouin scattering suppression by means of applying strain distribution to fiber with cabling,” *Journal of Lightwave Technology*, vol. 11, no. 10, pp. 1518–1522, 1993.
- [62] J. Hansryd, F. Dross, M. Westlund, P. Andrekson, and S. Knudsen, “Increase of the SBS threshold in a short highly nonlinear fiber by applying a temperature distribution,” *Journal of lightwave technology*, vol. 19, no. 11, p. 1691, 2001.
- [63] F. Willems and W. Muys, “Suppression of interferometric noise in externally modulated lightwave AM-CATV systems by phase modulation,” *Electronics letters*, vol. 29, no. 23, pp. 2062–2063, 1993.

REFERENCES

- [64] M. Pelusi, K. Solis-Trapala, H. N. Tan, T. Inoue, and S. Namiki, “Multi-tone counter dithering of terabit/s polarization multiplexed signals for enhanced FWM with a single pump,” in *2015 European Conference on Optical Communication (ECOC)*. IEEE, 2015, pp. 1–3.
- [65] A. Mussot, M. Le Parquier, and P. Szriftgiser, “Thermal noise for SBS suppression in fiber optical parametric amplifiers,” *Optics Communications*, vol. 283, no. 12, pp. 2607–2610, 2010.
- [66] J. C. Cartledge, F. P. Guiomar, F. R. Kschischang, G. Liga, and M. P. Yankov, “Digital signal processing for fiber nonlinearities,” *Optics Express*, vol. 25, no. 3, pp. 1916–1936, 2017.
- [67] J. C. Cartledge, A. D. Ellis, A. Shiner, A. A. El-Rahman, M. McCarthy, M. Reimer, A. Borowiec, and A. Kashi, “Signal processing techniques for reducing the impact of fiber nonlinearities on system performance,” in *Optical Fiber Communication Conference*. Optical Society of America, 2016, pp. Th4F–5.
- [68] G. Liga, T. Xu, A. Alvarado, R. I. Killey, and P. Bayvel, “On the performance of multi-channel digital backpropagation in high-capacity long-haul optical transmission,” *Optics Express*, vol. 22, no. 24, pp. 30 053–30 062, 2014.
- [69] R. Dar and P. J. Winzer, “On the limits of digital back-propagation in fully loaded WDM systems,” *IEEE Photonics Technology Letters*, vol. 28, no. 11, pp. 1253–1256, 2016.
- [70] L. Galdino, D. Semrau, D. Lavery, G. Saavedra, C. B. Czegledi, E. Agrell, R. I. Killey, and P. Bayvel, “On the limits of digital back-propagation in the presence of transceiver noise,” *Optics Express*, vol. 25, no. 4, pp. 4564–4578, 2017.
- [71] M. Schetzen, “The Volterra and Wiener theories of nonlinear systems,” 1980.
- [72] K. V. Peddanarappagari and M. Brandt-Pearce, “Volterra series transfer function of single-mode fibers,” *Journal of Lightwave Technology*, vol. 15, no. 12, pp. 2232–2241, 1997.

-
- [73] M. Schetzen, "Theory of pth-order inverses of nonlinear systems," *IEEE Transactions on Circuits and Systems*, vol. 23, no. 5, pp. 285–291, 1976.
- [74] F. P. Guiomar, J. D. Reis, A. L. Teixeira, and A. N. Pinto, "Digital postcompensation using Volterra series transfer function," *IEEE Photonics Technology Letters*, vol. 23, no. 19, pp. 1412–1414, 2011.
- [75] L. Liu, L. Li, Y. Huang, K. Cui, Q. Xiong, F. N. Hauske, C. Xie, and Y. Cai, "Intra-channel nonlinearity compensation by inverse Volterra series transfer function," *Journal of Lightwave Technology*, vol. 30, no. 3, pp. 310–316, 2011.
- [76] J. D. Reis and A. L. Teixeira, "Unveiling nonlinear effects in dense coherent optical WDM systems with Volterra series," *Optics Express*, vol. 18, no. 8, pp. 8660–8670, 2010.
- [77] M. Gagni, F. P. Guiomar, S. Wabnitz, and A. N. Pinto, "Simplified high-order Volterra series transfer function for optical transmission links," *Optics Express*, vol. 25, no. 3, pp. 2446–2459, 2017.
- [78] J.-H. Lee, D.-H. Han, and B.-Y. Choi, "Analysis of fiber nonlinearities by perturbation method," *Journal of the Optical Society of Korea*, vol. 9, no. 1, pp. 6–12, 2005.
- [79] Z. Tao, L. Dou, W. Yan, L. Li, T. Hoshida, and J. C. Rasmussen, "Multiplier-free intrachannel nonlinearity compensating algorithm operating at symbol rate," *Journal of Lightwave Technology*, vol. 29, no. 17, pp. 2570–2576, 2011.
- [80] M. Malekiha, I. Tselniker, and D. V. Plant, "Efficient nonlinear equalizer for intra-channel nonlinearity compensation for next generation agile and dynamically reconfigurable optical networks," *Optics Express*, vol. 24, no. 4, pp. 4097–4108, 2016.
- [81] L. Dou, Z. Tao, L. Li, W. Yan, T. Tanimura, T. Hoshida, and J. C. Rasmussen, "A low complexity pre-distortion method for intra-channel nonlinearity," in *2011 Optical Fiber Communication Conference and Exposition and the National Fiber Optic Engineers Conference*. IEEE, 2011, pp. 1–3.

REFERENCES

- [82] A. Ghazisaeidi, I. F. de Jauregui Ruiz, L. Schmalen, P. Tran, C. Simonneau, E. Awwad, B. Uscumlic, P. Brindel, and G. Charlet, "Submarine transmission systems using digital nonlinear compensation and adaptive rate forward error correction," *Journal of Lightwave Technology*, vol. 34, no. 8, pp. 1886–1895, 2016.
- [83] D. M. Pepper and A. Yariv, "Compensation for phase distortions in nonlinear media by phase conjugation," *Optics letters*, vol. 5, no. 2, pp. 59–60, 1980.
- [84] X. Liu, A. Chraplyvy, P. Winzer, R. Tkach, and S. Chandrasekhar, "Phase-conjugated twin waves for communication beyond the Kerr nonlinearity limit," *Nature Photonics*, vol. 7, no. 7, pp. 560–568, 2013.
- [85] A. Yariv, D. Fekete, and D. M. Pepper, "Compensation for channel dispersion by nonlinear optical phase conjugation," *Optics Letters*, vol. 4, no. 2, pp. 52–54, 1979.
- [86] R. A. Fisher, B. Suydam, and D. Yevick, "Optical phase conjugation for time-domain undoing of dispersive self-phase-modulation effects," *Optics letters*, vol. 8, no. 12, pp. 611–613, 1983.
- [87] S. L. Jansen, S. Spalter, G.-D. Khoe, H. de Waardt, H. E. Escobar, L. Marshall, and M. Sher, "16× 40 Gb/s over 800 km of SSMF using mid-link spectral inversion," *IEEE Photonics Technology Letters*, vol. 16, no. 7, pp. 1763–1765, 2004.
- [88] P. Minzioni, "Nonlinearity compensation in a fiber-optic link by optical phase conjugation," *Fiber and Integrated Optics*, vol. 28, no. 3, pp. 179–209, 2009.
- [89] S. Watanabe, T. Naito, and T. Chikama, "Compensation of chromatic dispersion in a single-mode fiber by optical phase conjugation," *IEEE photonics technology letters*, vol. 5, no. 1, pp. 92–95, 1993.
- [90] A. Gnauck, R. Jopson, and R. Derosier, "10-Gb/s 360-km transmission over dispersive fiber using midsystem spectral inversion," *IEEE photonics technology letters*, vol. 5, no. 6, pp. 663–666, 1993.

-
- [91] S. Watanabe and T. Chikama, "Cancellation of four-wave mixing in multichannel fibre transmission by midway optical phase conjugation," *Electronics Letters*, vol. 30, no. 14, pp. 1156–1157, 1994.
- [92] R. Jopson, A. Gnauck, and R. Derosier, "Compensation of fibre chromatic dispersion by spectral inversion," *Electronics Letters*, vol. 29, no. 7, pp. 576–578, 1993.
- [93] D. J. Richardson, R. I. Laming, D. Taverner, and D. N. Payne, "Simulation of 50GHz transmission over 50km of standard fibre using mid-point spectral inversion for dispersion compensation," *Proc. Nonlinear guided wave phenomena*, 1993.
- [94] M. Tatham, G. Sherlock, and L. Westbrook, "Compensation fibre chromatic dispersion by optical phase conjugation in a semiconductor laser amplifier," *Electronics letters*, vol. 29, no. 21, pp. 1851–1852, 1993.
- [95] A. Gnauck, R. Jopson, P. Iannone, and R. Derosier, "Transmission of two wavelength-multiplexed 10 Gbit/s channels over 560 km of dispersive fibre," *Electronics Letters*, vol. 30, no. 9, pp. 727–728, 1994.
- [96] X. Zhang, F. Ebskamp, and B. F. Jørgensen, "Long-distance transmission over standard fiber by use of mid-way phase conjugation," *IEEE photonics technology letters*, vol. 7, no. 7, pp. 819–821, 1995.
- [97] S. Watanabe, G. Ishikawa, T. Naito, and T. Chikama, "Generation of optical phase-conjugate waves and compensation for pulse shape distortion in a single-mode fiber," *Journal of lightwave technology*, vol. 12, no. 12, pp. 2139–2146, 1994.
- [98] K. Kikuchi, "Elimination of four-wave mixing in dispersion-shifted optical fibers by using midway optical phase conjugation in a semiconductor optical amplifier," in *Lasers and Electro-Optics, 1996. CLEO'96., Summaries of papers presented at the Conference on. IEEE*, 1996, pp. 42–43.
- [99] P. Minzioni, P. Harper, V. Pusino, L. Barker, C. Langrock, M. M. Fejer, J.-D. Ania-Castanon, I. Cristiani, and V. Degiorgio, "Optical phase conjugation for dispersion and

REFERENCES

- nonlinearity compensation in a 1600km, 42 Gb/s quasi-lossless system,” in *Nonlinear Optics: Materials, Fundamentals and Applications*. Optical Society of America, 2009, p. NThA5.
- [100] A. Ellis, M. Tatham, D. Davies, D. Nasset, D. Moodie, and G. Sherlock, “40 Gbit/s transmission over 202 km of standard fibre using midspan spectral inversion,” *Electronics Letters*, vol. 31, no. 4, pp. 299–301, 1995.
- [101] D. Marcenac, D. Nasset, A. Kelly, M. Brierly, A. Ellis, D. Moodie, and C. Ford, “40 Gbit/s transmission over 406 km of NDSF using mid-span spectral inversion by four-wave-mixing in a 2 mm long semiconductor optical amplifier,” *Electronics Letters*, vol. 33, no. 10, pp. 879–880, 1997.
- [102] D. Marcenac, D. Nasset, A. Kelly, and D. Gavrilovic, “40 Gbit/s transmission over 103 km of NDSF using polarisation independent mid-span spectral inversion by four-wave mixing in a semiconductor optical amplifier,” *Electronics Letters*, vol. 34, no. 1, pp. 100–101, 1998.
- [103] U. Feiste, R. Ludwig, C. Schmidt, E. Dietrich, S. Diez, H. Ehrke, E. Patzak, H. Weber, and T. Merker, “80-Gb/s transmission over 106-km standard-fiber using optical phase conjugation in a Sagnac-interferometer,” *IEEE Photonics Technology Letters*, vol. 11, no. 8, pp. 1063–1065, 1999.
- [104] J. Inoue, H. Sotobayashi, W. Chujo, and H. Kawaguchi, “80 Gbit/s OTDM signal transmission over 208km standard fibre using midspan optical phase conjugation based on four-wave mixing in semiconductor optical amplifiers,” *Electronics Letters*, vol. 38, no. 15, p. 1, 2002.
- [105] I. Brener, B. Mikkelsen, K. Rottwitt, W. Burkett, G. Raybon, J. Stark, K. Parameswaran, M. Chou, M. Fejer, E. Chaban *et al.*, “Cancellation of all Kerr nonlinearities in long fiber spans using a LiNbO₃ phase conjugator and Raman amplification,” in *Optical Fiber Communication Conference*. Optical Society of America, 2000, p. PD33.
- [106] S. Set, R. Girardi, E. Riccardi, B. Olsson, M. Puleo, M. Ibsen, R. Laming, P. Andrekson, F. Cisternino, and H. Geiger, “40Gbit/s field transmission over standard fibre using

- midspan spectral inversion for dispersion compensation,” *Electronics Letters*, vol. 35, no. 7, pp. 581–582, 1999.
- [107] A. Chowdhury, G. Raybon, R.-J. Essiambre, J. H. Sinsky, A. Adamiecki, J. Leuthold, C. R. Doerr, and S. Chandrasekhar, “Compensation of intrachannel nonlinearities in 40-Gb/s pseudolinear systems using optical-phase conjugation,” *Journal of lightwave technology*, vol. 23, no. 1, p. 172, 2005.
- [108] S. Radic, R. Jopson, C. McKinstrie, A. Gnauck, S. Chandrasekhar, and J. Centanni, “Wavelength division multiplexed transmission over standard single mode fiber using polarization insensitive signal conjugation in highly nonlinear optical fiber,” in *Optical Fiber Communications Conf.(OFC03), Atlanta, GA, 2003*.
- [109] S. L. Jansen, S. Spälter, G.-D. Khoe, H. de Waardt, H. E. Escobar, M. Sher, D. Woll, and D. Zhou, “10Gbit/s, 25GHz spaced transmission over 800km without using dispersion compensation modules,” in *Optical Fiber Communication Conference*. Optical Society of America, 2004, p. ThT1.
- [110] A. Chowdhury, G. Raybon, R. Essiambre, and C. Doerr, “Optical phase conjugation in a WDM CSRZ pseudo-linear 40 Gb/s system for 4800 km transmission,” in *Eur. Conf. Optical Communication (ECOC), Stockholm, Sweden, 2004*.
- [111] S. Jansen, G.-D. Khoe, H. de Waardt, S. Spälter, C.-J. Weiske, A. Schöpflin, S. Field, H. Escobar, and M. Sher, “Mixed data rate and format transmission (40-Gbit/s non-return-to-zero, 40-Gbit/s duobinary, and 10-Gbit/s non-return-to-zero) by mid-link spectral inversion,” *Optics letters*, vol. 29, no. 20, pp. 2348–2350, 2004.
- [112] S. L. Jansen, D. van den Borne, C. Climent, M. Serbay, C.-J. Weiske, H. Suche, P. Krummrich, S. Spaelter, S. Calabró, N. Hecker-Denschlag *et al.*, “10,200 km 22x2x10Gbit/s RZ-DQPSK Dense WDM Transmission without inline dispersion compensation through optical phase conjugation,” in *Optical Fiber Communication Conference*. Optical Society of America, 2005, p. PDP28.

REFERENCES

- [113] S. Ayotte, H. Rong, S. Xu, O. Cohen, and M. J. Paniccia, “Multichannel dispersion compensation using a silicon waveguide-based optical phase conjugator,” *Optics letters*, vol. 32, no. 16, pp. 2393–2395, 2007.
- [114] M. Pelusi, F. Luan, D.-Y. Choi, S. Madden, D. Bulla, B. Luther-Davies, and B. Eggleton, “Optical phase conjugation by an As₂S₃ glass planar waveguide for dispersion-free transmission of WDM-DPSK signals over fiber,” *Optics Express*, vol. 18, no. 25, pp. 26 686–26 694, 2010.
- [115] L. Marazzi, P. Parolari, P. Martelli, R. Siano, P. Boffi, M. Ferrario, A. Righetti, M. Martinelli, V. Pusino, P. Minzioni *et al.*, “Real-time 100-Gb/s POLMUX RZ-DQPSK transmission over uncompensated 500 km of SSMF by optical phase conjugation,” in *Optical Fiber Communication Conference*. Optical Society of America, 2009, p. JWA44.
- [116] H. Hu, R. Nouroozi, R. Ludwig, C. Schmidt-Langhorst, H. Suche, W. Sohler, and C. Schubert, “110 km transmission of 160 Gbit/s RZ-DQPSK signals by midspan polarization-insensitive optical phase conjugation in a Ti: PPLN waveguide,” *Optics letters*, vol. 35, no. 17, pp. 2867–2869, 2010.
- [117] D. Rafique and A. D. Ellis, “Various nonlinearity mitigation techniques employing optical and electronic approaches,” *IEEE photonics technology letters*, vol. 23, no. 23, pp. 1838–1840, 2011.
- [118] B.-E. Olsson, C. Larsson, J. Martensson, and A. Alping, “Experimental demonstration of electro-optical mid-span spectrum inversion for mitigation of non-linear fiber effects,” in *European Conference and Exhibition on Optical Communication*. Optical Society of America, 2012, pp. Th-1.
- [119] X. Chen, X. Liu, S. Chandrasekhar, B. Zhu, and R. Tkach, “Experimental demonstration of fiber nonlinearity mitigation using digital phase conjugation,” in *Optical Fiber Communication Conference*. Optical Society of America, 2012, pp. OTh3C-1.

-
- [120] L. B. Du, M. M. Morshed, and A. J. Lowery, “604-Gb/s coherent optical OFDM over 800 km of S-SMF with mid-span spectral inversion,” in *2012 17th Opto-Electronics and Communications Conference*, 2012.
- [121] M. Morshed, L. B. Du, B. Foo, M. D. Pelusi, and A. J. Lowery, “Optical phase conjugation for nonlinearity compensation of 1.21-Tb/s pol-mux coherent optical OFDM,” in *OptoElectronics and Communications Conference and Photonics in Switching*. Optical Society of America, 2013, p. PD3_4.
- [122] F. Da Ros, I. Sackey, R. Elschner, T. Richter, C. Meuer, M. Nölle, M. Jazayerifar, K. Petermann, C. Peucheret, and C. Schubert, “Kerr nonlinearity compensation in a 5×28 -GBd PDM 16-QAM WDM system using fiber-based optical phase conjugation,” in *40th European Conference on Optical Communication (ECOC 2014)*. IEEE, 2014, pp. paper-P.
- [123] I. Sackey, F. Da Ros, M. Jazayerifar, T. Richter, C. Meuer, M. Nölle, L. Molle, C. Peucheret, K. Petermann, and C. Schubert, “Kerr nonlinearity mitigation in 5×28 -GBd PDM 16-QAM signal transmission over a dispersion-uncompensated link with backward-pumped distributed Raman amplification,” *Optics Express*, vol. 22, no. 22, pp. 27 381–27 391, 2014.
- [124] I. Phillips, M. Tan, M. F. Stephens, M. McCarthy, E. Giacomidis, S. Sygletos, P. Rosa, S. Fabbri, S. T. Le, T. Kanesan *et al.*, “Exceeding the nonlinear-Shannon limit using Raman laser based amplification and optical phase conjugation,” in *Optical Fiber Communication Conference*. Optical Society of America, 2014, pp. M3C-1.
- [125] D. Vukovic, J. Schröder, F. Da Ros, L. B. Du, C. J. Chae, D.-Y. Choi, M. D. Pelusi, and C. Peucheret, “Multichannel nonlinear distortion compensation using optical phase conjugation in a silicon nanowire,” *Optics Express*, vol. 23, no. 3, pp. 3640–3646, 2015.
- [126] A. Ellis, I. Phillips, M. Tan, M. Stephens, M. McCarthy, M. Al Kahteb, M. Iqbal, A. Perentos, S. Fabbri, V. Gordienko *et al.*, “Enhanced superchannel transmission using phase conjugation,” 2015.

REFERENCES

- [127] M. A. Al-Khateeb, M. Tan, M. A. Iqbal, A. Ali, M. E. McCarthy, P. Harper, and A. D. Ellis, “Experimental demonstration of 72% reach enhancement of 3.6 Tbps optical transmission system using mid-link optical phase conjugation,” *Optics Express*, vol. 26, no. 18, pp. 23 960–23 968, 2018.
- [128] K. Solis-Trapala, M. Pelusi, H. N. Tan, T. Inoue, S. Suda, and S. Namiki, “Doubled transmission reach for DP-64QAM signal over field-deployed legacy fiber systems enabled by MSSSI,” in *Optical Communication (ECOC), 2015 European Conference on*. IEEE, 2015, pp. 1–3.
- [129] S. Yoshima, Y. Sun, K. Bottrill, F. Parmigiani, P. Petropoulos, and D. Richardson, “Non-linearity mitigation through optical phase conjugation in a deployed fibre link with full bandwidth utilization,” 2015.
- [130] S. Yoshima, Z. Liu, Y. Sun, K. R. Bottrill, F. Parmigiani, P. Petropoulos, and D. J. Richardson, “Nonlinearity mitigation for multi-channel 64-QAM signals in a deployed fiber link through optical phase conjugation,” in *Optical Fiber Communication Conference*. Optical Society of America, 2016, pp. Th4F–4.
- [131] H. Hu, R. M. Jopson, A. Gnauck, M. Dinu, S. Chandrasekhar, X. Liu, C. Xie, M. Montoliu, S. Randel, and C. McKinstrie, “Fiber nonlinearity compensation of an 8-channel WDM PDM-QPSK signal using multiple phase conjugations,” in *Optical Fiber Communication Conference*. Optical Society of America, 2014, pp. M3C–2.
- [132] K. Solis-Trapala, M. Pelusi, H. N. Tan, T. Inoue, and S. Namiki, “Transmission optimized impairment mitigation by 12 stage phase conjugation of WDM 24×48 Gb/s DP-QPSK signals,” in *2015 Optical Fiber Communications Conference and Exhibition (OFC)*. IEEE, 2015, pp. 1–3.
- [133] H. Hu, R. M. Jopson, A. Gnauck, D. Pileri, S. Randel, and S. Chandrasekhar, “Fiber non-linearity compensation by repeated phase conjugation in 2.048-Tbit/s WDM transmission of PDM 16-QAM Channels,” in *Optical Fiber Communication Conference*. Optical Society of America, 2016, pp. Th4F–3.

-
- [134] S. Watanabe and M. Shirasaki, “Exact compensation for both chromatic dispersion and Kerr effect in a transmission fiber using optical phase conjugation,” *Journal of Lightwave Technology*, vol. 14, no. 3, pp. 243–248, 1996.
- [135] K. Solis-Trapala, T. Inoue, and S. Namiki, “Nearly-ideal optical phase conjugation based nonlinear compensation system,” in *Optical Fiber Communication Conference*. Optical Society of America, 2014, pp. W3F–8.
- [136] M. McCarthy, M. Al Kahteb, F. Ferreira, and A. Ellis, “PMD tolerant nonlinear compensation using in-line phase conjugation,” *Optics Express*, vol. 24, no. 4, pp. 3385–3392, 2016.
- [137] A. Mecozzi, C. B. Clausen, M. Shtaif, S.-G. Park, and A. Gnauck, “Cancellation of timing and amplitude jitter in symmetric links using highly dispersed pulses,” *IEEE Photonics Technology Letters*, vol. 13, no. 5, pp. 445–447, 2001.
- [138] P. Minzioni and A. Schiffrini, “Unifying theory of compensation techniques for intrachannel nonlinear effects,” *Optics Express*, vol. 13, no. 21, pp. 8460–8468, 2005.
- [139] T. Freckmann, R.-J. Essiambre, P. Winzer, G. Foschini, and G. Kramer, “Fiber capacity limits with optimized ring constellations,” *IEEE Photonics Technology Letters*, vol. 21, no. 20, pp. 1496–1498, 2009.
- [140] T. Lotz, X. Liu, S. Chandrasekhar, P. Winzer, H. Haunstein, S. Randel, S. Corteselli, B. Zhu, and D. Peckham, “Coded PDM-OFDM transmission with shaped 256-iterative-polar-modulation achieving 11.15-b/s/Hz intrachannel spectral efficiency and 800-km reach,” *Journal of Lightwave Technology*, vol. 31, no. 4, pp. 538–545, 2012.
- [141] L. Beygi, E. Agrell, J. M. Kahn, and M. Karlsson, “Rate-adaptive coded modulation for fiber-optic communications,” *Journal of Lightwave Technology*, vol. 32, no. 2, pp. 333–343, 2013.
- [142] J. Cho and P. J. Winzer, “Probabilistic constellation shaping for optical fiber communications,” *Journal of Lightwave Technology*, vol. 37, no. 6, pp. 1590–1607, 2019.

REFERENCES

- [143] F. Buchali, F. Steiner, G. Böcherer, L. Schmalen, P. Schulte, and W. Idler, “Rate adaptation and reach increase by probabilistically shaped 64-QAM: An experimental demonstration,” *Journal of Lightwave Technology*, vol. 34, no. 7, pp. 1599–1609, 2016.
- [144] A. Shiner, M. Reimer, A. Borowiec, S. O. Gharan, J. Gaudette, P. Mehta, D. Charlton, K. Roberts, and M. ÓSullivan, “Demonstration of an 8-dimensional modulation format with reduced inter-channel nonlinearities in a polarization multiplexed coherent system,” *Optics Express*, vol. 22, no. 17, pp. 20 366–20 374, 2014.
- [145] C. Behrens, S. Makovejs, R. I. Killey, S. J. Savory, M. Chen, and P. Bayvel, “Pulse-shaping versus digital backpropagation in 224Gbit/s PDM-16QAM transmission,” *Optics Express*, vol. 19, no. 14, pp. 12 879–12 884, 2011.
- [146] B. Châtelain, C. Laperle, K. Roberts, M. Chagnon, X. Xu, A. Borowiec, F. Gagnon, and D. V. Plant, “A family of Nyquist pulses for coherent optical communications,” *Optics Express*, vol. 20, no. 8, pp. 8397–8416, 2012.
- [147] P. Poggiolini, A. Carena, Y. Jiang, G. Bosco, and F. Forghieri, “On the ultimate potential of symbol-rate optimization for increasing system maximum reach,” in *2015 European Conference on Optical Communication (ECOC)*. IEEE, 2015, pp. 1–3.
- [148] M. Qiu, Q. Zhuge, X. Xu, M. Chagnon, M. Morsy-Osman, and D. V. Plant, “Subcarrier multiplexing using DACs for fiber nonlinearity mitigation in coherent optical communication systems,” in *Optical Fiber Communication Conference*. Optical Society of America, 2014, pp. Tu3J–2.
- [149] X. Liu, S. Chandrasekhar, P. Winzer, R. W. Tkach, and A. R. Chraplyvy, “406.6-Gb/s PDM-BPSK superchannel transmission over 12,800-km TWRS fiber via nonlinear noise squeezing,” in *2013 Optical Fiber Communication Conference and Exposition and the National Fiber Optic Engineers Conference (OFC/NFOEC)*. IEEE, 2013, pp. 1–3.
- [150] A. Ghazisaeidi, J. Renaudier, M. Salsi, P. Tran, G. Charlet, and S. Bigo, “System benefits of digital dispersion pre-compensation for non-dispersion-managed PDM-WDM transmis-

-
- sion,” in *39th European Conference and Exhibition on Optical Communication (ECOC 2013)*. IET, 2013, pp. 1–3.
- [151] M. I. Yousefi and F. R. Kschischang, “Information transmission using the nonlinear Fourier transform, part I: Mathematical tools,” *IEEE Transactions on Information Theory*, vol. 60, no. 7, pp. 4312–4328, 2014.
- [152] S. K. Turitsyn, J. E. Prilepsky, S. T. Le, S. Wahls, L. L. Frumin, M. Kamalian, and S. A. Derevyanko, “Nonlinear Fourier transform for optical data processing and transmission: advances and perspectives,” *Optica*, vol. 4, no. 3, pp. 307–322, 2017.
- [153] I. T. Lima, V. S. Grigoryan, M. O’Sullivan, and C. R. Menyuk, “Computational complexity of nonlinear transforms applied to optical communications systems with normal dispersion fibers,” in *2015 IEEE Photonics Conference (IPC)*. IEEE, 2015, pp. 277–278.
- [154] X. Liu, “Twin-wave-based optical transmission with enhanced linear and nonlinear performances,” *Journal of Lightwave Technology*, vol. 33, no. 5, pp. 1037–1043, 2015.
- [155] Y. Han and G. Li, “Polarization diversity transmitter and optical nonlinearity mitigation using polarization-time coding,” in *Coherent Optical Technologies and Applications*. Optical Society of America, 2006, p. CThC7.
- [156] Y. Yu, W. Wang, P. D. Townsend, and J. Zhao, “Modified phase-conjugate twin wave schemes for spectral efficiency enhancement,” in *Optical Communication (ECOC), 2015 European Conference on*. IEEE, 2015, pp. 1–3.
- [157] S. T. Le, M. E. McCarthy, N. Mac Suibhne, A. D. Ellis, and S. K. Turitsyn, “Phase-conjugated pilots for fibre nonlinearity compensation in CO-OFDM transmission,” *Journal of Lightwave Technology*, vol. 33, no. 7, pp. 1308–1314, 2015.
- [158] T. Yoshida, T. Sugihara, K. Ishida, and T. Mizuoichi, “Spectrally-efficient dual phase-conjugate twin waves with orthogonally multiplexed quadrature pulse-shaped signals,” in *Optical Fiber Communication Conference*. Optical Society of America, 2014, pp. M3C–6.

REFERENCES

- [159] Y. Tian, Y.-K. Huang, S. Zhang, P. R. Prucnal, and T. Wang, "Demonstration of digital phase-sensitive boosting to extend signal reach for long-haul WDM systems using optical phase-conjugated copy," *Optics Express*, vol. 21, no. 4, pp. 5099–5106, 2013.
- [160] H. Eliasson, P. Johannisson, M. Karlsson, and P. A. Andrekson, "Mitigation of nonlinearities using conjugate data repetition," *Optics Express*, vol. 23, no. 3, pp. 2392–2402, 2015.
- [161] "S1A : Optical Experiments and Testing: With or without FEC? Workshop," in *the 2019 Optical Fiber Communication Conference, San Diego, 2019*.
- [162] A. Alvarado, E. Agrell, D. Lavery, R. Maher, and P. Bayvel, "Replacing the soft-decision FEC limit paradigm in the design of optical communication systems," *Journal of Lightwave Technology*, vol. 34, pp. 707–721, 2016.
- [163] R.-J. Essiambre, G. Kramer, P. J. Winzer, G. J. Foschini, and B. Goebel, "Capacity limits of optical fiber networks," *Journal of Lightwave Technology*, vol. 28, no. 4, pp. 662–701, 2010.
- [164] I. E. Commission *et al.*, "Fibre optic communication subsystem test procedures: part 1-3," IEC 61280-1-3 2010, Tech. Rep.
- [165] W. Moench and E. Loecklin, "Measurement of optical signal-to-noise-ratio in coherent systems using polarization multiplexed transmission," in *2017 Optical Fiber Communications Conference and Exhibition (OFC)*. IEEE, 2017, pp. 1–3.
- [166] R. Schmogrow, B. Nebendahl, M. Winter, A. Josten, D. Hillerkuss, S. Koenig, J. Meyer, M. Dreschmann, M. Huebner, C. Koos *et al.*, "Error vector magnitude as a performance measure for advanced modulation formats," *IEEE Photonics Technology Letters*, vol. 24, no. 1, pp. 61–63, 2011.
- [167] S. T. Le, M. E. McCarthy, N. Mac Suibhne, E. Giacoumidis, N. J. Doran, A. D. Ellis, and K. J. Blow, "Comparison of bit error rate estimation methods for QPSK CO-OFDM transmission," *IEEE Photonics Technology Letters*, vol. 26, no. 22, pp. 2244–2247, 2014.

-
- [168] S. T. Le, K. J. Blow, V. K. Mezentsev, and S. K. Turitsyn, “Bit error rate estimation methods for QPSK CO-OFDM transmission,” *Journal of Lightwave Technology*, vol. 32, no. 17, pp. 2951–2959, 2014.
- [169] T. M. Cover and J. A. Thomas, *Elements of information theory*. John Wiley & Sons, 2012.
- [170] R. R. Müller, “Advanced modulation formats and signal processing for high speed spectrally efficient optical communications,” Ph.D. dissertation, 2016.
- [171] A. Splett, C. Kurtzke, and K. Petermann, “Ultimate transmission capacity of amplified optical fiber communication systems taking into account fiber nonlinearities,” vol. 2, pp. 41–44, 1993.
- [172] H. Louchet, A. Hodzic, and K. Petermann, “Analytical model for the performance evaluation of DWDM transmission systems,” *IEEE Photon. Technol. Lett.*, vol. 15, no. 9, pp. 1219–1221, Sept 2003.
- [173] A. Carena, V. Curri, G. Bosco, P. Poggiolini, and F. Forghieri, “Modeling of the impact of nonlinear propagation effects in uncompensated optical coherent transmission links,” *Journal of Lightwave technology*, vol. 30, no. 10, pp. 1524–1539, 2012.
- [174] X. Chen and W. Shieh, “Closed-form expressions for nonlinear transmission performance of densely spaced coherent optical OFDM systems,” *Optics Express*, vol. 18, no. 18, pp. 19 039–19 054, 2010.
- [175] P. Poggiolini, A. Carena, V. Curri, G. Bosco, and F. Forghieri, “Analytical modeling of nonlinear propagation in uncompensated optical transmission links,” *IEEE Photonics technology letters*, vol. 23, no. 11, pp. 742–744, 2011.
- [176] P. Poggiolini, G. Bosco, A. Carena, V. Curri, and F. Forghieri, “A simple and accurate model for non-linear propagation effects in uncompensated coherent transmission links,” in *2011 13th International Conference on Transparent Optical Networks*. IEEE, 2011, pp. 1–6.

REFERENCES

- [177] G. Bosco, P. Poggiolini, A. Carena, V. Curri, and F. Forghieri, “Analytical results on channel capacity in uncompensated optical links with coherent detection,” *Optics Express*, vol. 19, no. 26, pp. B440–B451, 2011.
- [178] P. Poggiolini, “The GN model of non-linear propagation in uncompensated coherent optical systems,” *Journal of Lightwave Technology*, vol. 30, no. 24, pp. 3857–3879, 2012.
- [179] E. Torrenco, R. Cigliutti, G. Bosco, A. Carena, V. Curri, P. Poggiolini, A. Nespola, D. Zeolla, and F. Forghieri, “Experimental validation of an analytical model for nonlinear propagation in uncompensated optical links,” *Optics Express*, vol. 19, no. 26, pp. B790–B798, 2011.
- [180] P. Poggiolini, G. Bosco, A. Carena, V. Curri, Y. Jiang, and F. Forghieri, “The GN-model of fiber non-linear propagation and its applications,” *Journal of lightwave technology*, vol. 32, no. 4, pp. 694–721, 2013.
- [181] P. Johannisson and M. Karlsson, “Perturbation analysis of nonlinear propagation in a strongly dispersive optical communication system,” *Journal of Lightwave Technology*, vol. 31, no. 8, pp. 1273–1282, 2013.
- [182] A. Bononi, O. Beucher, and P. Serena, “Single-and cross-channel nonlinear interference in the Gaussian noise model with rectangular spectra,” *Optics Express*, vol. 21, no. 26, pp. 32 254–32 268, 2013.
- [183] A. Mecozzi and R.-J. Essiambre, “Nonlinear Shannon limit in pseudolinear coherent systems,” *Journal of Lightwave Technology*, vol. 30, no. 12, pp. 2011–2024, 2012.
- [184] Y. Fan, L. Dou, Z. Tao, L. Lei, S. Oda, T. Hoshida, and J. C. Rasmussen, “Modulation format dependent phase noise caused by intra-channel nonlinearity,” in *2012 38th European Conference and Exhibition on Optical Communications*. IEEE, 2012, pp. 1–3.
- [185] R. Dar, M. Feder, A. Mecozzi, and M. Shtaif, “Properties of nonlinear noise in long, dispersion-uncompensated fiber links,” *Optics Express*, vol. 21, no. 22, pp. 25 685–25 699, 2013.

-
- [186] A. Carena, G. Bosco, V. Curri, Y. Jiang, P. Poggiolini, and F. Forghieri, “EGN model of non-linear fiber propagation,” *Optics Express*, vol. 22, no. 13, pp. 16 335–16 362, 2014.
- [187] P. Poggiolini, G. Bosco, A. Carena, V. Curri, Y. Jiang, and F. Forghieri, “A simple and effective closed-form GN model correction formula accounting for signal non-Gaussian distribution,” *Journal of Lightwave Technology*, vol. 33, no. 2, pp. 459–473, 2015.
- [188] P. Serena and A. Bononi, “A time-domain extended Gaussian noise model,” *Journal of Lightwave Technology*, vol. 33, no. 7, pp. 1459–1472, 2015.
- [189] R. Dar, M. Feder, A. Mecozzi, and M. Shtaif, “Accumulation of nonlinear interference noise in fiber-optic systems,” *Optics Express*, vol. 22, no. 12, pp. 14 199–14 211, 2014.
- [190] —, “Inter-channel nonlinear interference noise in WDM systems: modeling and mitigation,” *Journal of Lightwave Technology*, vol. 33, no. 5, pp. 1044–1053, 2014.
- [191] —, “Pulse collision picture of inter-channel nonlinear interference in fiber-optic communications,” *Journal of Lightwave Technology*, vol. 34, no. 2, pp. 593–607, 2016.
- [192] V. Pechenkin and I. J. Fair, “Analysis of four-wave mixing suppression in fiber-optic OFDM transmission systems with an optical phase conjugation module,” *Journal of Optical Communications and Networking*, vol. 2, no. 9, pp. 701–710, 2010.
- [193] I. Kim, O. Vassilieva, P. Palacharla, M. Sekiya, and T. Ikeuchi, “Analysis of nonlinearity mitigation using spectral inversion for superchannel transmission,” *IEEE Photonics Journal*, vol. 8, no. 5, pp. 1–8, 2016.
- [194] X. Xiao, C. Yang, and P. Shum, “Analytical design of SPM-limited systems with optical phase conjugation,” *IEEE Photonics Technology Letters*, vol. 20, no. 7, pp. 472–474, 2008.
- [195] M. A. Al-Khateeb, M. E. McCarthy, and A. D. Ellis, “Performance enhancement prediction for optical phase conjugation in systems with 100km amplifier spacing,” in *2017 European Conference on Optical Communication (ECOC)*. IEEE, 2017, pp. 1–3.

REFERENCES

- [196] A. A. Ali, C. S. Costa, M. A. Al-Khateeb, F. M. Ferreira, and A. D. Ellis, “An expression for nonlinear noise in optical phase conjugation systems with lumped amplifiers,” *IEEE Photonics Technology Letters*, vol. 30, no. 23, pp. 2056–2059, 2018.
- [197] I. Sackey, R. Elschner, C. Schmidt-Langhorst, T. Kato, T. Tanimura, S. Watanabe, T. Hoshida, and C. Schubert, “Novel wavelength-shift-free optical phase conjugator used for fiber nonlinearity mitigation in 200-Gb/s PDM-16QAM transmission,” in *Optical Fiber Communication Conference*. Optical Society of America, 2017, pp. Th3J–1.
- [198] K. Hill, D. Johnson, B. Kawasaki, and R. MacDonald, “CW three-wave mixing in single-mode optical fibers,” *Journal of Applied Physics*, vol. 49, no. 10, pp. 5098–5106, 1978.
- [199] D. Marcuse, “Pulse distortion in single-mode fibers,” *Applied Optics*, vol. 19, no. 10, pp. 1653–1660, 1980.
- [200] N. Shibata, R. Braun, and R. Waarts, “Phase-mismatch dependence of efficiency of wave generation through four-wave mixing in a single-mode optical fiber,” *IEEE Journal of Quantum Electronics*, vol. 23, no. 7, pp. 1205–1210, 1987.
- [201] A. Carena, G. Bosco, V. Curri, P. Poggiolini, M. Taiba, and F. Forghieri, “Statistical characterization of PM-QPSK signals after propagation in uncompensated fiber links,” in *36th European Conference and Exhibition on Optical Communication (ECOC)*, Torino, Sept 2010, pp. 1–3.
- [202] F. Vacondio, C. Simonneau, L. Lorcy, J.-C. Antona, A. Bononi, and S. Bigo, “Experimental characterization of Gaussian-distributed nonlinear distortions,” in *37th European Conference and Exhibition on Optical Communication (ECOC)*, Geneva, Sept 2011, pp. 1–3.
- [203] T. M. Schmidl and D. C. Cox, “Robust frequency and timing synchronization for OFDM,” *IEEE transactions on communications*, vol. 45, no. 12, pp. 1613–1621, 1997.

-
- [204] G. Gao, X. Chen, and W. Shieh, “Analytical expressions for nonlinear transmission performance of coherent optical OFDM systems with frequency guard band,” *Journal of Lightwave Technology*, vol. 30, no. 15, pp. 2447–2454, 2012.
- [205] P. Poggiolini, “A generalized GN-model closed-form formula,” *arXiv preprint arXiv:1810.06545*, 2018.
- [206] G. Saavedra, D. Semrau, M. Tan, M. A. Iqbal, D. Elson, L. Galdino, P. Harper, R. Killely, and P. Bayvel, “Inter-channel stimulated Raman scattering and its impact in wideband transmission systems,” in *2018 Optical Fiber Communications Conference and Exposition (OFC)*. IEEE, 2018, pp. 1–3.
- [207] K. Minoguchi, S. Okamoto, F. Hamaoka, A. Matsushita, M. Nakamura, E. Yamazaki, and Y. Kisaka, “Experiments on stimulated Raman scattering in S-and L-bands 16-QAM signals for ultra-wideband coherent WDM systems,” in *Optical Fiber Communication Conference*. Optical Society of America, 2018, pp. Th1C–4.
- [208] A. D. Ellis, M. Tan, M. A. Iqbal, M. A. Z. Al-Khateeb, V. Gordienko, G. S. Mondaca, S. Fabbri, M. F. Stephens, M. E. McCarthy, A. Perentos *et al.*, “4 Tb/s transmission reach enhancement using 10×400 Gb/s super-channels and polarization insensitive dual band optical phase conjugation,” *Journal of lightwave technology*, vol. 34, no. 8, pp. 1717–1723, 2016.
- [209] K. Torii and S. Yamashita, “Efficiency improvement of optical fiber wavelength converter without spectral spread using synchronous phase/frequency modulations,” *Journal of lightwave technology*, vol. 21, no. 4, p. 1039, 2003.
- [210] A. A. Cuyt, V. Petersen, B. Verdonk, H. Waadeland, and W. B. Jones, *Handbook of continued fractions for special functions*. Springer Science & Business Media, 2008.
- [211] R. Elschner, T. Richter, L. Molle, C. Schubert, and K. Petermann, “Single-pump FWM-wavelength conversion in HNLF using coherent receiver-based electronic compensation,” in *36th European Conference and Exhibition on Optical Communication*. IEEE, 2010, pp. 1–3.

REFERENCES

- [212] H. Hu, R. M. Jopson, A. H. Gnauck, S. Randel, and S. Chandrasekhar, "Fiber nonlinearity mitigation of WDM-PDM QPSK/16-QAM signals using fiber-optic parametric amplifiers based multiple optical phase conjugations," *Optics Express*, vol. 25, no. 3, pp. 1618–1628, 2017.
- [213] I. Sackey, F. Da Ros, T. Richter, R. Elschner, M. Jazayerifar, C. Meuer, C. Peucheret, K. Petermann, and C. Schubert, "Design and performance evaluation of an OPC device using a dual-pump polarization-independent FOPA," in *2014 The European Conference on Optical Communication (ECOC)*. IEEE, 2014, pp. 1–3.
- [214] T. Hasegawa, K. Inoue, and K. Oda, "Polarization independent frequency conversion by fiber four-wave mixing with a polarization diversity technique," *IEEE photonics technology letters*, vol. 5, no. 8, pp. 947–949, 1993.
- [215] R. Jopson and R. Tench, "Polarisation-independent phase conjugation of lightwave signals," *Electronics Letters*, vol. 29, no. 25, pp. 2216–2217, 1993.
- [216] K. Inoue, "Polarization independent wavelength conversion using fiber four-wave mixing with two orthogonal pump lights of different frequencies," *Journal of lightwave technology*, vol. 12, no. 11, pp. 1916–1920, 1994.
- [217] F. Yang, M. Marhic, and L. Kazovsky, "CW fibre optical parametric amplifier with net gain and wavelength conversion efficiency ≥ 1 ," *Electronics Letters*, vol. 32, no. 25, pp. 2336–2338, 1996.
- [218] H. N. Tan, T. Inoue, K. Solis-Trapala, S. Petitz, Y. Oikawaz, S. Takasakayy, T. Yagiyy, M. Pelusi, and S. Namiki, "First demonstration of wavelength conversion of DP-64QAM signal using an improved counter-dithering pump scheme," in *2015 Opto-Electronics and Communications Conference (OECC)*. IEEE, 2015, pp. 1–3.
- [219] K. Inoue, "Spectral inversion with no wavelength shift based on four-wave mixing with orthogonal pump beams," *Optics letters*, vol. 22, no. 23, pp. 1772–1774, 1997.

-
- [220] P. Winzer, A. Gnauck, A. Konczykowska, F. Jorge, and J.-Y. Dupuy, “Penalties from in-band crosstalk for advanced optical modulation formats,” in *European Conference and Exposition on Optical Communications*. Optical Society of America, 2011, pp. Tu–5.
- [221] A. A. I. Ali, M. Tan, M. A. Z. Al-khateeb, C. Laperle, and A. D. Ellis, “First demonstration of optical phase conjugation with real time commercial transceiver,” in *45th European Conference and Exhibition on Optical Communications (ECOC)*, Dublin, Sept 2019, pp. 1–3.
- [222] A. A. Ali, F. Ferreira, M. Al-Khateeb, D. Charlton, C. Laperle, and A. D. Ellis, “The impact of dispersion slope on fiber nonlinearity in ultra-wideband optical communication system,” in *2018 European Conference on Optical Communication (ECOC)*. IEEE, 2018, pp. 1–3.
- [223] P. Minzioni, I. Cristiani, V. Degiorgio, L. Marazzi, M. Martinelli, C. Langrock, and M. Fejer, “Experimental demonstration of nonlinearity and dispersion compensation in an embedded link by optical phase conjugation,” *IEEE photonics technology letters*, vol. 18, no. 9, pp. 995–997, 2006.
- [224] P. Minzioni, V. Pusino, I. Cristiani, L. Marazzi, M. Martinelli, C. Langrock, M. Fejer, and V. Degiorgio, “Optical phase conjugation in phase-modulated transmission systems: experimental comparison of different nonlinearity-compensation methods,” *Optics Express*, vol. 18, no. 17, pp. 18 119–18 124, 2010.
- [225] A. Ali, M. Al-Khateeb, T. Zhang, F. Ferreira, and A. Ellis, “Enhanced nonlinearity compensation efficiency of optical phase conjugation system,” in *2019 Optical Fiber Communications Conference and Exhibition (OFC)*. IEEE, 2019, pp. 1–3.
- [226] T. Richter, J. Pan, and S. Tibuleac, “Comparison of WDM bandwidth loading using individual transponders, shaped, and flat ASE noise,” in *2018 Optical Fiber Communications Conference and Exposition (OFC)*. IEEE, 2018, pp. 1–3.

REFERENCES

- [227] A. Dochhan, S. Smolorz, H. Rohde, and W. Rosenkranz, “Fbg dispersion compensation in a 43 gbit/s wdm system: comparing different fbg types and modulation formats,” in *2009 11th International Conference on Transparent Optical Networks*. IEEE, 2009, pp. 1–4.
- [228] I. Sackey, F. Da Ros, J. K. Fischer, T. Richter, M. Jazayerifar, C. Peucheret, K. Petermann, and C. Schubert, “Kerr nonlinearity mitigation: mid-link spectral inversion versus digital backpropagation in 5×28 -GBd PDM 16-QAM signal transmission,” *Journal of Lightwave Technology*, vol. 33, no. 9, pp. 1821–1827, 2015.
- [229] M. Reimer, M. O’Sullivan, Q. Zhuge, S. O. Gharan, A. Borowiec, L. Berg, and P. Mehta, “Prospects for real-time compensation of fiber nonlinearities,” in *ECOC 2016; 42nd European Conference on Optical Communication*. VDE, 2016, pp. 1–3.
- [230] K. Solis-Trapala, T. Inoue, and S. Namiki, “Signal power asymmetry tolerance of an optical phase conjugation-based nonlinear compensation system,” in *2014 The European Conference on Optical Communication (ECOC)*. IEEE, 2014, pp. 1–3.
- [231] P. Rosa, S. T. Le, G. Rizzelli, M. Tan, and J. D. Ania-Castanón, “Signal power asymmetry optimisation for optical phase conjugation using Raman amplification,” *Optics Express*, vol. 23, no. 25, pp. 31 772–31 778, 2015.
- [232] M. Al-Khateeb, M. Tan, T. Zhang, and A. D. Ellis, “Combating fiber nonlinearity using dual-order Raman amplification and OPC,” *IEEE Photonics Technology Letters*, vol. 31, no. 11, pp. 877–880, 2019.
- [233] A. Ellis, S. Le, M. McCarthy, and S. Turitsyn, “The impact of parametric noise amplification on long haul transmission throughput,” in *2015 17th International Conference on Transparent Optical Networks (ICTON)*. IEEE, 2015, pp. 1–4.
- [234] M. A. Al-Khateeb, M. McCarthy, C. Sánchez, and A. Ellis, “Effect of second order signal–noise interactions in nonlinearity compensated optical transmission systems,” *Optics letters*, vol. 41, no. 8, pp. 1849–1852, 2016.

REFERENCES

- [235] M. Tan, P. Rosa, S. Le, V. Dvoyrin, M. A. Iqbal, S. Sugavanam, S. Turitsyn, and P. Harper, “RIN mitigation and transmission performance enhancement with forward broadband pump,” *IEEE Photonics Technology Letters*, vol. 30, no. 3, pp. 254–257, 2017.
- [236] A. Ellis, N. Mac Suibhne, F. G. Gunning, and S. Sygletos, “Expressions for the nonlinear transmission performance of multi-mode optical fiber,” *Optics Express*, vol. 21, no. 19, pp. 22 834–22 846, 2013.
- [237] F. M. Ferreira, N. Mac Suibhne, C. Sánchez, S. Sygletos, and A. Ellis, “Advantages of strong mode coupling for suppression of nonlinear distortion in few-mode fibers,” in *2016 Optical Fiber Communications Conference and Exhibition (OFC)*. IEEE, 2016, pp. 1–3.
- [238] K. Inoue, “Four-wave mixing in an optical fiber in the zero-dispersion wavelength region,” *Journal of lightwave technology*, vol. 10, no. 11, pp. 1553–1561, 1992.
- [239] R. Tkach, A. Chraplyvy, F. Forghieri, A. Gnauck, and R. Derosier, “Four-photon mixing and high-speed WDM systems,” *Journal of Lightwave Technology*, vol. 13, no. 5, pp. 841–849, 1995.

REFERENCES

Appendix A

FWM Power in Multi-Span System Employing OPC with Pre-Dispersion

In order to derive the FWM power for a multi-span lumped amplification system, employing mid-link OPC with pre-dispersion to improve the symmetry, we use Fig.(3.1) All the spans are

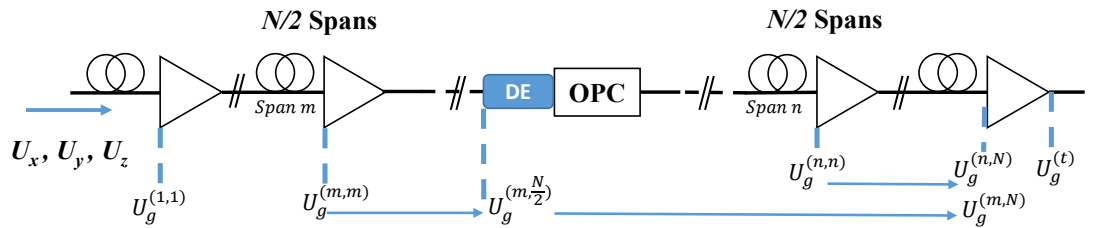


Figure A.1. Mid-link optical phase conjugation system with pre-dispersion. DE: dispersion element, $U_g^{(1,1)}$: The four-wave mixing field in the first span and N: number of spans

assumed to have the same dispersion and attenuation and the FWM power generated from each span is propagated linearly to the end of the transmission link.

A.1 Single Span FWM

The wave equation for the FWM idler U_g generated from the co-propagation of three waves U_x , U_y and U_z can be written as [198],

$$\frac{\partial^2 U_g}{\partial z^2} - \frac{n^2}{c^2} \frac{\partial^2 U_g}{\partial t^2} - \frac{\alpha n}{c} \frac{\partial U_g}{\partial t} = \frac{4\pi^2 D \chi}{c^2} \frac{\partial^2}{\partial t^2} U_x U_y U_z^* \quad (\text{A.1})$$

where z is the propagation distance, t is the time, n is the refractive index, α is the attenuation coefficient, χ is the third-order susceptibility, D is the degeneracy factor or number of permutations and U_g for an arbitrary span m can be written as,

$$U_g^{(m)} = A_g^{(m)}(z) e^{-j\omega_g t} e^{j\beta_g(z - \sum_{j=1}^{m-1} l_j)} \quad (\text{A.2})$$

where l_j is the j th span length, β_g is the idler propagation constant, ω_g is the idler angular frequency and $A_g(z)$ is the small varying envelope, while the three waves U_x , U_y and U_z in span m can be written as,

$$U_i^{(m)} = A_i^{(m)}(z) e^{-j\omega_i t} e^{(-\frac{\alpha}{2} + j\beta_i)(z - \sum_{j=1}^{m-1} l_j)}, (i = x, y, \text{ or } z) \quad (\text{A.3})$$

By substituting Eq.(A.2) and Eq.(A.3) into Eq.(A.1), we can write Eq.(A.1) as the following,

$$\begin{aligned} & e^{-j\omega_g t} e^{j\beta_g(z - \sum_{j=1}^{m-1} l_j)} \frac{\partial^2 A_g^{(m)}}{\partial z^2} + 2j\beta_g e^{-j\omega_g t} e^{j\beta_g(z - \sum_{j=1}^{m-1} l_j)} \frac{\partial A_g^{(m)}}{\partial z} + (j\beta_g)^2 e^{-j\omega_g t} e^{j\beta_g(z - \sum_{j=1}^{m-1} l_j)} A_g^{(m)}(z) \\ & - \frac{n^2}{c^2} e^{-j\omega_g t} e^{j\beta_g(z - \sum_{j=1}^{m-1} l_j)} A_g^{(m)}(z) - \frac{\alpha n}{c} (-j\omega_g) e^{-j\omega_g t} e^{j\beta_g(z - \sum_{j=1}^{m-1} l_j)} A_g^{(m)}(z) \\ & = \frac{4\pi D \chi}{c^2} (j\omega_g)^2 A_x^{(m)} A_y^{(m)} A_z^{(m)*} e^{-j\omega_g t} e^{-\frac{3}{2}\alpha(z - \sum_{j=1}^{m-1} l_j)} e^{(\beta_x + \beta_y - \beta_z)(z - \sum_{j=1}^{m-1} l_j)} \end{aligned} \quad (\text{A.4})$$

Using the fact that $\beta_g = \frac{n\omega_g}{c}$, the phase mismatch $\Delta\beta = \beta_x + \beta_y - \beta_z - \beta_g$ and the assumption that the envelope $A_g(z)$ of the the forward-travelling wave $U_g^{(m)}$ varies slowly in time and space compared with the carrier frequency (slow varying envelope approximation), therefore, $\frac{\partial^2 A_g^{(m)}}{\partial z^2} \approx$

0, and Eq.(A.4) can be simplified as,

$$\frac{dA_g^{(m)}(z)}{dz} = -\frac{\alpha}{2}A_g^{(m)}(z) + j\frac{2\pi\omega D\chi}{nc}A_x^{(m)}A_y^{(m)}A_z^{(m)*}e^{(-\frac{3}{2}\alpha+\Delta\beta)(z-\sum_{j=1}^{m-1}l_j)} \quad (\text{A.5})$$

Equation (A.5) is a standard first-order differential equation and can be written in the form,

$$\frac{dA_g(z)}{dz} + P(z)A_g(z) = Q(z) \rightarrow A_g(z) = \frac{1}{w(z)} \int w(z)Q(z) \text{ and } w(z) = e^{\int P(z)dz} \quad (\text{A.6})$$

Therefore, $A_g^{(m)}(z)$ can be written as,

$$A_g^{(m)}(z) = j\frac{2\pi\omega D\chi}{nc}e^{-\frac{\alpha}{2}l_m} \frac{e^{(-\alpha+j\Delta\beta)l_m} - 1}{-\alpha + j\Delta\beta} A_x^{(m)} A_y^{(m)} A_z^{*(m)} \quad (\text{A.7})$$

A.2 Spans Before the OPC

For the spans before the OPC, Eq.(A.7) can be written as a function of the input electric field (slow varying envelope) to the link as,

$$A_i^{(m)}(z) = A_i^{(1)}(z)e^{(-\frac{\alpha}{2}+j\beta_i)\sum_{j=1}^{m-1}l_j} \prod_{j=1}^{m-1} \sqrt{G_j}, \quad i = x, y \text{ or } z \quad (\text{A.8})$$

By substituting Eq.(A.8) into Eq.(A.7) and the FWM propagates through l_m as $A_g(z)e^{j\beta_g l_m}$ (Eq.(A.2) for $z = l_m + \sum_{j=1}^{m-1} l_j$), we can write Idler field from span m as a function of the input field to the link measured at the end of span m as the following,

$$A_g^{(m,m)}(z) = j\frac{2\pi\omega D\chi}{nc}A_x^{(1)}A_y^{(1)}A_z^{*(1)}e^{(-\frac{\alpha}{2}+j\beta_g)l_m} \frac{e^{(-\alpha+j\Delta\beta)l_m} - 1}{-\alpha + j\Delta\beta} e^{(-\frac{3}{2}\alpha+j(\Delta\beta+\beta_g)\sum_{j=1}^{m-1}l_j)} \prod_{j=1}^{m-1} (G_j)^{\frac{3}{2}} \quad (\text{A.9})$$

We define new notation $A_g^{(i,j)}$ as the idler field from span i measured at the end of span j . For the case of multi-span system without OPC, $A_g^{(m,m)}$ will be estimated at the end of the link after the linear propagation in the spans from span $m + 1$ to span N , then the idler field from all the spans is calculated by taking the summation of $\sum_{m=1}^N A_g(z)^{(m,N)}$ and this is left for the reader

APPENDIX A

for practice to get the FWM in multi-span lumped amplification system mentioned in [53–56]. The idler or FWM field $A_g^{(m,m)}$ in Eq.(A.9) will propagate linearly to the middle of the link as the following,

$$A_g^{(m,\frac{N}{2})}(z) = A_g^{(m,m)}(z)e^{(-\frac{\alpha}{2}+j\beta_g)\sum_{j=m+1}^{\frac{N}{2}}l_j}\prod_{j=m}^{\frac{N}{2}}\sqrt{G_j} \quad (\text{A.10})$$

Then $A_g^{(m,\frac{N}{2})}$ will linearly propagate through the DE as $A_g^{(m,\frac{N}{2})}e^{j\beta_{gd}L_d}$ where β_{gd} is the propagation constant of A_g inside the DE. To match the SSMF spans notations, it is assumed that the DE has a length L_d and dispersion β_{2d} . Next, $A_g^{(m,\frac{N}{2})}e^{j\beta_{gd}L_d}$ will be conjugated using the OPC then propagate linearly to the end of the link as the following,

$$A_g^{(m,N)}(z) = A_g^{*(m,\frac{N}{2})}(z)e^{-j\beta_{gd}L_d}e^{(-\frac{\alpha}{2}+j\beta_g)\sum_{j=\frac{N}{2}+1}^Nl_j}\prod_{j=\frac{N}{2}+1}^N\sqrt{G_j} \quad (\text{A.11})$$

By substituting Eq.(A.9) into Eq.(A.10) then the result is substituted into Eq.(A.11), we get the idler field resulted from span m and measured at the end of the link as the following,

$$A_g^{(m,N)}(z) = -j\frac{2\pi\omega D\chi}{nc}A_x^{*(1)}A_y^{*(1)}A_z^{(1)}\frac{e^{(-\alpha-j\Delta\beta)l_m}-1}{-\alpha-j\Delta\beta}e^{(-\frac{3}{2}\alpha-j\Delta\beta\sum_{j=1}^{m-1}l_j)}\prod_{j=1}^{m-1}(G_j)^{\frac{3}{2}} \\ e^{-j\beta_g\sum_{j=1}^{\frac{N}{2}}l_j}e^{-j\beta_{gd}L_d}e^{j\beta_g\sum_{j=\frac{N}{2}+1}^Nl_j}e^{-\frac{\alpha}{2}\sum_{j=m}^Nl_j}\prod_{j=m}^N\sqrt{G_j} \quad (\text{A.12})$$

We assume that the amplifiers ideally compensate the attenuation in each span, then $A_g^{(m,N)}(z)$ can be written as the following,

$$A_g^{(m,N)}(z) = -j\frac{2\pi\omega D\chi}{nc}A_x^{*(1)}A_y^{*(1)}A_z^{(1)}\frac{e^{(-\alpha-j\Delta\beta)l_m}-1}{-\alpha-j\Delta\beta}e^{(-j\Delta\beta\sum_{j=1}^{m-1}l_j)} \\ e^{-j\beta_g\sum_{j=1}^{\frac{N}{2}}l_j}e^{-j\beta_{gd}L_d}e^{j\beta_g\sum_{j=\frac{N}{2}+1}^Nl_j} \quad (\text{A.13})$$

A.3 Spans After the OPC

For the spans after the OPC, Eq.(A.7) will be used to describe the idler field from arbitrary span n after the OPC as the following,

$$A_g^{(n)}(z) = j \frac{2\pi\omega D\chi}{nc} e^{-\frac{\alpha}{2}l_n} \frac{e^{(-\alpha+j\Delta\beta)l_n} - 1}{-\alpha + j\Delta\beta} A_x^{(n)} A_y^{(n)} A_z^{*(n)} \quad (\text{A.14})$$

However, the relation between $A_i^{(n)}$ and $A_i^{(1)}$ is not straightforward like the relation in Eq.(A.8), to find $A_i^{(n)}$ as a function of $A_i^{(1)}$, we use Eq.(A.8) to find $A_i^{(\frac{N}{2})}$ as the following,

$$A_i^{(\frac{N}{2})}(z) = A_i^{(1)}(z) e^{(-\frac{\alpha}{2}+j\beta_i)\sum_{j=1}^{\frac{N}{2}} l_j} \prod_{j=1}^{\frac{N}{2}} \sqrt{G_j}, \quad i = x, y \text{ or } z \quad (\text{A.15})$$

Then $A_i^{(\frac{N}{2})}(z)$ will propagate through the DE and conjugated through the OPC then propagate to the beginning of span n , and $A_i^{(n)}$ can be written as,

$$A_i^{(n)}(z) = A_i^{*(1)}(z) e^{(-\frac{\alpha}{2}-j\beta_i)\sum_{j=1}^{\frac{N}{2}} l_j} \prod_{j=1}^{\frac{N}{2}} \sqrt{G_j} e^{-j\beta_{id}L_d} e^{(-\frac{\alpha}{2}+j\beta_i)\sum_{j=\frac{N}{2}+1}^{n-1} l_j} \prod_{j=\frac{N}{2}+1}^{n-1} \sqrt{G_j} \quad (\text{A.16})$$

And $A_x^{(n)} A_y^{(n)} A_z^{*(n)}$ can be written as,

$$A_x^{(n)} A_y^{(n)} A_z^{*(n)} = A_x^{*(1)} A_y^{*(1)} A_z^{(1)} e^{-j(\Delta\beta+\beta_g)\sum_{j=1}^{\frac{N}{2}} l_j} e^{-j(\Delta\beta_1+\beta_{gd})L_d} e^{j(\Delta\beta+\beta_g)\sum_{j=\frac{N}{2}+1}^{n-1} l_j} e^{-\frac{3}{2}\alpha\sum_{j=1}^{n-1} l_j} \prod_{j=1}^{n-1} (G_j)^{\frac{3}{2}} \quad (\text{A.17})$$

where $\Delta\beta_1$ is the equivalent phase-mismatch in the DE. Similar to Eq.(A.9), we can write $A_g^{(n,n)}(z)$ as the following,

$$A_g^{(n,n)}(z) = j \frac{2\pi\omega D\chi}{nc} A_x^{*(1)} A_y^{*(1)} A_z^{(1)} e^{(-\frac{\alpha}{2}+j\beta_g)l_n} \frac{e^{(-\alpha+j\Delta\beta)l_n} - 1}{-\alpha + j\Delta\beta} e^{-j(\Delta\beta+\beta_g)\sum_{j=1}^{\frac{N}{2}} l_j} e^{-j(\Delta\beta_1+\beta_{gd})L_d} e^{j(\Delta\beta+\beta_g)\sum_{j=\frac{N}{2}+1}^{n-1} l_j} e^{-\frac{3}{2}\alpha\sum_{j=1}^{n-1} l_j} \prod_{j=1}^{n-1} (G_j)^{\frac{3}{2}} \quad (\text{A.18})$$

APPENDIX A

Again, $A_g^{(n,n)}(z)$ will propagate to the end of the link as the following,

$$A_g^{(n,N)}(z) = A_g^{(n,n)}(z) e^{(-\frac{\alpha}{2} + j\beta_g) \sum_{j=n+1}^N l_j} \prod_{j=n}^N \sqrt{G_j} \quad (\text{A.19})$$

Using the same assumption that all the amplifiers ideally compensate the span losses, $A_g^{(n,N)}$ can be written as,

$$A_g^{(n,N)}(z) = j \frac{2\pi\omega D\chi}{nc} A_x^{*(1)} A_y^{*(1)} A_z^{(1)} \frac{e^{(-\alpha + j\Delta\beta)l_n} - 1}{-\alpha + j\Delta\beta} e^{-j(\Delta\beta + \beta_g) \sum_{j=1}^{\frac{N}{2}} l_j} e^{j\beta_g l_n} e^{-j(\Delta\beta_1 + \beta_{gd})L_d} e^{j(\Delta\beta + \beta_g) \sum_{j=\frac{N}{2}+1}^{n-1} l_j} e^{j\beta_g \sum_{j=n+1}^N l_j} \quad (\text{A.20})$$

A.4 Total FWM Field and Power

As a special case, we assume that we have identical span lengths for all the spans after and before the OPC ($l_j = L$), then $A_g^{(m,N)}(z)$ and $A_g^{(n,N)}(z)$ can be simplified as the following,

$$A_g^{(m,N)}(z) = -j \frac{2\pi\omega D\chi}{nc} A_x^{*(1)} A_y^{*(1)} A_z^{(1)} \frac{e^{(-\alpha - j\Delta\beta)L} - 1}{-\alpha - j\Delta\beta} e^{-j(m-1)\Delta\beta L} e^{-j\beta_{gd}L_d} \quad (\text{A.21})$$

$$A_g^{(n,N)}(z) = j \frac{2\pi\omega D\chi}{nc} A_x^{*(1)} A_y^{*(1)} A_z^{(1)} \frac{e^{(-\alpha + j\Delta\beta)L} - 1}{-\alpha + j\Delta\beta} e^{j(n-N-1)\Delta\beta L} e^{-j(\Delta\beta_1 + \beta_{gd})L_d} \quad (\text{A.22})$$

Now, we sum the idler field from all the spans after and before the OPC as the following,

$$A_g^{(t)} = \sum_{m=1}^{\frac{N}{2}} A_g^{(m,N)} + \sum_{n=\frac{N}{2}+1}^N A_g^{(n,N)} \quad (\text{A.23})$$

$$\begin{aligned}
A_g^{(t)} = j \frac{2\pi\omega D\chi}{nc} A_x^{*(1)} A_y^{*(1)} A_z^{(1)} e^{-j\beta_{gd}L_d} & \left(\frac{e^{(-\alpha-j\Delta\beta)L} - 1}{\alpha + j\Delta\beta} \sum_{m=1}^{\frac{N}{2}} e^{-j(m-1)\Delta\beta L} \right. \\
& \left. + \frac{e^{(-\alpha+j\Delta\beta)L} - 1}{-\alpha + j\Delta\beta} e^{-j\Delta\beta_1 L_d} e^{-j\frac{N}{2}\Delta\beta L} \sum_{n=\frac{N}{2}+1}^N e^{j(n-\frac{N}{2}-1)\Delta\beta L} \right)
\end{aligned} \quad (\text{A.24})$$

By evaluating the summation as the following,

$$\sum_{m=1}^{\frac{N}{2}} e^{-j(m-1)\Delta\beta L} = \frac{1 - e^{-j\frac{N}{2}\Delta\beta L}}{1 - e^{-j\Delta\beta L}} = e^{-j\frac{N}{4}\Delta\beta L} e^{j\frac{\Delta\beta L}{2}} \frac{\sin(\frac{N}{4}\Delta\beta L)}{\sin(\frac{\Delta\beta L}{2})} \quad (\text{A.25})$$

$$\sum_{n=\frac{N}{2}+1}^N e^{j(n-\frac{N}{2}-1)\Delta\beta L} = \frac{1 - e^{j\frac{N}{2}\Delta\beta L}}{1 - e^{j\Delta\beta L}} = e^{j\frac{N}{4}\Delta\beta L} e^{-j\frac{\Delta\beta L}{2}} \frac{\sin(\frac{N}{4}\Delta\beta L)}{\sin(\frac{\Delta\beta L}{2})} \quad (\text{A.26})$$

Then substituting the series summation into Eq.(A.24), we can rewrite $A_g^{(t)}$ as the following,

$$\begin{aligned}
A_g^{(t)} = j \frac{2\pi\omega D\chi}{nc} A_x^{*(1)} A_y^{*(1)} A_z^{(1)} e^{-j\beta_{gd}L_d} e^{-j\frac{N}{4}\Delta\beta L} e^{-j\frac{\Delta\beta_1 L_d}{2}} & \frac{\sin(\frac{N}{4}\Delta\beta L)}{\sin(\frac{\Delta\beta L}{2})} \\
& \left(\frac{e^{(-\alpha-j\Delta\beta)L} - 1}{\alpha + j\Delta\beta} e^{j(\Delta\beta_1 L_d + \Delta\beta L)/2} + \frac{e^{(-\alpha+j\Delta\beta)L} - 1}{-\alpha + j\Delta\beta} e^{-j(\Delta\beta_1 L_d + \Delta\beta L)/2} \right)
\end{aligned} \quad (\text{A.27})$$

$$\begin{aligned}
A_g^{(t)} = \frac{4\pi\omega D\chi}{nc} A_x^{*(1)} A_y^{*(1)} A_z^{(1)} e^{-j\beta_{gd}L_d} e^{-j\frac{N}{4}\Delta\beta L} e^{-j\frac{\Delta\beta_1 L_d}{2}} & \frac{\sin(\frac{N}{4}\Delta\beta L)}{\sin(\frac{\Delta\beta L}{2})} \frac{1}{(\alpha^2 + \Delta\beta^2)} \\
& \left[\alpha \left(e^{-\alpha L} \sin\left(\frac{\Delta\beta L - \Delta\beta_1 L_d}{2}\right) + \sin\left(\frac{\Delta\beta L + \Delta\beta_1 L_d}{2}\right) \right) + \right. \\
& \left. \Delta\beta \left(e^{-\alpha L} \cos\left(\frac{\Delta\beta L - \Delta\beta_1 L_d}{2}\right) - \cos\left(\frac{\Delta\beta L + \Delta\beta_1 L_d}{2}\right) \right) \right]
\end{aligned} \quad (\text{A.28})$$

By following a similar way to that presented in [198], the FWM power from a multi-span system employing mid-link OPC and DE can be written as,

$$P_g = \frac{4096\pi^6 (D\chi)^2}{n^4 \lambda^2 c^2 A_{eff}^2} P_x P_y P_z \left(\frac{\sin(\frac{N}{4}\Delta\beta L)}{\sin(\frac{\Delta\beta L}{2})} \right)^2 \frac{1}{(\alpha^2 + \Delta\beta^2)^2} \kappa^2 \quad (\text{A.29})$$

APPENDIX A

where κ can be written as,

$$\begin{aligned} \kappa = & \alpha \left(e^{-\alpha L} \sin\left(\frac{\Delta\beta L - \Delta\beta_1 L_d}{2}\right) + \sin\left(\frac{\Delta\beta L + \Delta\beta_1 L_d}{2}\right) \right) + \\ & \Delta\beta \left(e^{-\alpha L} \cos\left(\frac{\Delta\beta L - \Delta\beta_1 L_d}{2}\right) - \cos\left(\frac{\Delta\beta L + \Delta\beta_1 L_d}{2}\right) \right) \end{aligned} \quad (\text{A.30})$$

The power of the new generated signal (idler or FWM) in Eq.(A.29) is measured in the electrostatic system of units (esu) [239], where χ is measured in units cm^3/erg [198] and using the relation [38, 54, 239],

$$\chi[\text{esu}] = \frac{cn^2}{480\pi^2} n_2 [m^2/W], \quad \text{and} \quad \gamma = \frac{2\pi f}{cA_{eff}} n_2, \quad (\text{A.31})$$

equation (A.29) can be written in the international system of units (SI units) as the following [53, 196],

$$P_g = \frac{4D^2}{9} \gamma^2 P_x P_y P_z \left(\frac{\sin(\frac{N}{4} \Delta\beta L)}{\sin(\frac{\Delta\beta L}{2})} \right)^2 \frac{1}{(\alpha^2 + \Delta\beta^2)^2} \kappa^2 \quad (\text{A.32})$$

